SPACE
PRODUCTS
DEVELOPMENT
GROUP

A CONTROL MOMENT GYRO FINE ATTITUDE CONTROL SYSTEM

FINAL TECHNICAL REPORT

NASA CONTRACT NO. NAS9-10363

Prepared By R. Van Riper
R. Van Riper

Approved By J. Harrison
J. Harrison

SPERRY FLIGHT SYSTEMS DIVISION
PHOENIX, ARIZONA

COPY NO. _____ PRINTED IN U.S.A. AUGUST 1970 PUB. NO. 70-1304-00-00

FOREWORD

This report, which summarizes the results of an 8-month study, satisfies the requirements of Article II, Item 5 of the contract schedule, NASA Contract No. NAS9-10363. All work was performed at the Sperry Flight Systems Division, Phoenix, Arizona, by the Space Products Development Group of the Research and Development Department. Mr. John Harrison served as the Program Manager, Mr. Richard Van Riper as Project Engineer, and Mr. Frank Cappelletto as Systems Analyst.

The contract was administered by the NASA Houston, Manned Spacecraft Center, Guidance and Control Division. Mr. William A. McMahon was the Technical Monitor.

TABLE OF CONTENTS

TABLE OF CONTENTS (cont)

TABLE OF CONTENTS (cont)

LIST OF ILLUSTRATIONS

LIST OF ILLUSTRATIONS (cont)

LIST OF ILLUSTRATIONS (cont)

SECTION I

INTRODUCTION

SECTION I

INTRODUCTION

The purpose of the Control Moment Gyro (CMG) Fine Attitude Control System (FACS) Study was to identify, analyze, design, and specify an attitude control system capable of providing fine pointing accuracy and very low attitude drift rates. This study elected to conduct detailed sizing and system design predicated on the Apollo CSM since characteristic data was readily available for this vehicle. The CMG system discussed, however, is applicable to any orbiting planetary or lunar spacecraft which requires fine pointing accuracy, has a moderate disturbance torque profile, and requires high reliability and long lifetime. Such a spacecraft presently being investigated is the free flying experiment module to be used with an earth orbiting space station.

The principal tasks accomplished during this study were the following:

- Competitive Control Systems Compared
- A Fine Attitude Control System Synthesized
- Dynamic Analysis by Analog Simulation Conducted
- CMG Momentum and Stability Envelopes Established
- CMG Steering Laws Investigated
- CMG Momentum Unloading Techniques Investigated
- Failure Modes and Effects Analysis Conducted
- Reliability Analysis Conducted
- Monitoring and Failure Detection Techniques Established
- Operational Procedures and Performance Specifications Established

Initially, the study was to consider only manned missions which dictate the use of large control torque and system bandwidth capability. Midway through the study, however, a decision was made to consider unmanned missions as well, therefore providing for a more comprehensive and meaningful investigation. The results of both studies are presented in this report. Most of the analog computer studies were conducted for the system satisfying the manned mission requirements.

SECTION II

STATEMENT OF THE PROBLEM

SECTION II

STATEMENT OF THE PROBLEM

Attitude control of a satellite or space vehicle is required for two major reasons. One is to ensure that rocket thrusts from vehicle referenced rocket engines are properly directed. The other is to facilitate information flow from or to the vehicle. These reasons may result from using the vehicle as a stable platform while photographing the moon or earth, conducting telescopic observations of celestial bodies, inspecting other spaceborne objects, conducting orbital and geophysical experiments, forming part of a space-ground or space-communication link, and many others. Each mission has a set of attitude requirements related to the investigations and experiments it is intended to accomplish, and these dictate the form of the attitude control system. The simplest attitude control technique is employed by a free spinning satellite using the principle that a spinning body will tend to maintain its attitude in a force free space. This represents one end of a spectrum. The manned Apollo spacecraft using a three-axis, stabilized, inertial measuring unit; rate gyro stabilization; complex digital computer; and supplementary star sight updating represents the other end. Most space vehicle attitude stabilization requirements will call for a system complexity between these two extremes.

The primary attitude control requirements usually specified are attitude or (pointing) accuracy and attitude rate. Attitude accuracy can be classified as follows:

- Precision: less than 0.01 degree
- Fine: 0.01 to 0.2 degree
- Moderate: 0.2 to 1.0 degree
- Coarse: 1.0 to 5.0 degree

The Apollo Telescope Mount (ATM) represents a typical precision attitude accuracy mission, 2.5 arc second; and the Application Technology Satellite represents a fine-moderate accuracy requirement. Advanced systems proposed for use in the 1975 - 1980 period such as for Free Flying Experiment Modules and High Energy Astronomical Observatory (HEAO) Satellites will require attitude accuracies of 0.005 to 0.5 arc second.

The attitude rate attained during pointing within the allowable attitude accuracy influences the imaging of cameras and telescopes and puts errors into precision, on-board experiments; therefore, the minimum rate must also be considered as well as the static accuracy specification. Typically, the rate requirement in degrees per second is between 0.05 and 0.5 of the accuracy requirements expressed in degrees (i.e., 0.1 deg attitude and 0.01 deg/sec rate). For some applications an additional tracking specification is imposed which requires the vehicle to turn or slew at a given rate while maintaining attitude accuracy.

To achieve these requirements, the attitude control system must oppose every disturbance torque which acts on the vehicle and attempts to produce an undesirable attitude change. Disturbance torques can be classified by point of origin as either external or internal, and also by form as cyclic or secular. External torque sources such as solar, magnetic, gravity gradient, and aerodynamic disturbances can be cyclic at a multiple of the orbital frequency or they can be secular in only one direction. Internal torque sources such as rotating machinery and gas venting can produce secular torques; whereas, crew torques are large, cyclic disturbances at a relatively high frequency and of a rather random nature.

As a consequence of this large gamut of possible attitude control requirements and disturbance torques, there does not exist one "best" system design which can be applied cookbook fashion to each mission. Instead, each attitude control system design is able to satisfy a particular combination of requirements better than others and can be said to possess an area of superior performance. Unfortunately, the area of superior performance is not completely separated for each system design and many overlaps occur which may ultimately require a final decision based on good engineering judgment. References* 1 and 2 discuss many such tradeoffs and indicate the complexity involved in selecting the "best" attitude control system for a particular mission objective.

This study, therefore, attempts to investigate the mission requirements, identify their impact on system choice, and design an attitude control system capable of achieving fine attitude accuracies.

*All references cited are listed in Section XII.

SECTION III

ATTITUDE CONTROL SYSTEM REQUIREMENTS

SECTION III

ATTITUDE CONTROL SYSTEM REQUIREMENTS

The initial effort in defining a spacecraft attitude control system is to establish a basic set of control requirements. These requirements are derived from consideration of the vehicle configuration, mission plan, on-board experiments, operational modes, orbit geometry, in-orbit orientation, available power, life, and reliability. Once established, such requirements as attitude and attitude rate accuracies, tracking errors, response time, bandwidth, damping, control torque, momentum storage, minimum impulse, power and reliability constitute common criteria to use in performing a control system comparison study and serve as a design goal during system synthesis and implementation.

A. DESIGN MISSION DESCRIPTION

To create a meaningful study and avoid a superficial investigation of many different type vehicles, orbits, and systems, a "design mission" has been selected as representative of the many possibilities. This technique allows a set of system requirements to be generated and a design conducted which not only identifies the important technical areas and techniques used in designing the attitude control system but also creates a starting point for conducting other mission designs.

The design mission selected for this study is shown in Figure 3-1. An Apollo CSM vehicle is shown in a 250-nautical-mile circular earth orbit with a 33-degree inclination. The vehicle is oriented so that the X or longitudinal axis is pointed at the sun and the Y or pitch axis is held in the orbital plane. This orientation is maintained for at least 60 minutes per orbit. The Apollo CSM was selected as the design spacecraft because configuration data was readily available and its size and configuration is typical of many present and future orbiting space vehicles. The attitude hold requirements, which are presented in Table 3-1, call for 3-axis attitude hold with an attitude error less than 0.1 degree and attitude rate of less than 0.01 degree per second. To achieve sun re-acquisition with minimum maneuvering when leaving the earth's shadow, the allowable attitude reference drift when not locked on the sun is 0.10 degree per hour maximum. The mission duration is 14 to 60 days and a probability of overall system success greater than 0.95 for 1000 hours is necessary. No maneuvering or slewing is to be done by the fine attitude control system since this is accomplished by a parallel high torque level, reaction jet control system.

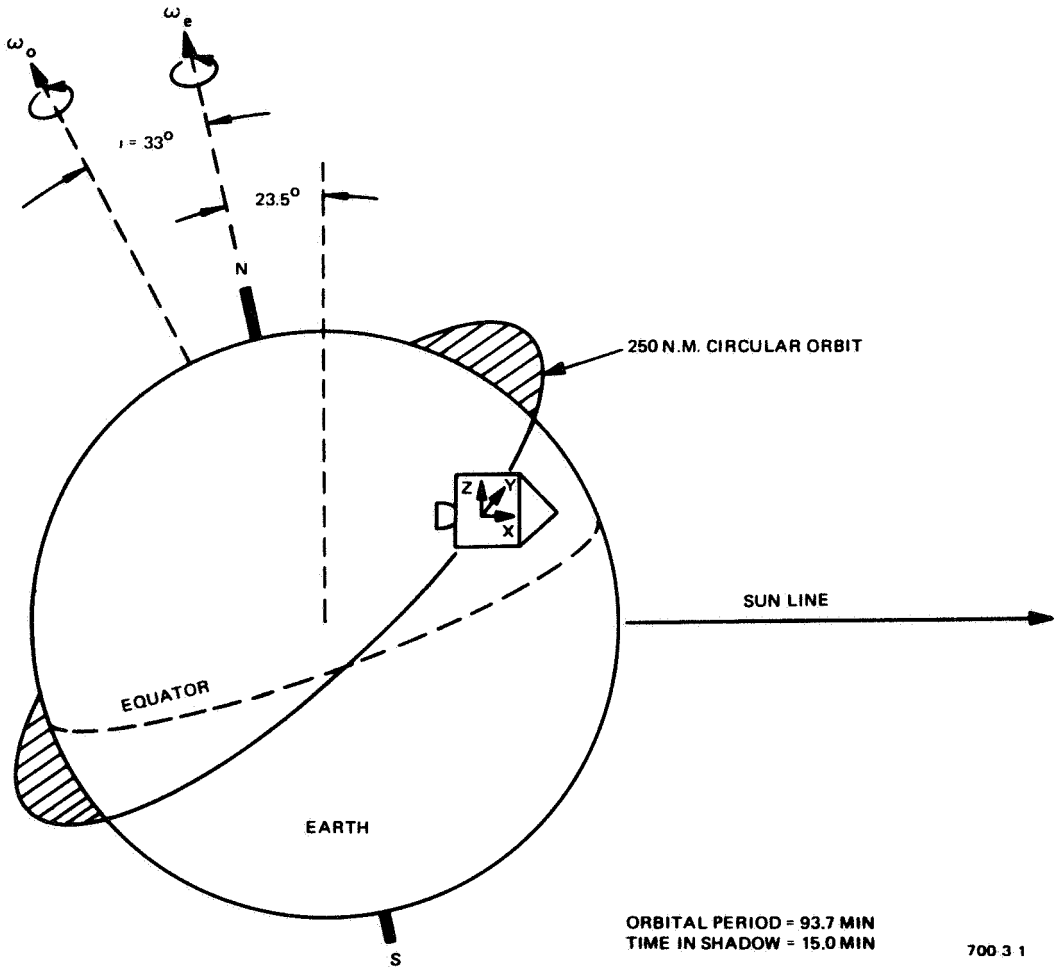

Figure 3-1
Orbit Geometry

Both manned and unmanned vehicles, which are considered, required significantly different system designs. Moderate crew torques are allowed during the attitude hold period in the manned missions. The electrical power is derived for on-board hydrogen-oxygen fuel cells which have a maximum available electrical power of 1000 watts at 28 volts dc over the mission duration.

TABLE 3-1
ATTITUDE HOLD REQUIREMENTS
(MANNED)

Parameter	Pitch	Roll	Yaw	Unit
Maximum Attitude Error	<0.1	<0.1	<0.1	Deg
Maximum Attitude Rate	<0.01	<0.01	<0.01	Deg/Sec
Attitude Drift (while in shadow)	0.1	0.1	0.1	Deg/Hr

B. DISTURBANCE TORQUES

Both external and internal disturbance torques, which act on the orbiting spacecraft, must be countered by an opposing control torque to maintain fine attitude hold. The magnitude of the combined disturbances establishes the maximum control torque needed, and the waveshape defines the required system bandwidth during attitude hold. The torques present at a 250-nautical-mile earth orbit are the following:

External	Internal
Magnetic	Crew Motion
Solar	Internal Machinery
Gravity	Fuel or Gas Venting
Aerodynamic	

The magnetic torque produced by the interaction of the earth's magnetic field and currents within the spacecraft is approximately $2(10)^{-7}$ foot-pounds for this mission and can be neglected (Ref 3). The torque produced by the solar radiation pressure on the spacecraft is very low (approximately 10^{-10} foot-pounds) because the vehicle's X-axis is oriented at the sun during attitude hold and geometrical symmetry exists about the axis.

The gravity gradient torques due to the non-equal vehicle moments of inertia and the aerodynamic torques caused by atmospheric molecules are both significant for the 250-nautical-mile orbit. Derivation of torques due to these sources is presented in Appendix A; resulting equations are the following:

$$\begin{bmatrix} L_x \\ L_y \\ L_z \end{bmatrix} = \begin{bmatrix} 0.613 \sin 2\omega_o t \\ -3.63 \ (1 + \cos 2\omega_o t) \\ 3.96 \sin 2\omega_o t \end{bmatrix}_{gr} 10^{-2} + \begin{bmatrix} -0.5 \, D_n(t) \cos \omega_o t \\ -1.95 \, D_n(t) \sin \omega_o t \\ 2.67 \, D_n(t) \cos \omega_o t \end{bmatrix}_{aero} 10^{-2} \quad (3\text{-}1)$$

where:

$$D_n(t) = 0.12 \ (1 - 0.3 \sin^2 \omega_o t)^{1/2}$$

Torques and accumulated momentum about each axis are shown in Figures 3-2 through 3-7.

These torques, which are strongly influenced by orbit altitude, attitude orientation, and vehicle configuration, should be considered characteristic (not absolute) for this type mission. For instance, at this orbital altitude (250 nautical miles) the aerodynamic torques are approximately 10 percent of the gravity-gradient torques; for a 170-nautical-mile orbit, the aerodynamic torques increase ten times and are approximately equal to the gravity-gradient torque. Likewise, only a 7 percent change in the Y-axis moment-of-inertia will double the X-axis gravity-gradient torque. All the torques are cyclic at twice the orbital frequency and accumulate zero net angular momentum except the Y-axis gravity gradient torque, which has a constant secular contribution of -0.0363 foot-pounds. This torque causes angular momentum to be accumulated about the Y-axis and creates a need for desaturation of a momentum storage-type control system or periodic pulsing of a mass expulsion reaction jet control system. An alternate orientation with the X-axis in the orbital plane that would decrease the secular torque significantly is presented in Appendix A.

Internal disturbance torques result from the following: internal moving parts (rotating machinery and on-board experiments); venting or leakage of fuel and gases; and crew motions. For the design mission, only crew-generated torques are considered. Crew torques are quite a random phenomena which are characterized by large magnitude, high frequency cyclic torques relative to the external disturbances and, therefore, must be approximated when establishing a system design. Laboratory studies have been conducted (ref 4, 5) which identify typical crew disturbances in an Apollo vehicle and idealize them as a single sinewave torque pulse as shown in Figure 3-8 and listed in Table 3-2. For this study a design torque of 25 foot-pound peak with a 1-Hz frequency has been selected as representing a moderate crew disturbance. The influence of crew torques on the attitude hold control system is the requirement of larger control torques and a higher system bandwidth than necessary for the low magnitude, slowly varying gravity and aerodynamic disturbances. Unlike the case of gravity torques, however, very little stored momentum requirement due to crew torques exists because an equal and opposite reaction occurs very soon after the initial disturbance.

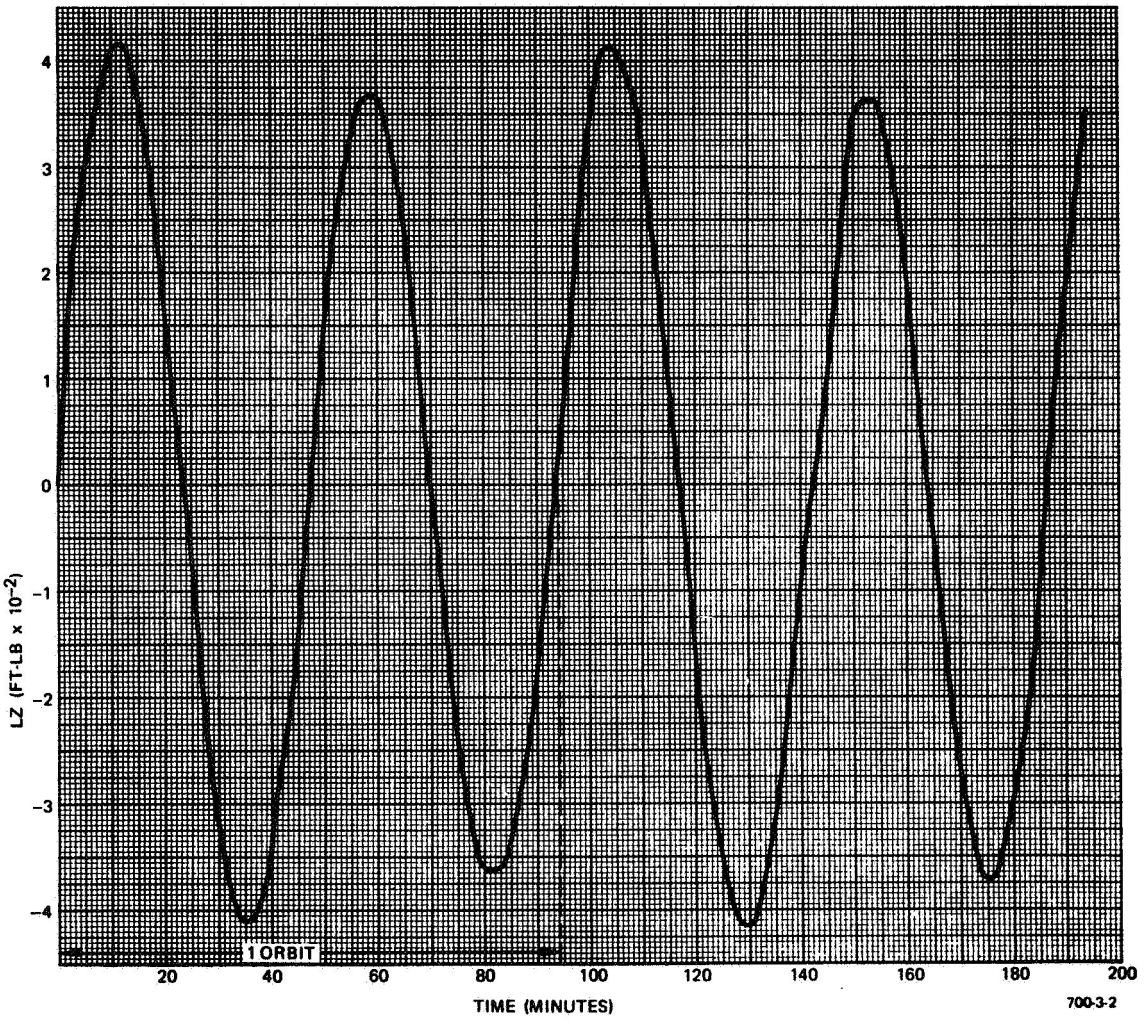

Figure 3-2
Z-Axis Torque versus Time

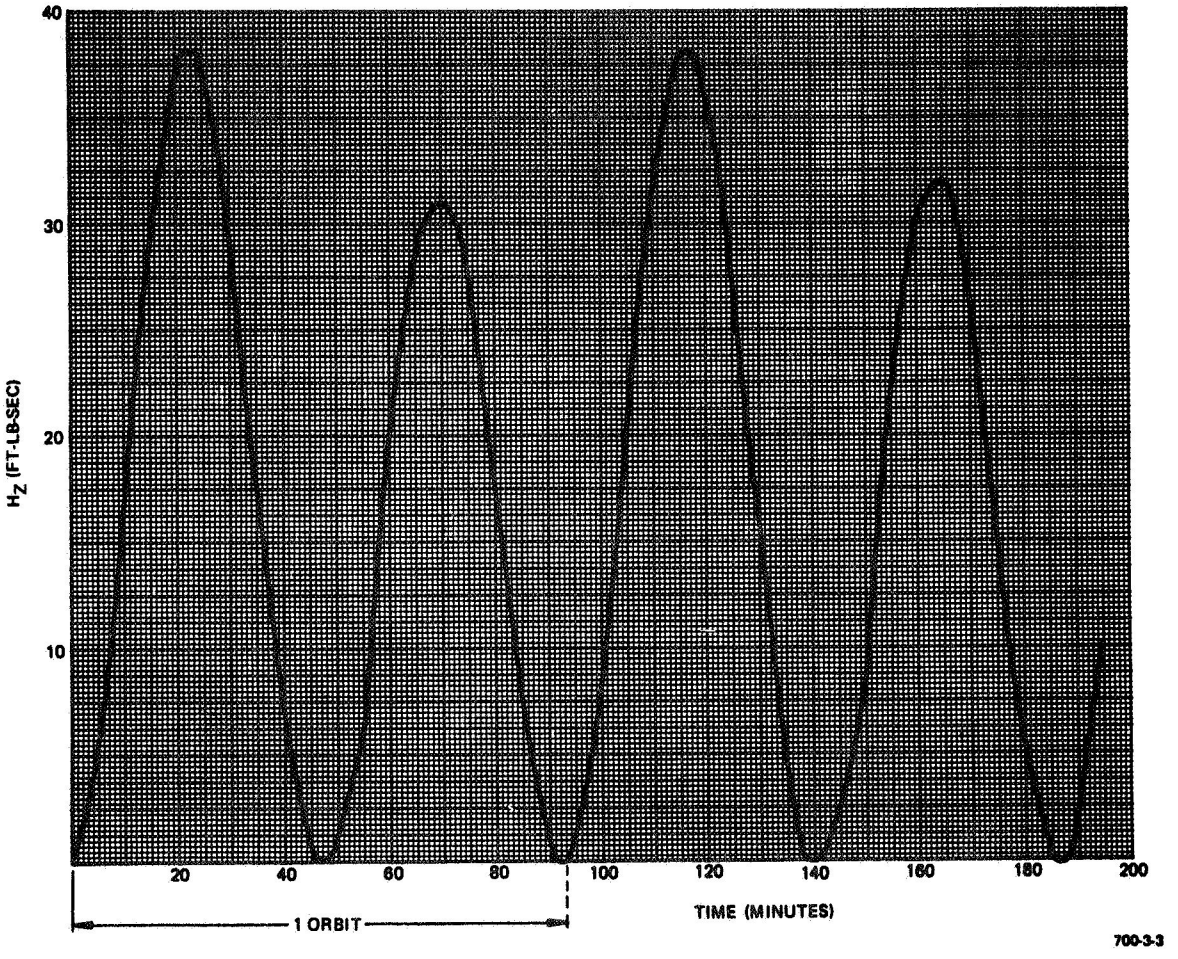

Figure 3-3
Z-Axis Momentum versus Time

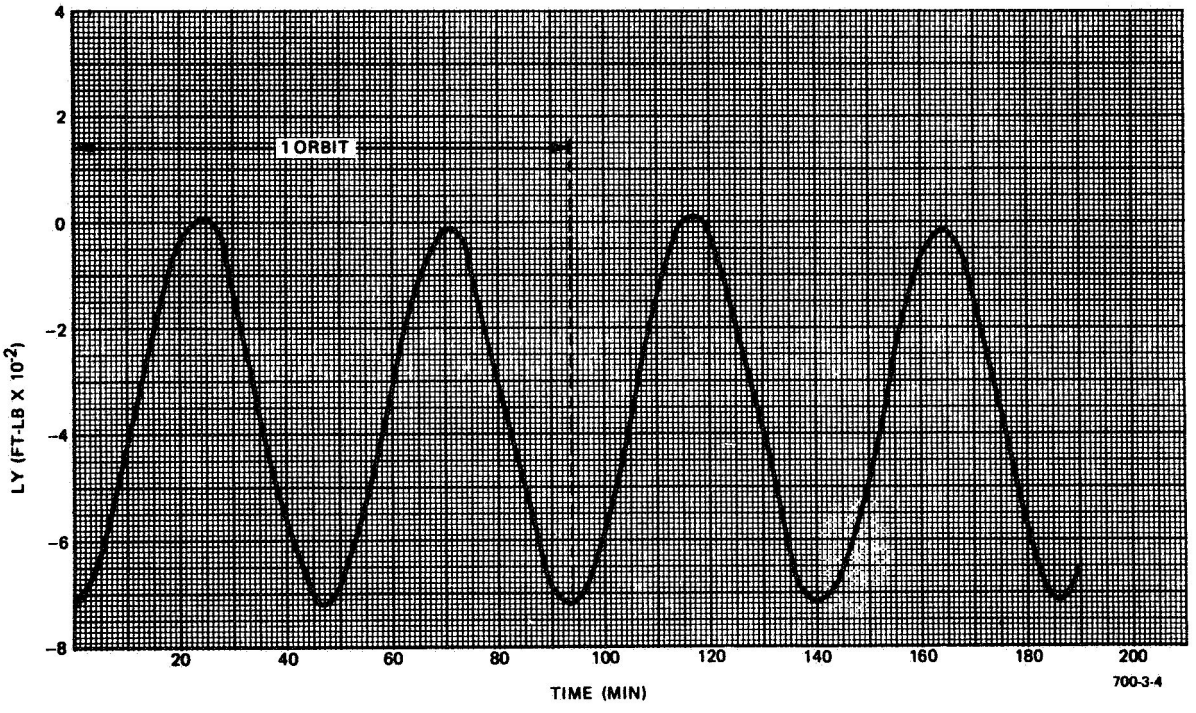

Figure 3-4
Y-Axis Torque versus Time

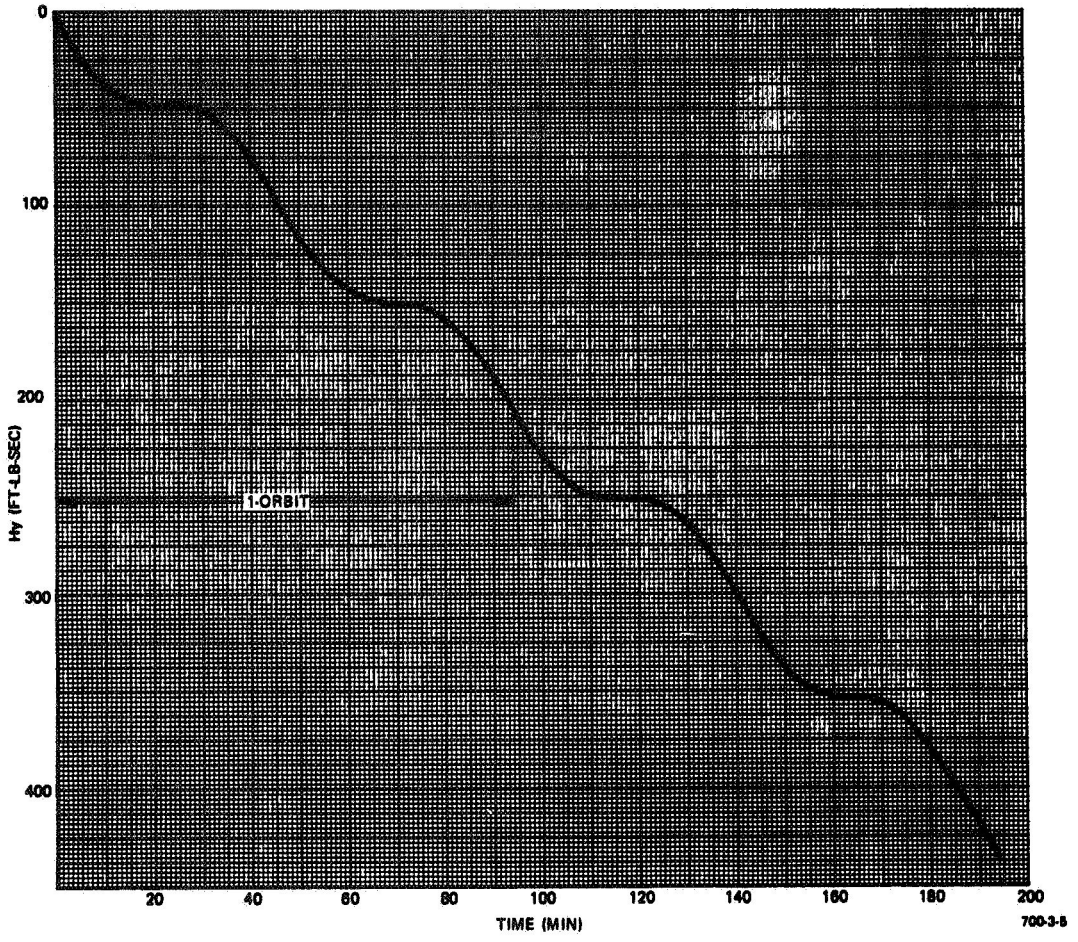

Figure 3-5
Y-Axis Momentum versus Time

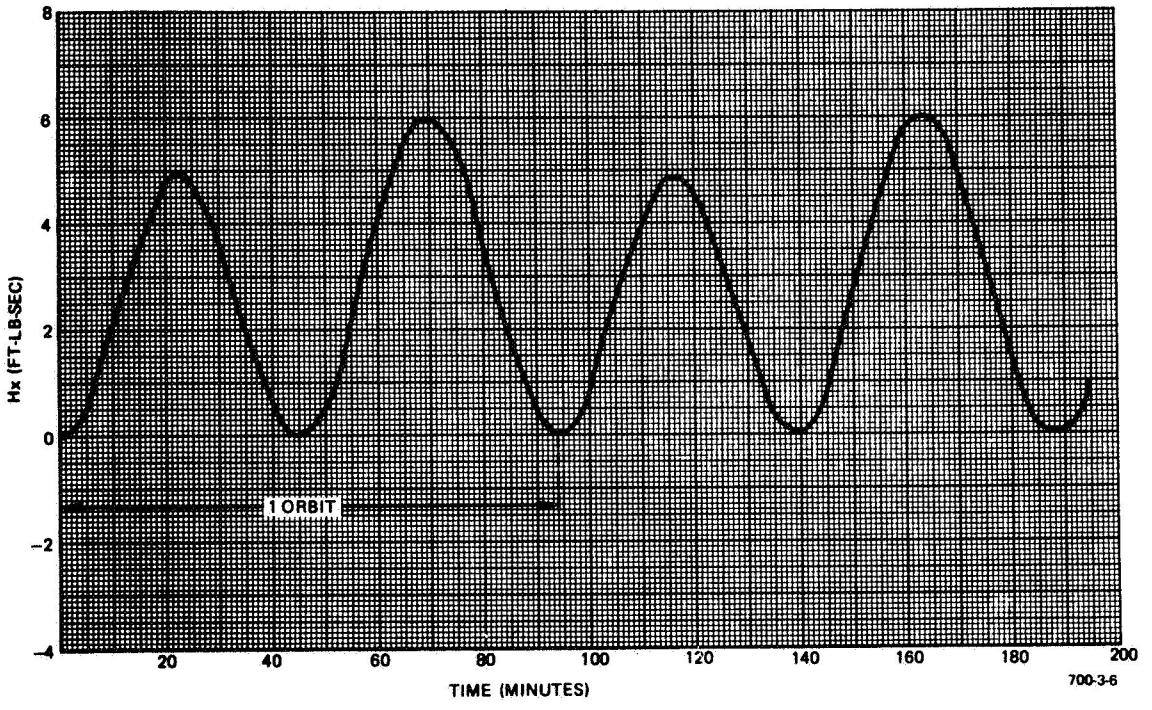

Figure 3-6
X-Axis Momentum versus Time

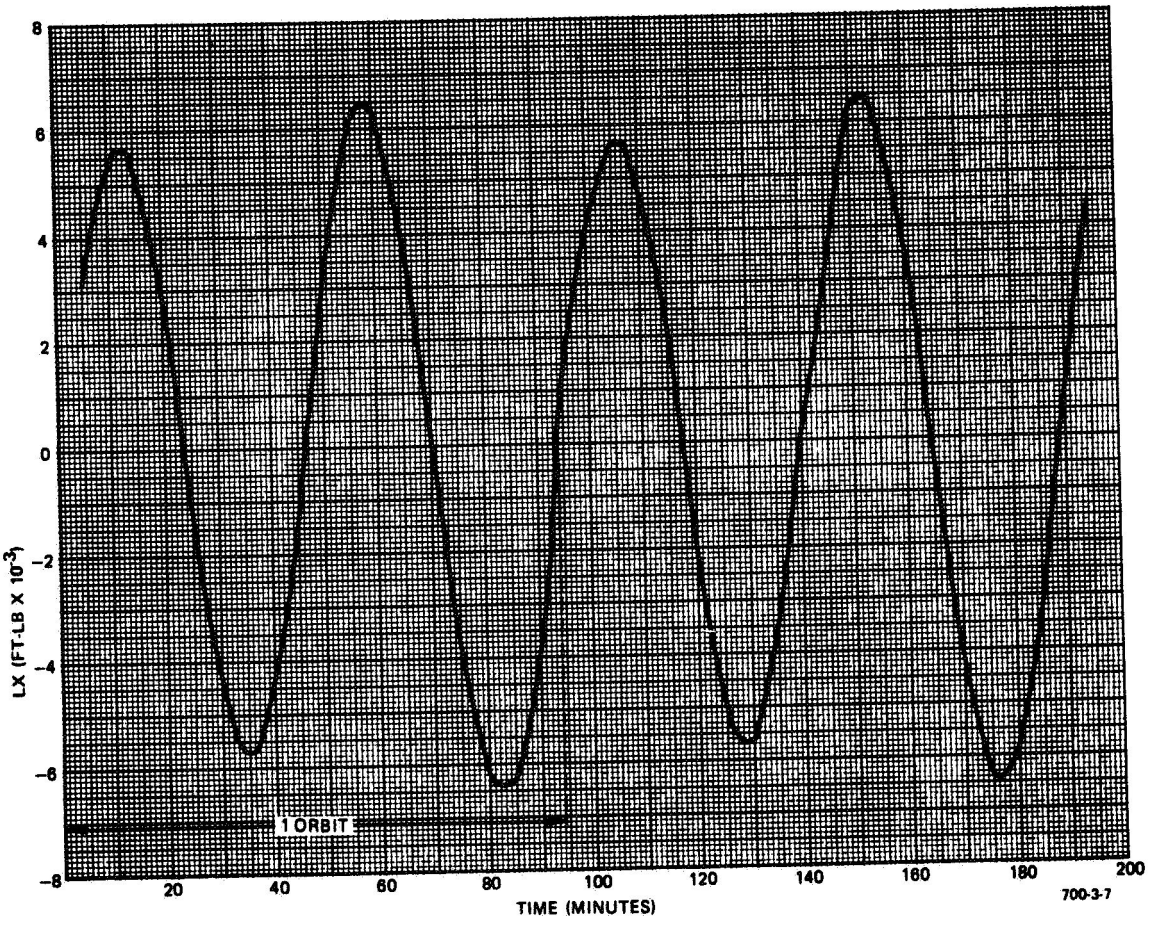

Figure 3-7
X-Axis Torque versus Time

For unmanned missions only external torques need be considered; therefore, a low level control torque system with a small bandwidth is required. With low level torques present, a much more precise attitude accuracy can be achieved.

TABLE 3-2
TYPICAL CREW DISTURBANCES IDEALIZED AS A SINGLE SINEWAVE TORQUE PULSE

Activity	T_{MX} (ft-lb)	T_{MY} (ft-lb)	T_{MZ} (ft-lb)	Frequency (Hz)
Breathing	0.12	1.0	0.15	0.83
Coughing	-8.0	-30.0	6.0	1.0
Sneezing	3.0	-20.0	3.1	1.0
Panel Operation	5.0	5.0	-2.6	0.5
Arm Movement	-16	12	20	1.0

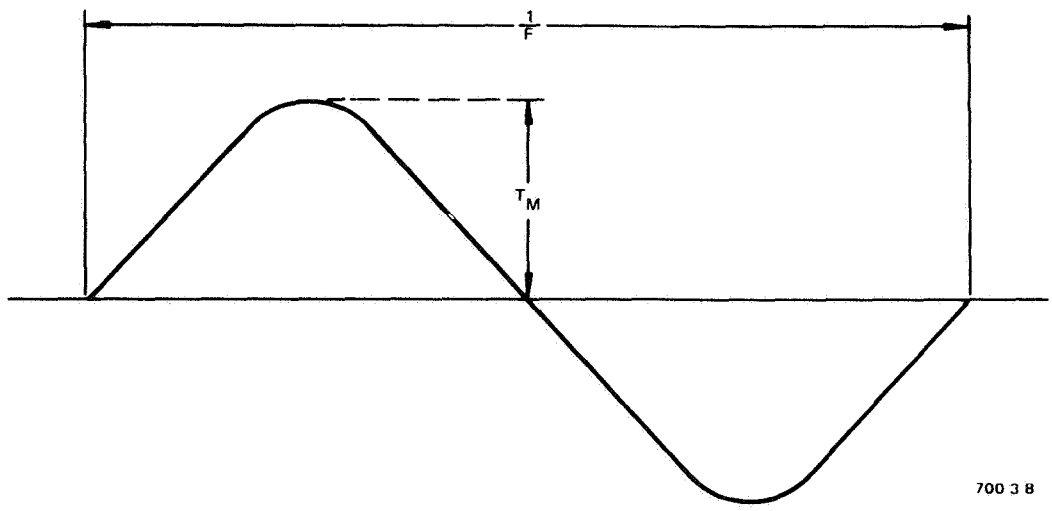

Figure 3-8
Crew Torques

C. MOMENTUM REQUIREMENTS

Establishing momentum requirements in each axis is important because it strongly influences the selection and size of the CMG configuration. Each CMG configuration possesses a characteristic momentum envelope which signifies its maximum momentum storage capability. After this momentum limit is reached, the CMG configuration must be desaturated by an RJC system or other means. By selecting a CMG configuration whose momentum envelope is compatible with the momentum requirements, a smaller and more efficient gyro system can be developed.

For the manned mission and the disturbance torques identified in Subsection III.B, the stored momentum requirements are

- X Axis = 7 ft-lb-sec
- Y Axis = 142 ft-lb-sec (60 min)
  205 ft-lb-sec (1 orbit)
- Z Axis = 38 ft-lb-sec
- Plus 8 ft-lb-sec per crew torque disturbance

The momentum envelope (Figure 3-9) is derived by adding all the disturbance torque momentum vectors along each vehicle axis and forming a box-type envelope. The effect of the secular gravity-gradient torque is to increase the requirement along the Y axis and elongate the envelope. The path that the total momentum vector traces out, an ascending spiral, is also shown in Figure 3-9.

For an unmanned mission, the momentum requirements are essentially unchanged, although,the 8 ft-lb-sec crew torque momentum is not needed.

D. SUMMARY

The fine attitude control system requirements have been established by reviewing the design mission selected, deriving the disturbance torque time profiles, and developing a momentum envelope. The attitude accuracies, available power, and reliability are dictated directly by mission requirements. The crew disturbances establish the maximum control torque and system bandwidth requirement; the gravity-gradient and aerodynamic torque time integrals establish the stored momentum requirements. The principal system requirements are summarized in Table 3-3.

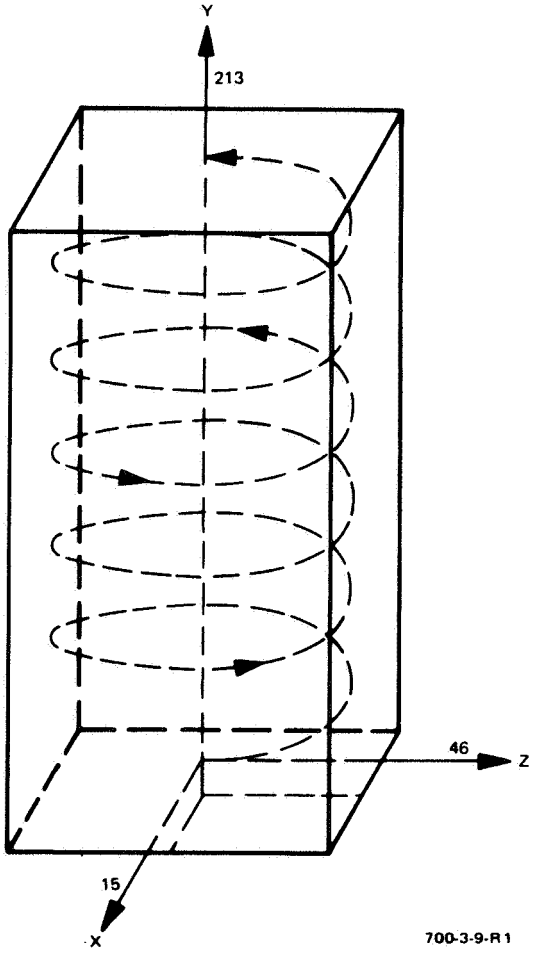

Figure 3-9
Momentum Envelope

TABLE 3-3

ATTITUDE CONTROL SYSTEM REQUIREMENTS

Parameter	Manned	Unmanned	Unit
Attitude hold accuracy	<0.1	<0.001	degrees
Attitude hold rate	< 0.01	< 0.0001	deg/sec
Maximum control torque	25	2	ft-lb
Maximum system bandwidth	3	1	Hz
Maximum stored momentum	213	208	ft-lb-sec
Maximum available power	1000	1000	watts
Minimum probability of success for 1000 hours	0.95	0.95	---

SECTION IV

4-FACS CMG CONFIGURATION

SECTION IV

4-FACS CMG CONFIGURATION

The Sperry 4-FACS CMG configuration is a unique arrangement of four single gimbal gyros which has been selected to provide fine attitude hold capability with a simple, linear, constant gain steering law and to permit operation with one gyro failed by making a small steering law modification.

A. OPERATIONAL DESCRIPTION

This selected configuration, identified as the Sperry 4-FACS CMG configuration, is shown in Figure 4-1. The model shown in this illustration does not represent a physical model of an actual system, but simply illustrates the relative orientations of the gimbal axes and the angular momentum vectors (shown as black arrows). The four gimbal axes lie in the xz-plane of the vehicle coordinate system, with directions of 45, 135, 225, and 315 degrees from the z-axis. The respective gimbal angles, denoted by $\alpha = \{\alpha_1, \ldots, \alpha_4\}$, are the angles of the h-vectors (angular momentum vectors) about the gimbal axes. The reference directions of the h-vectors lie in the xz-plane and in the counterclockwise direction about the y-axis. The figure shows gimbal angles of $\alpha = \{+45°, -45°, +45°, -45°\}$, which correspond to the initial gimbal angles for the case where all four gyros are operational.

A simplified description of the steering law is first presented, followed by an analytical presentation. Each pair of the four gyros for which the gimbal axes are colinear may be considered as a scissored pair. Denote the net angular momentum vector of gyros 1 and 3 (counted from the z-axis in the counterclockwise direction) by H_a, and that of gyros 2 and 4 by H_b. H_a and H_b and the planes in which they may rotate are shown in Figure 4-2. For the initial gimbal angles, H_a lies in the +y direction, H_b lies in the -y direction. Both have the magnitude of $\sqrt{2}\,h$ where h is the angular momentum magnitude of each gyro (all assumed equal). In general, the magnitude of H_a is $2h \sin\left[(\alpha_1 + \alpha_3)/2\right]$ and that of H_b is $2h \sin\left[(\alpha_2 + \alpha_4)/2\right]$. The angle of H_a from the +y axis (see Figure 4-2) is given by $\alpha_a = (\alpha_1 - \alpha_3)/2$, and similarly, $\alpha_b = (\alpha_4 - \alpha_2)/2$.

To produce H (the net angular momentum of the system) in the +y direction starting from α_0, $|H_a|$ (the magnitude of H_a) is increased by increasing α_1 and α_3 by equal amounts, and $|H_b|$ is decreased by increasing α_2 and α_4 by equal amounts. To produce H in the +z direction, α_a and α_b are increased by equal amounts, and $|H_a|$ and $|H_b|$ are held constant. Similarly, H in the +x direction may be produced by decreasing α_a and increasing α_b by equal amounts without changing $|H_a|$ and $|H_b|$.

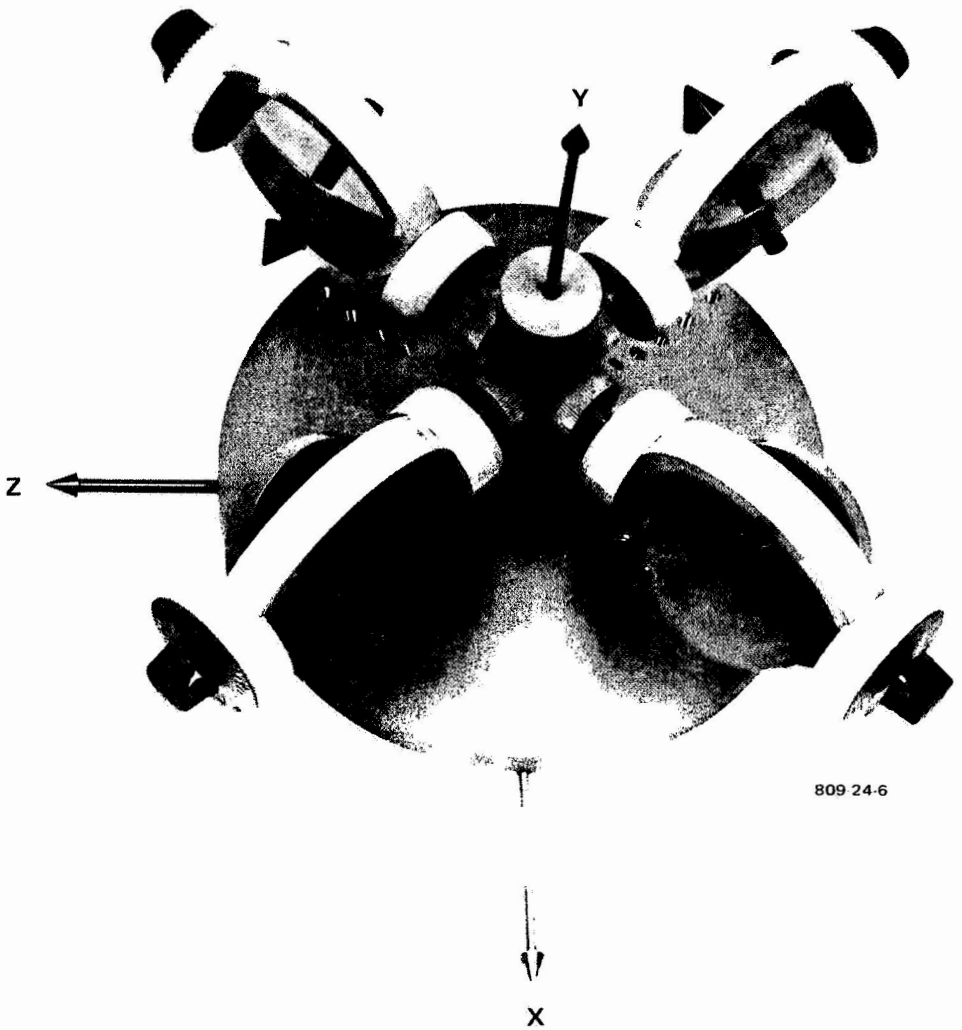

Figure 4-1
Model Showing Sperry 4-FACS CMG Configuration

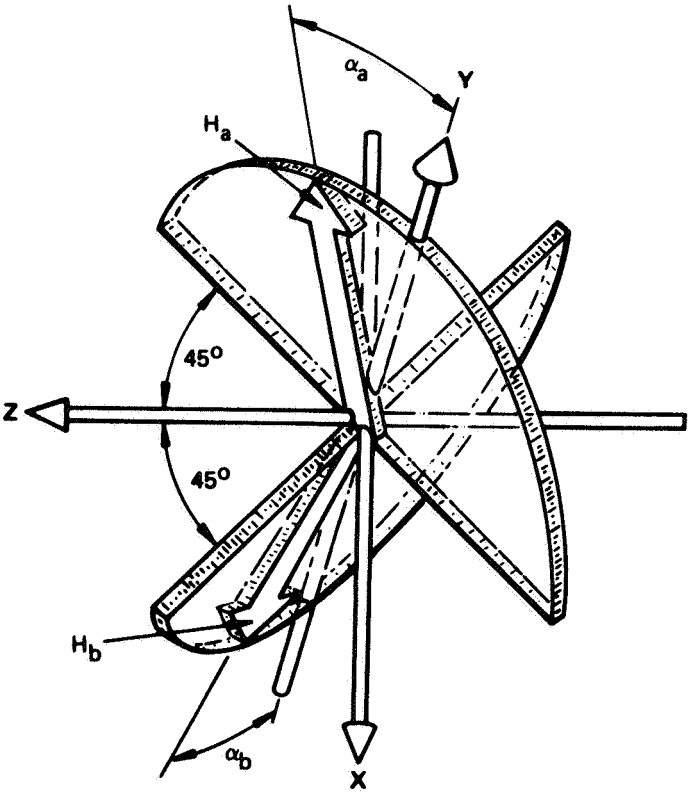

Figure 4-2
H_a and H_b

When the commanded change in H does not start with $\alpha = \alpha_0$, cross-coupling occurs, and the outer attitude loop or other steering law corrections are relied on to remove the attitude errors thus produced.

B. GYRO MOMENTUM AND TORQUE

In analytical terms, the net angular momentum of this configuration is

$$\begin{aligned} H_y &= h(S_1 + S_2 + S_3 + S_4) \\ H_z &= \frac{h}{\sqrt{2}}(-C_1 - C_2 + C_3 + C_4) \\ H_x &= \frac{h}{\sqrt{2}}(C_1 - C_2 - C_3 + C_4) \end{aligned} \tag{4-1}$$

where h is the angular momentum magnitude of each gyro (all equal), and where $S_i = \sin \alpha_i$, and $C_i = \cos \alpha_i$. The reaction torque acting on the vehicle due to a changing net angular momentum of the CMG system is the negative time-derivative of these equations (4-1) with respect to inertial space. The torque due to the vehicle attitude rate during attitude hold is negligibly small compared with the torque due to gimbal rates so the torques may be given by:

$$\begin{bmatrix} T_y \\ T_z \\ T_x \end{bmatrix} = -h \begin{bmatrix} C_1 & C_2 & C_3 & C_4 \\ S_1/\sqrt{2} & S_2/\sqrt{2} & -S_3/\sqrt{2} & -S_4/\sqrt{2} \\ -S_1/\sqrt{2} & S_2/\sqrt{2} & S_3/\sqrt{2} & -S_4/\sqrt{2} \end{bmatrix} \begin{bmatrix} \dot{\alpha}_1 \\ \dot{\alpha}_2 \\ \dot{\alpha}_3 \\ \dot{\alpha}_4 \end{bmatrix} \tag{4-2}$$

where $\dot{\alpha}_i = d\alpha_i/dt$.

C. CONSTANT GAIN STEERING LAW

A control moment gyro system provides precise attitude control of a spacecraft by imparting the correct combination of three axis torques in response to vehicle disturbances or maneuvering commands. These gyro torques are created by driving each gyro in the CMG configuration at a particular gimbal rate; however, for configurations with more than three gyros one unique set of gyro gimbal rates that produce a particular three axis torque combination does not exist. Steering law computers, therefore, are necessary to continuously translate the vehicle command signals (usually a function of rate and attitude error) into a preferred set of gimbal rate commands. An "exact" steering law would generate gimbal command signals so that the open-loop vehicle response

would follow the vehicle command signals without any cross-axis coupling and minimize the torquer power consumed. Such a steering law would require a complex computer capable of solving many equations in a short period of time. Instead, to increase system reliability, the following simple constant gain steering law has been derived which is "exact" when all gimbal angles are at their initial condition $(\alpha_0) = (45°, -45°, 45°, -45°)$, but deviates from the exact solution otherwise.

$$\begin{bmatrix} \dot{\alpha}_{1c} \\ \dot{\alpha}_{2c} \\ \dot{\alpha}_{3c} \\ \dot{\alpha}_{4c} \end{bmatrix} = -\frac{1}{h} \begin{bmatrix} \frac{\sqrt{2}}{4} & \frac{1}{2} & -\frac{1}{2} \\ \frac{\sqrt{2}}{4} & -\frac{1}{2} & -\frac{1}{2} \\ \frac{\sqrt{2}}{4} & -\frac{1}{2} & \frac{1}{2} \\ \frac{\sqrt{2}}{4} & \frac{1}{2} & \frac{1}{2} \end{bmatrix} \begin{bmatrix} T_{yc} \\ T_{zc} \\ T_{xc} \end{bmatrix} \qquad (4\text{-}3)$$

where $T_c = \{T_{yc}, T_{zc}, T_{xc}\}$ are the torques commanded by the fine attitude controller, and $\dot{\alpha}_c = \{\dot{\alpha}_{1c}, \ldots, \dot{\alpha}_{4c}\}$ are the gimbal rates commanded to the gimbal controller. With this steering law, the torque applied to the vehicle due to T_c is (for $\dot{\alpha} = \dot{\alpha}_c$)

(4-4)

$$\begin{bmatrix} T_y \\ T_z \\ T_x \end{bmatrix} = \begin{bmatrix} \frac{\sqrt{2}}{4}(C_1 + C_2 + C_3 + C_4) & \frac{1}{2}(C_1 - C_2 - C_3 + C_4) & \frac{1}{2}(-C_1 - C_2 + C_3 + C_4) \\ \frac{1}{4}(S_1 + S_2 - S_3 - S_4) & \frac{\sqrt{2}}{4}(S_1 - S_2 + S_3 - S_4) & \frac{\sqrt{2}}{4}(-S_1 - S_2 - S_3 - S_4) \\ \frac{1}{4}(-S_1 + S_2 + S_3 - S_4 & \frac{\sqrt{2}}{4}(-S_1 - S_2 - S_3 - S_4) & \frac{\sqrt{2}}{4}(S_1 - S_2 + S_3 - S_4) \end{bmatrix} \begin{bmatrix} T_{yc} \\ T_{zc} \\ T_{xc} \end{bmatrix}$$

When $\alpha = \alpha_0$, the above matrix equals the identity matrix. As disturbance torque integrals on the vehicle accumulate, α wanders away from α_0 and the above matrix becomes cross-coupled.

The amount that α is allowed to differ from α_0 is defined as the deviation angle $\Delta\alpha$. The maximum $\Delta\alpha$ is determined by the maximum allowable gyro gimbal rates, the permissable cross axis transients imparted to the vehicle, and the the configuration stability requirements.

To determine the gyro gimbal rates required for all possible combinations of deviation angles would be a very lengthy task employing a digital computer routine and many iterative runs. Instead, a conservative worst case type design can be obtained by considering a torque applied colinear with the gyro gimbal axis. To generate torque in this direction only the two gyros with orthogonal gimbal axes contribute torque; the other two gyros don't help but only act to eliminate cross-axis torques. With only two gyros producing the required torques the gimbal rates obtained are very high for large deviation angles. Consider simultaneous equal X and Z axis torques, T_x and T_z which require a gyro torque along the gimbal axis of gyro 1 and 3; then

$$1.4\ T_{x,z} = 2h\ \dot{\alpha}\ \sin\ (-45^\circ + \Delta\alpha) \qquad (4\text{-}5)$$

The net angular momentum transferred into the Y-axis derived from equation (4-1) is:

$$H_y = 2h\ \left[\sin\ (45^\circ + \Delta\alpha) - \sin\ (45^\circ - \Delta\alpha)\right] \qquad (4\text{-}6)$$

or

$$H_y = 2\sqrt{2}\ h\ \sin\ (\Delta\alpha) \qquad (4\text{-}7)$$

Equations (4-5) and (4-7) are normalized and shown in Figure 4-3. Beyond $\Delta\alpha = 30$ degrees the gimbal rate starts to increase rapidly, whereas, the incremental angular momentum that is being transferred into the Y-axis with increasing deviation angle is diminishing. A limit, therefore, must be established for $\Delta\alpha$ since an increasing gimbal rate puts more load on the spin and gimbal bearings and requires more torque motor power. A limit has been established at $\Delta\alpha = 40$ degrees where the gyro bearing torque is 8.11 times the output axis control torque.

This condition is a special worst case in which two gyros are incapable of supplying any torque in the required direction. Only the failed gyro case would require greater torques. Normally, all four gyros contribute to the net output torque and require significantly lower gyro bearing torques, $h\dot{\alpha}$, to produce the desired output torque.

The vehicle cross-axis transients created by gyro cross coupling at non-initial angles are a function of the overall vehicle control system bandwidth, disturbance torque characteristics, vehicle inertias, and gyro momentum.

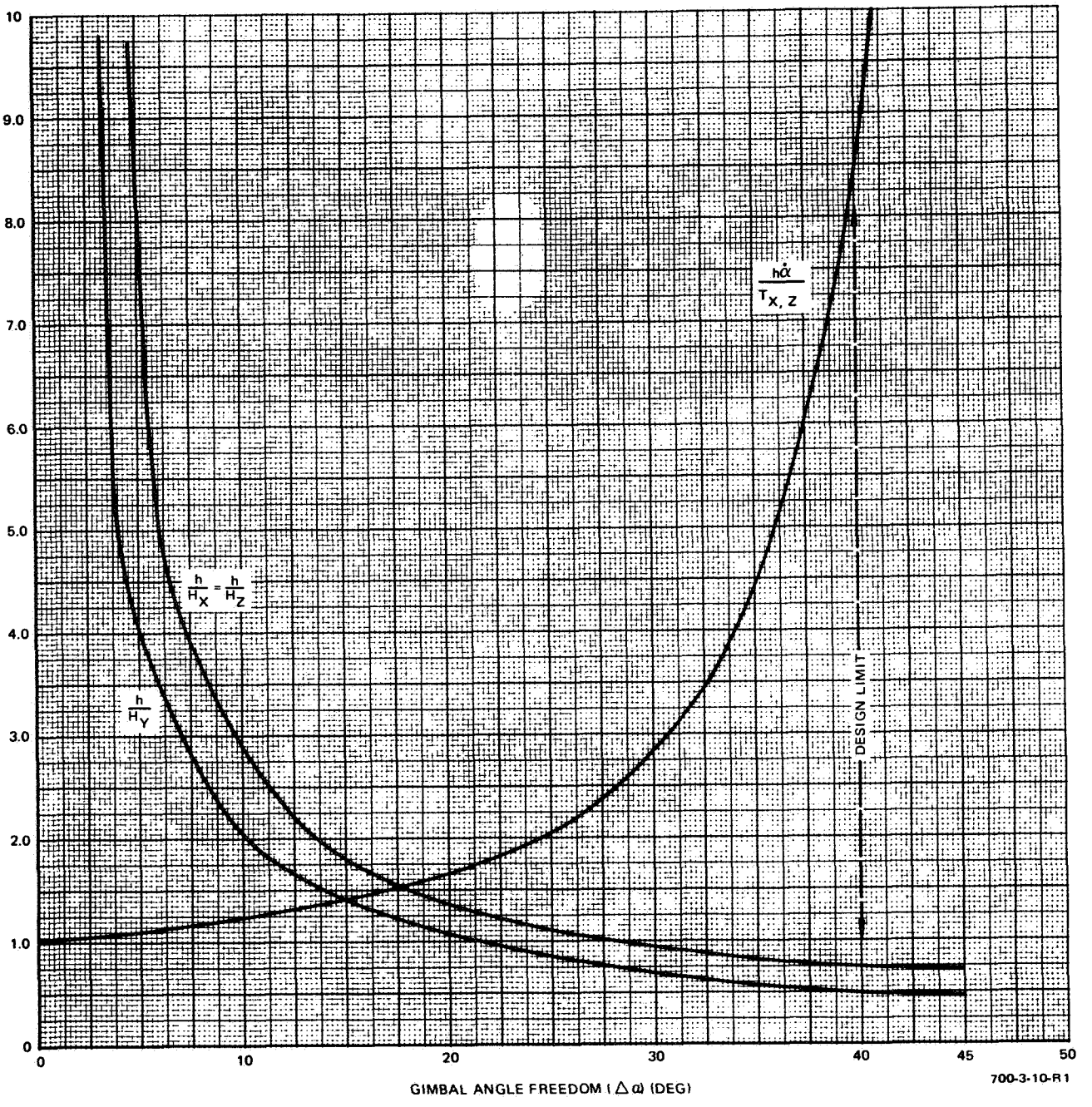

Figure 4-3
Normalized 4-FACS Parameters versus Gimbal Angle Deviation

If equation (4-4) is rewritten as a function of the deviation angle, $\Delta\alpha$, then for stored momentum in the Z axis:

$$\begin{bmatrix} T_y \\ T_z \\ T_x \end{bmatrix} = \begin{bmatrix} \cos(\Delta\alpha) & o & \sqrt{2}\sin(\Delta\alpha) \\ o & \cos(\Delta\alpha) & o \\ \frac{-\sin(\Delta\alpha)}{\sqrt{2}} & o & \cos(\Delta\alpha) \end{bmatrix} \begin{bmatrix} T_{yc} \\ T_{zc} \\ T_{xc} \end{bmatrix} \qquad (4\text{-}8)$$

and in the Y axis:

$$\begin{bmatrix} T_y \\ T_z \\ T_x \end{bmatrix} = \begin{bmatrix} \cos(\Delta\alpha) & o & o \\ o & \cos(\Delta\alpha) & -\sin(\Delta\alpha) \\ o & -\sin(\Delta\alpha) & \cos(\Delta\alpha) \end{bmatrix} \begin{bmatrix} T_{yc} \\ T_{zc} \\ T_{xc} \end{bmatrix} \qquad (4\text{-}9)$$

and finally for the X axis

$$\begin{bmatrix} T_y \\ T_x \\ T_x \end{bmatrix} \begin{bmatrix} \cos(\Delta\alpha) & \sqrt{2}\sin(\Delta\alpha) & o \\ \frac{-\sin(\Delta\alpha)}{\sqrt{2}} & \cos(\Delta\alpha) & o \\ o & o & \cos(\Delta\alpha) \end{bmatrix} \begin{bmatrix} T_{yc} \\ T_{zc} \\ T_{xc} \end{bmatrix} \qquad (4\text{-}10)$$

These equations, which indicate the effect of momentum storage on cross-axis torque coupling, can be used as an indication of the relative transient cross-coupling that can occur before the outer attitude loop takes effect and adjusts the torque commands to eliminate cross-coupling. In each case only two axis are coupled; the one with stored momentum remains uncoupled. For instance, in equation (4-9) with momentum stored in the Y-axis, X and Z are coupled; and at $\Delta\alpha = 45°$ an X-axis torque command, T_{xc}, produces an equal X and Z axis gyro output torque. The vehicle Z-axis control system must now force this torque to zero.

D. PSEUDO-TORQUE FEEDBACK STEERING LAW

The pseudo-torque feedback steering law effectively eliminates the cross coupling present with the constant gain law at the expense of added circuit complexity. The steering law mechanization, the gyro, and the vehicle transformations are shown in Figure 4-4. A linearized electronic analog of the CMG rate to torque transformation is created by applying the commanded rates to a gyro transfer matrix, $[\hat{B}]$, which represents the gimbal rate loops and the gyro configuration. This matrix transformation, equation (4-2), is a function of the sine and cosine of the gyro gimbal angles; therefore, the steering law generates the sine and cosine of each gimbal angle and applies it to the transfer matrix. The matrix outputs are the electrically derived or pseudo-torques representing those torques applied to the vehicle. They are fed back to be compared with the commanded torques. If an error exists, an integrator corrects the input to the constant gain steering law so that a set of gimbal rates are obtained which create the desired torque combination.

This pseudo-torque feedback signal acts to correct the input to the constant gain steering law, instead of requiring the outer vehicle loop to make the necessary response. The torque feedback loop response is adjusted to be much faster than the vehicle loop and gimbal loop response. The torque feedback loop, therefore, serves as a high bandwidth computer which rapidly solves for a correct set of four gimbal angle rates in response to three axis torque commands. The CMG gimbal rate loops are therefore presented with the correct commands to generate output torques without cross coupling.

The electronic analog matrix $[\hat{B}]$ is linearized, except for trigonometric functions; and therefore, does not represent the gyro loop nonlinearities. These differences between the analog model and the actual hardware result in small cross-coupling torques which are removed by the outer vehicle loop.

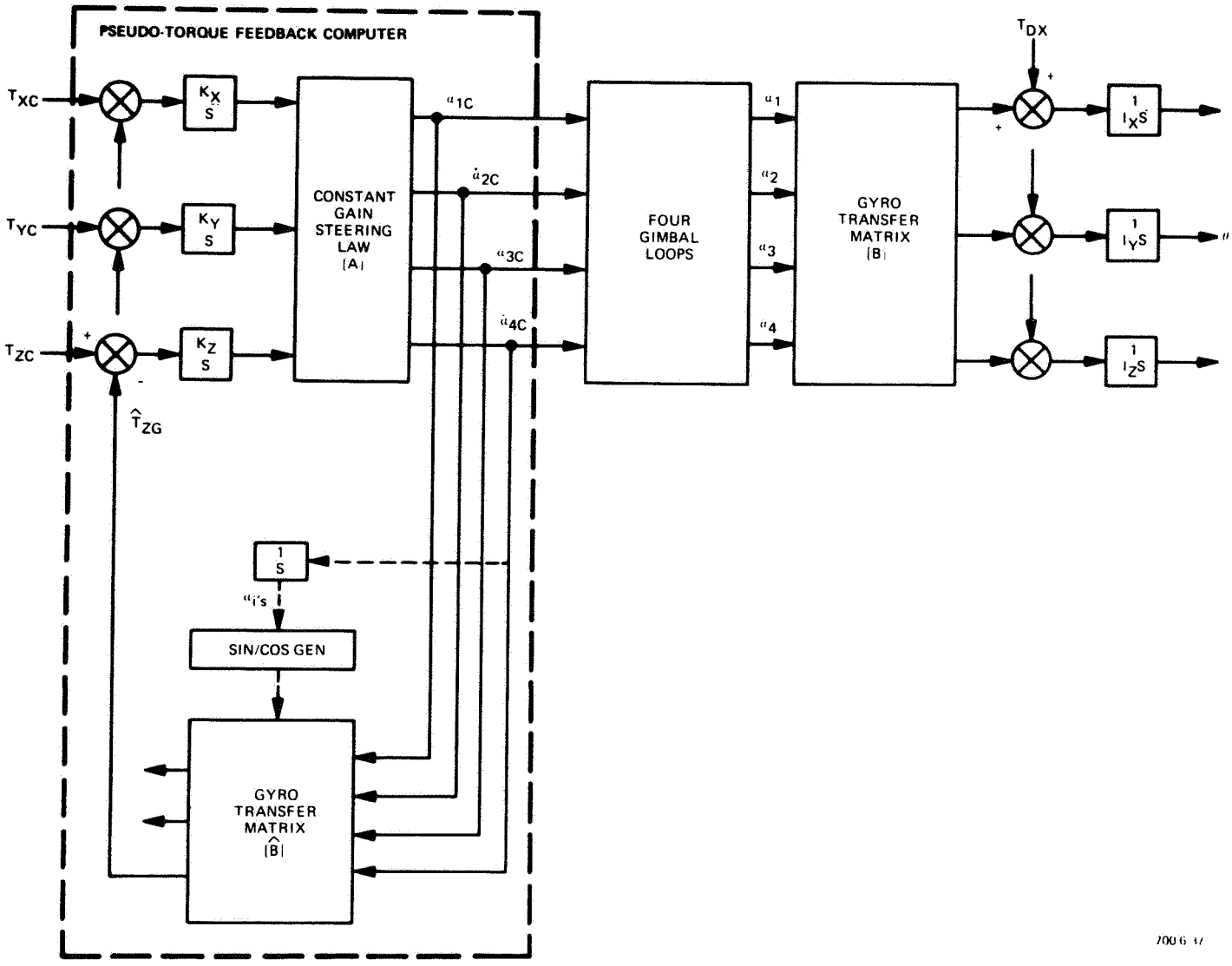

Figure 4-4
Pseudo-Torque Feedback Steering Law

Since the design mission system with manned disturbances required a gimbal loop bandwidth approximately equal to the outer loop bandwidth, the pseudo-torque was derived as a function of commanded gimbal rates to attain a rapid response loop. In applications where the gyro gimbal rate loop bandwidth is significantly higher than the vehicle loop bandwidth, the actual gimbal rates could be used to derive the pseudo-torques and hence include any nonlinearities inherent in the CMG hardware.

Another alternate mechanization is to mount a resolver on each CMG gimbal and derive the $\dot{\alpha}_{ic} \sin \alpha_i$ and $\dot{\alpha}_{ic} \cos \alpha_i$ signals directly from the gyro. This technique would eliminate the need for electronically computing the trigonometric functions and employ the actual gyro angles.

The technique employed in this study is to derive the pseudo-torques from the gimbal rate commands and process these rates through gimbal-mounted resolvers.

E. ONE GYRO FAILED OPERATION

A unique feature of the 4-FACS CMG configuration which enhances the reliability is its ability to operate in a backup mode with one gyro failed and still maintain vehicle control. To do this, the initial angles, α_0, of the three remaining gyros must be re-oriented and the steering law must be slightly altered.

With one gyro failed, the remaining gyro of the corresponding scissored pair is steered similarly to the previous net H of that pair. For example, if gyro 1 has failed, gyro 3 is changed to $\alpha_3 = +90$ degrees and is steered as H_a was, except that its magnitude is constant at $H_a = h$. The initial angles for α_2 and α_4 are changed to -30 degrees so that $H_b = h$ and cancels H_a. Only H_b can now be changed to produce H in the y direction, but otherwise, the gimbal steering is the same as described in Subsection IV.C.

With one of the gyros failed, only one solution to equation (4-2) exists. The initial gimbal angles for the failed mode where gyro number i has failed is $\alpha_0 = \{+30°, -30°, +30°, -30°\}$, except that gyro number $i \pm 2$ is changed to $-(-1)^i\ 90°$, and gyro number i is, of course, ignored. For example, if gyro number 3 has failed, $\alpha_0 = (90°, -30°, -, -30°)$. The solution to equation (4-2) for $\alpha = \alpha_0$ and with $\alpha_i = 0$ (where gyro number i has failed) is given by:

$$\begin{bmatrix} \dot{\alpha}_{1c} \\ \dot{\alpha}_{2c} \\ \dot{\alpha}_{3c} \\ \dot{\alpha}_{4c} \end{bmatrix} = -\frac{1}{h} \begin{bmatrix} \frac{1}{\sqrt{3}} & \frac{1}{\sqrt{2}} & -\frac{1}{\sqrt{2}} \\ \frac{1}{\sqrt{3}} & -\frac{1}{\sqrt{2}} & -\frac{1}{\sqrt{2}} \\ \frac{1}{\sqrt{3}} & -\frac{1}{\sqrt{2}} & \frac{1}{\sqrt{2}} \\ \frac{1}{\sqrt{3}} & \frac{1}{\sqrt{2}} & \frac{1}{\sqrt{2}} \end{bmatrix} \begin{bmatrix} T_{yc} \\ T_{zc} \\ T_{xc} \end{bmatrix} \qquad (4\text{-}11)$$

except that the first term in row $i \pm 2$ is changed to zero and $\dot{\alpha}_{ic} = 0$.

The constant gain steering law for all cases may be implemented as shown in Figure 4-5. With no failures, all switches are closed, $K_y = \sqrt{2}/4$, and $K_x = K_z = 1/2$. With gyro number i failed, switches S_i and S_i' are opened, $K_x = 1/\sqrt{3}$, and $K_y = K_z = 1/\sqrt{2}$. In changing from the no-failure mode to a one-failure mode, the gimbal angles must also be changed to the modified initial conditions, and the failed gyro should be despun. The steering law modification due to a failure may be simplified by not changing the gains, K_x, K_y and K_z.

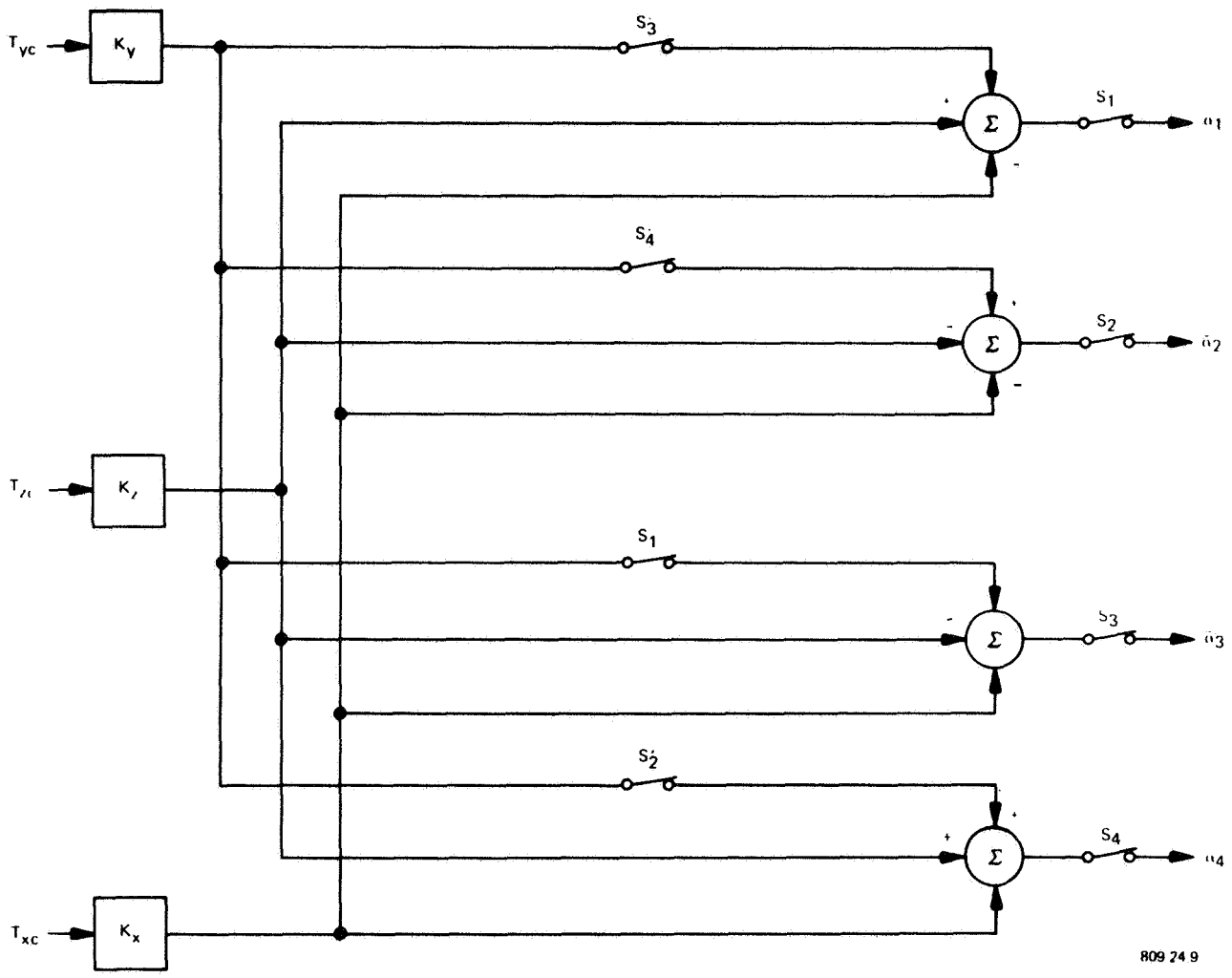

Figure 4-5
Constant Gain Steering Law

The loss in the attitude control-loop gain will then be reduced by 39 percent in the y axis and 29 percent in the x and z axes. This loss in gain will lower the system bandwidth and increase the static error, although, it may be acceptable for some system requirements.

A preliminary analog circuit mechanization is shown in Figure 4-6 and indicates the simplicity of the complete 4-FACS constant gain steering law computer.

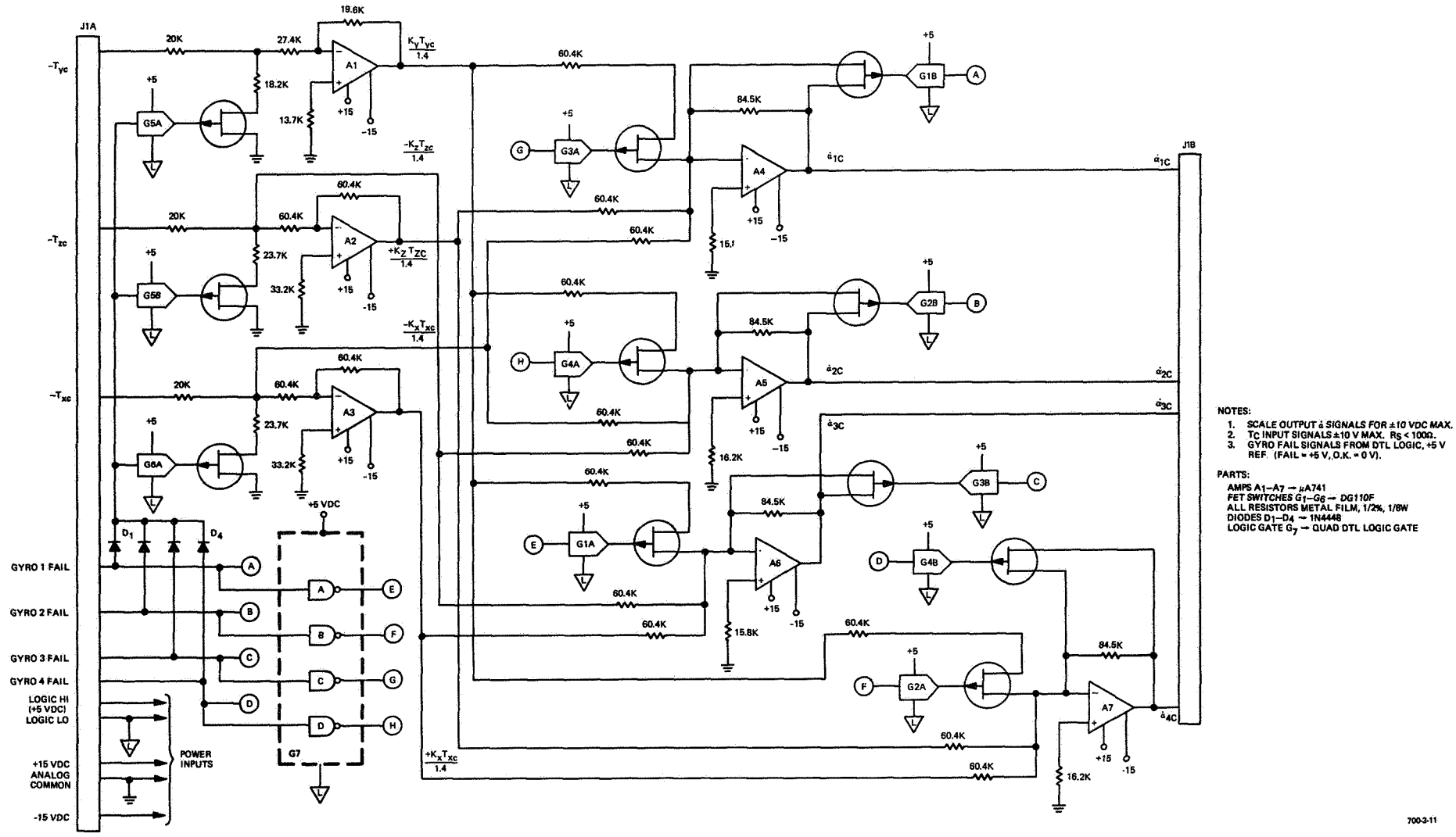

Figure 4-6
4-FACS Steering Law Computer,
Preliminary Schematic

F. 4-FACS MOMENTUM ENVELOPE

The 4-FACS momentum envelope shown in Figure 4-7 represents the upper half of the three-dimensional surface of maximum momentum which this configuration can absorb with the gimbal deviation angle, $\Delta\alpha$, limited to ±40 degrees and a constant gain steering law employed. The figure indicates that maximum storage capability occurs along each individual axis; $|H_y| = 1.82h$ and $|H_z| = |H_x| = 1.35h$ and for combined axis storage the capability per axis decreases. For instance, with $H_y = 0$ (at the base of Figure 4-7) the momentum that can be stored in either the x- or z-axis individually is $|H_x| = |H_z| = 1.35h$; however, if equal momentum is stored in each axis the allowable single-axis momentum is limited to $|H_x| = |H_z| = 0.64h$ with the net angular momentum vector reduced to 0.90h. This envelope is especially well suited to missions which have moderate cyclic torques about two axes (x and z) and a secular torque about the third axis. The net momentum vector then remains close to and spirals up the y-axis.

The momentum envelope was generated by using a digital program to solve for the gimbal angle time histories as a function of disturbance torque inputs (Figure 4-8). A closed loop was formed which included the constant gain steering law, an identity gimbal loop matrix, a gyro transfer matrix, and an integrator block; an angle detector monitored all four gimbal angles and stopped the program whenever any angle moved more than 40 degrees from its initial angle, α_0. Various planes of stored y-axis momentum were derived by: initializing the gimbal angles at α_0; injecting a y-axis step torque for the time needed to establish the desired stored H_y; and then injecting combinations of x- and z-axis torques to establish the momentum limits on the selected H_y plane. This process was repeated at 15-degree intervals about the y-axis for each of the eight H_y planes investigated. From this data the solid model shown in Figure 4-7 was constructed. The envelope contours at each of the eight planes is shown in Figure 4-9.

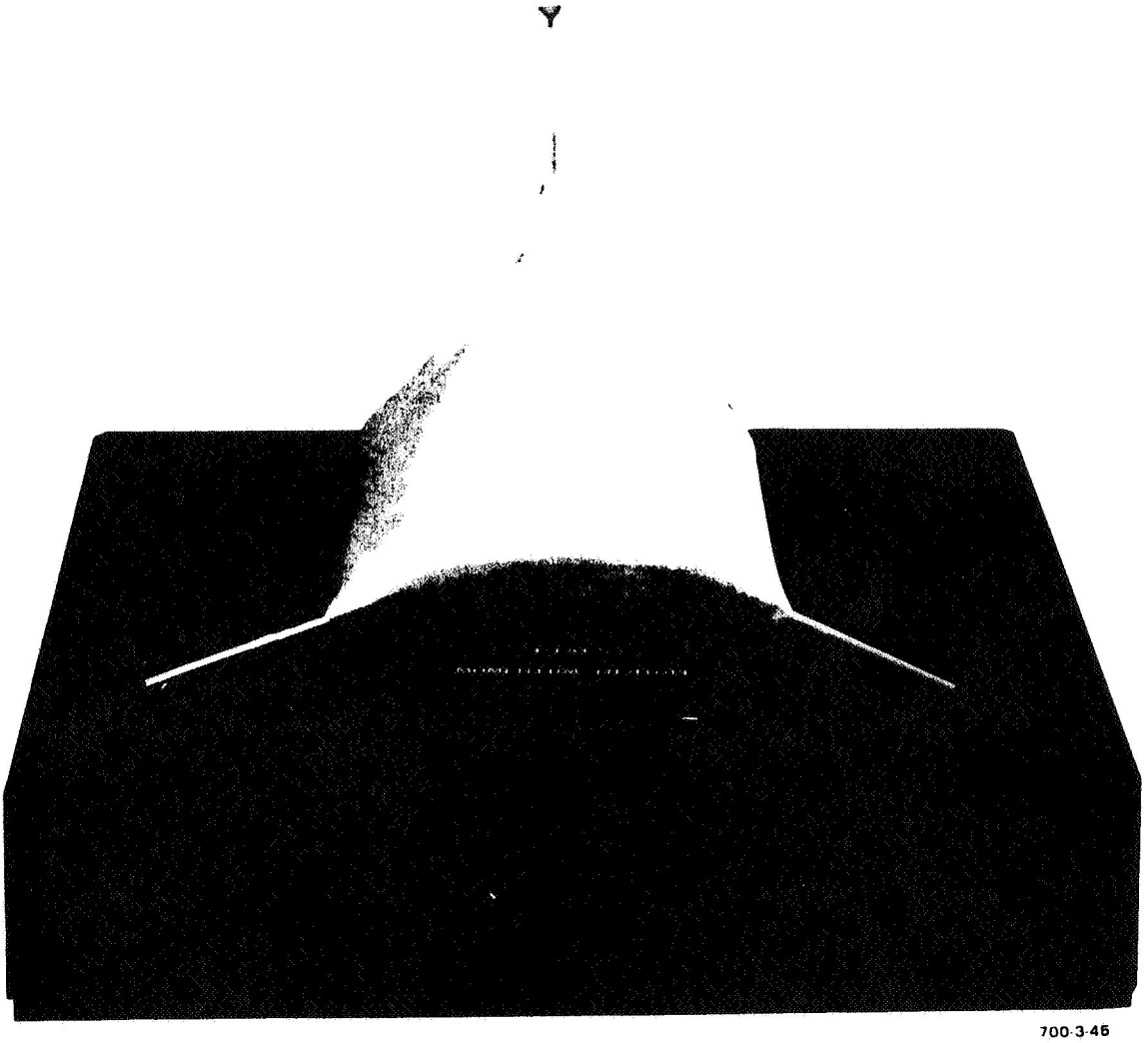

Figure 4-7
4-FACS Momentum Envelope with Four
Gyros Operating, Upper Half Only

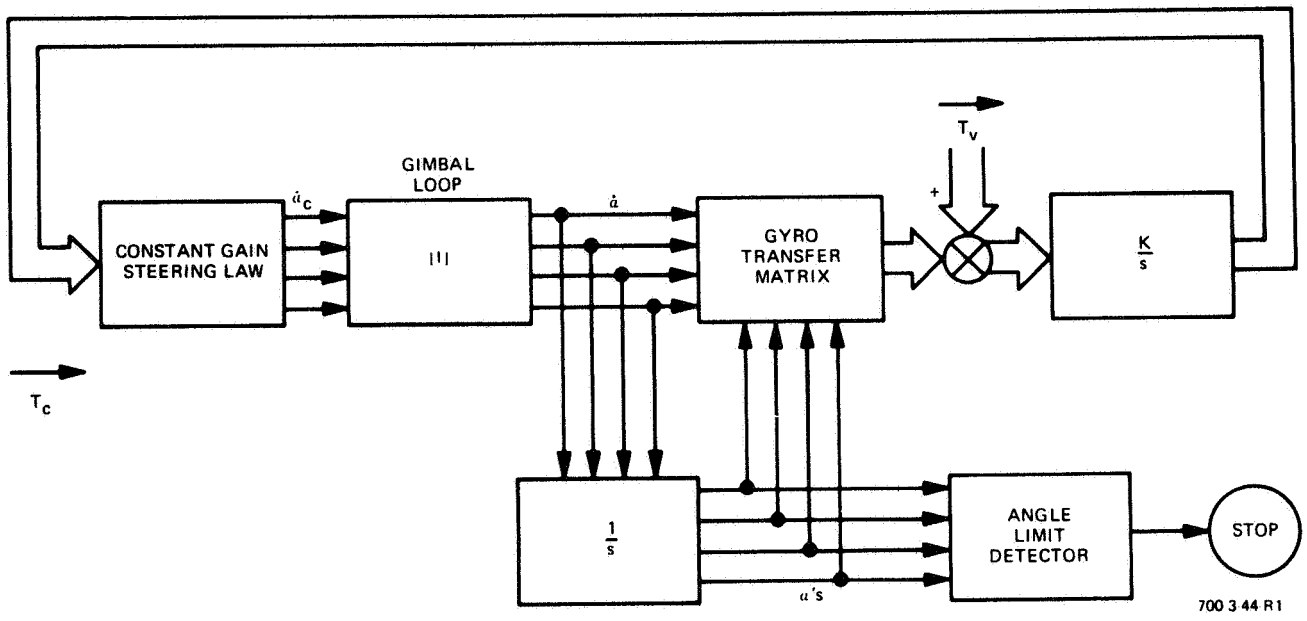

Figure 4-8
Momentum Envelope Generator

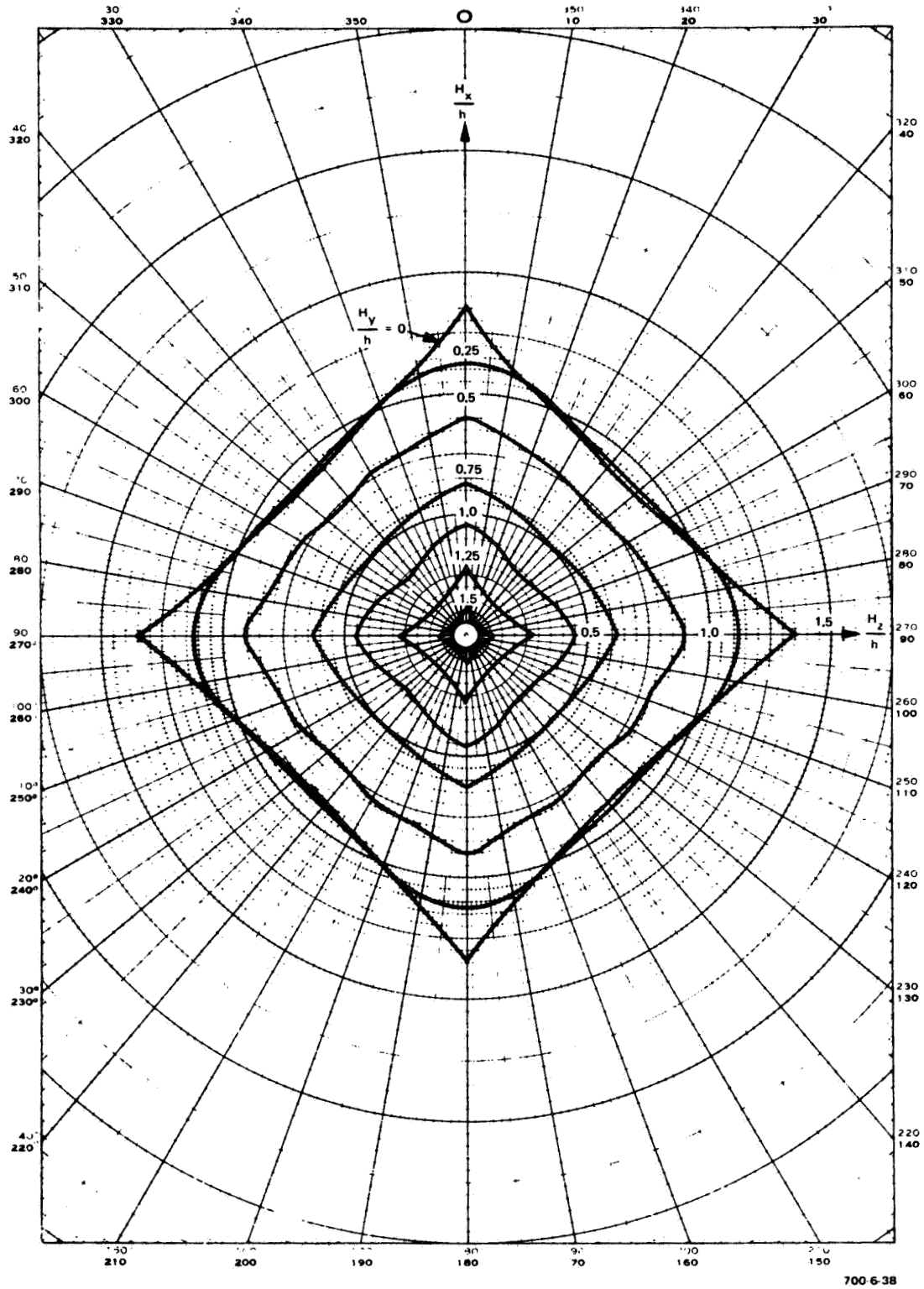

Figure 4-9
4-FACS Momentum Envelope Contours
with Four Gyros Operating

The momentum envelope with one gyro failed is shown in Figure 4-10. This envelope represents the complete three-dimensional surface of maximum momentum that this configuration can absorb with the gimbal deviation angle, $\Delta\alpha$, limited to ±85 degrees for the CMG with a colinear gimbal axis with the failed gyro, and +25 and -55 degrees for the two orthogonal CMG's. The unequal deviation angles are necessary to obtain a sufficiently large envelope for momentum stored in the negative y-axis direction and yet maintain stability when storing momentum in the positive y-axis direction.

Although the envelope has lower lobes which extend beyond the $H_y = -h$ plane, this area cannot be used since a forbidden region exists along the y-axis. Unlike the four gyro envelope, symmetry does not exist along the y-axis and more area is available in the x-z plane along the negative y-axis. If gyro 2 or 4 fails, however, the envelope is reversed and the positive axis has the most area available. Biasing the desaturated initial condition point away from $H_y = H_x = H_z = 0$ to take advantage of the envelope shape, therefore, could be accomplished if the torque history is known a priori, or if an average momentum circuit is employed to update the desaturated point. As in the four gyro case, the envelope is best suited to secular torque in one direction and cyclic torques along the orthogonal axis.

The positive y-axis can store $H_y = +0.83h$ and negative y-axis, $H_y = -0.99h$. The negative lobes extend to $H_y = -1.92h$ and the maximum $H_x = H_z = 1.21h$ along the $H_y = -0.75h$ plane. The envelope at each of nine planes is shown in Figure 4-11.

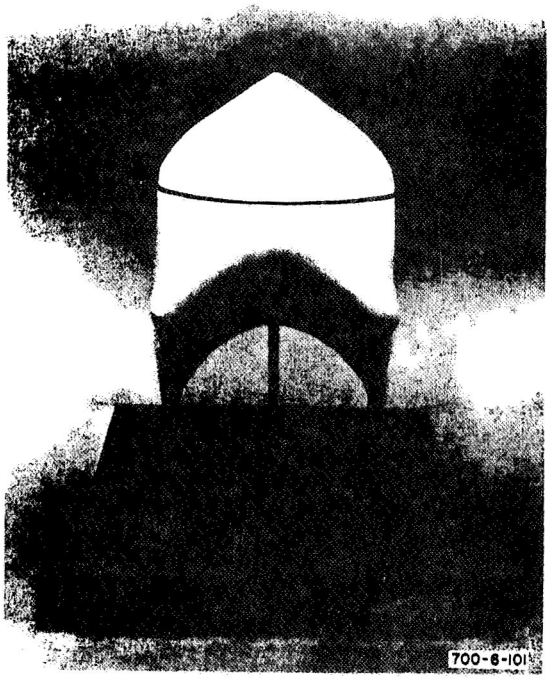

Figure 4-10
4-FACS Momentum Envelope with One Gyro Failed

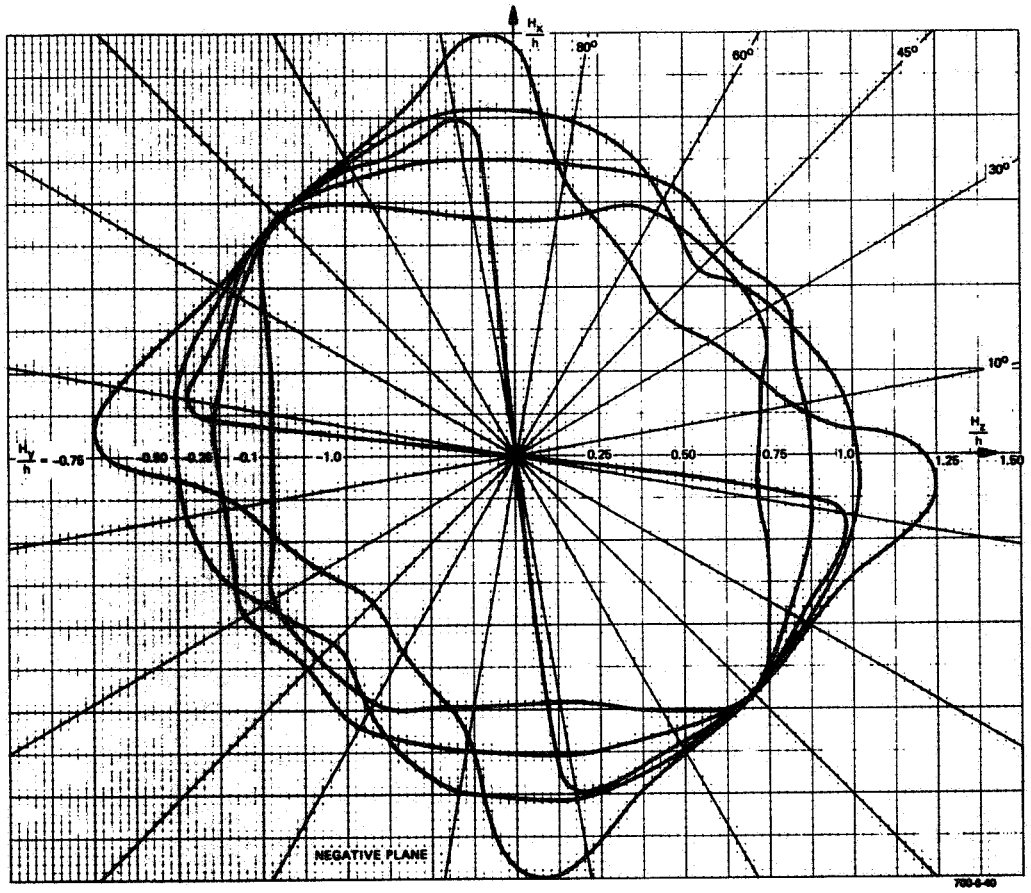

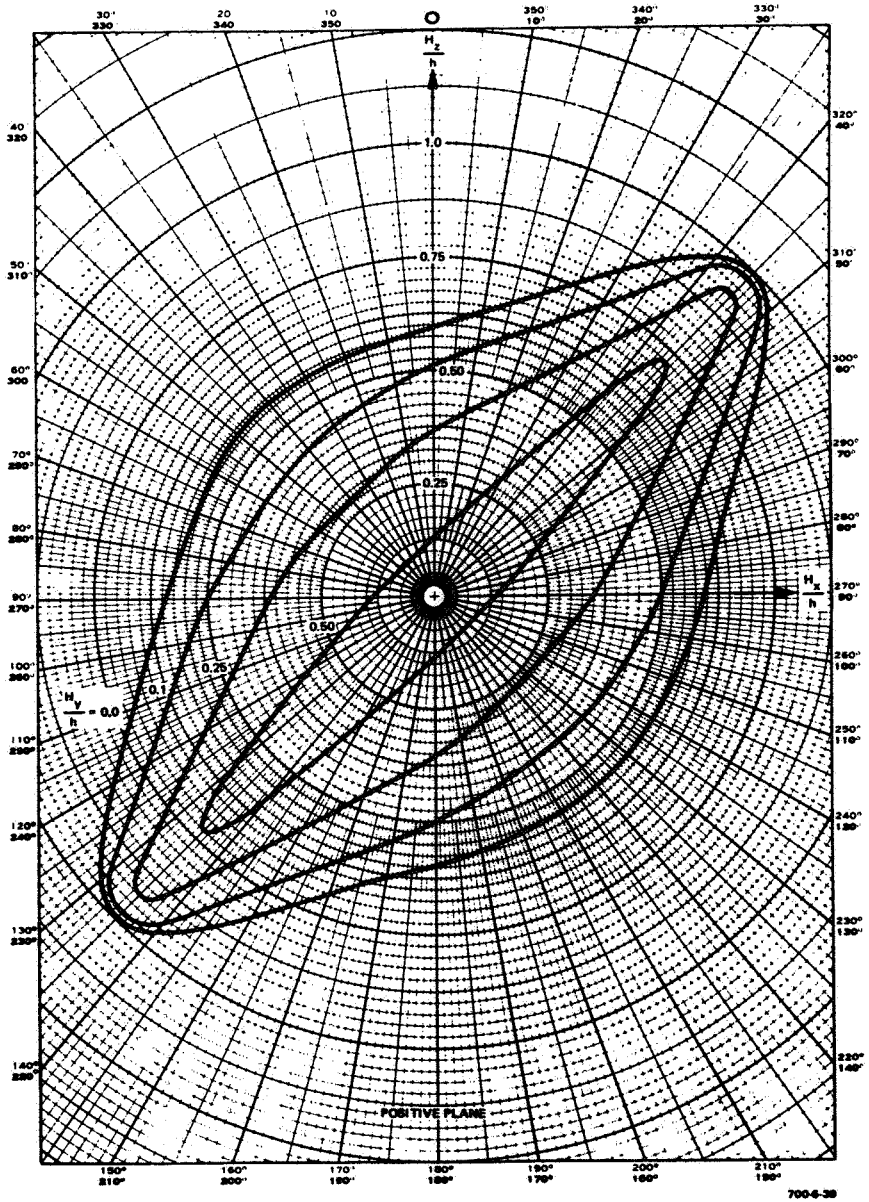

Figure 4-11
4-FACS Momentum Envelope Contours
with One Gyro Failed

G. STABILITY ENVELOPES

Stability envelope contours for the 4-FACS CMG configuration are depicted in Figures 4-12 and 4-13. These curves are similar to the momentum envelopes of Section IV.F, except they represent the maximum momentum which can be stored while maintaining system stability. No gimbal angular limits were established a priori; instead the momentum generation digital program, Figure 4-8, was used to determine the gimbal angle combination $\{\alpha_1, \cdots \alpha_4\}$ for a particular momentum (H_y, H_z, H_x). This set of angles was then inputted to a system stability matrix program which solved for the linear roots of the overall three-axis system. The resulting roots were then examined for unstable positive real axis plane roots. If none existed, then the momentum was incremented by ΔH along the same path, and a new set of gimbal angles were determined. These were again employed in the stability program to derive a new set of closed-loop system roots. This process was repeated until an unstable root was found and hence the maximum stability boundary of momentum determined. Along each H_y level, a contour of momentum was established and is plotted in Figure 4-12 for all four gyros operative, and in Figure 4-13 for the one gyro failed case. These figures can be compared directly with Figures 4-9 and 4-11, respectively which represent the momentum envelopes for the gimbal angle restrictions employed. It will be noted that in all cases a margin exists between the stability momentum limit and the momentum envelope employed, therefore, proving global stability over all selected conditions.

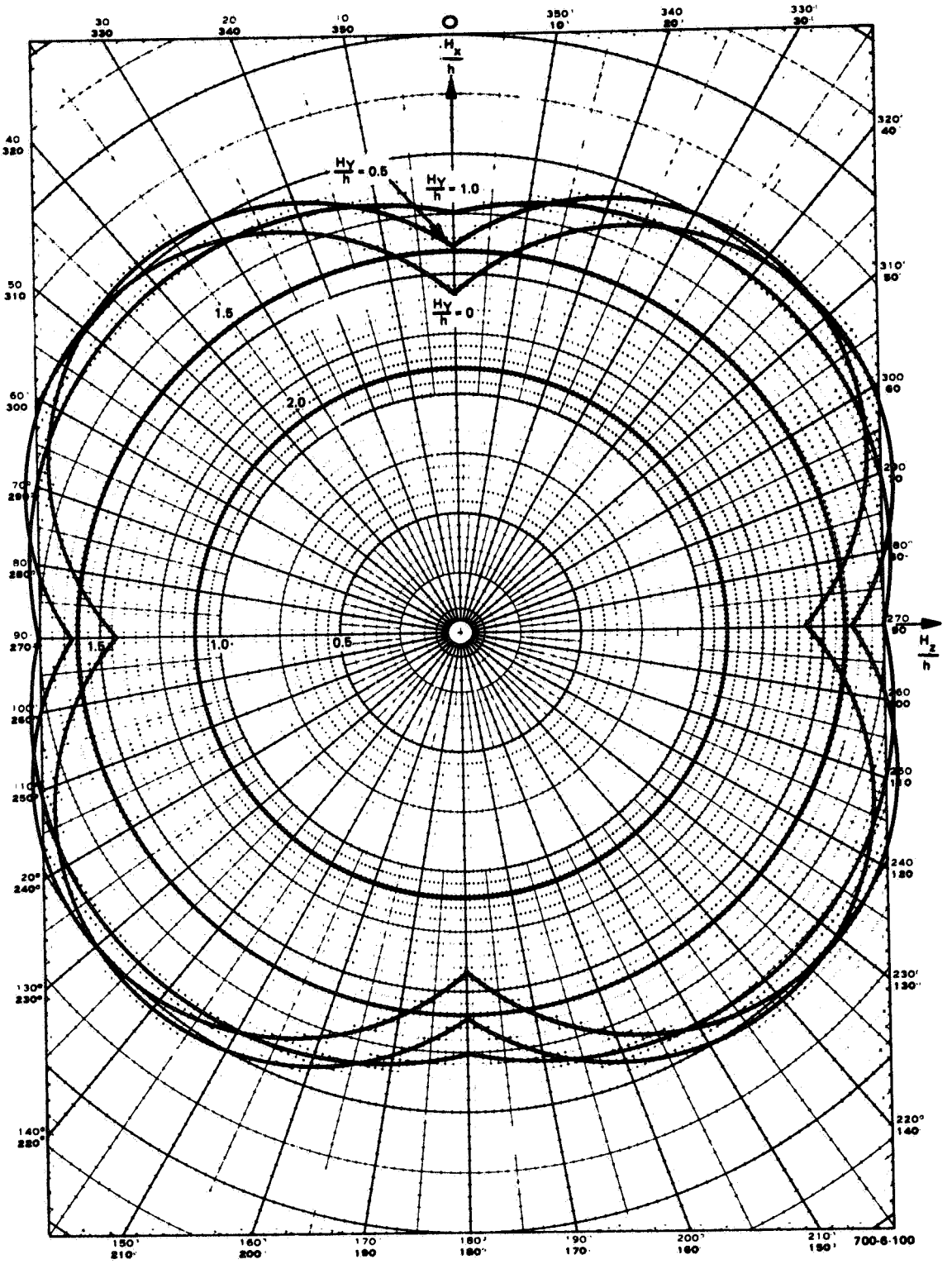

Figure 4-12
4-FACS Stability Envelope, Four Gyros Operative, Constant Gain Steering Law

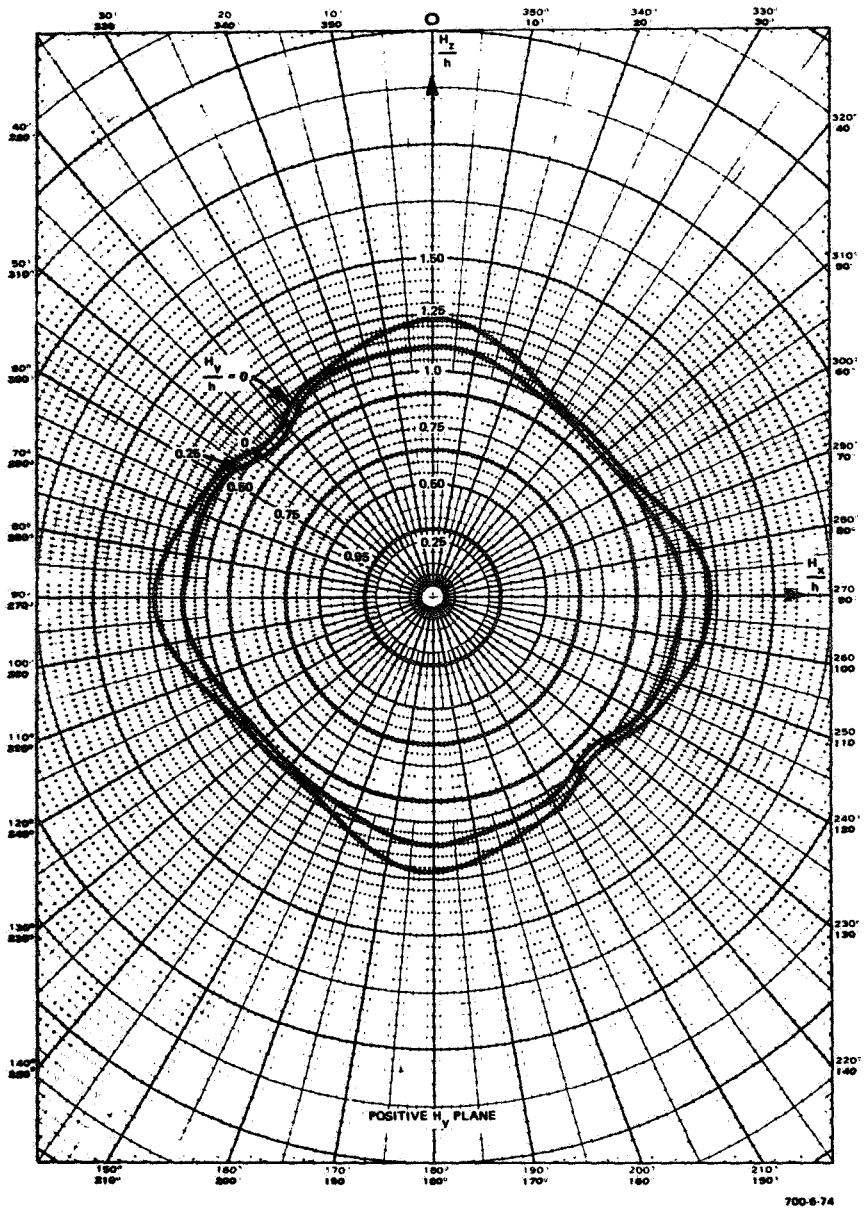

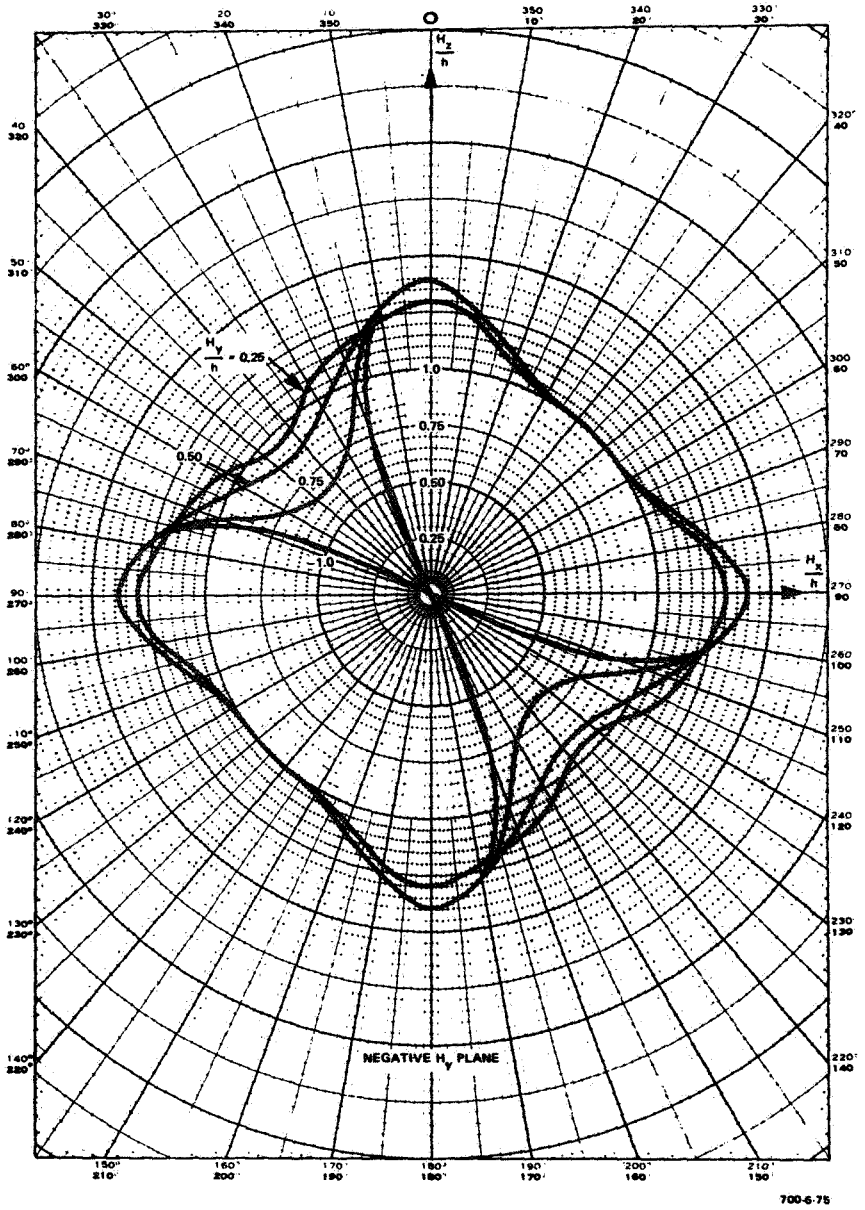

Figure 4-13
4-FACS Stability Envelope, Gyro No. 1
Failed, Constant Gain Steering Law

SECTION V

ATTITUDE CONTROL SYSTEM COMPARISON

SECTION V

ATTITUDE CONTROL SYSTEM COMPARISON

Four competitive fine attitude control systems are compared in this section in order to establish the relative merits and shortcomings of each and to chose a preferred system for the design mission. A system consisting of three reaction wheels; a six-gyro, scissored pair CMG system; a 4-FACS CMG configuration; and a reaction jet control system are compared for system weight, electrical power consumption, and reliability. The systems selected for comparison do not represent all possible candidate systems. Instead, they represent each of the most popular current fine attitude control techniques. Other gyro and reaction wheel configurations as well as hybrid combinations could be equally competitive for particular mission requirements. A comprehensive comparison of all conceivable systems, however, was beyond the scope of this study. The techniques used in this study for comparison of each system can be applied in analogous fashion to any other candidate systems.

As stated previously, two types of missions are considered within this study — manned and unmanned. The systems compared in this section, therefore, are for both types of missions. Primary differences are the control torque level and system bandwidth requirements. The momentum requirements dictated by the orbital disturbances and frequency of desaturation remain approximately the same for both missions.

To ensure that all systems were compared on an impartial basis with no special requirements to give one system a peculiar advantage, the following set of generalized requirements were used as system specifications:

- Only one size actuator (CMG, reaction wheel, jet thruster) is to be used to maintain commonality and cost effectiveness.
- Each axis must have a minimum momentum storage capability of 200 ft-lb-sec.
- Each axis must have a control torque capability of at least 25 ft-lb for manned and at least 2 ft-lb for unmanned missions.
- Each axis must have a bandwidth greater than 3 Hz for manned and 1 Hz for unmanned missions.
- Maximum available electrical power is 1000 watts at 28 volts dc nominal voltage.
- Desaturation allowed only once per orbit while in the earth's shadow.

A. REACTION WHEEL SYSTEM

A reaction wheel fine attitude control system consisting of 3 reaction wheels aligned with their spin axis along each of the principal vehicle axes is shown in Figure 5-1. When a disturbance torque is applied about the Y-axis, the angular momentum and speed of gyro 1 is changed in order to absorb the momentum. Thus,

$$\vec{H}_1 = I_1 \vec{\omega}_1 = -\int \vec{T}_{dy}\, dt \qquad (5\text{-}1)$$

where:

H_1 = Angular momentum of reaction wheel No. 1

I_1 = Polar moment of inertia of reaction wheel No. 1

ω_1 = Angular velocity of reaction wheel No. 1

T_{dy} = Disturbance torque about Y - vehicle axis

The vehicle remains stationary as the reaction wheel absorbs the total momentum imparted by the disturbance.

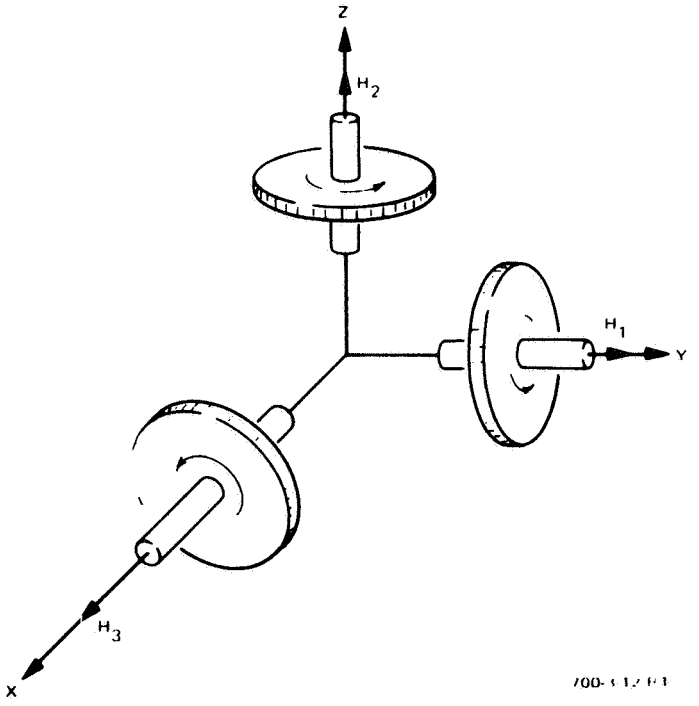

Figure 5-1
Reaction Wheel Configuration

$$\vec{H}_v = \vec{H}_d - \vec{H}_l = 0 \tag{5-2}$$

where

H_v = Vehicle angular momentum

H_d = Angular momentum imparted by disturbance torque

However, the reaction wheel must increase its speed as it absorbs momentum and will finally attain a maximum allowable speed, ω_{max}. At this speed, the reaction wheel is defined as saturated and reaction jets or other torque devices must be used to desaturate the wheel and decrease its speed. If only cyclic disturbance torques are present, the reaction wheel can be sized to absorb the peak momentum and never reach saturation; therefore, no reaction jet fuel will be expended while maintaining fine attitude hold.

The amount of momentum that the reaction wheel is required to absorb can be reduced by desaturating more frequently, and thus not allowing the secular torque to transfer a large amount of momentum to the reaction wheel. Often, however, the required attitude accuracies cannot be achieved during desaturation and, therefore, a tradeoff exists among the following: uninterrupted experiment duration; attitude hold to desaturation time ratio; and reaction wheel size and power requirements. This technique could also be employed to decrease the size of a CMG system in an analogous manner. For this comparison study only one desaturation per orbit was considered which allows a sixty-minute uninterrupted experiment duration.

Since the reaction wheel produces a torque equal to the disturbance torque at all wheel speeds, a large amount of power is consumed when the reaction wheel is near saturation. This power is of primary importance when considering a reaction wheel design.

To determine the "best" reaction wheel design for a given mission, an evaluation criteria or "cost function" is established which expresses the system weight and power consumption as a total equivalent weight, W_T:

$$W_T = W_R + W_H + W_M + W_P + W_E \tag{5-3}$$

where:

W_R = Rotor weight (lb)

W_H = Housing weight (lb)

W_M = Spin motor weight (lb)

W_P = Equivalent weight due to electrical power (lb)

W_E = Electronic control package weight (lb)

The rotor weight is a function of the reaction wheel speed, S, expressed in revolutions per minute, the maximum momentum, H (ft-lb-sec) which is stored, and the rotor radius, R, in inches

$$W_R = \frac{46{,}000\ H}{R^2\ S} + 0.2\ R^{1.4} \tag{5-4}$$

The housing weight, which contains the rotor and provides a near vacuum environment, is exponentially related to rotor size:

$$W_H = 0.027\ R^{2.75} \tag{5-5}$$

The spin motor weight is expressed as a function of maximum torque required and in the torque range of interest is

$$W_M = 1.5\ T_{max} \tag{5-6}$$

where

T_{max} = Maximum control torque (ft-lb)

The equivalent electrical power weight, W_p, is related to the type of power system on-board the space vehicle and the equivalent weight required to produce the electrical power and energy. For this study a fuel cell energy system is considered. The power penalties are 35 pounds per kilowatt which accounts for the fuel cell and power distribution system weight, and 0.8 pound per kilowatt-hour which represents the H_2 and O_2 weight needed to produce the energy.

The instantaneous electrical power input, P_{in}, required is

$$P_{in} = \frac{\vec{T} \cdot \vec{S}}{\eta\ (9.549)} \tag{5-7}$$

where

T = Instantaneous control torque (ft-lb)

η = Conversion efficiency from electrical input to mechanical shaft power

Considering cyclic torques about three axes plus a secular torque about the third axis, the average power is obtained by integrating and averaging the instantaneous power over an orbital period.

$$P_{(avg)} = \frac{P_{(max)}}{4}\left[\frac{3}{2\pi} + \frac{1}{2}\right] = 0.245\ P_{(max)} \tag{5-8}$$

Combining equations (5-7) and (5-8), and employing the power penalties previously mentioned, the equivalent electrical power weight, W_P, is

$$W_P = \frac{T_{max}\, S(0.245)}{\eta(9.549)} \left[0.035 + 0.0192\ D\right] \tag{5-9}$$

where

D = Time in orbit (days)

If solar cells were used as the power source, the equivalent weight would be independent of the time in orbit except as affected by the solar cell efficiency decreasing with age.

The electronic control package weight, W_E, is considered to be a constant 10 pounds for all designs. Structural mounting weight is not considered in the overall weight calculation.

Combining all the individual weights results in the total equivalent weight for one reaction wheel.

$$W_T = \frac{46{,}000\ H}{R^2\ S} + 0.2\ R^{1.4} + 0.027\ R^{2.75} + 1.5\ T_{(max)}$$

$$+ \frac{T_{(max)}\ S}{\eta} \left[0.0009 + 0.0005\ D\right] + 10 \tag{5-10}$$

In a reaction wheel design, the maximum momentum, H, maximum torque, $T_{(max)}$ conversion efficiency, η, and orbit lifetime, D, are known. The desired rotor size and speed are selected to minimize the total equivalent weight, W_T. A speed constraint is added to the optimization procedure which reflects the limited available power of one kilowatt.

$$S \leq \frac{3180\ \eta}{T_{(max)}} \tag{5-11}$$

A digital computer program has been developed at Sperry which solves equation (5-10) within the speed constraint of equation (5-11) by varying rotor radius and speed to obtain a minimum total equivalent weight. The results in parametric form for a system of three reaction wheels are shown in Figure 5-2 through 5-4. Figure 5-2 is plotted for various momentum requirements at $T_{(max)}$ = 1.0 ft-lb; Figure 5-3 is similar for $T_{(max)}$ = 2.0 ft-lb, and Figure 5-4 is plotted for various control torques at one fixed momentum, H = 200 ft-lb-sec. Each point on these curves represents a different reaction wheel design (rotor size and speed) which is optimized for that particular torque, momentum, and orbit duration.

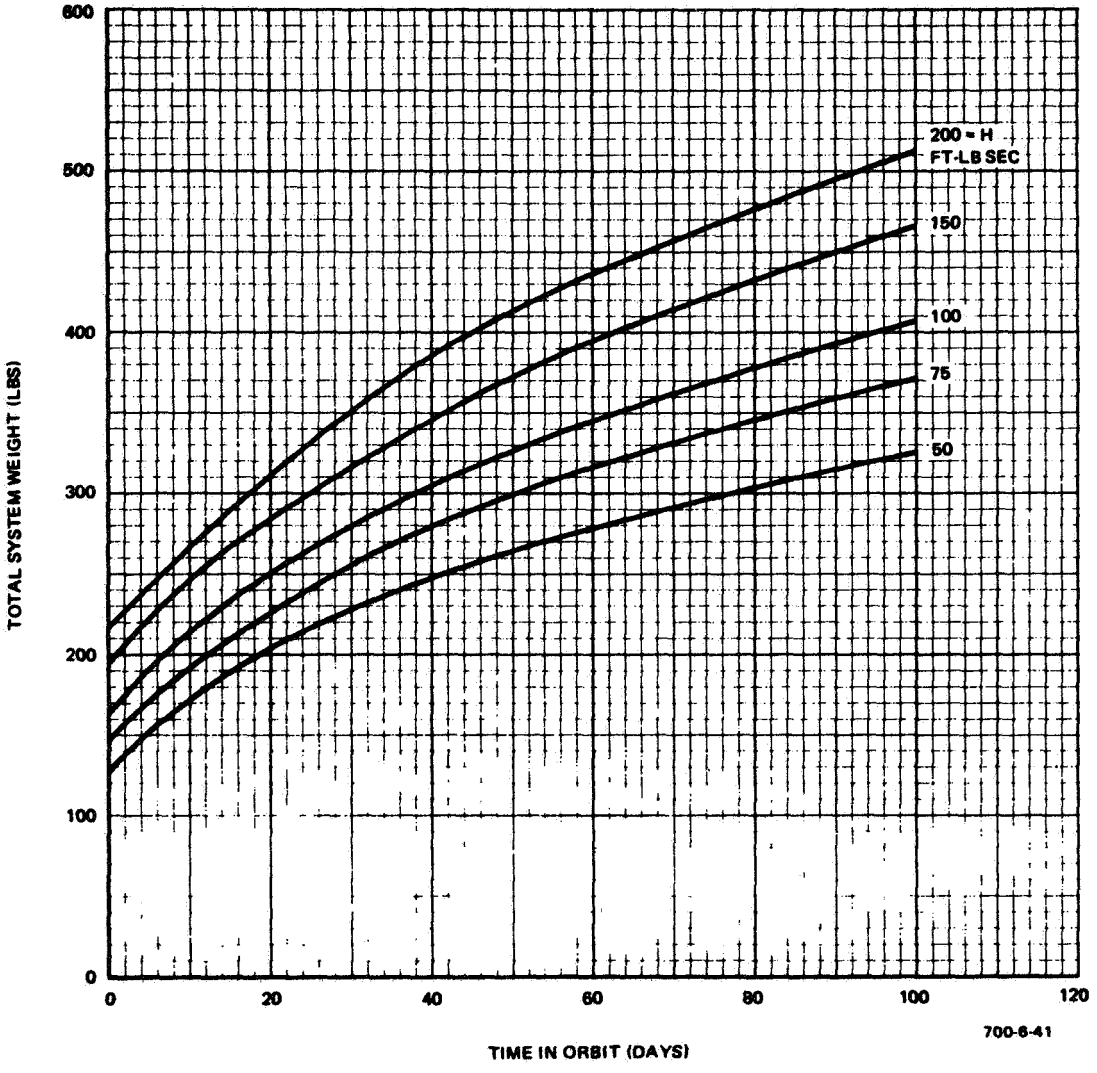

Figure 5-2
Reaction Wheel Optimum Equivalent Weights for
T_{PK} = 2.0 foot-pounds, η = 0.75

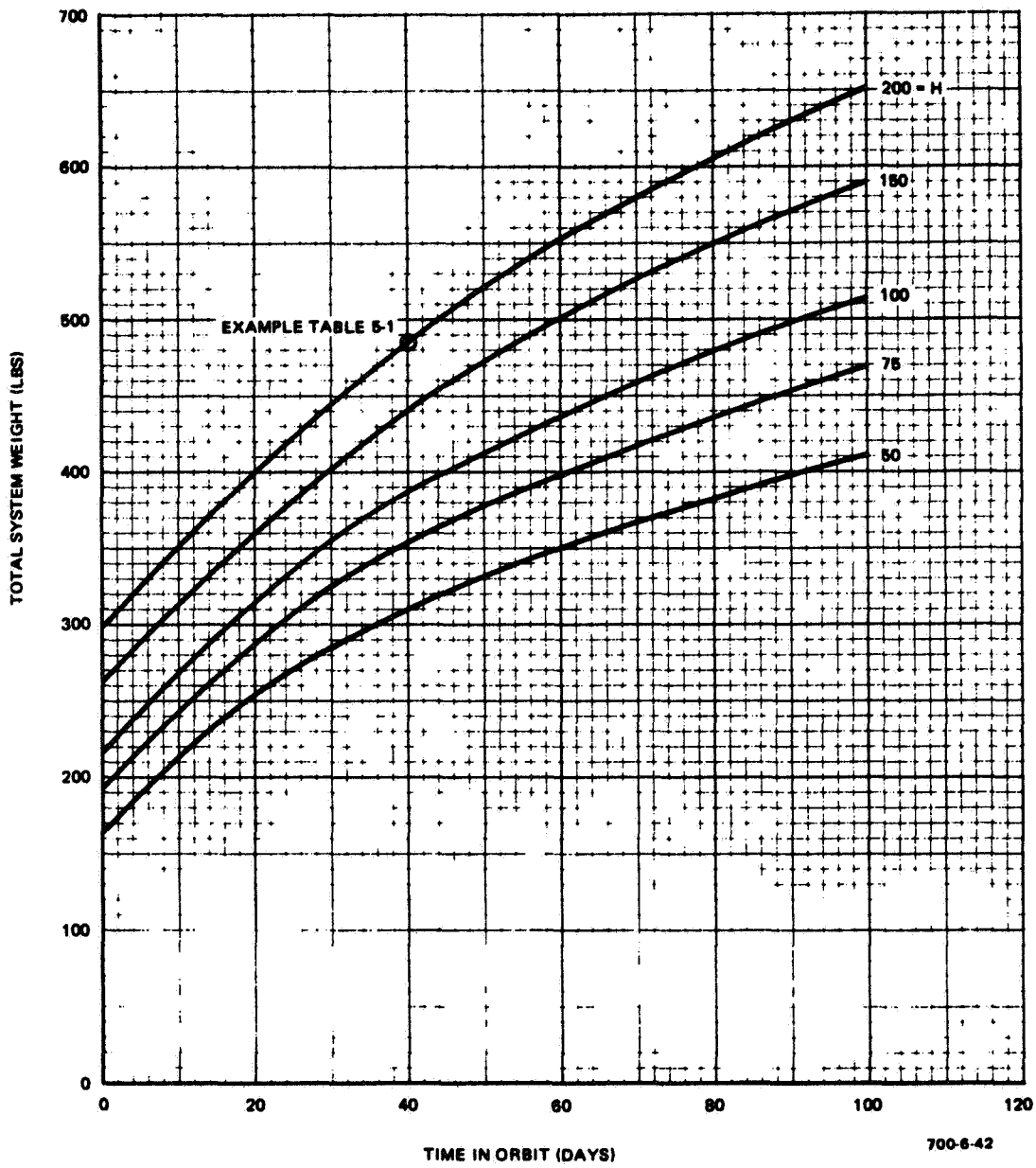

Figure 5-3
Reaction Wheel Optimum Equivalent Weights
for T_{PK} = 2.0 foot-pounds, η = 0.75

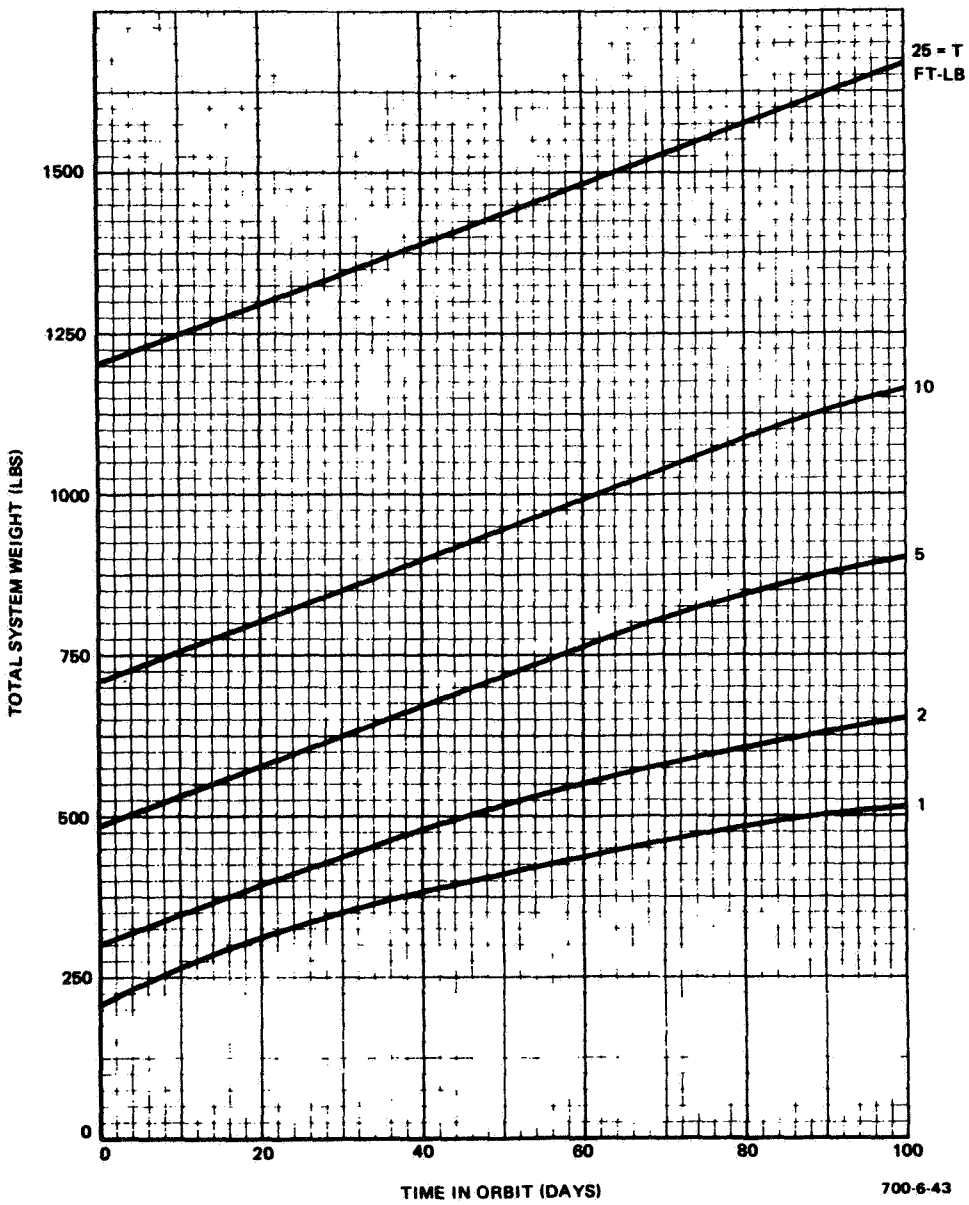

Figure 5-4
Reaction Wheel Equivalent Weights for
H = 200 foot-pound-seconds, $\eta = 0.75$

Typical computer results of the trials leading to the optimum solution for a 200 ft-lb-sec momentum, 2.0 ft-lb torque reaction wheel with an orbital operational period of 40 days are presented in Table 5-1. The program solved for the radius which gave the minimum weight at each speed selected. The weights obtained were then compared until the speed with the lowest weight was determined. In this example, the optimum design is a 13.5-inch radius rotor with a rotor, housing, and torquer-weight of 98.27 pounds, an electrical power equivalent weight of 53.11 pounds, a maximum speed of 953 rpm, and power of 266 watts per wheel. A total of 30 trial designs which the computer considered are tabulated in Table 5-1.

For a manned-type vehicle requiring $T_{(max)}$ = 25 ft-lb and momentum storage of 200 ft-lb-sec, the total equivalent weight at launch is 1206 pounds (Figure 5-4). This weight is extremely heavy compared to that of competitive systems; therefore, reaction wheels are not considered the best choice for this mission.

When considering unmanned missions with much lower torque requirements, reaction wheels become more competitive. This is considered in more detail in Subsection V.C. Again, however, because of high power requirements, lack of a backup capability, and high equivalent weight the reaction wheel system is eliminated from consideration. If a different power system were used, power were readily available, power generated heat could be transferred away easily, and if a redundant-skewed reaction wheel configuration were used in a mission with low torque duty cycle, then the reaction wheel system might be preferred.

TABLE 5-1

REACTION WHEEL OPTIMUM WEIGHT PRINTOUT

W_T (lb)	W_P (lb)	$W_R+W_H+W_M$ (lb)	Radius (in.)	Speed (rpm)	Power (watt)
1267.83	.56	1257.27	35.70	10.00	2.79
433.97	3.85	420.13	23.60	69.00	19.26
314.06	7.13	296.93	20.70	128.00	35.74
260.70	10.42	240.28	19.10	187.00	52.21
230.02	13.71	206.31	18.00	246.00	68.68
210.16	17.00	183.16	17.20	305.00	85.16
196.43	20.29	166.14	16.50	364.00	101.63
186.53	23.58	152.96	16.00	423.00	118.10
179.26	26.86	142.40	15.50	482.00	134.57
173.81	30.15	133.65	15.20	541.00	151.05
169.77	33.44	126.33	14.80	600.00	167.52
166.76	36.73	120.03	14.50	659.00	183.99
164.57	40.02	114.55	14.30	718.00	200.47
163.06	43.30	109.76	14.00	777.00	216.94
162.08	46.59	105.49	13.80	836.00	233.41
161.55	49.88	101.67	13.60	895.00	249.88
161.40	53.17	98.23	13.40	954.00	266.36
161.57	56.46	95.11	13.20	1013.00	282.83
161.53	56.18	95.35	13.30	1008.00	281.43
161.51	55.90	95.61	13.30	1003.00	280.04
161.48	55.62	95.86	13.40	998.00	278.64
161.46	55.34	96.12	13.40	993.00	277.25
161.45	55.06	96.38	13.40	988.00	275.85
161.43	54.79	96.65	13.40	983.00	274.45
161.42	54.51	96.91	13.40	978.00	273.06
161.41	54.23	97.18	13.40	973.00	271.66
161.40	53.95	97.45	13.50	968.00	270.27
161.39	53.67	97.72	13.50	963.00	268.87
161.39	53.39	98.00	13.50	938.00	267.47
161.38	**53.11**	**98.27**	**13.50**	**953.00**	**266.08**

Momentum, H = 200 ft-lb-sec

Efficiency, η = 0.75

Torque, $T_{(max)}$ = 2.0 ft-lb

Duration, D = 40 days

Optimum

B. SCISSORED PAIR CMG CONFIGURATION

The scissored-pair CMG configuration (Figure 5-5) consists of six constant-speed, single-degree-of-freedom gimballed gyros which are used in pairs to provide three momentum vectors aligned with the three vehicle axes. By slaving two gyros of each pair together either electrically or mechanically so that they are driven to equal gimbal angles, the torque produced is aligned along only one vehicle axis and no cross-coupling occurs. This freedom from cross-coupling, however, is obtained at the expense of requiring six gyros for control of only three degrees of freedom.

The angular momentum from each gyro pair is

$$H = 2h \sin \alpha \tag{5-12}$$

where

H = Single-axis angular momentum (ft-lb-sec)

h = Single-gyro angular momentum (ft-lb-sec)

α = Gimbal angle (radian)

and the output torque, T_o, the gyro imparts to the vehicle axis is

$$T_o = 2h\dot{\alpha} \cos \alpha \tag{5-13}$$

where

$\dot{\alpha}$ = Gimbal angular rate, $\frac{d\alpha}{dt}$ (rad/sec)

The manned mission requiring 25 ft-lb torque and a 3 Hz bandwidth is considered first.

For purposes of sizing, equations (5-12) and (5-13) can be normalized and written as a function of gimbal angle, α,

$$\frac{h}{H} = \frac{1}{2 \sin \alpha} \tag{5-14}$$

and

$$\frac{T_B}{T_o} = \frac{h\dot{\alpha}}{T_o} = \frac{1}{2 \cos \alpha} \tag{5-15}$$

where

T_B= Radial torque on gyro bearings (ft-lb)

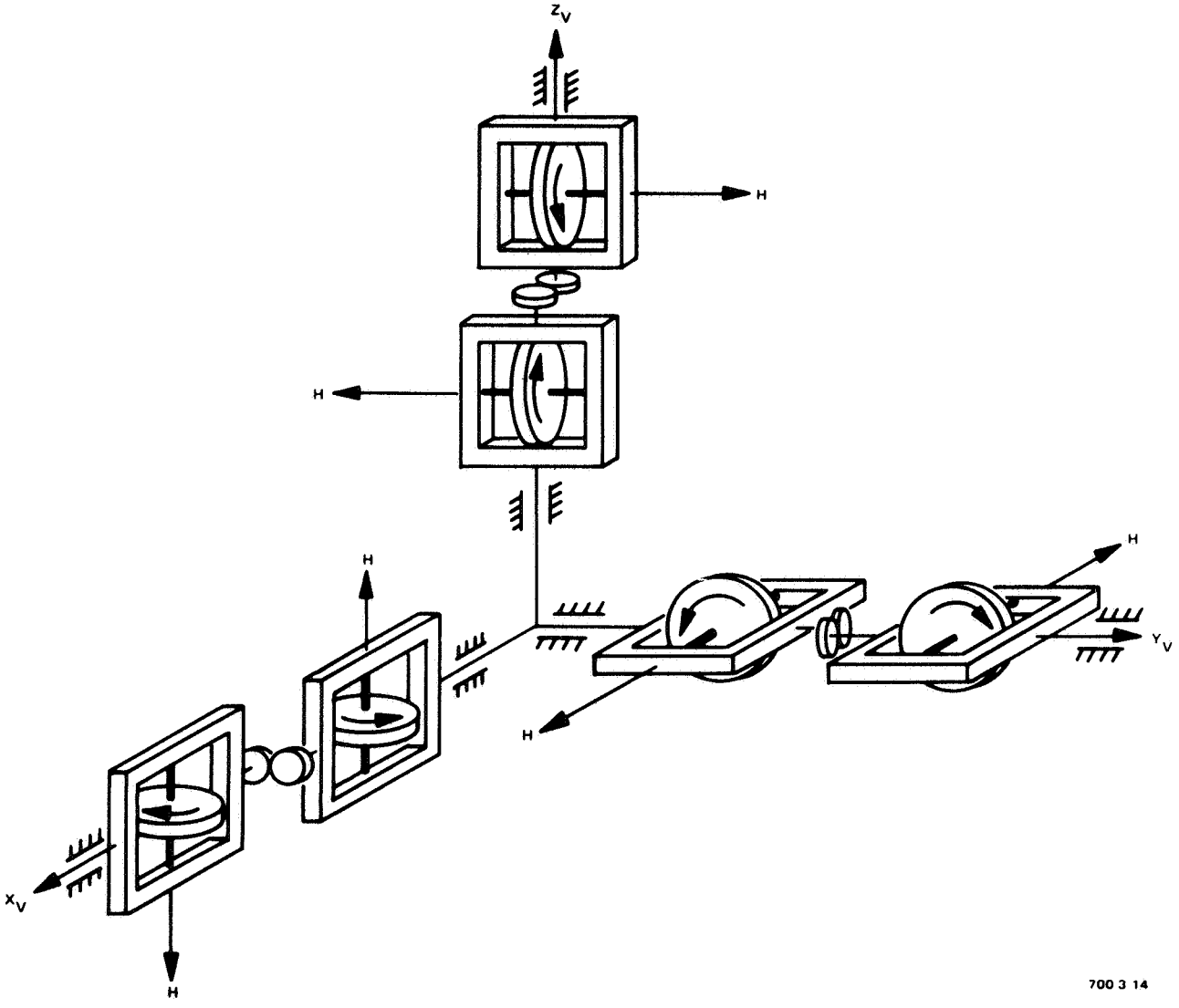

Figure 5-5
Three-Axis CMG Scissored-Pair Configuration

These equations are plotted in Figure 5-6. For small gimbal angles, small gimbal rates and bearing torques are required, but a large gyro angular momentum, h, is necessary. Whereas, for gimbal angles beyond 60 degrees, the gyro momentum, h, required is almost constant but the necessary gimbal rates are rapidly increasing. Since larger gimbal rates require more torquer power and exert more load on the spin and gimbal bearings, a limit exists on the maximum gimbal angle. For this study 60 degrees was selected, and thus the required gyro parameters are

$$h = 0.58\ H = 116\ \text{ft-lb-sec} \tag{5-16}$$

$$\dot{\alpha} = \frac{T_o}{h} = 0.218\ \text{rad/sec} \tag{5-17}$$

To obtain the desired system bandwidth of 3 Hz, the gyro must meet an additional angular acceleration requirement of 1.37 radians per second per second.

These requirements were inputted to the Sperry CMG optimum sizing digital computer program which selects the "best" gyro design predicated on weight, power, and reliability considerations, (Ref 6). The selected gyro parameters are:

Rotor Diameter	14 inches
Rotor Speed	7729 rpm
Rotor Weight	17 pounds
Inner Gimbal Weight	29 pounds
Torquer Weight	11 pounds
Outer Gimbal Weight	9 pounds
Total Gyro Weight	49 pounds
Spin Motor Shaft Power	3.6 watts
Gyro Average Power	8 watts
Peak Torquer Power	30 watts

The system specifications presented in Table 5-2 are the result of using six gyros in the system, and allotting 10 pounds of weight and 10 watts of power for the control electronics and 30 pounds for the mounting structure which mates the gyro to the vehicle. The equivalent system weight includes a penalty of 35 pounds per kilowatt for fuel cell weight and 0.8 pound per kilowatt-hour for the weight of hydrogen and oxygen required by the fuel cell.

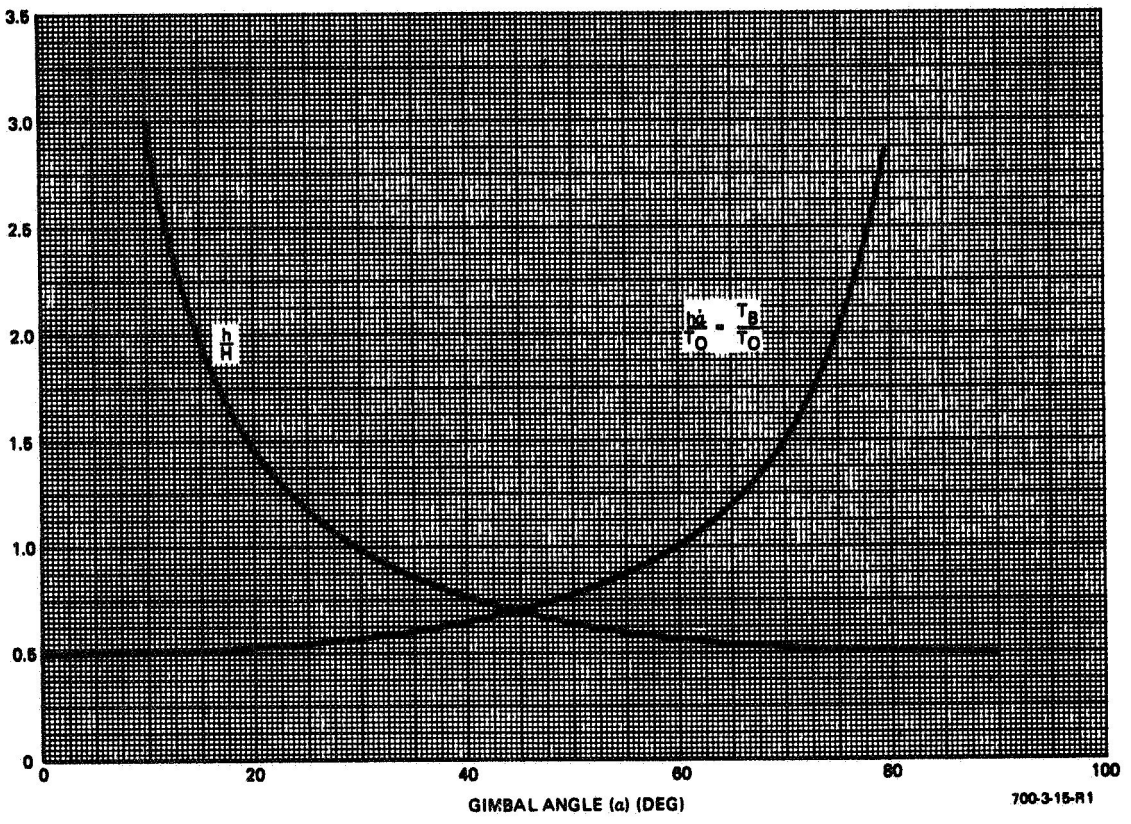

Figure 5-6
Normalized Scissored-Pair Parameters versus Gimbal Angle

TABLE 5-2
CMG COMPARISON DATA (MANNED MISSION)

Parameter	4-FACS	Scissored-Pair	Unit
Momentum	200	116	ft-lb-sec
Maximum Control Torque	25	25	ft-lb
Maximum Bearing Torque	203	25	ft-lb
Maximum Gimbal Rate	1.01	0.218	rad/sec
Effective Gimbal Inertia	1.1	0.46	$sl\text{-}ft^2$
Maximum Gimbal Torque	5.0	2.0	ft-lb
Rotor Diameter	16	14	in.
Rotor Speed	7729	7729	rpm
Single Gyro Weight	61	49	lb
Total Gyro Weight	244	294	lb
Total System Weight	280	334	lb
System Average Power	52	58	W
System Run-Up Power	260	290	W
Equivalent System Weight	290 + D	344 + 1.1 D	lb
D = Time Independent weight factor, lb/day			

C. 4-FACS CMG CONFIGURATION

The sizing technique used for the 4-FACS CMG configuration described in Section IV is similar to that employed for the scissored pair gyro configuration. With the deviation angle, $\Delta\alpha$ limited to ±40 degrees (from Figure 4-3)

$$\frac{h}{H_x} = \frac{h}{H_z} = 0.775 \tag{5-18}$$

and

$$\frac{h\dot{\alpha}}{T_{x,z}} = 8.11 \tag{5-19}$$

These equations, however, express the capability along only a single axis. Since each gyro contributes momentum which is coupled to combined axes simultaneously, the gyros should be sized larger than just the single-axis requirement indicates. In mission designs where the required momentum envelope shape is known a priori, a more precise method of sizing the gyro momentum would be to "fit" the required envelope to those 4-FACS envelopes shown in Subsection IV.F. For this study, a single-gyro momentum of 200 ft-lb-sec with a gimbal rate requirement of one radian per second has been selected. To obtain the desired system bandwidth of 3 Hz, the gyro must have an angular acceleration capability

of 3.2 radians per second per second. As with the scissored pair, the gyro requirement data was inputted to the Sperry CMG optimum sizing digital computer program; the selected gyro parameters are:

Rotor Diameter	16 inches
Rotor Speed	7729 rpm
Rotor Weight	22 pounds
Inner Gimbal Weight	37 pounds
Torquer Weight	13 pounds
Outer Gimbal Weight	11 pounds
Total Gyro Weight	61 pounds
Spin Motor Shaft Power	5.2 watts
Gyro Average Power	10.4 watts
Peak Torquer Power	132 watts

The specifications presented in Table 5-2 are the result of using four gyros in the system and allotting 10 pounds weight and 10 watts power for the control electronics and 25 pounds for the mounting structure which mates the gyro to the vehicle. The same power weight penalties are employed to derive the system equivalent weight as those previously used for the scissored pair configuration.

For the unmanned mission the gyro requirements change to the following:

Momentum	200 ft-lb-sec
Gimbal Rate	0.16 rad/sec
Control Torque	2 ft-lb
Gimbal Torque	1 ft-lb

A comparison between the gyro designs obtained for both manned and unmanned missions is presented in Table 5-3. The gyro selected for the lower torque unmanned mission runs at a faster speed than the high torque design because bearing loads are lighter, and thus allow a smaller rotor design. More electrical power, however, is consumed by the motor and makes the equivalent weights equal between the two designs after a mission time, D, of 102 days.

TABLE 5-3
4-FACS CMG CONFIGURATION COMPARISON

Parameter	Low Torque	High Torque	Unit
Momentum	200	200	ft-lb-sec
Maximum Control Torque	2.0	25	ft-lb
Maximum Gimbal Torque	1.0	5	ft-lb
Rotor Diameter	14	16	in.
Rotor Speed	8833	7729	rpm
Single Gyro Weight	48	61	lb
Total System Weight	227	280	lb
System Average Power	77	52	W
System Run-Up Power	385	260	W
Equivalent System Weight	240 + 1.48D	290 + D	lb
D = Time independent weight factor, lb/day			

The equivalent system weight obtained for the low torque design is shown in Figure 5-7 and compared to the optimum reaction wheel curves. The entire 4-FACS curve represents only one design which is optimized at approximately 50 days, whereas, each point on the reaction wheel curves represents an individual design optimized for that particular orbital duration as discussed in Subsection V.A.

D. REACTION JET CONTROL SYSTEM

A low level reaction jet system was considered as a competitive fine attitude control system. Both manned and unmanned missions were considered. The system (Figure 5-8) consists of twelve low-level thrusters which produce pure rotational couples about each vehicle axis. For the manned mission two-pound hydrazine thrusters were selected to provide the required control torque of 25 ft-lb and a high effective specific impulse, I_{sp}. The minimum thruster impulse bit per axis, I_m, is

$$I_m = 2T_j(\Delta t) = 0.06 \text{ lb-sec} \qquad (5\text{-}20)$$

where

Δt = Thruster minimum impulse delay time, 15 milliseconds

T_j = Rocket thrust (pounds)

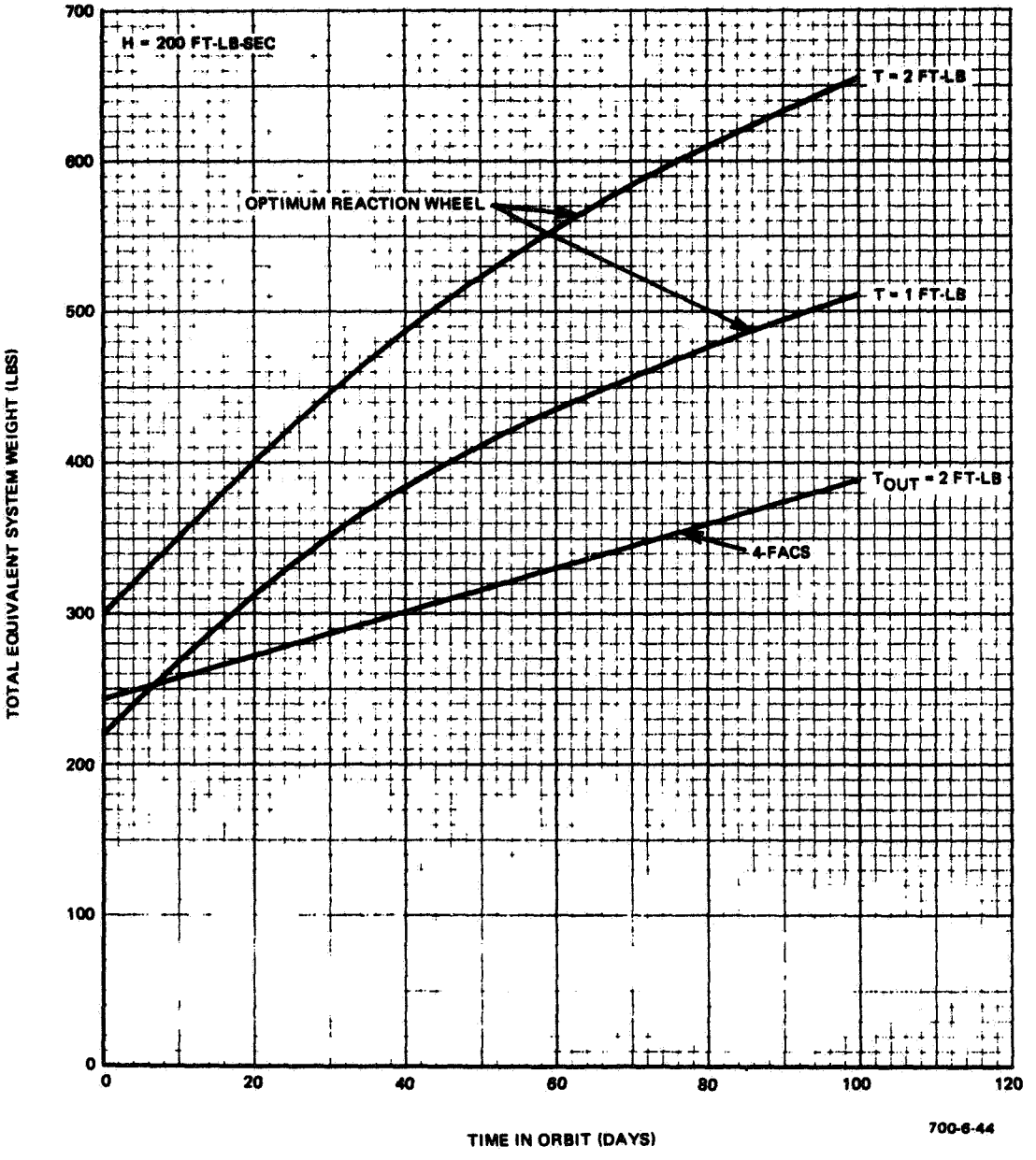

Figure 5-7
4-FACS versus Reaction Wheel Comparison for
Low Torque Mission, H = 200 foot-pound-seconds

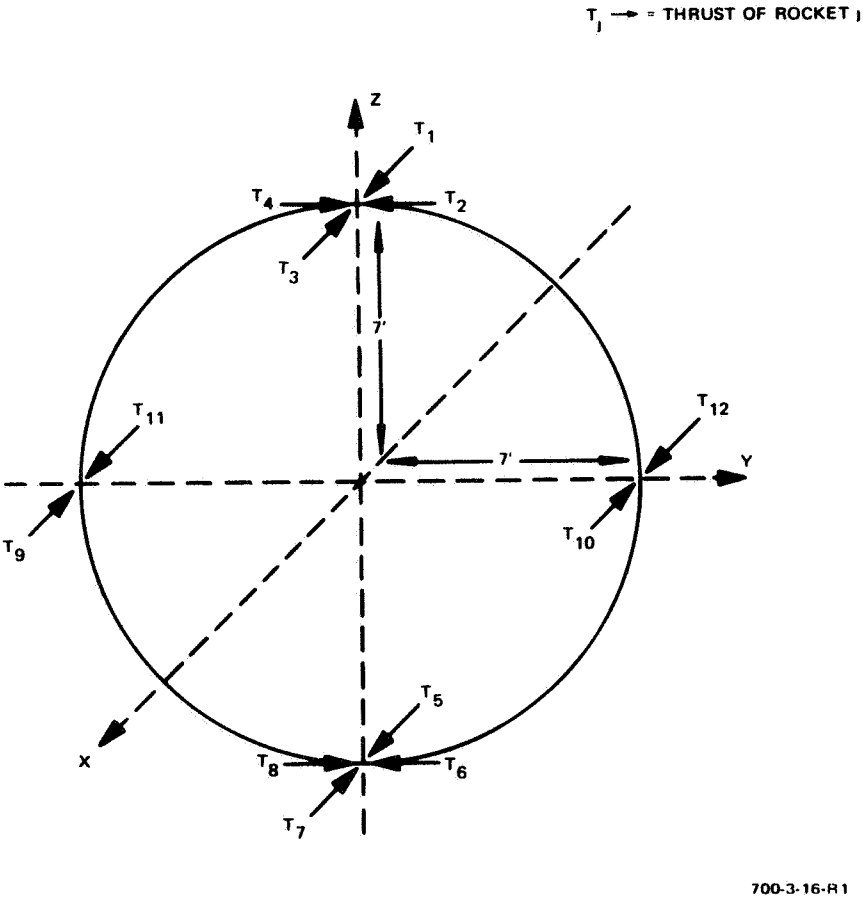

Figure 5-8
Reaction Jet Thruster Configuration

The "dry" or unfueled system weight, which varies between 60 and 80 pounds, includes the fuel tanks, tubing, regulators, thrusters, solenoids, and electronic package weights. To this weight must be added the required fuel weight which is a function of limit cycle and disturbance torque requirements. For the "design mission" system with 0.01 deg/sec rate and 0.1 degree attitude deadbands, the limit cycle fuel required is only 0.33 pound per day with an I_{sp} = 190. When considering the fuel requirements to overcome external torque disturbances, the secular torques are neglected because both CMG and RCJ systems require the same amount of fuel to control these torques. Considering only the cyclic torques, therefore, the fuel requirement is 3.1 pounds per day. Finally, the fuel required to overcome crew torques is estimated by allowing for one disturbance per axis every 5 minutes for a total momentum requirement of 870 ft-lb-sec per day. The additional fuel needed is 0.33 pound per day; therefore, the total fuel weight needed is 3.76 pounds per day.

Electrical power is required in the RJC system for the control computer electronics and power supplies, the jet logic and failure detection networks, and the thruster solenoids. A continuous power of 10 watts is needed with peak requirements during thrusting of 160 watts.

An equivalent system weight comparison between the manned mission CMG configurations and the RJC system is shown in Figure 5-9. The RJC system is plotted with a conservative I_{sp} = 190 sec as used in the previous calculations, and an optimistic I_{sp} = 215 sec as could be expected in advanced RJC hydrazine systems. For short duration missions, less than 75 days, the RJC system weighs less than either CMG configuration. Beyond 90 days where large amounts of RJC fuel are needed, the 4-FACS CMG configuration is the lightest system, weighing approximately 380 pounds at 90 days.

For unmanned missions requiring very precise attitude control rates (0.0001 deg/sec) the reaction jet control system is limited by the minimum impulse bit achievable. From equation (5-20) and with a vehicle inertia, I_v, the minimum impulse rate achievable is

$$\dot{\theta}_{(min)} = \frac{2T_j (\Delta t) L}{I_v} \qquad (5\text{-}21)$$

where

L = Rocket moment arm (ft)

$\dot{\theta}_{(min)}$ = Minimum impulse rate (rad/sec)

and the control torque or moment, M_v, imparted to the vehicle by the jet couple is

$$M_v = 2T_j L \qquad (5\text{-}22)$$

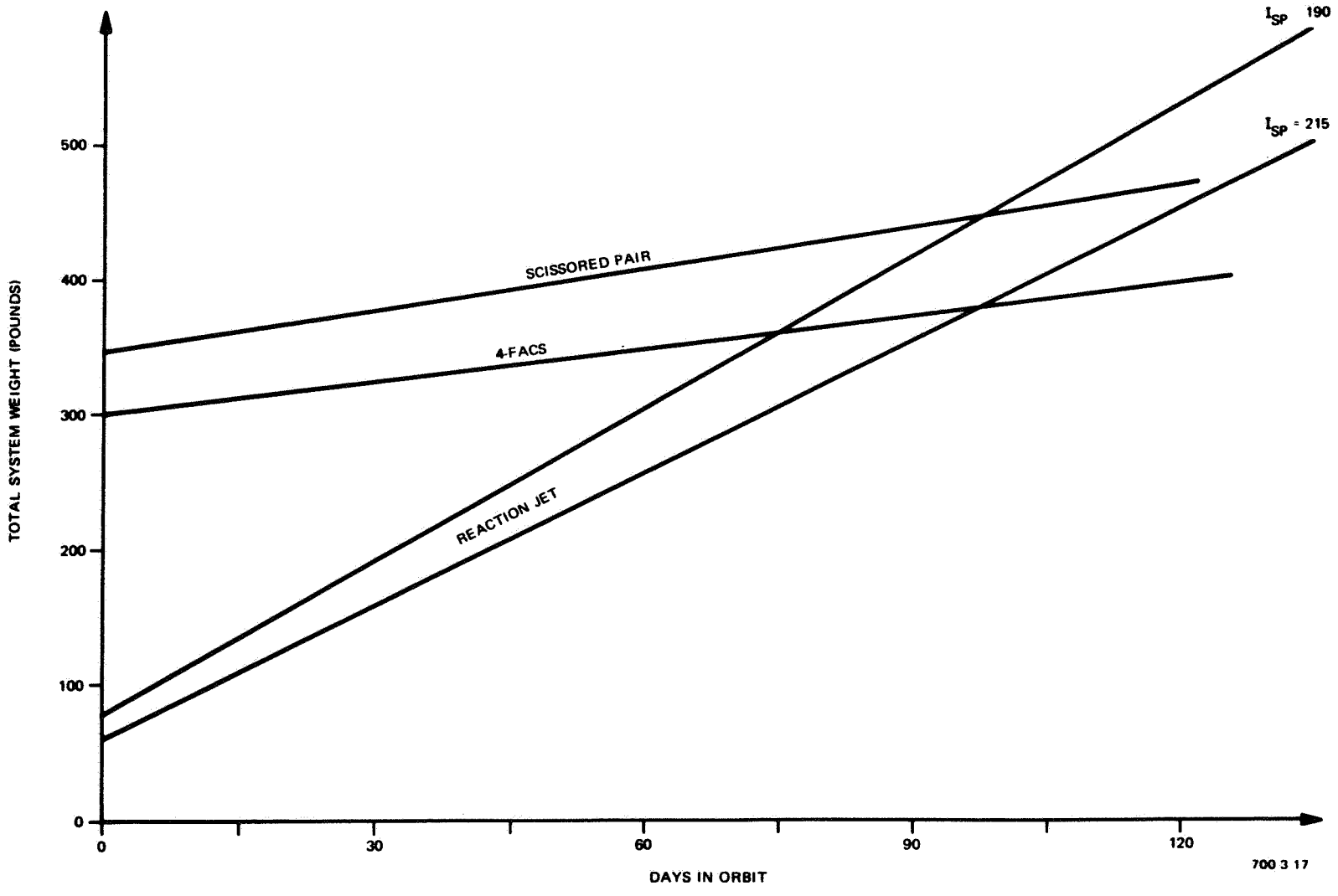

Figure 5-9
System Weight Comparison, Manned Mission

Combining equations (5-21) and (5-22) gives the maximum allowable moment for a given minimum rate.

$$M_{V_{(max)}} = \frac{\dot{\theta}_{(min)} I_V}{(\Delta t)} \qquad (5\text{-}23)$$

This expression for three values of vehicle inertia and a miminum thruster delay time, Δt, of 15 milliseconds is shown in Figure 5-10. For a vehicle with I_V = 20,000 slug-ft^2, the control torque must be limited below 2.3 ft-lb to achieve minimum impulse attitude rates of 10^{-4} degrees per second. With a system requirement of 2.0 ft-lb and 10^{-4} deg/sec rate accuracy, the RJC system would barely meet the accuracy requirement and not allow for any system or thruster tolerance variations.

The amount of fuel per day required for unmanned and manned missions is similar. The difference is only 0.33 pound per day depending on the presence of crew disturbances.

Another problem existing with the low torque RJC system is reliability. Since the miminum impulse bit is very small, a large number of thruster firings are necessary to oppose continuously the gravity and aerodynamic torques that are present. This is discussed in further detail in the following section.

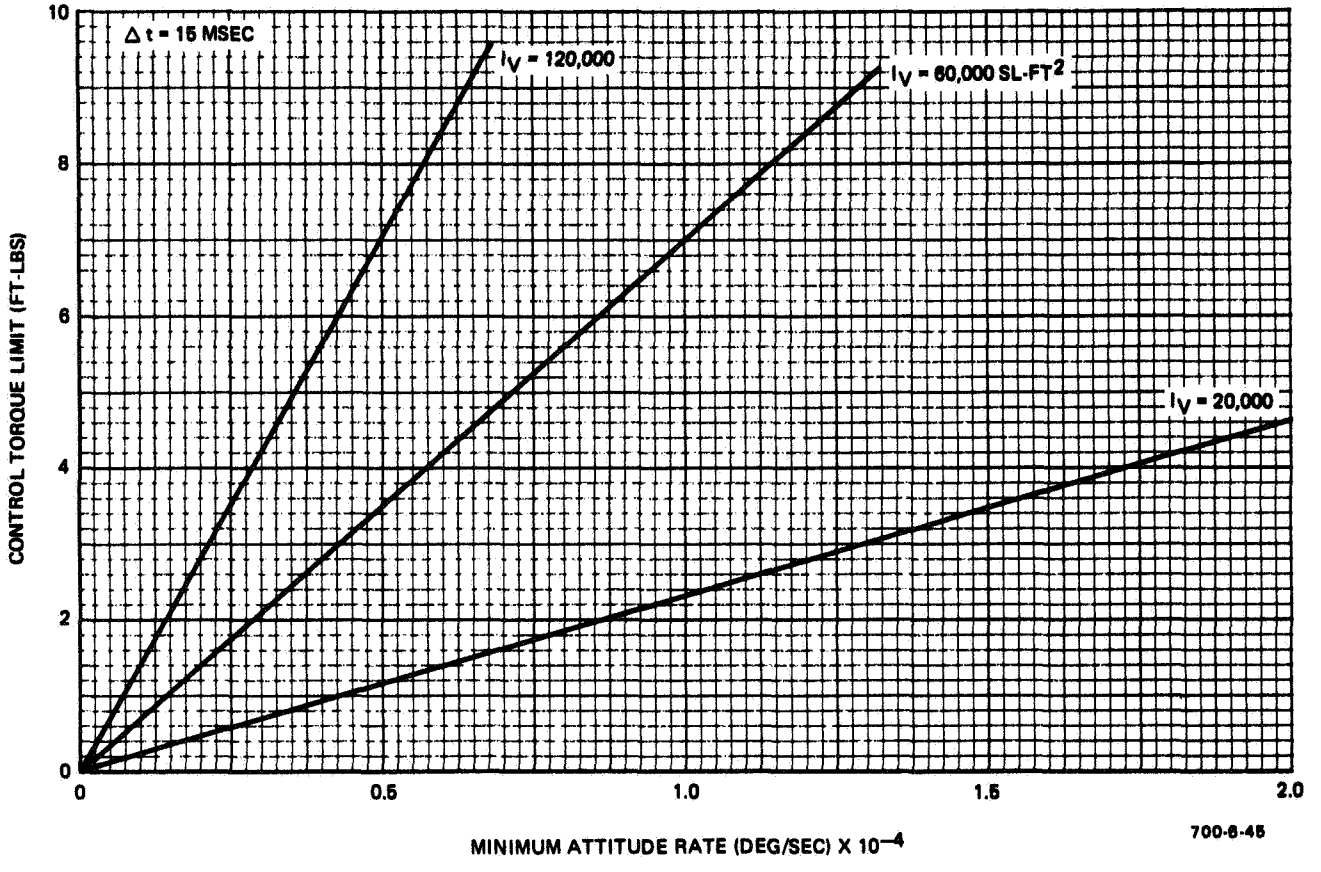

Figure 5-10
RJC Torque Limit versus Minimum Attitude Rate

E. RELIABILITY COMPARISON

A reliability comparison of the CMG configuration and RJC system was conducted for the manned mission; the results are presented in Figure 5-11. Unlike the overall system reliability analysis of Section IX, only the torque actuator portion of the system is considered in the comparison; other system components (i.e., attitude reference, telemetry, etc) are common to all systems under study. Each system is divided into major subsystems and probability of success numbers for a 1000-hour mission are derived for each subsystem in a similar manner. The reliability estimates used are derived from many standard sources (ref 7, 8); breakdown of some of the major system components are tabulated in Appendix E.

The 4-FACS CMG system (which can continue to operate successfully after any single gyro failure) requires a steering law computer, at least three of the four gyros and gimbal loops, and associated electronics to complete a fine attitude hold mission. The computer block includes all the electronics (the compensation networks, CMG vehicle loop computer, and CMG steering law computer) needed to translate the vehicle attitude error and rate signals into gimbal loop commands. The gimbal loop block comprises the gimbal loop electronics, torque motor, gimbal bearings, rate sensor, and all hardware used to maneuver the gyro's momentum vector. The gyro rotor block includes the spin motor and bearings, tachometer, speed control electronics, and associated gyro inner gimbal hardware.

Allowing for any single-gyro failure, the probability of success for the 4-FACS configuration over a 1000-hour mission is 0.9935, the highest of the systems studied. The non-redundant computer is the primary source of failure for this configuration. A redundant computer was not considered for two reasons: a comparison for a simple 4-FACS system was desired while added redundancy complicate the system to gain higher reliability; and more CMG systems reliability does not significantly enhance the overall control system reliability unless redundancy is used throughout as shown in Section IX.

Two different configurations are considered for the scissored pair CMG system. Configuration A is the "classical" scissored pair in which each gyro pair is mechanically connected or electrically slaved together to always work in a scissored fashion as described in Subsection V.B. This configuration has the disadvantage of requiring all six gyro wheels operating to obtain the required control capability. With one gyro failed, the cross coupling is so great that the gimbal angle must be severely limited and the momentum exchange capability is considerably decreased. A more reliable CMG scissored pair system can be implemented by employing an electronic steering law to re-orient and position the gyros after a failure as is done in the 4-FACS configuration.

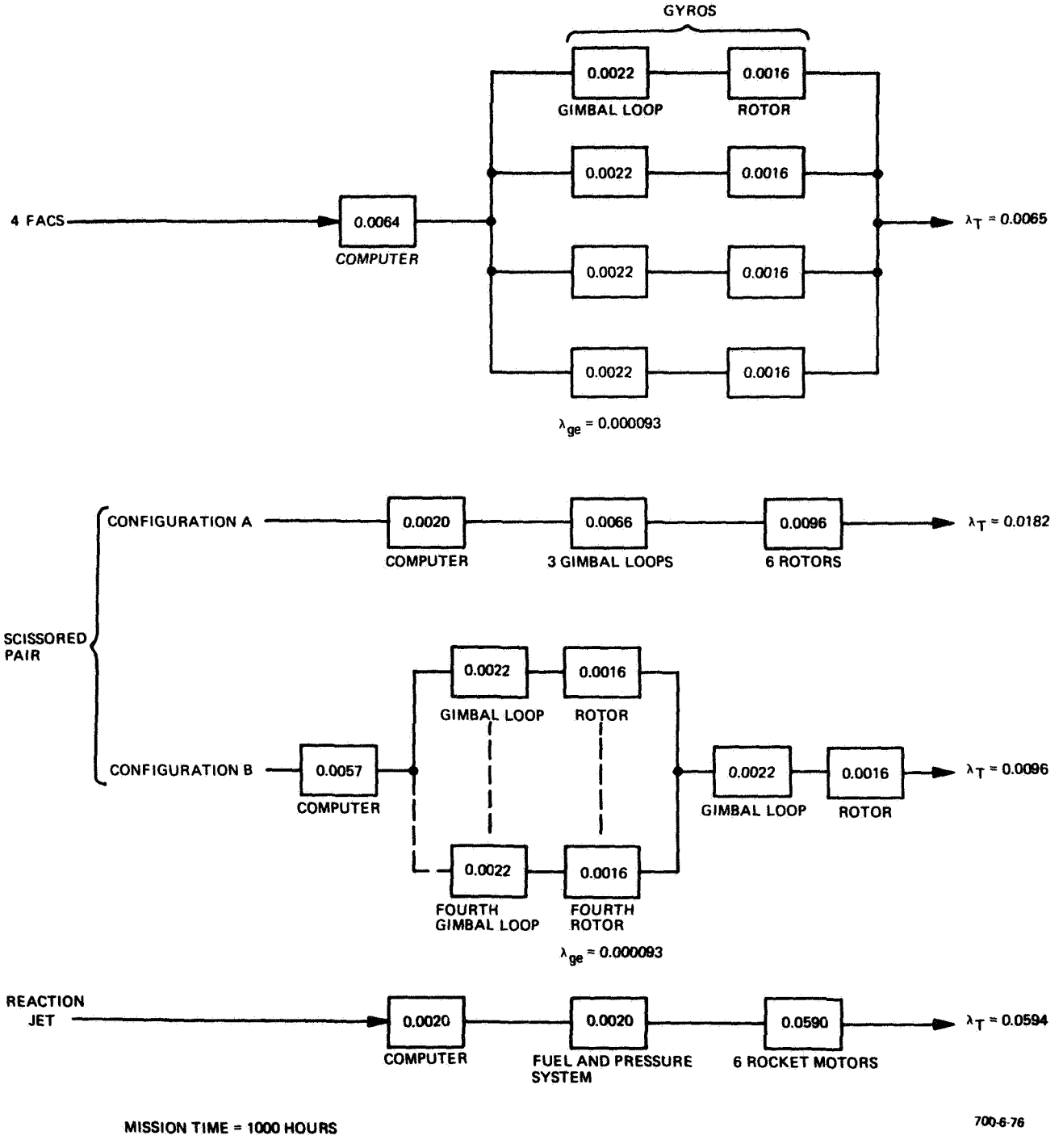

Figure 5-11
Reliability Comparison, High Torque Systems

This allows the scissored pair system to successfully complete the mission with one gyro failed. The momentum vectors of the gyros are re-oriented to a new "initial angle condition" or net zero angular momentum position after failure of gyro 1 (Figure 7-53). To produce control torque along the X axis, gyros 3 and 4 are still driven in a scissored fashion and gyro 2 is held fixed. For control torque along the Y axis, gyro 2 is driven to produce the necessary torque, and gyros 3 and 4 are driven in the same direction (clockwise or counter-clockwise) to maintain zero torque along the X-axis. With this operating technique, an increased probability of success $P_s = 0.9904$ is obtained, yet still not as high as the 4-FACS configuration.

The RJC system has the lowest reliability with $P_s = 0.941$ for a 1000-hour mission. The RJC system was divided into three blocks consisting of computer, fuel and pressure system, and rocket motors.

The computer includes all the electronics needed to translate attitude error signals into RJC solenoid commands. The fuel and pressure system block comprises the fuel and pressure gas tanks, tubing, regulators, control valves, and associated hardware and electronics. The rocket motors are the least reliable RJC system component and strongly determine the overall system reliability. Six rocket motors are considered sufficient to maintain vehicle control, although translation would be present and only one-half the normal control torque would be available. If pure rotational couples at full torque are necessary, all twelve rocket motors are necessary and the reliability decreases even further.

The unmanned, low torque mission system reliability remains approximately equal to the high torque system for the CMG configurations. Only a small difference due to lower torque to momentum ratio may be present. As shown in Figure 5-12, however, a significant difference in reliability exists between high and low torque RJC systems. The lower reliability for lower torque missions is a direct indication of the lower minimum impulse bit required for lower torque, higher accuracy systems. As the minimum impulse bit is decreased for the same orbital momentum requirements, more reaction jet actuation cycles are required, and hence, a lower reliability results.

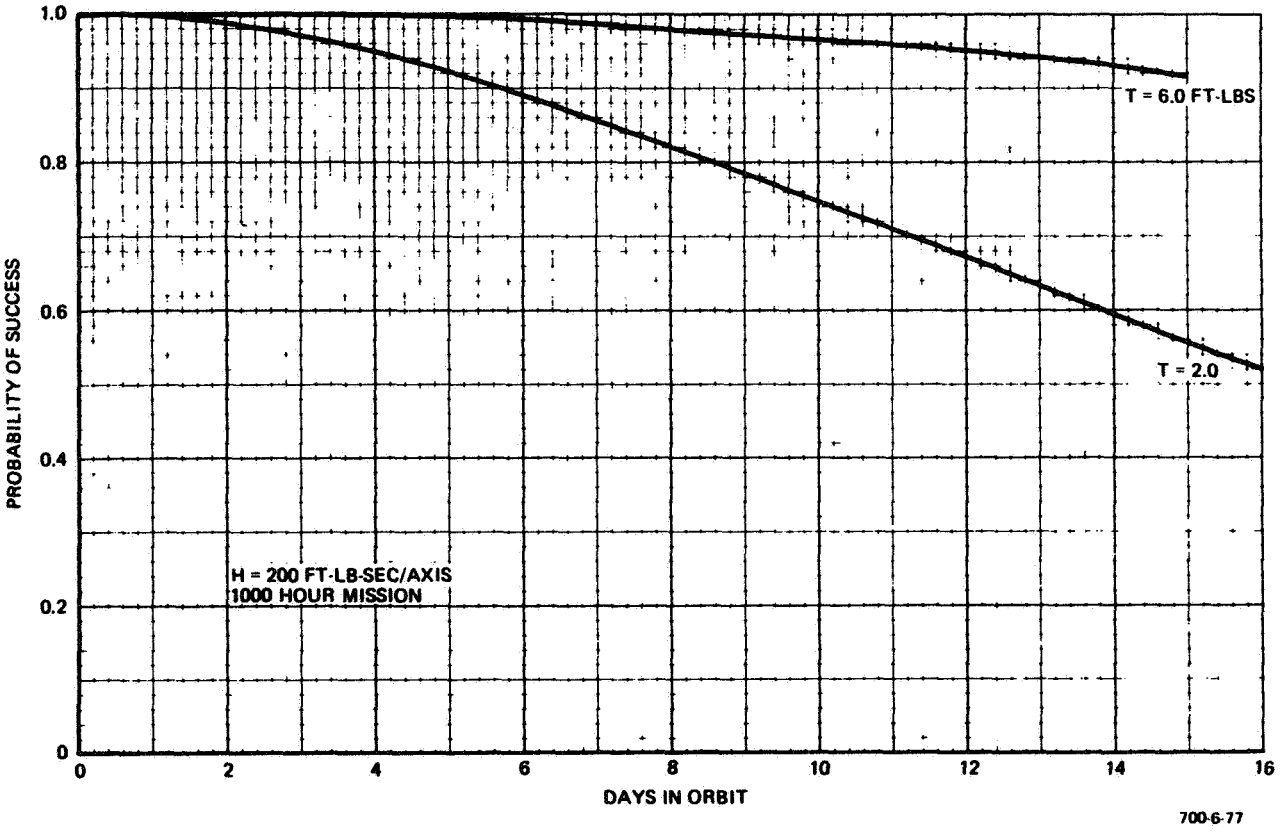

Figure 5-12
Low Torque RJC System Reliability,
T = 2 and 6 foot-pounds

F. SUMMARY

Four competitive fine attitude control systems have been compared in this section for a manned, high torque system and an unmanned, low torque system. The comparison was predicated on system weight, electrical power consumption, and reliability.

The manned mission systems requiring a 25 foot-pound control torque, 3-Hz bandwidth can be summarized as follows:

- Reaction Wheel: Requires most power and weight
- Scissored Pair CMG: Heavier than and less reliable than 4-FACS CMG
- 4-FACS CMG: Most reliable system and lightest CMG configuration
- RJC System: Least reliable, lightest weight system

The competitive fine attitude control systems have been compared equally for system weight, electrical power consumption, and reliability. The reaction wheel system, which consumes the most electrical power, (1000 watts), is the heaviest at 1200 pounds initial weight. As a result, it was eliminated from consideration first. The lightest weight system for missions less than 1000 hours is the RJC system, but it is also one of the least reliable systems. For short duration missions, therefore, a tradeoff must be conducted between system weight and reliability. For a manned mission or a highly expensive and critical "one of a type" mission, reliability is of primary importance and a CMG system should be selected. Of course, for missions beyond 1000 hours where large amounts of RJC fuel are needed, CMG systems are the best choice from both weight and reliability considerations. The 4-FACS CMG configuration is approximately 50 pounds lighter, consumes 6 watts less average electrical power, and is more reliable than the scissored pair CMG system. These advantages are primarily due to the 4-FACS configuration having only four gyro wheels (whereas, the scissored pair has six) and the 4-FACS capability of operating acceptably even after one of the four gyros has failed. The 4-FACS configuration, therefore, has been selected as the preferred fine attitude control system for a manned mission.

The unmanned, low torque mission systems requiring 2 foot-pounds and 1-Hz bandwidth can be summarized as follows:

- Reaction Wheel: High weight and power
- 4-FACS CMG: Most reliable system and lightest CMG configuration
- RJC System: Least reliable, lightest weight system

Although the reaction wheel weight and power requirements are decreased for the low torque mission, the requirement for desaturation once per orbit forces the reaction wheel to absorb a large amount of momentum and, thus, be heavy and consume great amounts of power. If desaturation were allowed during the attitude hold portion of the orbit, the momentum requirements could be lowered and a reaction wheel system might be desirable. Only a three reaction wheel system was considered for this study since this was ample to show a preference for CMG's. A redundant wheel or skewed arrangement of reaction wheels, however, should be considered for a competitive low torque study.

The 4-FACS CMG system studied is lighter than the reaction wheel system, more reliable than the RJC system, and appears to be capable of very precise accuracy when using a pseudo-torque feedback steering law. Until a detailed study is conducted to determine the ultimate accuracy that can be achieved with this type system, the effects of gyro loop non-linearities, as well as dual speed operation techniques on system performance can only be estimated. At present, CMG's are believed to be capable of achieving one arc-second accuracy. One or two orders of magnitude better accuracy, however, is very questionable until more study and hardware data is accumulated.

Considering these factors, the 4-FACS CMG configuration has been selected as the preferred system for the low torque mission also.

SECTION VI

ATTITUDE CONTROL SYSTEM SYNTHESIS

SECTION VI

ATTITUDE CONTROL SYSTEM SYNTHESIS

In this section the selected 4-FACS CMG configuration is synthesized to establish the loop gains and compensation networks required for obtaining the desired system response and bandwidth, defining the operational modes and system interfaces, and creating a starting point for an analog computer simulation. The manned high control torque mission is synthesized first; most of the system analysis effort during the study concentrated on this system. The unmanned, low torque system is discussed briefly. Primary differences between the types of systems which satisfy these missions are described.

A. SYSTEM DESCRIPTION

The 4-FACS CMG fine attitude control system block diagram shown in Figure 6-1 consists of a CMG steering law, four gimbal rate loops, a CMG gyro transfer matrix, an uncoupled rigid body vehicle, attitude error plus rate feedback, and a lead-lag compensation network. A high-level RJC system always connected in parallel with the CMG system is used for damping large initial rates, desaturation of the CMG configuration, and control during periods when fine attitude hold is not necessary. During desaturation, a gimbal angle loop is closed around the CMG to drive all gimbal angles back to their initial conditions. Except for gimbal angle rate and supply voltage limiting, the system has been linearized and all hardware non-linearities have been neglected in order to obtain a clear understanding of the basic 4-FACS configuration capabilities and avoid becoming involved with complicating details which are not germane to the basic system operation.

During the study, certain improvements were made to this preliminary system design, including the following: the addition of a torque feedback loop to the steering law; torque command limiting; and a direct reaction jet desaturation technique. The torque feedback steering law is discussed in Subsection IV.D and the desaturation technique is explained in Subsection VI.D. A detailed block diagram of the final overall system is presented in Appendix F and described in Section X.

When the system is in operation, the gyros are initially off and have their gimbals locked during launch and de-boost. The RJC system damps out initial de-boost rates and establishes a limit cycle within its operating deadband (0.2 deg/sec and 0.5 deg). The gyros are then brought up to speed with the RJC system cancelling out the spin motor reaction torques during startup.

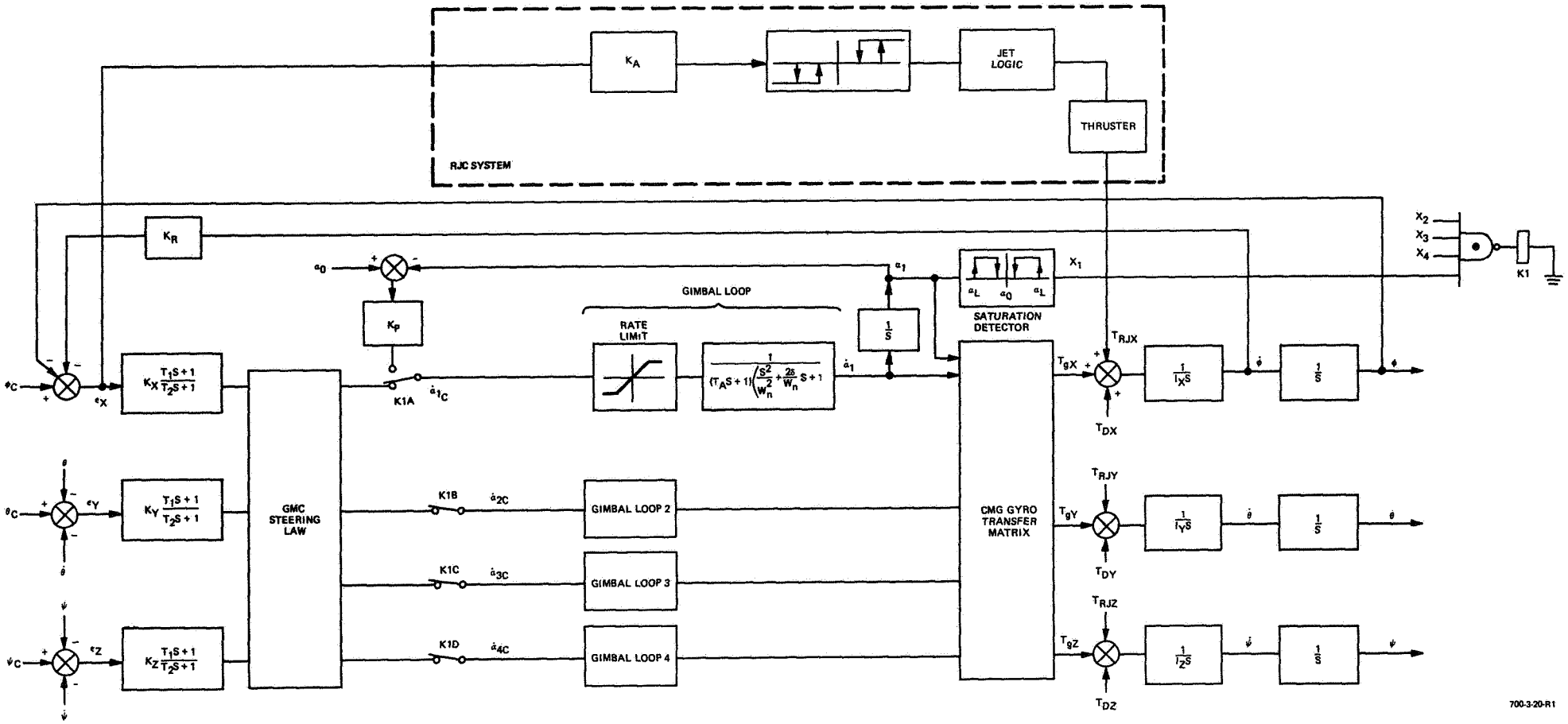

Figure 6-1
4-FACS Control System,
Simplified Block Diagram

After the gyros have attained a constant running speed, the gimbals are released, initial gimbal angles commanded, and the fine attitude hold mode initiated. In this mode, the gyros maintain the vehicle rate and attitude error within 0.01 deg/sec and 0.1 deg respectively as they absorb the momentum imparted onto the vehicle by disturbance torques. Secular torques finally cause the gyro configuration to reach a maximum gimbal angle and saturate. A saturation detector, which monitors each gimbal angle, combined with a loss of sun signal initiates the desaturation mode. In the design mission, the gyros are sized so that desaturation is necessary only once per orbit and would take place during the period when the vehicle is in the earth's shadow and attitude hold is not required. During desaturation the gyro gimbal angles are all driven back to their initial angles simultaneously and consequently impart torque to the vehicle. The RJC system is used to counter the gyro torque and maintain vehicle attitude and rate during desaturation. When the gyro configuration has returned to its zero-stored momentum configuration, the desaturation loop is disengaged and fine attitude hold mode is resumed.

B. GIMBAL CONTROL LOOP

The gimbal control loop shown in Figure 6-2 employs a direct drive torque motor and tachometer to provide a gimbal rate command mode. A direct drive torquer has been selected since it simplifies the analysis (no backlash or deadzone as in a geared torquer) and provides a clear insight into control loop operation. A torquer current feedback loop is used to provide tight torque control and make the system insensitive to amplifier and torque motor variations, and hardware non-linearities. An integrator is employed in the loop to create a first order system with zero steady-state error. The current loop gain is adjusted to create a double real axis pole at $\omega_c = \frac{1}{2\ T_M}$. The outer loop employs gimbal rate feedback and when closed creates a third order system consisting of a complex pole pair and a real axis pole. For the design mission, a 5-ft-lb torquer with T_M = 10 milliseconds was selected; the gimbal inertia was J_G = 1.1 slug-ft^2 and the loop gain was adjusted to give the following response:

$$\frac{\dot{\alpha}}{\dot{\alpha}_c} = \frac{72\ (22)^2}{(S + 72)\left[S^2 + 2\ (0.62)\ 22\ S + (22)^2\right]} \qquad (6\text{-}1)$$

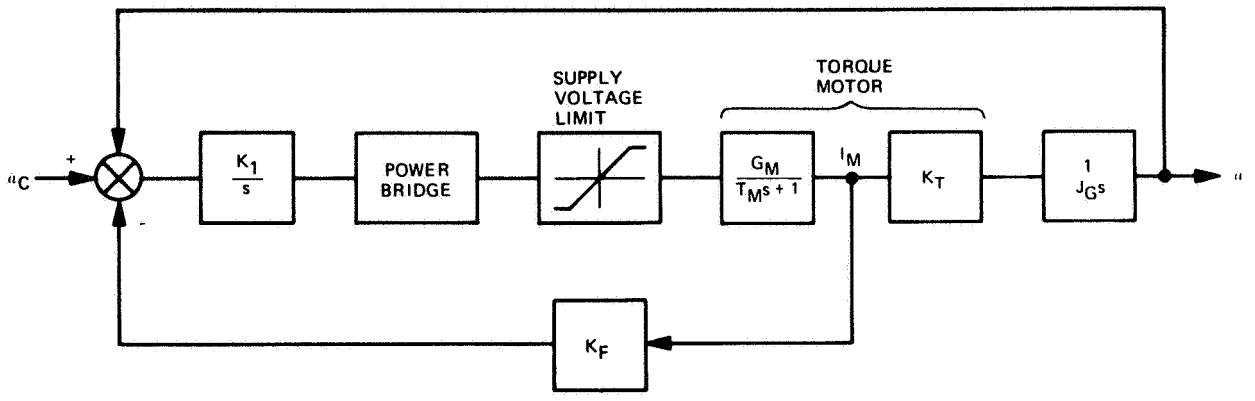

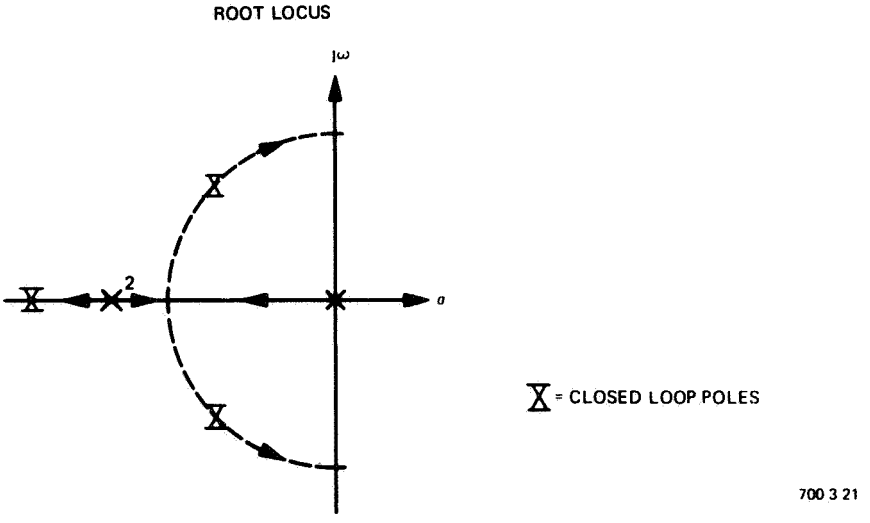

Figure 6-2
Gimbal Loop Block Diagram, Direct Drive Torquer

C. SINGLE-AXIS VEHICLE LOOP

The single axis attitude control loop (Figure 6-3) was created to establish the loop gain and compensation networks needed to attain a system bandwidth greater than 3 Hz. The loop consists of the gimbal rate command loop discussed in Subsection VI.B., the gyro torque/gimbal rate transformation, the rigid body vehicle dynamics, attitude error and rate feedback, a lead-lag compensation network, the steering law matrix in-axis diagonal gain, and a gimbal rate limiter.

For the "design mission" problem with h = 200 ft-lb-sec and I_y = 56,000 slug-ft^2, a rate feedback gain K_R = 0.25 sec and compensation time constants T_1 = 0.1 sec and T_2 = 0.02 sec that were selected provided the root locus of Figure 6-4. The vehicle poles at the origin approximately cancel with the compensation zeros and the gimbal loop complex pole pair determines the permissible open loop gain and closed loop bandwidth. A gain of $K_y = 1.25(10)^6$ that was selected provides the closed loop frequency response shown in Figure 6-5. The gimbal rate limiter is adjusted so that the gyro torque, T_{gy}, is sufficiently large to counter the disturbance torques but not produce excessive load on the gyro bearings. The other two vehicle axes are synthesized in an identical manner and the gains K_x and K_z are adjusted to obtain the same open loop gain. Therefore, an identical, uncoupled closed loop response is obtained in all three vehicle axes.

D. DESATURATION AND MOMENTUM UNLOADING

When the gyro configuration has absorbed its maximum momentum and the gimbal angles reach saturation, the gyro configuration must be returned to its initial zero angular momentum state. To accomplish this, the RJC system must expel an amount of momentum exactly equal to that stored in the gyro configuration at the initiation of desaturation. If the RJC system momentum unloading is inexact as a result of the rocket system having a minimum impulse bit, the remaining momentum is again absorbed by the gyro, consumes part of its momentum envelope, and does not return the gyro to its zero momentum state. Therefore, consideration must be given to the CMG/RJC interface when sizing the gyros and rocket thrusters so that the minimum impulse bit of the RJC system is sufficiently small to allow the gyro to reach near complete desaturation.

Another desirable, but not always necessary, requirement of the desaturation technique is that it maintain the vehicle attitude and rates near null during desaturation.

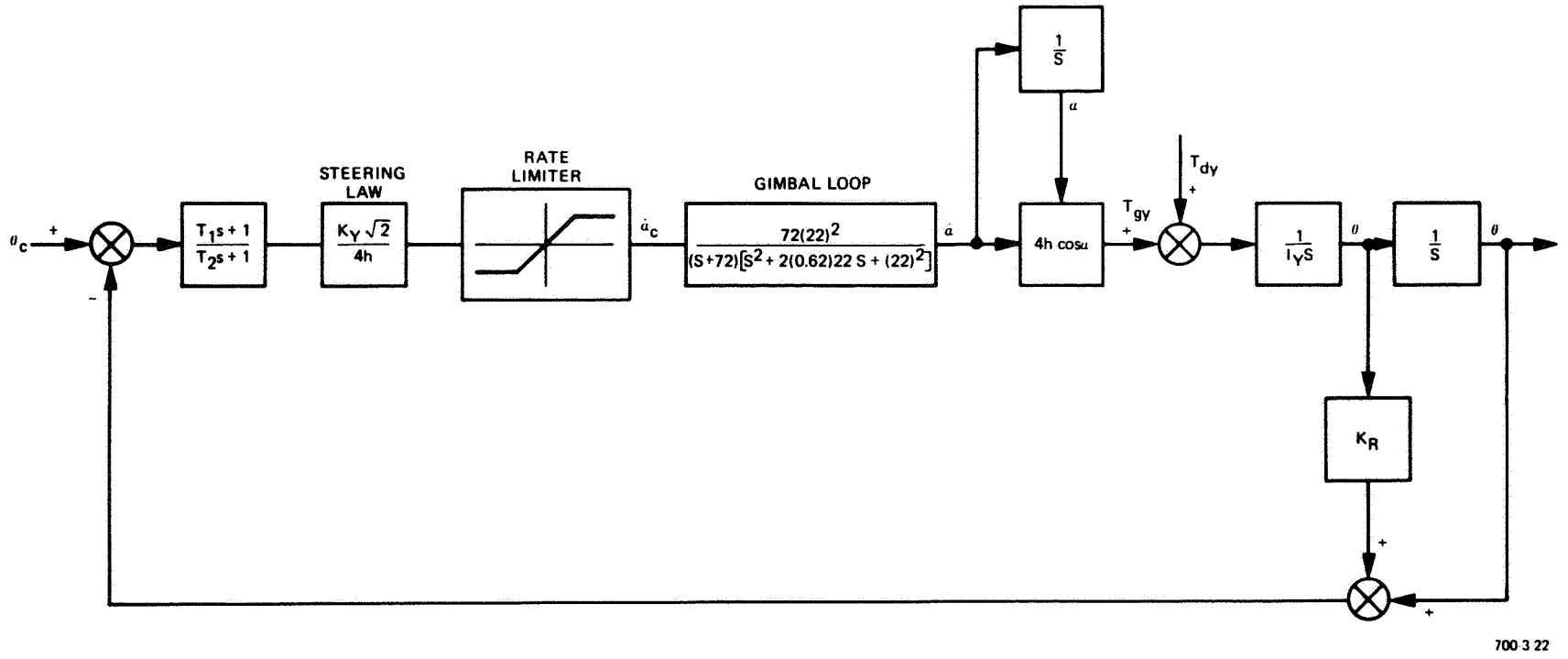

Figure 6-3
Overall Single-Axis Vehicle Loop Block Diagram

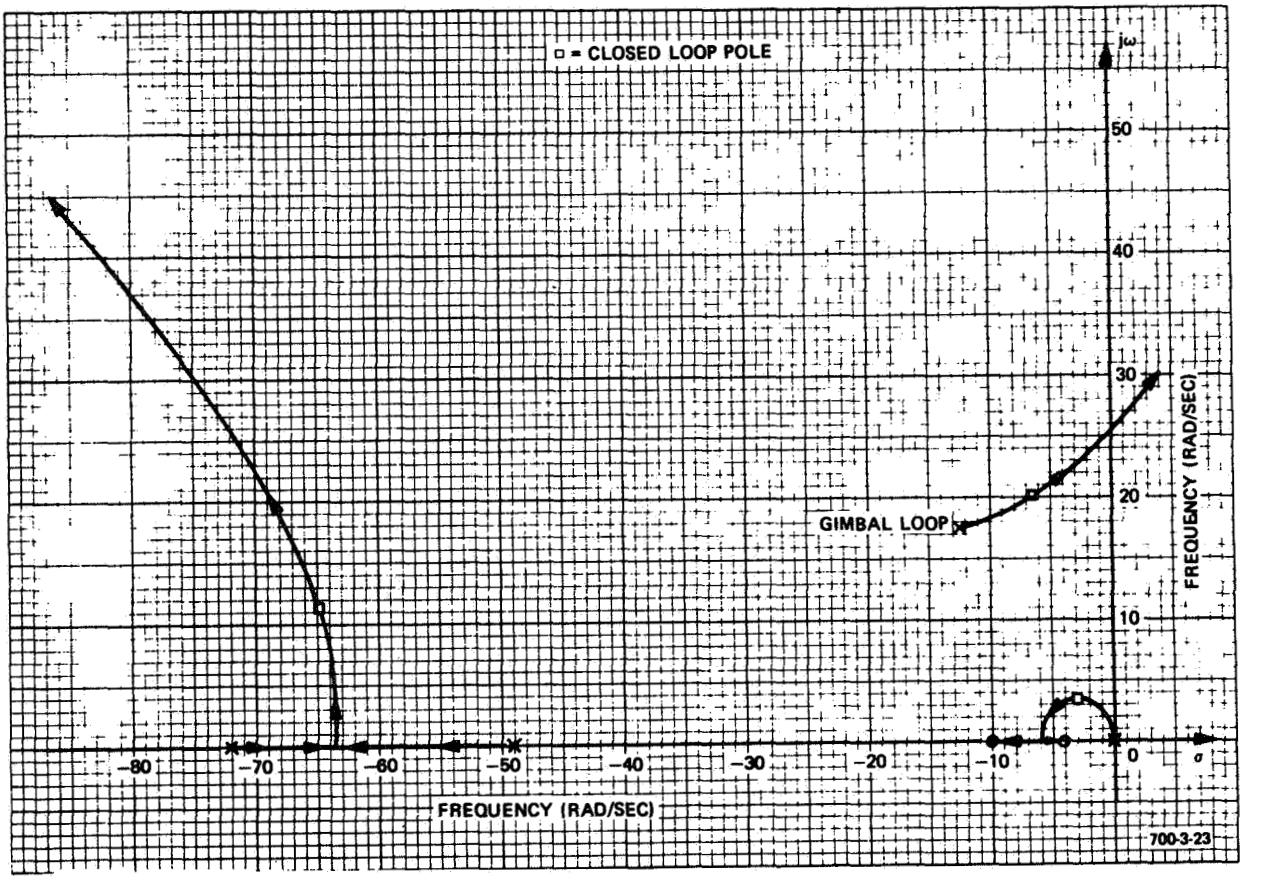

Figure 6-4
4-FACS Root Locus at Initial Gimbal Angles

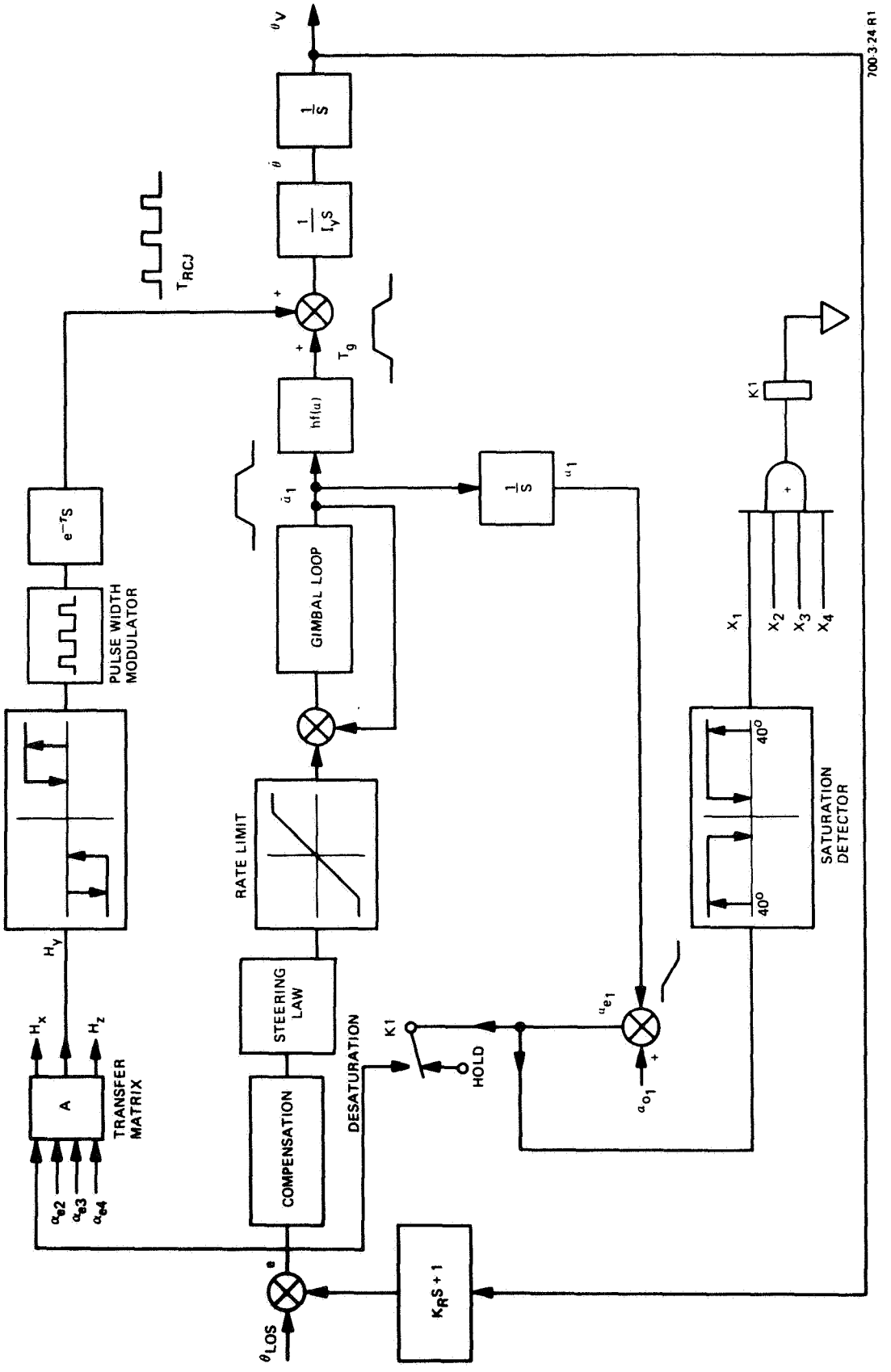

Figure 6-5
RJC Desaturation Block Diagram

Two principal methods of desaturation were considered in this study. The first and most direct method (Figure 6-1) is to close a gimbal position loop and command each gyro to return to its zero angular momentum position. As the gyros are driven to their initial angles, a torque is produced on the vehicle and the RJC system is used to cancel the torque and maintain attitude control. Relay K1 (Figure 6-1) disconnects the attitude error signal to the CMG's during desaturation. When the gyro angles reach their initial condition, relay K1 returns to the attitude hold position and the gyros must null out any remaining vehicle attitude rate. This remaining rate must be minimized because it creates a vehicle momentum which the gyros will be forced to absorb and thereby offset their initial angles. Analog computer studies were conducted to determine the ability of the system to re-orient the gyro to its null condition during combined axes desaturation; the results are presented in Subsection VII.E.

The second method (Figure 6-5) is to transform the gimbal angle errors to RJC pulse commands which cause the gyro to produce an opposing vehicle torque and thus unload its stored momentum. During desaturation, the RJC thrusters are pulse modulated at a duty cycle which allows the CMG system sufficient authority to maintain attitude control.

Although this method requires slightly more system complexity (angle transformation and pulse modulator), the vehicle rate can be maintained very low during desaturation since the CMG system maintains fine attitude control and subsequently the gyro angles can be returned very close to their initial angles (zero net momentum). An analog computer simulation was conducted and proved this method desaturated the gyros more thoroughly and in a more repeatable manner than the first technique.

E. UNMANNED (LOW TORQUE) SYSTEM

The unmanned system requiring lower bandwidths and control torques can eliminate some of the complexity present in the manned, higher response system. Since the gimbal loop bandwidth at approximately 22 rad/sec is much higher than the required outer loop bandwidth, 5 rad/sec, the lead compensation in the forward loop can be removed. Therefore, in Figure 6-1, $T_1 = T_2 = 0$ and only the gain K_x exists in the forward loop path.

Since very high attitude accuracy is desired and no integration is employed to "washout" an attitude error during a steady disturbance input, a lower limit, $K_{x(min)}$, must be placed on the compensation gain so that:

$$K_{x(min)} \geq \frac{T_{x(max)}}{\phi_e}$$

where

$T_{x(max)}$ = Maximum X-axis output torque (ft-lb)

ϕ_e = Allowable attitude error (radians)

For the design requirements of $T_{x(max)} = 2$ ft-lb and $\phi_e = 0.001$ deg, $K_{x(min)} \geq 1.15\ (10)^5$. Since the requirements are the same in all three axis K_y and K_z must also be equal to or greater than $K_{x(min)}$.

Another possible modification with the low torque system is to derive the feedback signals for the pseudo-torque feedback steering law directly from the gyro gimbal rates and angles, and thus, enclose the gyro within the steering law loop. This technique allows gyro nonlinearities to be included within the steering law computations and avoids errors due to neglecting the gimbal loop dynamics and nonlinearities. The inner steering law closed loop bandwidth can still be made faster than the outer vehicle loop, and thus achieve low cross-axis coupling.

Also, since lower control torque is needed, the CMG design can be altered to achieve a lighter weight configuration. This is discussed in detail in Subsection V.C.

SECTION VII

ANALOG COMPUTER SIMULATION

SECTION VII

ANALOG COMPUTER SIMULATION

The 4-FACS gyro configuration and vehicle dynamics were simulated on two interconnected Applied Dynamics/Four analog computers. Both the constant gain and the pseudo-torque feedback CMG steering laws were modeled. The gimbal loop was simplified by representing the torque motor current control loop section as a double lag. The RJC system output was represented by a torque step with a delay of 12 milliseconds and a minimum duration of 15 milliseconds. A three-axis, rigid-body vehicle was modeled. Analog computer diagrams are shown in Appendix D.

Torque disturbances and vehicle attitude commands were imposed on each individual axis with and without stored momentum in the system. These tests were run with three and four gyros operative with the constant gain steering law and with the pseudo-torque feedback steering law. Momentum desaturation methods were investigated for various combinations of stored momentum. Phases of the mission profile were simulated. A scissored pair system with one gyro failed was simulated to compare its behavior with that of the 4-FACS configuration with one gyro failed. Finally, the behavior of an unmanned, low-torque system with lower bandwidth requirements was investigated.

The results of the analog computer study are presented in the remainder of this section.

A. SINGLE-AXIS (NO STORED MOMENTUM) RESULTS - FOUR GYROS OPERATIVE

Two types of torque disturbances were imposed on the 4-FACS system employing a constant gain steering law: a step input of 25 ft-lb for one second and a sinusoidal input of 50 ft-lb peak-to-peak at a frequency of 1 Hz. The results are summarized in Table 7-1; analog computer traces of step input responses in the pitch axis are shown in Figure 7-1. The responses in the other two vehicle axes have the same characteristics because the loop gain is identical in each axis.

As shown in Table 7-1, a step torque input on a vehicle without a fine attitude control system (open loop) produces attitude rates and errors that are roughly ten times the rates and errors obtained in a vehicle using the 4-FACS CMG fine attitude control system (closed loop) employing a constant gain steering law. The same table shows that the gyro response characteristics, as would be anticipated, are the same in the three axes; the lower maximum gimbal rate in the pitch axis is due to the higher torque capability of the 4-FACS configuration in that axis. The sinusoidal torque disturbance that was imposed on the vehicle is representative of disturbance torques due to crew motion that can be encountered

in the course of a manned mission. Table 7-1 shows that the 4-FACS system in the simulated configuration holds attitude error to well within the desired limit of 0.1 deg/sec and exceeds the limit on attitude rate by 20 percent only when the disturbance is in the roll axis because of lower inertia in that axis.

Attitude step commands of 0.015 degree and 0.1 degree were imposed on each axis with a constant gain steering law employed. The results are summarized in Table 7-2 and computer traces of pitch axis step reponses are shown in Figures 7-2 and 7-3. Because of the lead compensation gain, an attitude command of 0.015 degree is the largest command for which gyro gimbal rates do not reach the limit. Attitude step commands of 0.1 degree rate-limit the gimbals, causing higher overshoots and longer peak times, as well as, producing large excursions of gyro gimbal angles.

TABLE 7-1

SINGLE-AXIS RESPONSE TO TORQUE DISTURBANCE - CONSTANT GAIN STEERING LAW

Input			Pitch	Roll	Yaw	Unit
Step Input	Attitude Rate	Open Loop	0.0256	0.0796	0.0239	Deg/Sec
		Closed Loop	0.00325	0.008	0.0025	Deg/Sec
	Attitude Error	Open Loop	0.0128	0.0398	0.0119	Deg
		Closed Loop	0.00122	0.0035	0.0011	Deg
	Maximum Gimbal Rate		0.0525	0.075	0.075	Rad/Sec
	Peak Time		0.23	0.23	0.225	Sec
	Overshoot		18	18	18	Percent
Single Sine Input	Maximum Attitude Rate		0.00375	0.0120	0.0035	Deg/Sec
	Maximum Attitude Error		0.00063	0.0020	0.00067	Deg
	Maximum Gimbal Rate		0.0505	0.0720	0.0687	Rad/Sec
Step Input of 25 ft-lb for 1 second Sinusoidal Input of 50 ft-lb peak-peak at 1 Hz						

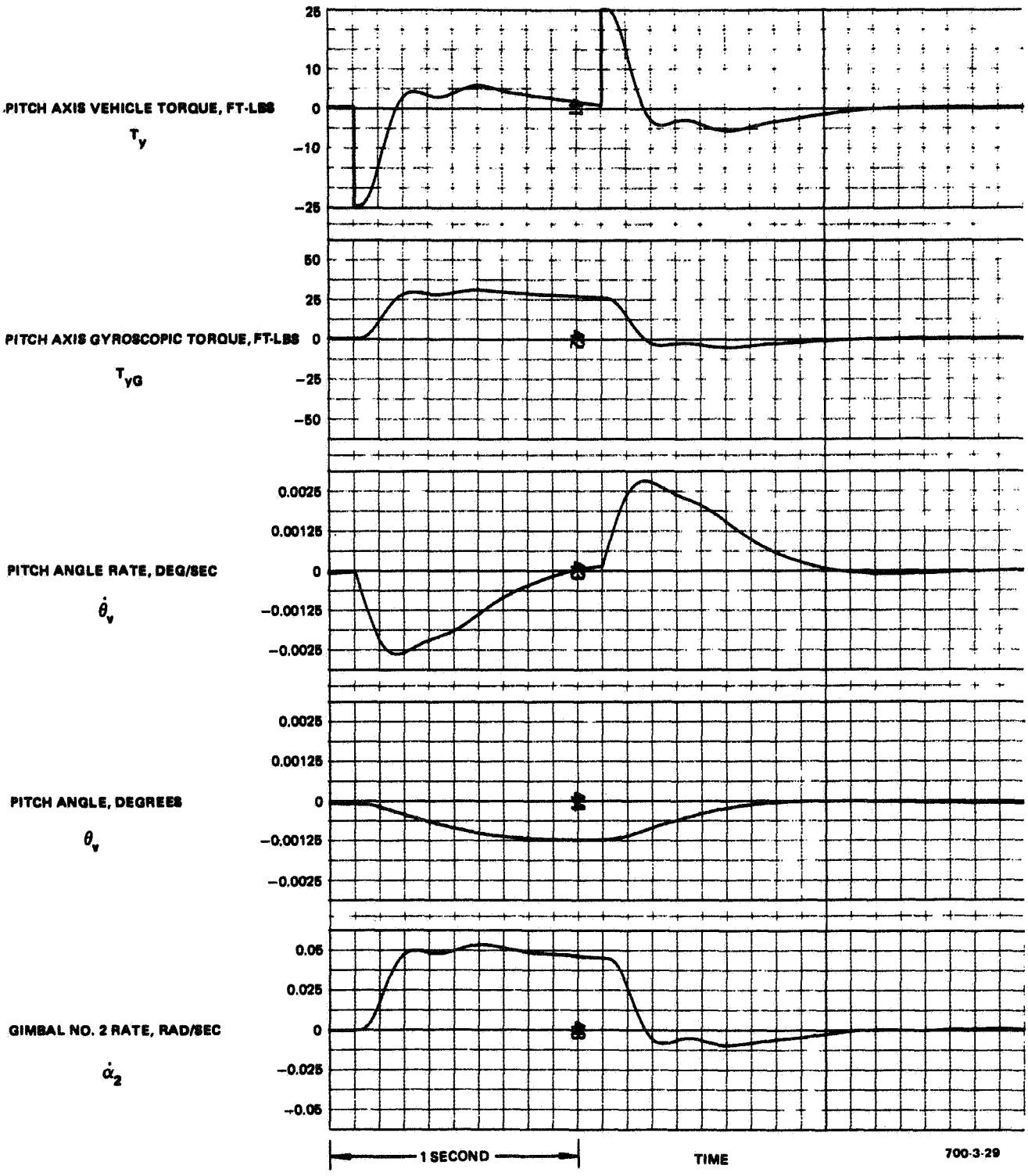

Figure 7-1
Step Torque Disturbance of 25 foot-pounds on
Pitch Axis for 1 second, Constant Gain Steering Law

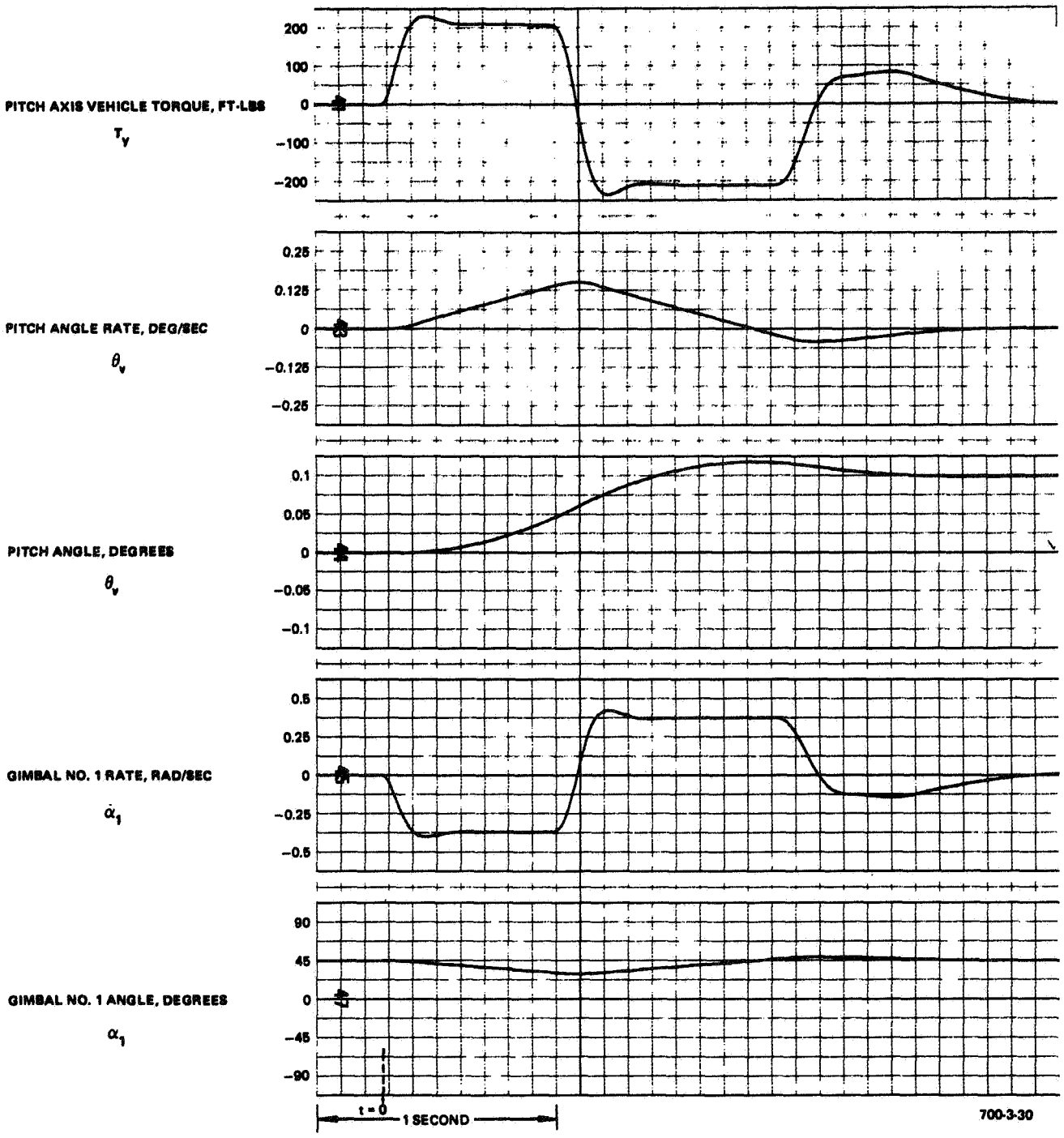

Figure 7-2
Step Response to Attitude Command of 0.1 degree in
Pitch Axis, Constant Gain Steering Law

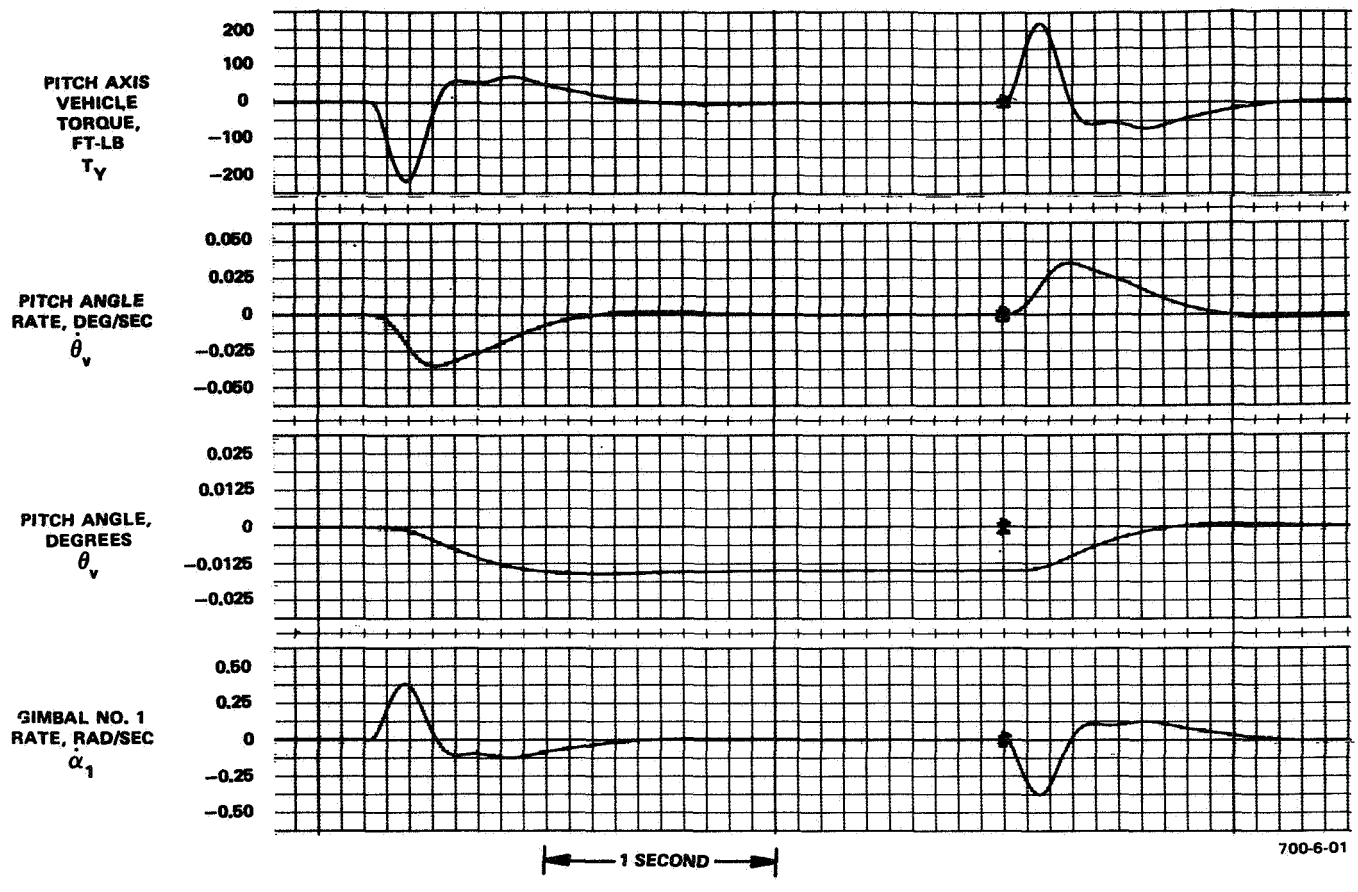

Figure 7-3
Step Response to Attitude Command of 0.015 degree in
Pitch Axis, Constant Gain Steering Law

TABLE 7-2

SINGLE AXIS ATTITUDE STEP
RESPONSE - CONSTANT GAIN STEERING LAW

Axis	Pitch (θ)		Roll (φ)		Yaw (ψ)		Units
Attitude Command	0.015	0.10	0.015	0.10	0.015	0.10	Deg
Maximum Attitude Rate	0.035	0.15	0.036	0.187	0.034	0.138	Deg/Sec
Attitude Peak Time	1.0	1.6	0.95	1.15	1.1	2	Sec
Attitude Overshoot	4.2	17.5	8.35	10.0	4.2	25	Percent
Maximum Torque	220	235	175	175	165	165	Ft-Lb
Maximum Gimbal Rate	0.382	0.425	0.424	0.424	0.400	0.400	Rad/Sec
Maximum Gimbal $\Delta\alpha$	4.5	15.75	0.8	9	4.5	20.2	Deg

Amplitude ratio and phase curves for the system with a constant gain steering law are shown in Figure 7-4. The frequency response is identical in each axis since the loop gain is the same. The curves show the system has a closed loop bandwidth of 3.9 Hz which is adequate to meet the design requirements of 3.0 Hz. The rise and dip at low frequencies are due to the inexact cancellation of the system compensation zeros and poles near the origin.

The pseudo-torque feedback steering law does not change appreciably the behavior of an uncoupled system (one in which no momentum is stored) because its only effect under these conditions is to add a pole at 200 rad/sec. The response to a step torque disturbance in the pitch axis for a system with pseudo-torque feedback steering law is shown in Figure 7-5. Comparison with Figure 7-1 shows the similarity in behavior between the two steering laws when zero momentum is stored.

B. SINGLE-AXIS (NO STORED MOMENTUM) RESULTS - ONE GYRO FAILED

Failure of one gyro causes the initial positions of the other three gyros to be modified. If the gains in the steering law are not modified accordingly, the loop gain when using the constant gain steering law will be reduced by 39 percent in the Y axis and 29 percent in the other two axes. If the pseudo-torque feedback steering law is adopted instead, no loss in bandwidth due to the loss of a gyro occurs because the steady-state value of gyroscopic torque is always equal to the steady-state value of commanded torque with no loss in loop gain. The frequency response of a three-gyro, uncoupled system using a constant gain steering law and the frequency response of the same system with a pseudo-torque feedback steering law is presented in Figure 7-6. The pseudo-torque feedback steering law has the effect of making the bandwidth of a three-gyro system the same as the bandwidth of a four-gyro system without requiring changes to the steering law matrix gains after a gyro fails.

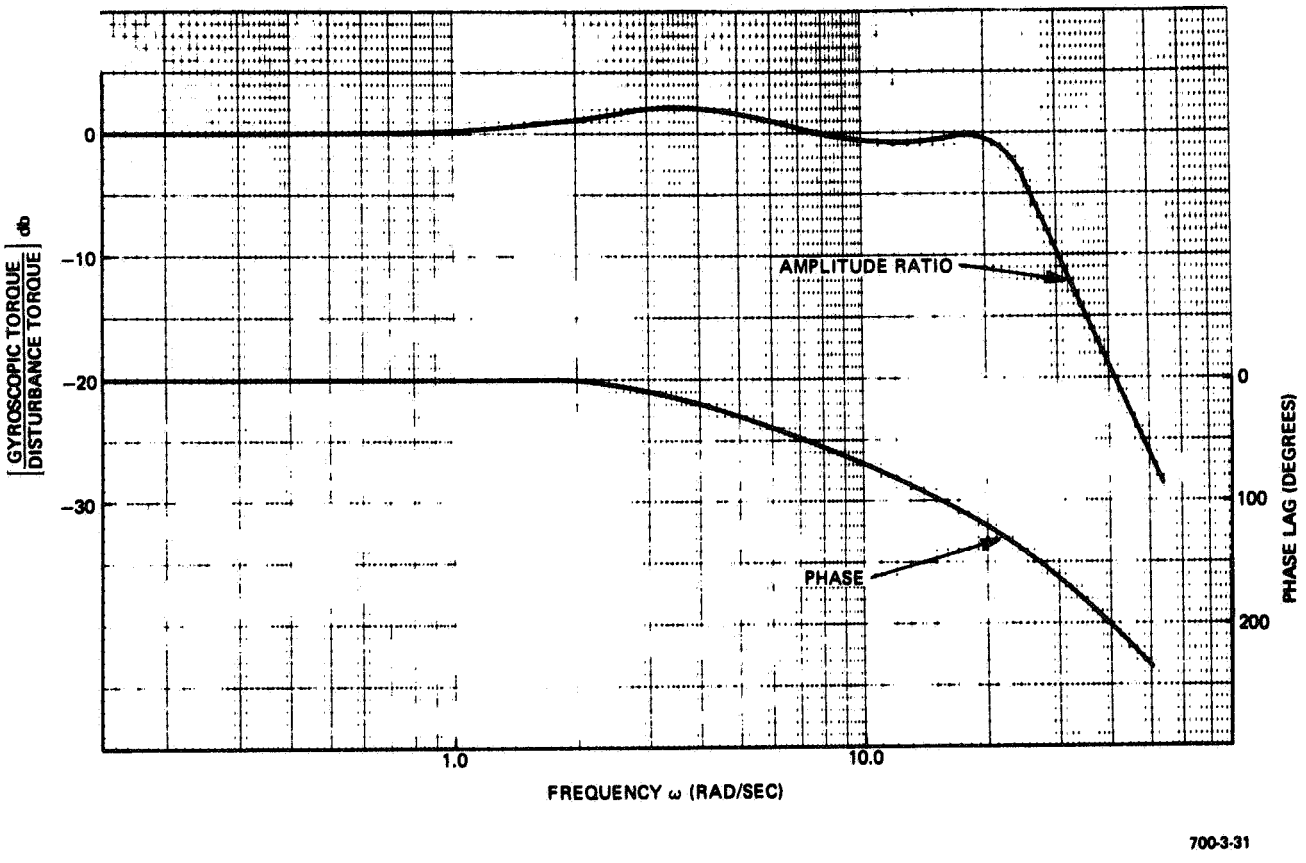

Figure 7-4
4-FACS Frequency Response, Initial Gimbal Angles, Constant Gain Steering Law

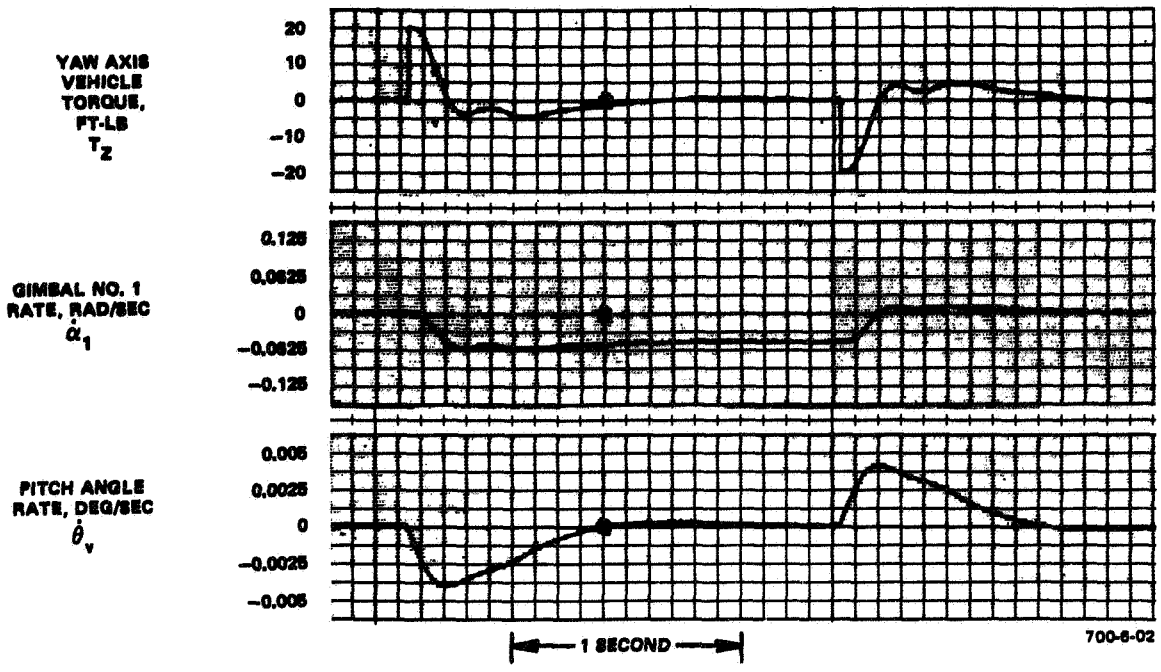

Figure 7-5
Step Torque Disturbance of 20 foot-pounds on
Yaw Axis, Pseudo-Torque Feedback Steering Law

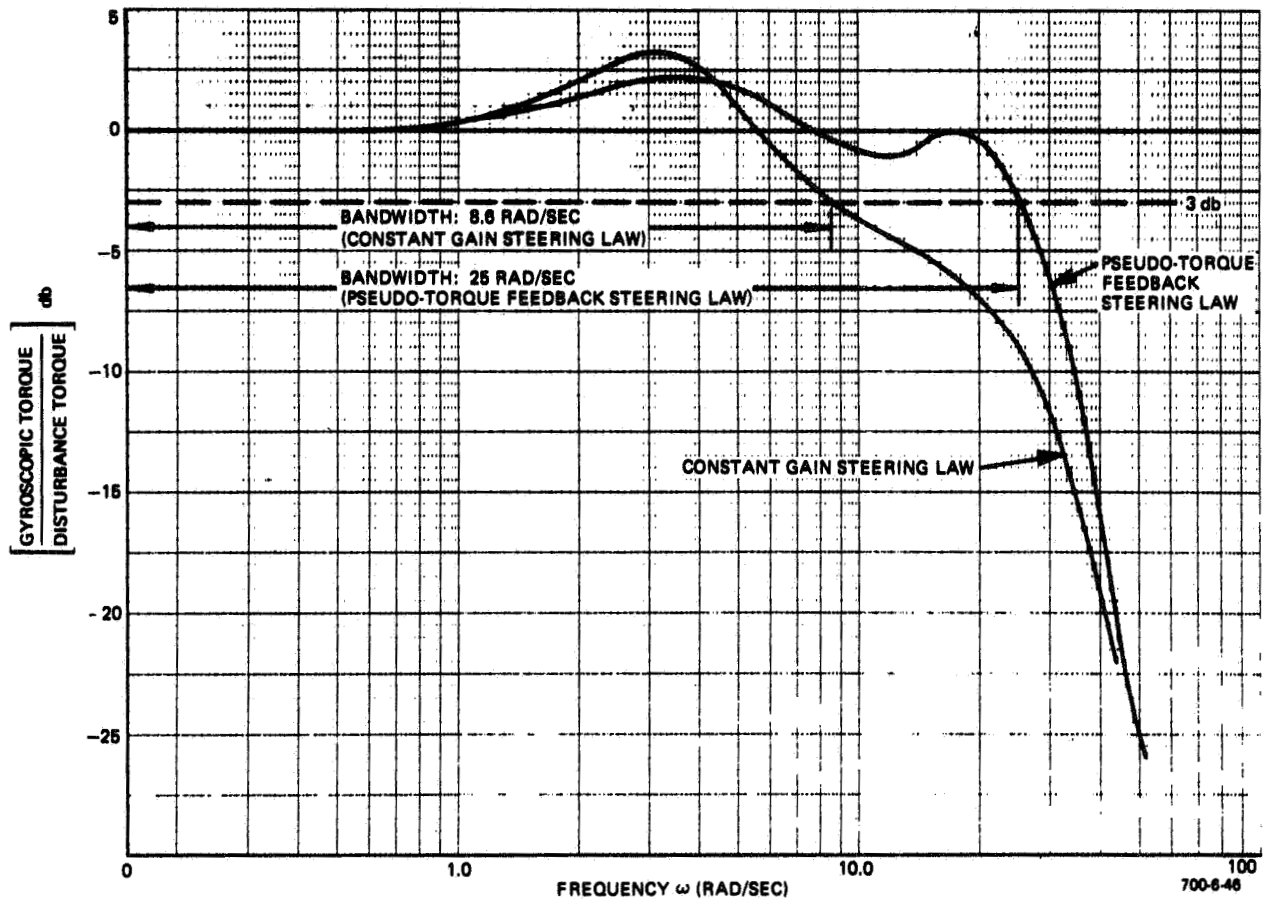

Figure 7-6
4-FACS Frequency Response, Gyro No. 1 Failed,
Comparison between Constant Gain and Pseudo-
Torque Feedback Steering Law, No Stored Momentum

Step torque disturbances of 20 ft-lb were imposed on a system with one gyro failed. The response of a system with constant gain steering law is shown in Figure 7-7; the response of a system with pseudo-torque feedback steering law is shown in Figure 7-8. The loss in loop gain with the constant gain steering law is evidenced by the larger peak time and consequently higher vehicle rate. The response of an uncoupled system to step torque disturbances for the various configurations studied is presented in Table 7-3. Although an uncoupled system with one failed gyro and the constant gain steering law still satisfies the maximum rate requirements, its performance is improved considerably by using the pseudo-torque feedback steering law.

Attitude step commands of 0.015 degree were imposed on each axis. The system response with constant gain steering is shown in Figure 7-9; the response when employing pseudo-torque feedback steering law is shown in Figure 7-10. Here again the lower loop gain of the constant gain steering law configuration is evident.

C. THREE-AXIS RESULTS - FOUR GYROS OPERATIVE

When momentum is stored in the system, the gimbal angles deviate from the ±45 degree initial positions and the constant gain steering law is not exact, thus causing cross-coupling between the axes, as discussed in subsection IV.C.

Typical responses to step torque disturbances with momentum stored in one axis and a constant gain steering law employed are shown in Figure 7-11 and 7-12. The effect of storing momentum is summarized in Figures 7-13 and 7-14. The effect of cross-coupling on vehicle rate is particularly noticeable: for large amounts of stored momentum, vehicle rate in the cross-axis is so large that it exceeds the magnitude of the in-axis rate. In all cases considered, however, attitude rate and error remained below the "design mission" limits.

The amount of cross-coupling is drastically reduced when the pseudo-torque feedback steering law is employed, as shown in Figure 7-15. The effect of the pseudo-torque feedback steering law on cross-coupling is summarized in Figures 7-16 and 7-17.

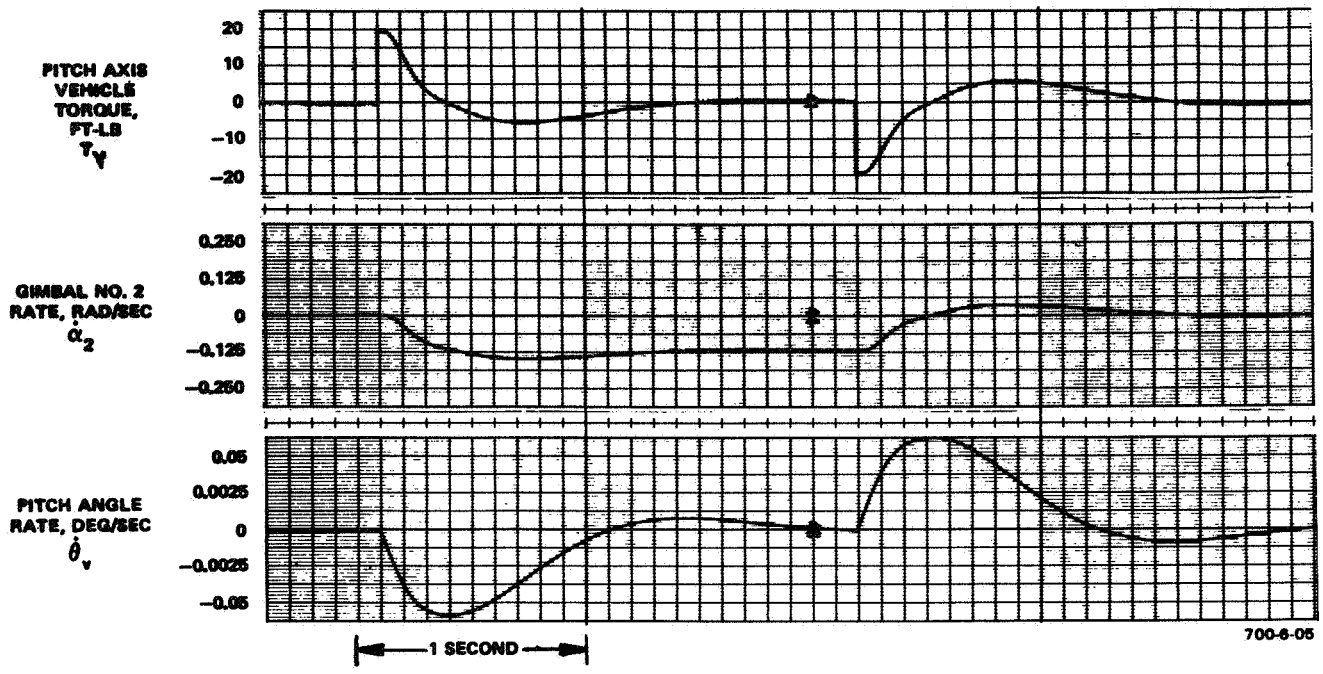

Figure 7-7
Step Torque Disturbance of 20 foot-pounds on Pitch Axis, Gyro No. 1 Failed, Constant Gain Steering Law

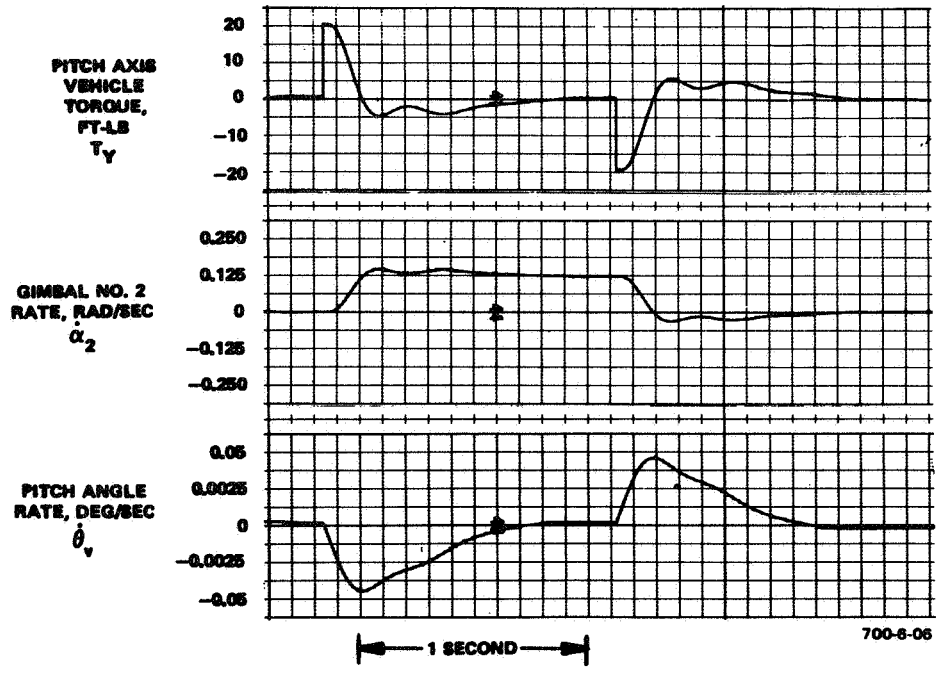

Figure 7-8
Step Torque Disturbance of 20 foot-pounds on Pitch Axis, Gyro No. 1 Failed, Pseudo-Torque Feedback Steering Law

TABLE 7-3

SINGLE-AXIS RESPONSE TO TORQUE DISTURBANCE

	Steering Law	Pitch		Roll		Yaw		Unit
		4 Gyros	3 Gyros	4 Gyros	3 Gyros	4 Gyros	3 Gyros	
Attitude Rate	Constant Gain	0.0024	0.0029	0.0067	0.0075	0.00225	0.0025	Deg/Sec
	Torque Feedback	0.002	0.002	0.007	0.007	0.002	0.0023	
Maximum Gimbal Rate	Constant Gain	0.046	0.075	0.068	0.088	0.068	0.088	Rad/Sec
	Torque Feedback	0.043	0.075	0.059	0.088	0.059	0.088	
Peak Time	Constant Gain	0.23	0.70	0.23	0.58	0.225	0.58	Seconds
	Torque Feedback	0.23	0.23	0.23	0.23	0.23	0.23	
Overshoot	Constant Gain	18	27.5	18	26	18	26	Percent
	Torque Feedback	25	25	25	25	25	25	

NOTES: 1. Step Input of 20 Ft-Lb

2. No stored momentum

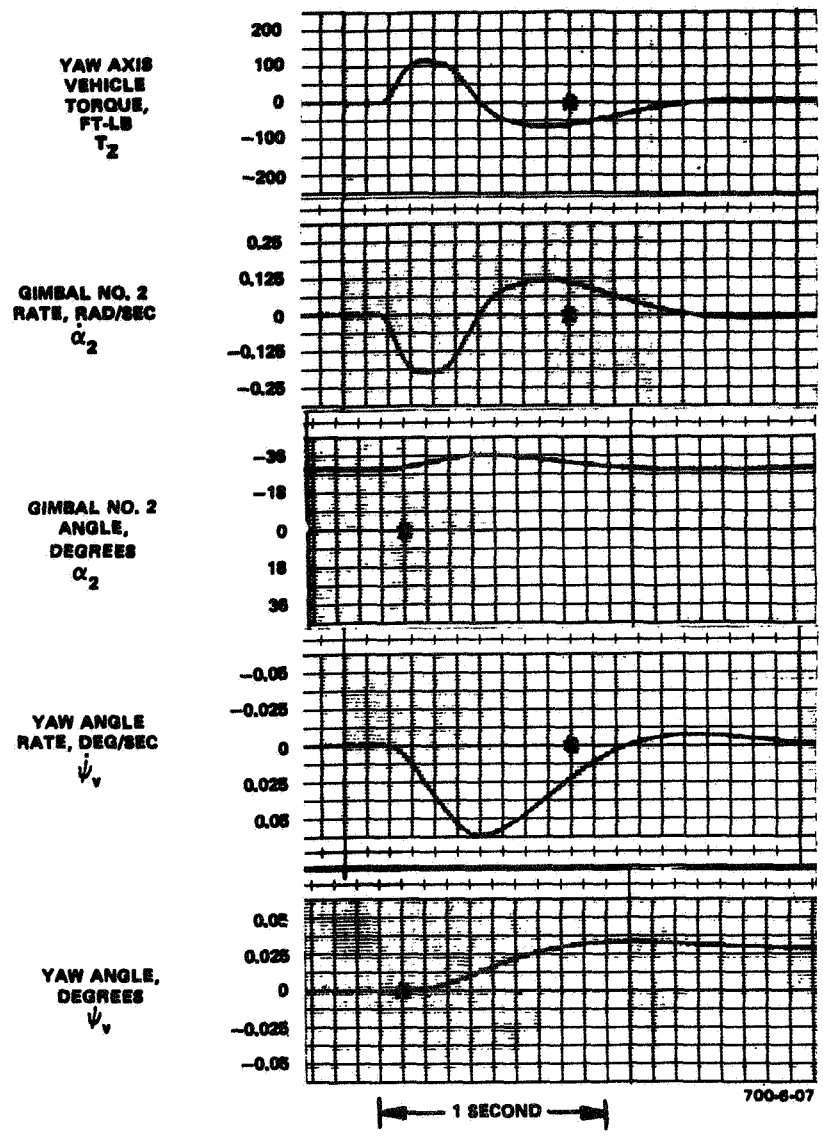

Figure 7-9
Step Response to Attitude Command of 0.015 degree in Yaw Axis, Gyro No. 1 Failed, Constant Gain Steering Law

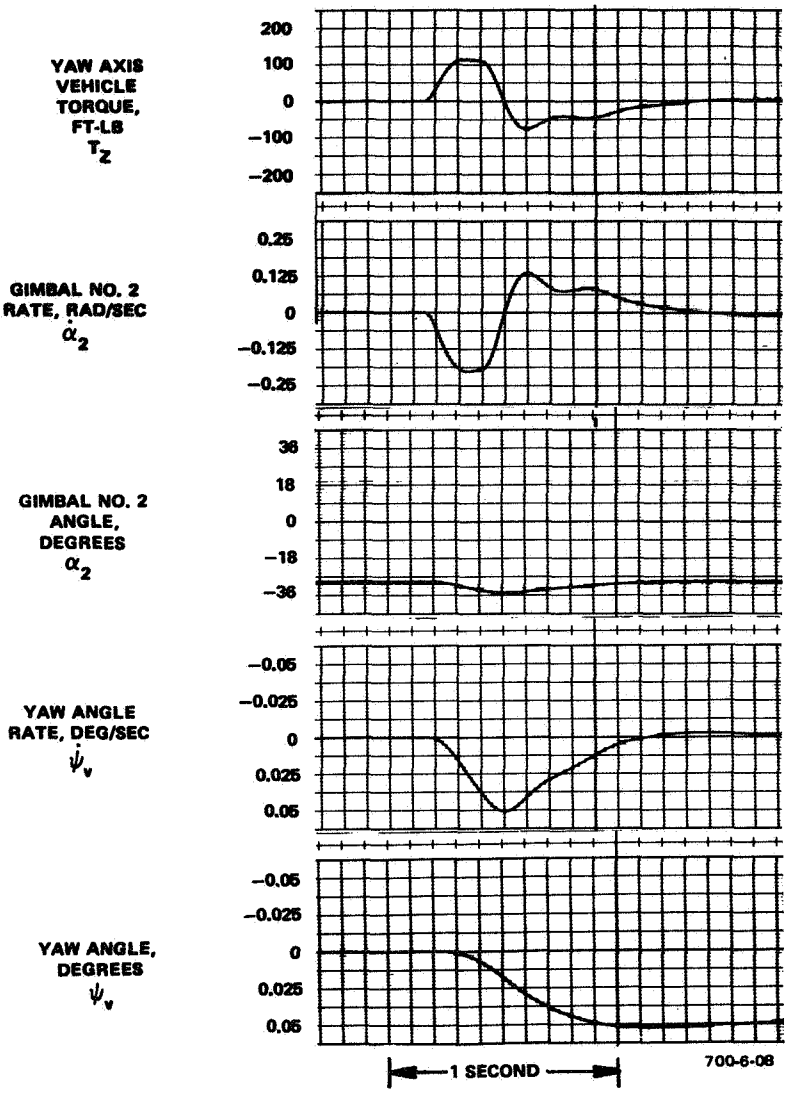

Figure 7-10
Step Response to Attitude Command of 0.015 degree in Yaw Axis, Gyro No. 1 Failed, Pseudo-Torque Feedback Law

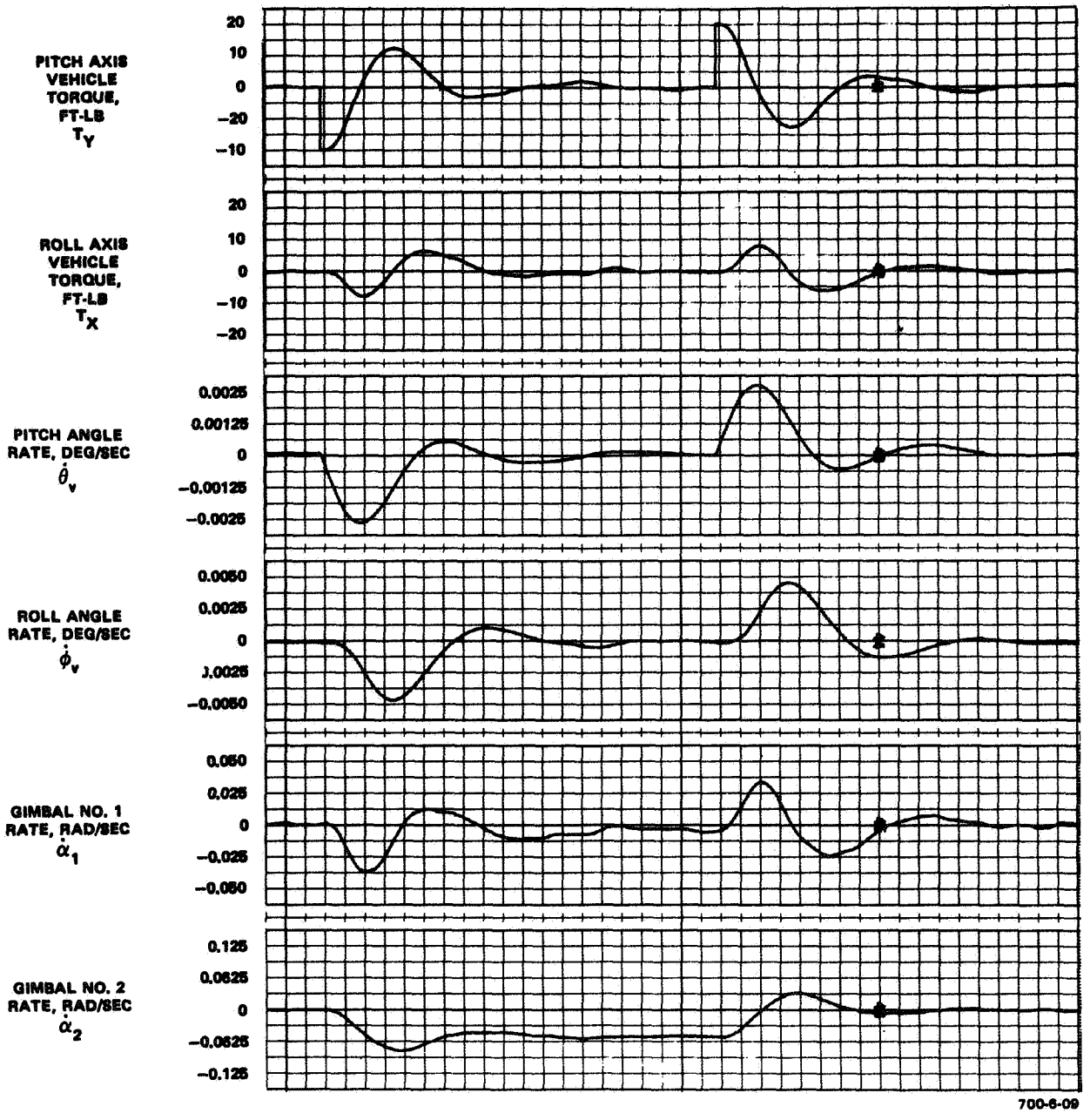

Figure 7-11
Step Torque Disturbance of 20 foot-pounds on Y-Axis for 2 seconds, $\left(\frac{H_z}{h}\right) = 1.145$, Constant Gain Steering Law

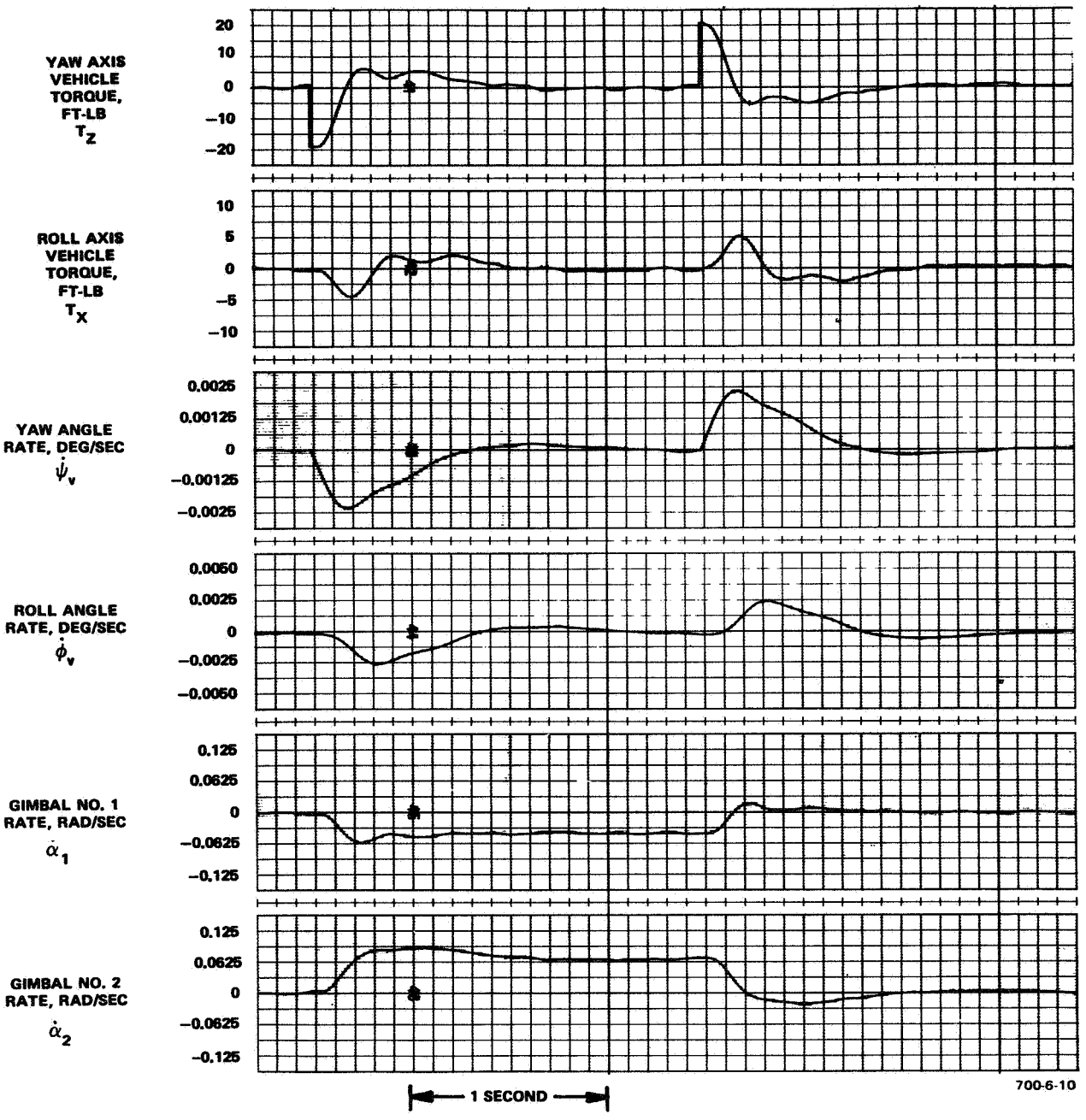

Figure 7-12
Step Torque Disturbance of 20 foot-pounds on Z-Axis for 2 seconds, $\left(\frac{H_v}{h}\right) = 0.73$, Constant Gain Steering Law

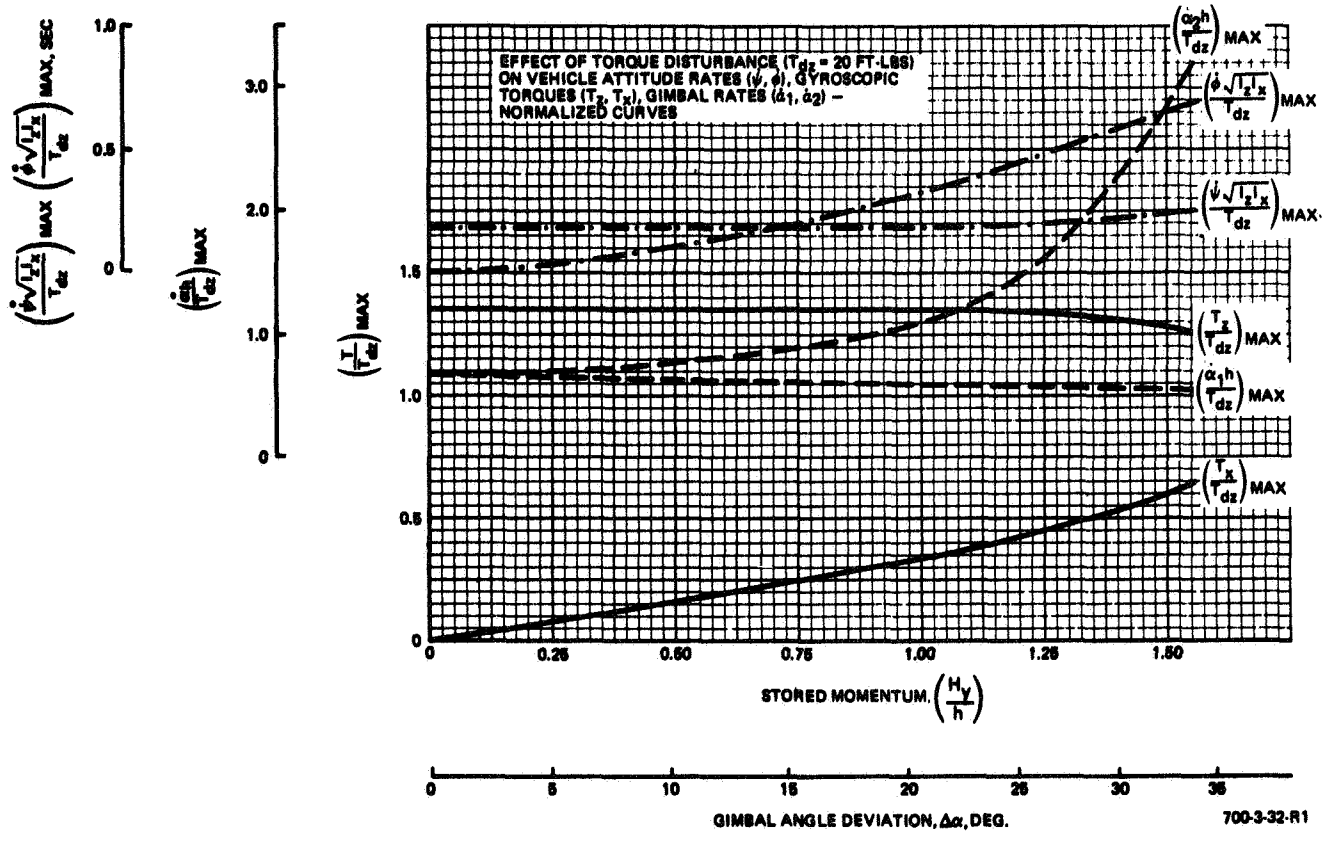

Figure 7-13
Step Response to Torque Disturbances, Stored
Momentum in Pitch (Y) Axis, Constant Gain Steering Law

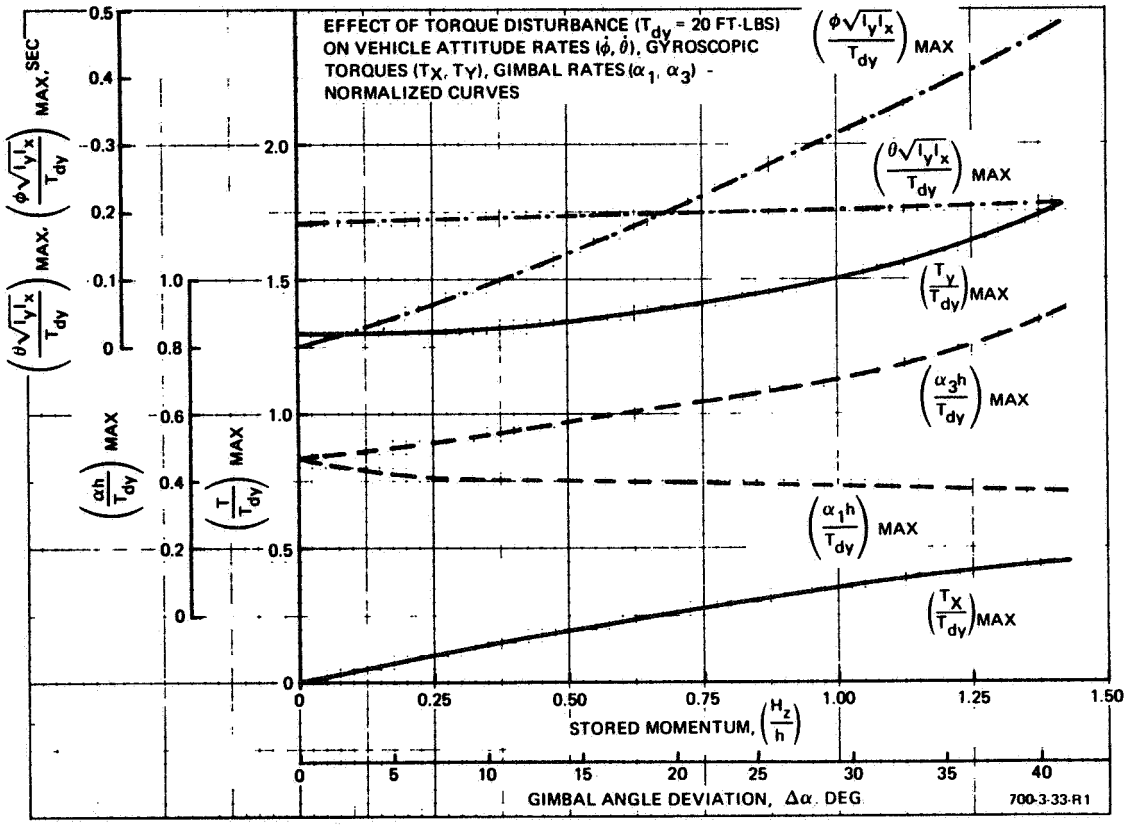

Figure 7-14
Step Response to Torque Disturbances, Stored Momentum in Yaw (Z) Axis, Constant Gain Steering Law

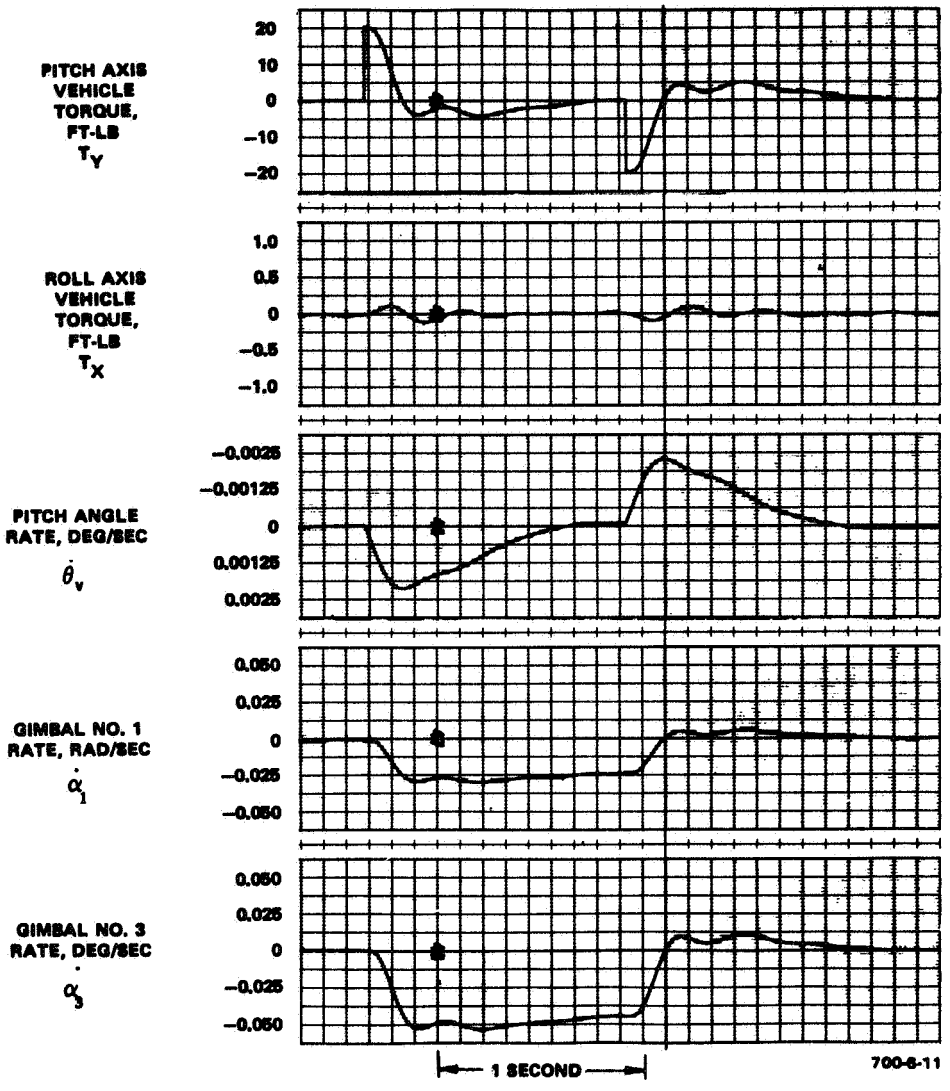

Figure 7-15
Step Torque Disturbance of 20 foot-pounds on Y-Axis,
$\left(\frac{H_Z}{h}\right) = 0.52$, Pseudo-Torque Feedback Steering Law

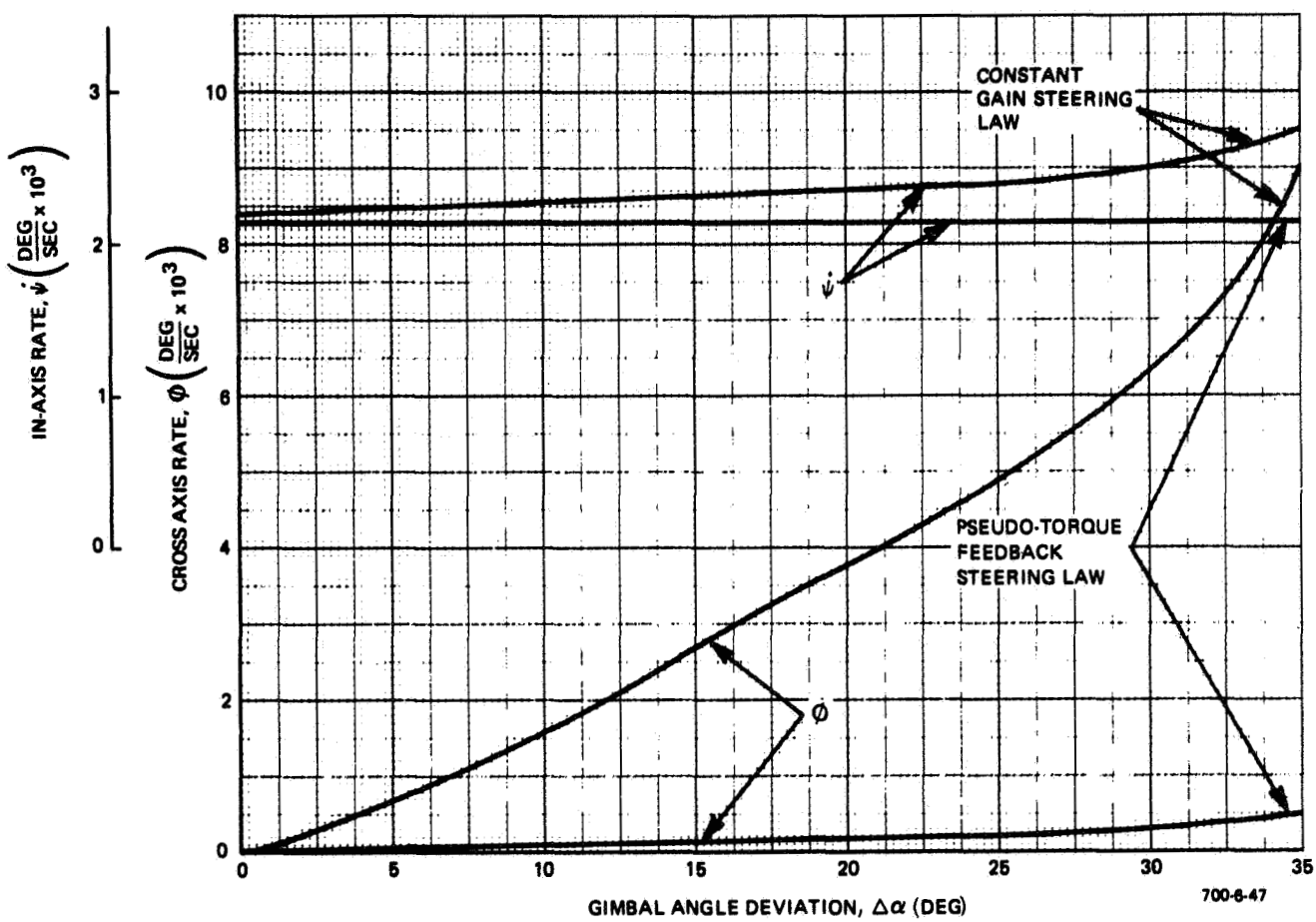

Figure 7-16
Vehicle Rate Response to Step Disturbance Torque,
Momentum Stored in Y-Axis, Step Torque
Disturbance of 20 foot-pounds in Z-Axis

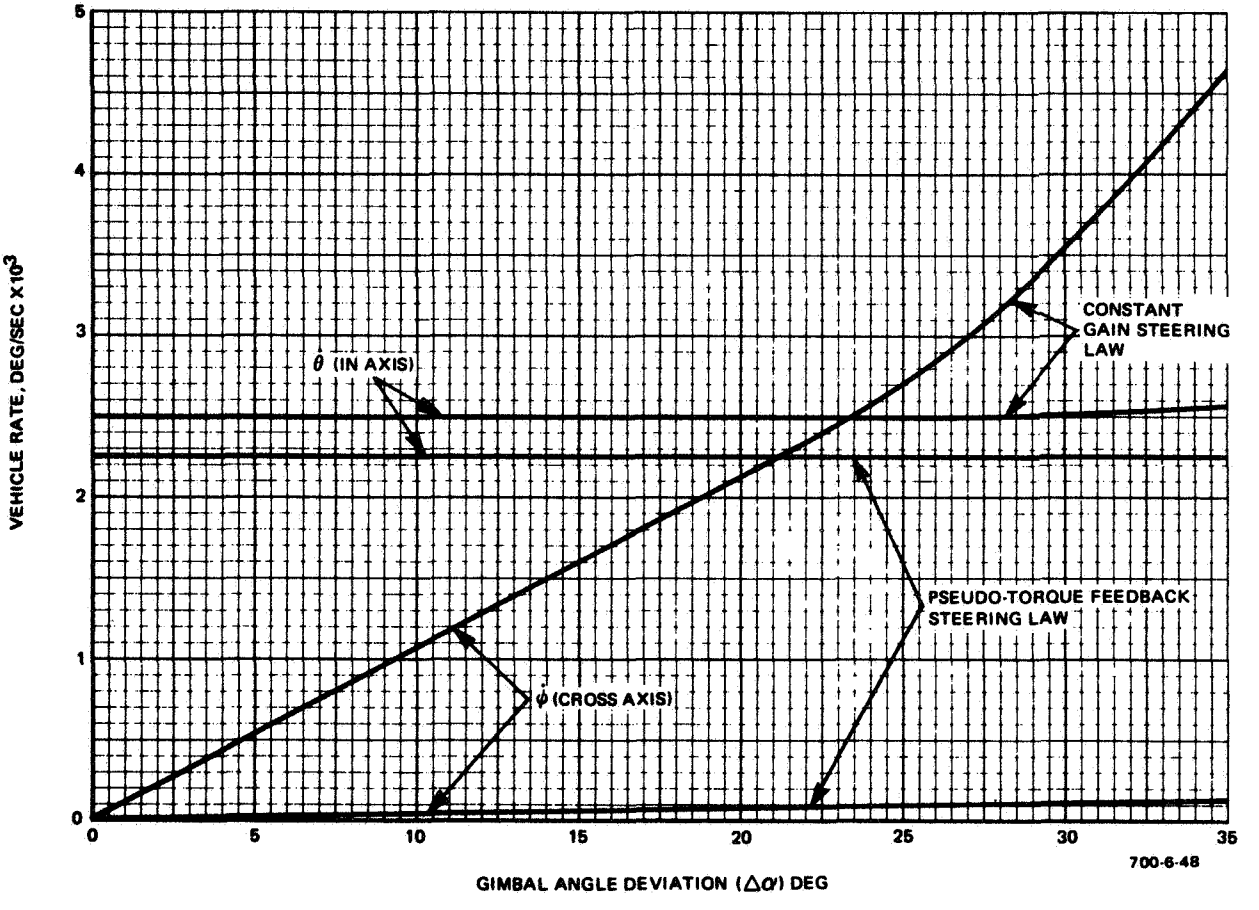

Figure 7-17
Vehicle Rate Response to Step Disturbance Torque,
Momentum Stored in Z-Axis, Step Torque
Disturbance of 20 foot-pounds in Y-Axis

Torque amplitude ratio and phase curves for the in-axis and cross-axis response with the constant gain steering law are shown in Figure 7-18 and 7-19 (input in Y axis) and in Figures 7-20 and 7-21 (input in Z axis). A significant amount of torque cross-coupling is within two octaves of the bandpass frequency - more so than is apparent from the step responses discussed previously. Stored momentum, however, does not affect the in-axis response as much.

When the pseudo-torque feedback steering law is adopted, stored momentum causes practically no cross-coupling even at high frequencies, and the in-axis response is also affected very little (Figure 7-22).

When the constant gain steering law is used (Figures 7-23 and 7-24), the gain margin of the system increases as more momentum is stored in one axis. (This characteristic was found to hold true also when momentum is stored in multiple axes.) The advantage of this characteristic is that each system axis can be designed independently as a single-axis system at zero stored momentum with the confidence that no point within the momentum envelope makes a system so designed unstable. When the pseudo-torque feedback steering law is adopted, the gain margin is 8 db in every axis and does not change when momentum is stored.

When an attitude step command is given in one axis with momentum stored in one axis, a system with constant gain steering law responds as shown in Figures 7-25 and 7-26. The amount of cross-coupling is reduced considerably when the pseudo-torque feedback steering law is employed (Figure 7-27). The effect of stored momentum in the Y axis on cross-axis vehicle rate for systems with constant gain and pseudo-torque feedback steering laws is summarized in Figure 7-28. With the pseudo-torque feedback steering law, the cross-axis rate does not exceed 0.01 degree/second. Similar results are obtained with momentum stored in the Z axis.

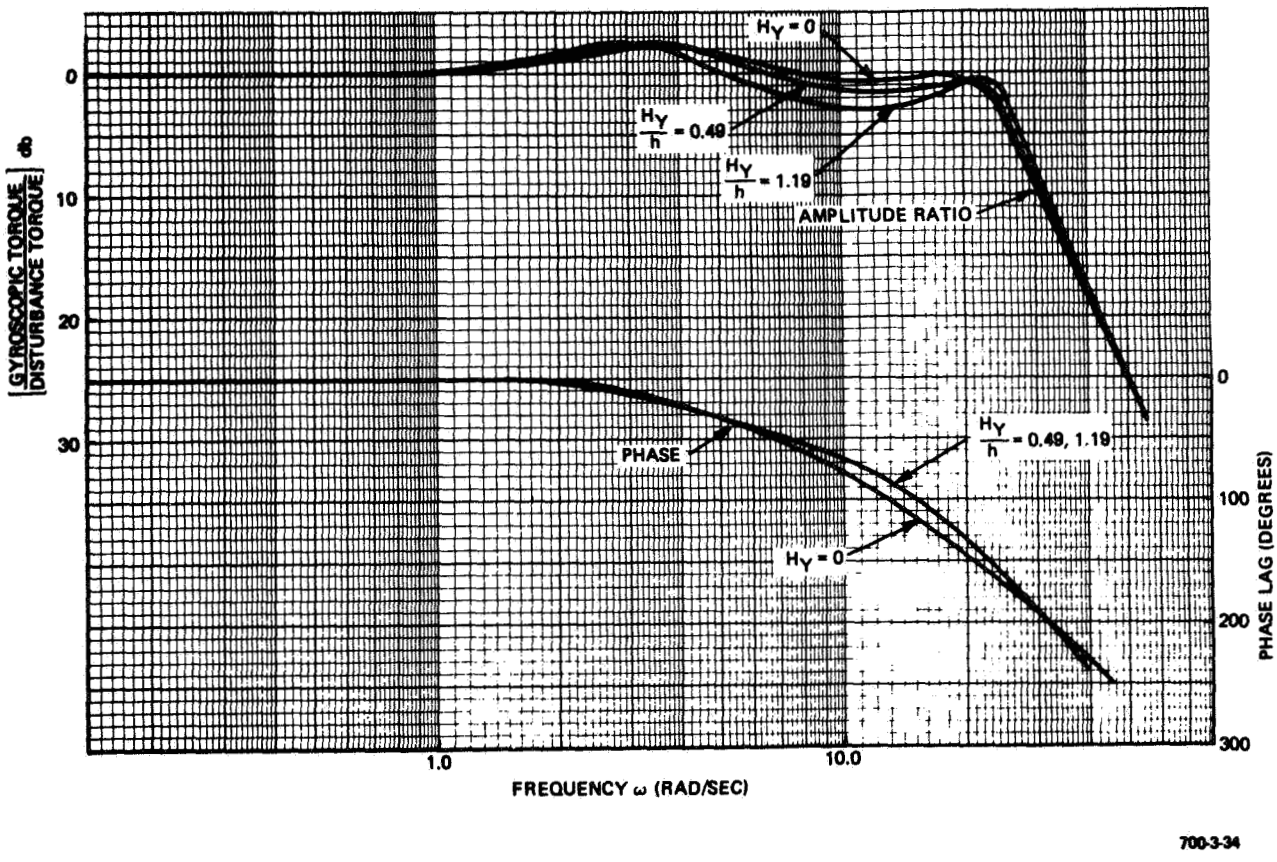

Figure 7-18
4-FACS Frequency Response, Effect of Stored Momentum in Pitch (Y) Axis, Response of In-Axis Torque, Constant Gain Steering Law

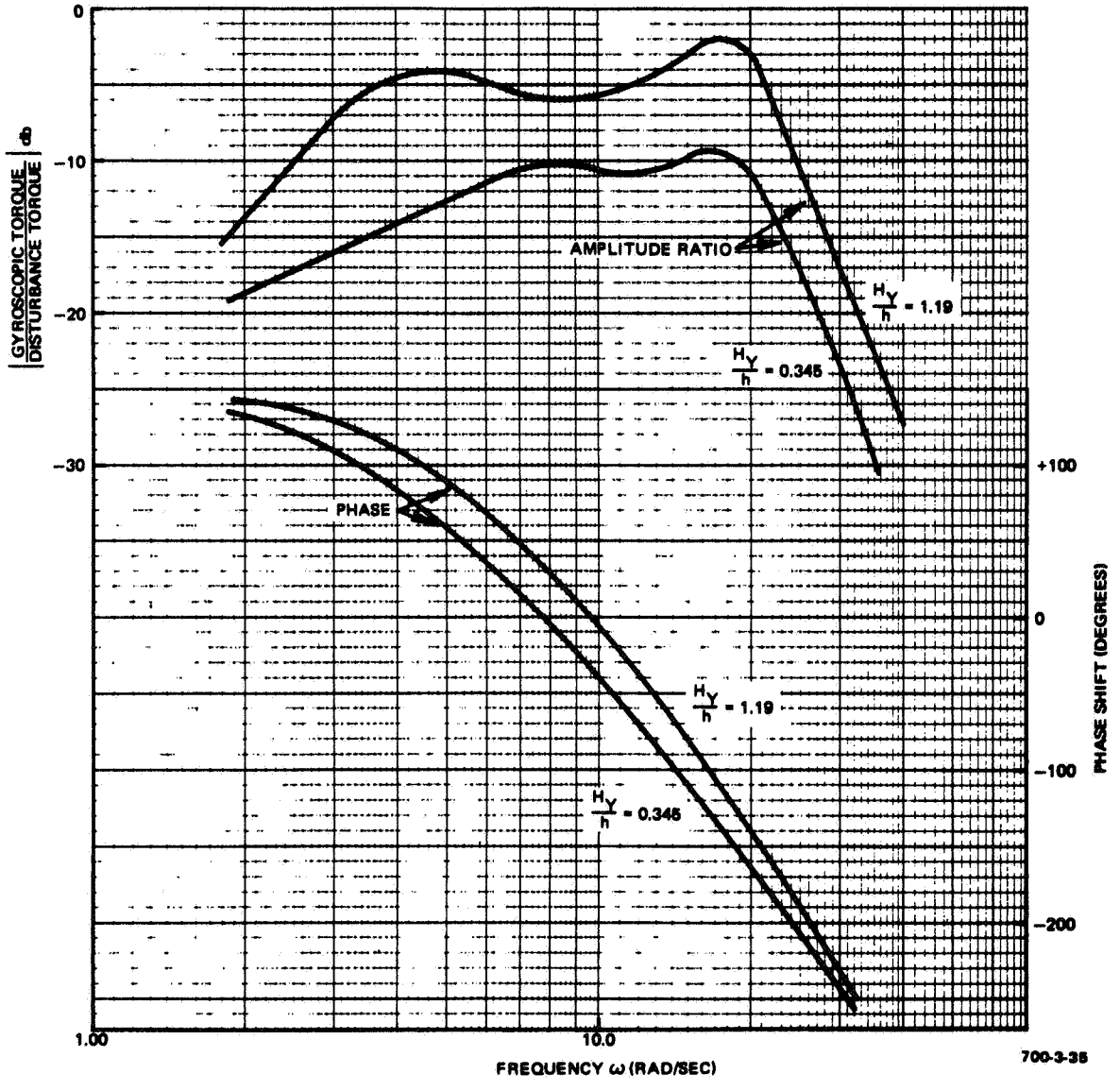

Figure 7-19
4-FACS Frequency Response, Effect of Stored Momentum in Pitch (Y) Axis, Response of Cross-Axis Torque, Constant Gain Steering Law

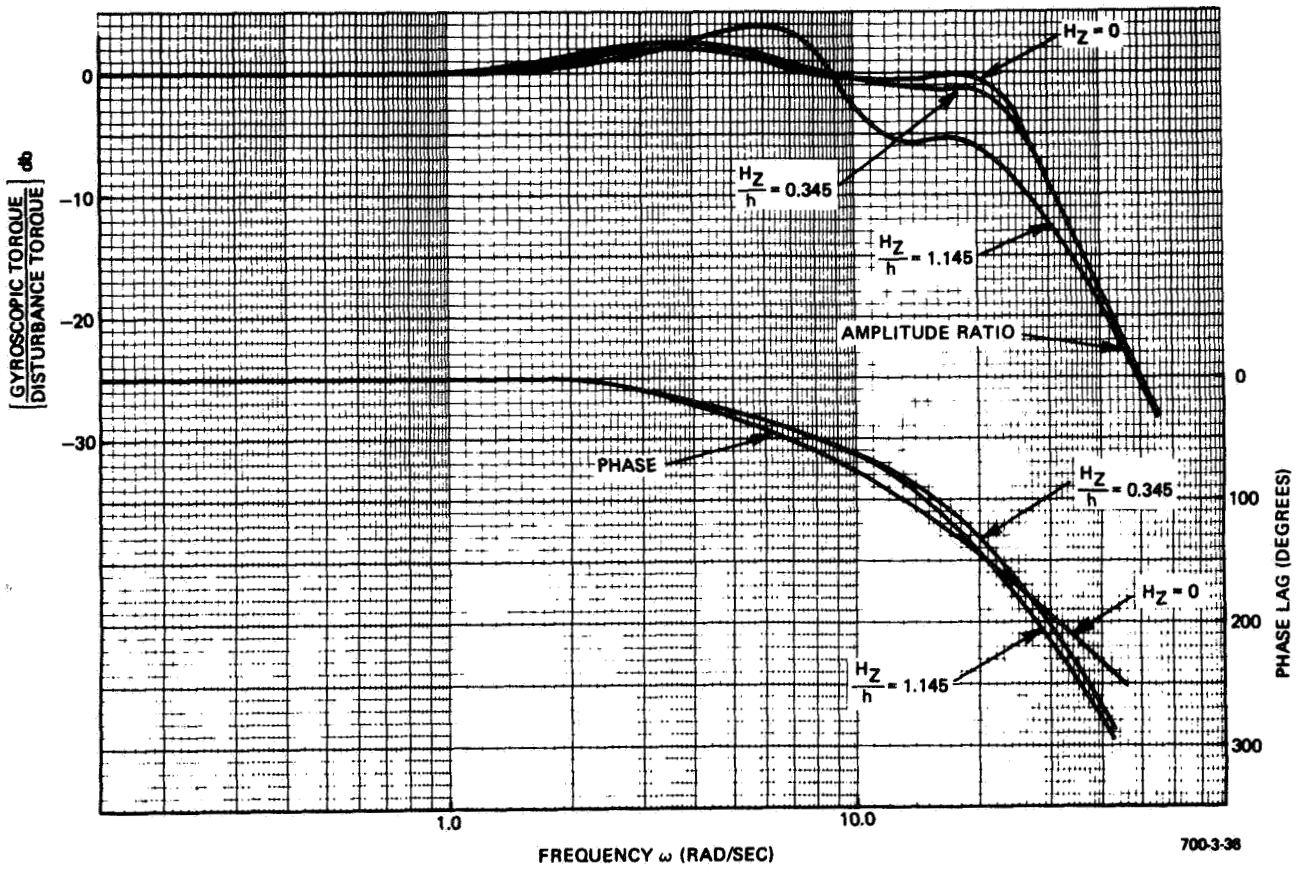

Figure 7-20
4-FACS Frequency Response, Effect of Stored Momentum in Yaw (Z) Axis, Response of In-Axis Torque, Constant Gain Steering Law

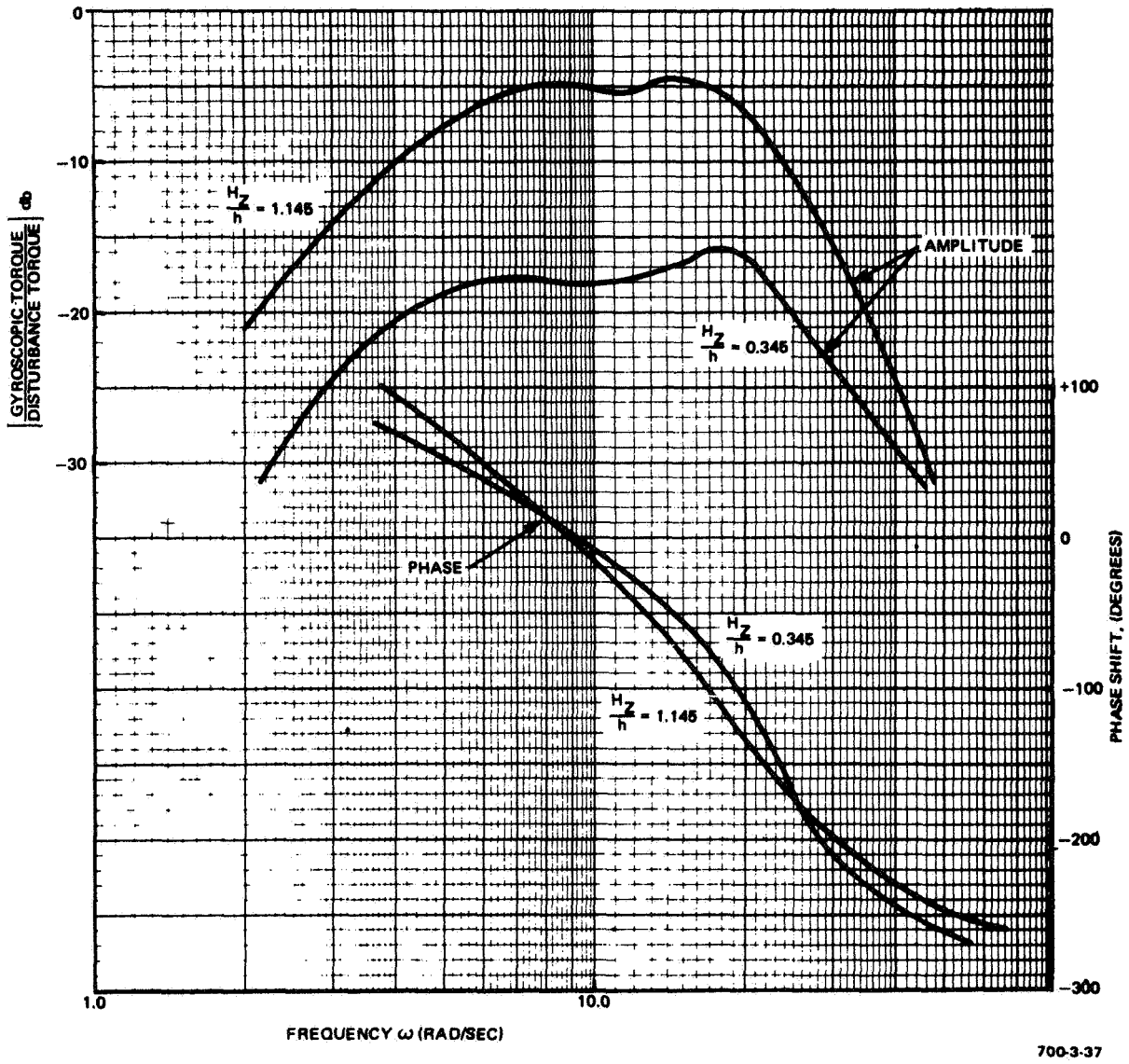

Figure 7-21
4-FACS Frequency Response, Effect of Stored Momentum in Yaw (Z) Axis, Response of Cross-Axis Torque, Constant Gain Steering Law

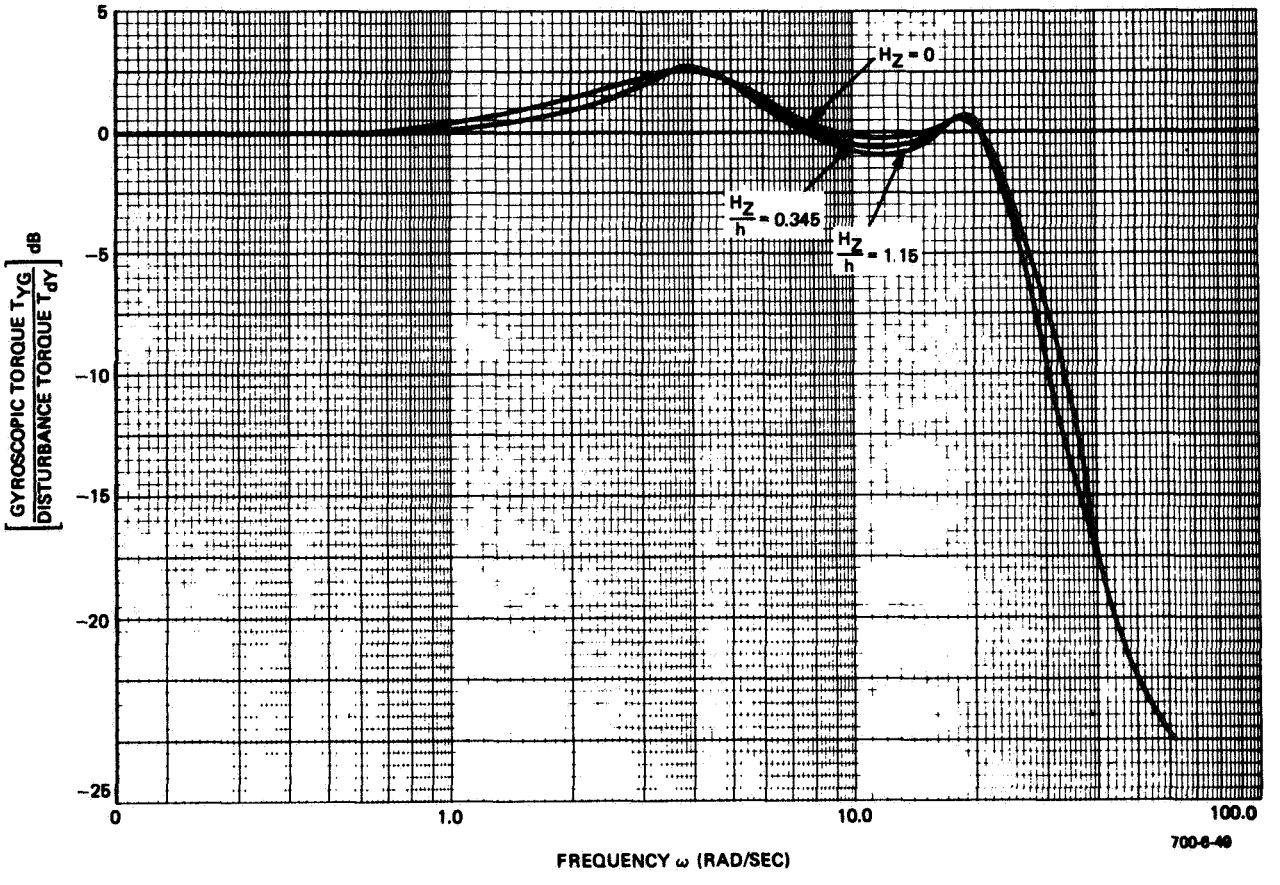

Figure 7-22
4-FACS Frequency Response, Pseudo-Torque Feedback Steering Law,
Effect of Stored Momentum in Vehicle Z-Axis, In-Axis Response

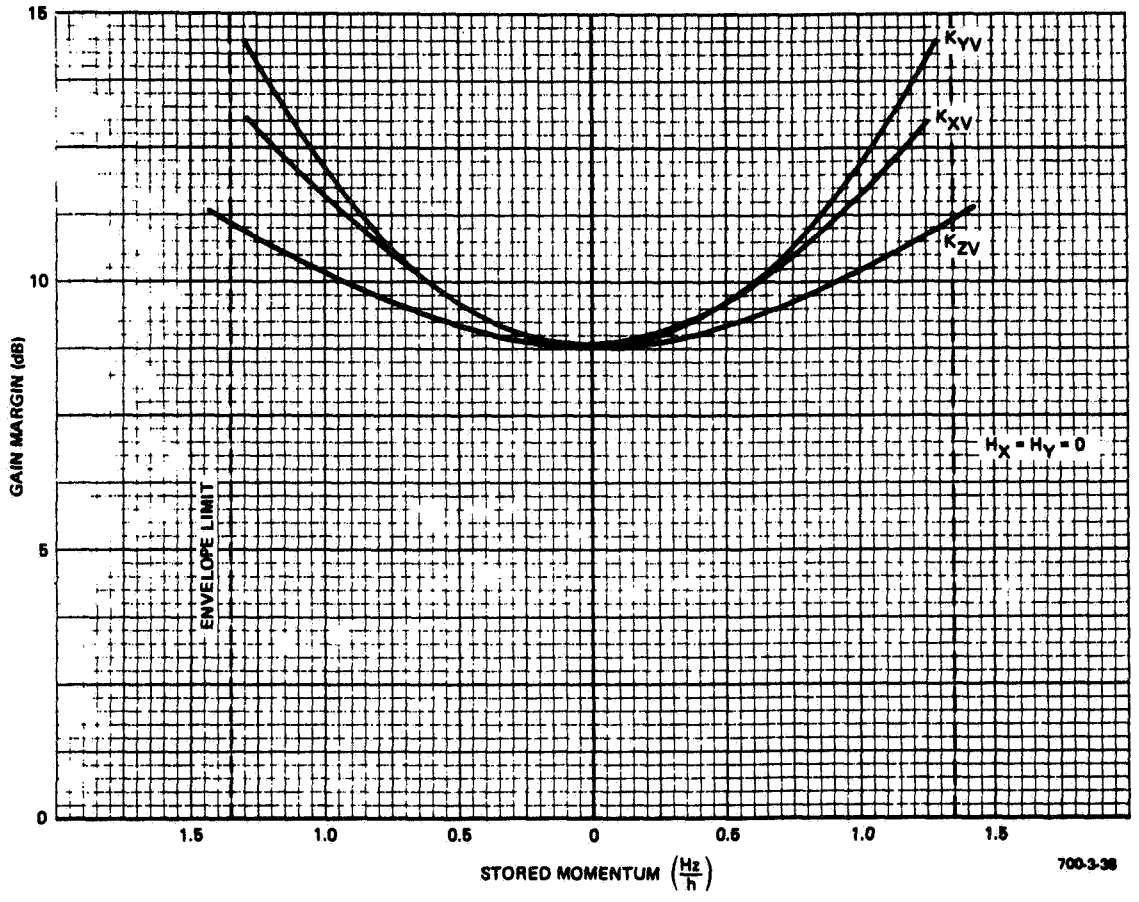

Figure 7-23
Effects of Stored Momentum in Z-Axis on
Stability Margin, Constant Gain Steering Law

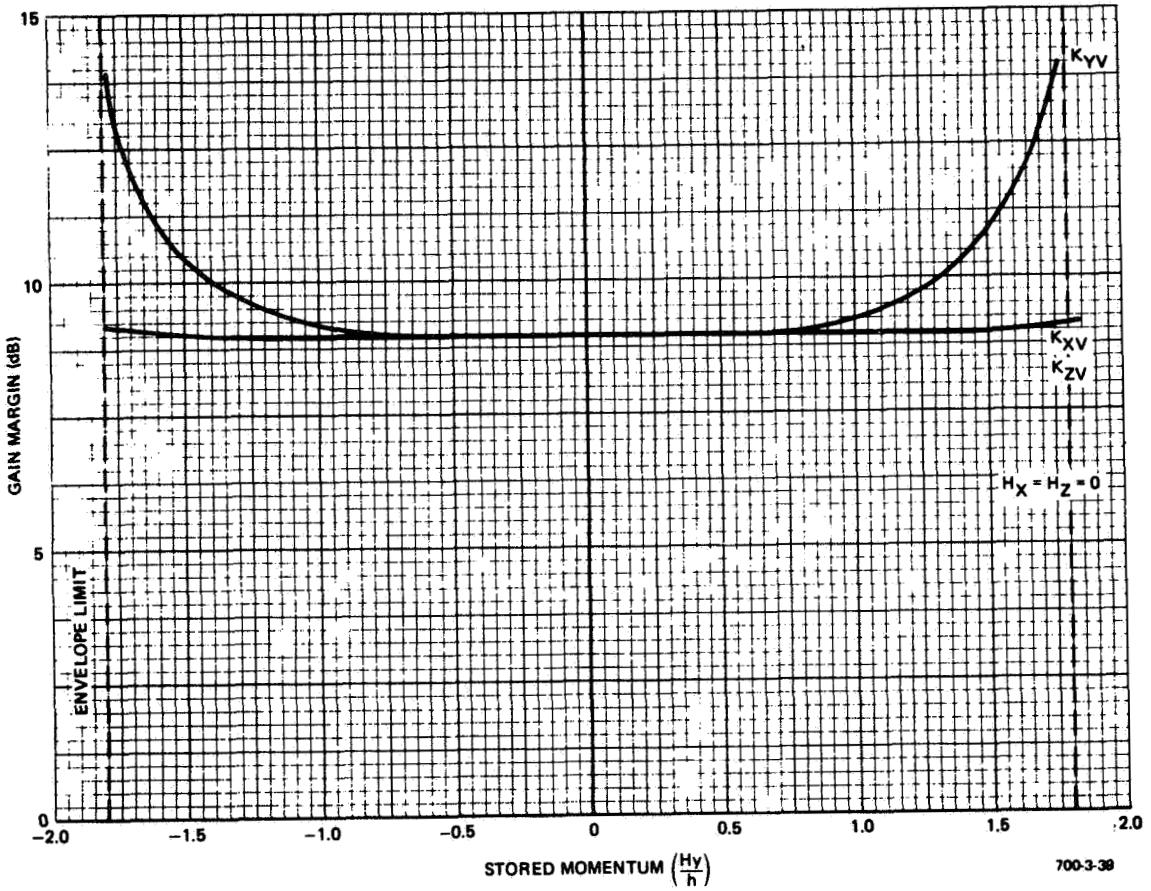

Figure 7-24
Effects of Stored Momentum in Y-Axis on Stability Margin, Constant Gain Steering Law

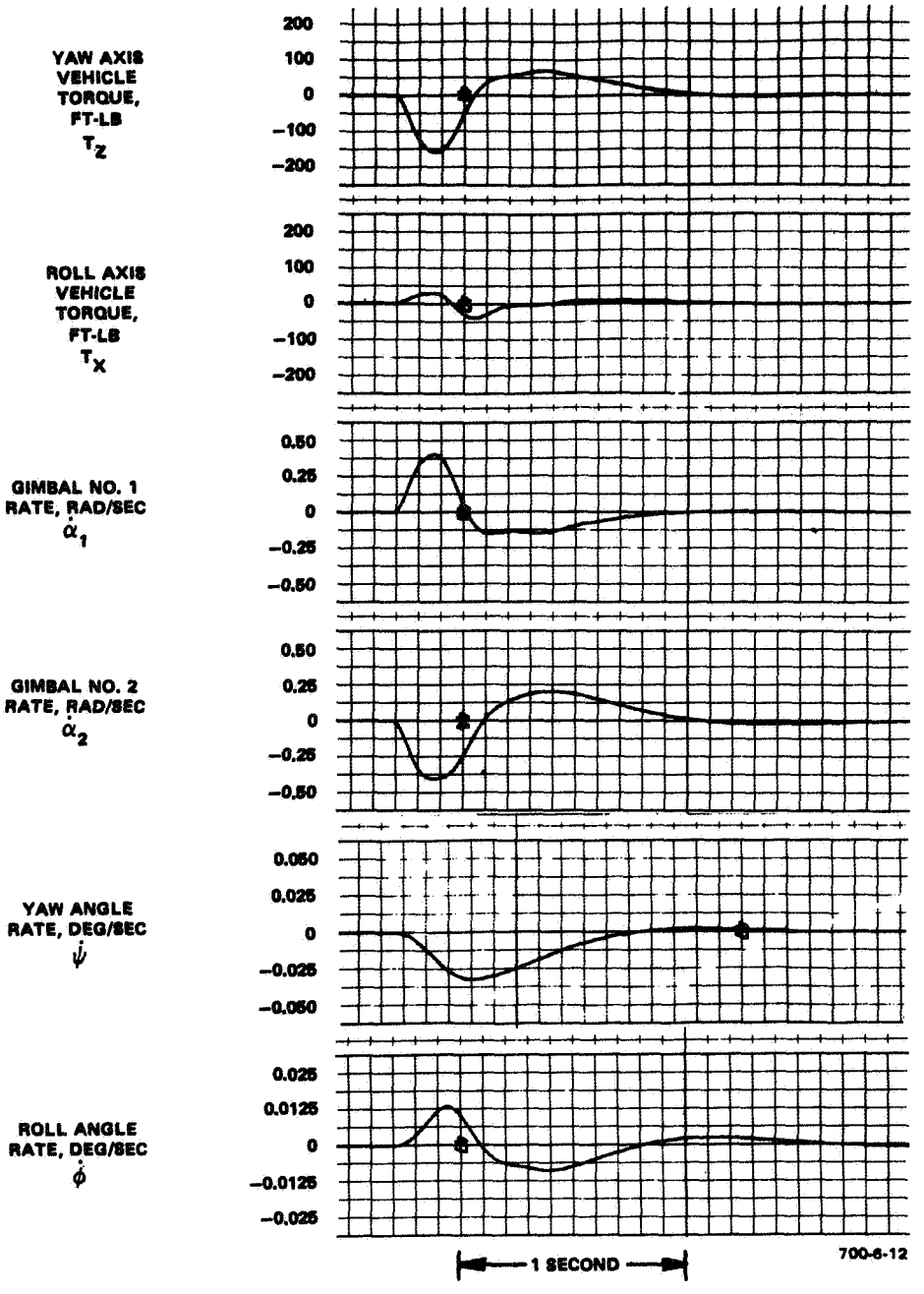

Figure 7-25
Step Response to Attitude Command of 0.015 degree in Z-Axis, $\left(\frac{H_v}{h}\right) = 0.49$, Constant Gain Steering Law

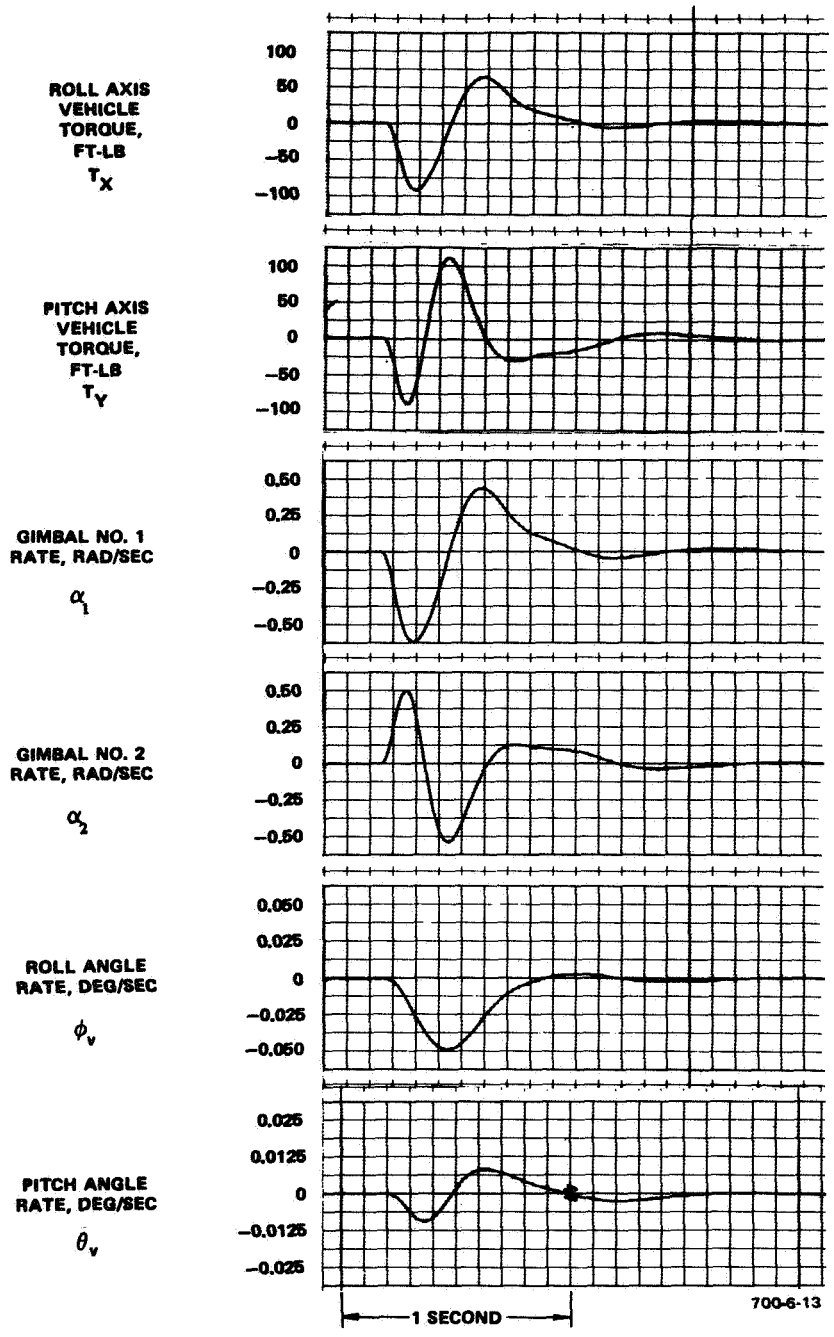

Figure 7-26
Step Response to Attitude Command of 0.015 degree in X-Axis, $\left(\frac{H_Z}{h}\right)$ = 1.29, Constant Gain Steering Law

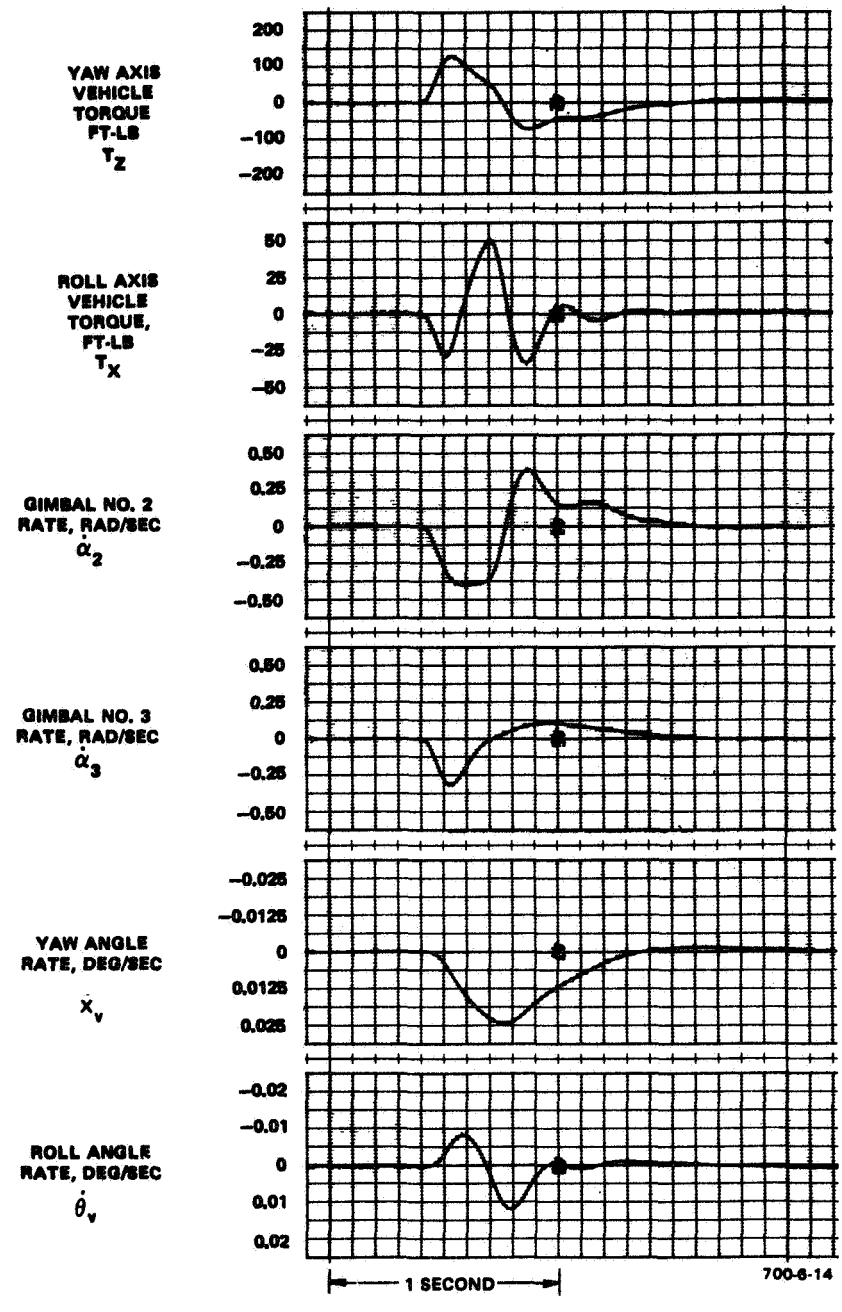

Figure 7-27
Step Response to Attitude Command of 0.015 degree in Z-Axis, $\left(\frac{H_y}{h}\right)$ = 0.73, Constant Gain Steering Law

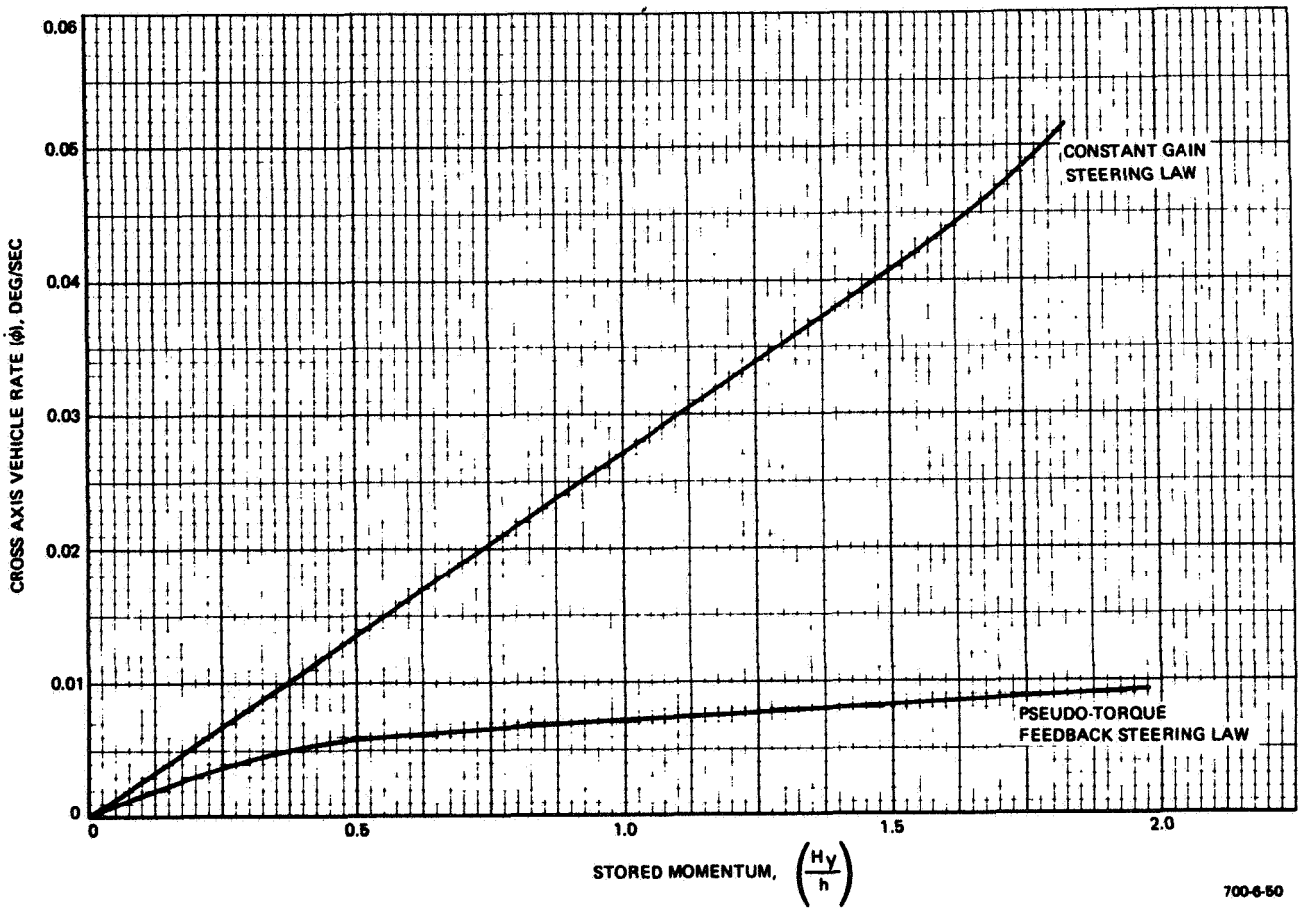

Figure 7-28
Response to Attitude Step Command of 0.015 degree in Z-Axis,
Effect of Stored Momentum in Y-Axis on Cross-Axis Vehicle Rate

D. THREE-AXIS RESULTS - ONE GYRO FAILED

Failure of one gyro reduces the momentum envelope of the system as discussed in Subsection IV.F and increases the amount of cross-coupling with stored momentum when the constant gain steering law is used. Responses to step torque disturbances when momentum is stored in one axis with the constant gain steering law are shown in Figure 7-29 and 7-30. The drop in loop gain that was noticeable in the single axis response (Figure 7-7) has a greater effect as momentum is stored. Adoption of the pseudo-torque feedback steering law, decreases cross-axis coupling and improves the performance of the system considerably. With lower coupling, a larger momentum envelope can be achieved for the same cross-axis rate. The amount of cross-coupling is greatly reduced as shown in Figure 7-31; comparison of Figure 7-31 with Figure 7-15 shows that when the pseudo-torque feedback steering law is employed, failure of one gyro causes no appreciable decrease in performance.

The effect of stored momentum on system response to step torque disturbances is summarized in Figures 7-32 and 7-33. When gyro No. 1 has failed, momentum is stored in the Y axis by increasing the gimbal angle (positive momentum) of gyros 2 and 4 or decreasing the angle (negative momentum). The initial position of the two gyros is -30 degrees. Since the sine and cosine curves are not symmetrical about -30 degrees, storing positive or negative momentum in the Y axis has different effects and explains the asymmetry of Figure 7-32. If gyro No. 2 had failed, the asymmetry would be opposite. When momentum is stored in the Z axis, on the other hand, gyros No. 2 and 4 move in opposite directions. Consequently, the same system response is obtained whether positive momentum or negative momentum is stored, and Figure 7-33 is symmetrical about zero stored momentum. Cross-coupling with three and four gyros operative is compared in Figures 7-34 and 7-35. With the exception of stored momentum in the negative Y axis (positive Y axis if gyro No. 2 is failed), failure of gyro No. 1 causes an increase in cross-coupling when the constant gain steering law is used. When the pseudo-torque feedback steering law is used, very little cross-coupling occurs in either case.

The asymmetry of storing momentum in the Y axis shows up again in the constant gain steering law frequency response curves shown in Figure 7-36 (in-axis response) and in Figure 7-37 (cross-axis response). Storing negative momentum in the Y axis increases the system bandwidth by as much as 1.5 octaves, while positive stored momentum has the effect of lowering the bandwidth. Less cross-coupling is caused by negative stored momentum than by positive. System bandwidth is not greatly affected by stored momentum; however, cross-coupling is very sensitive to it. When the pseudo-torque feedback is used, the response is practically the same as with all four gyros operative: storing momentum, which has very little effect on in-axis response, causes negligible cross-axis response.

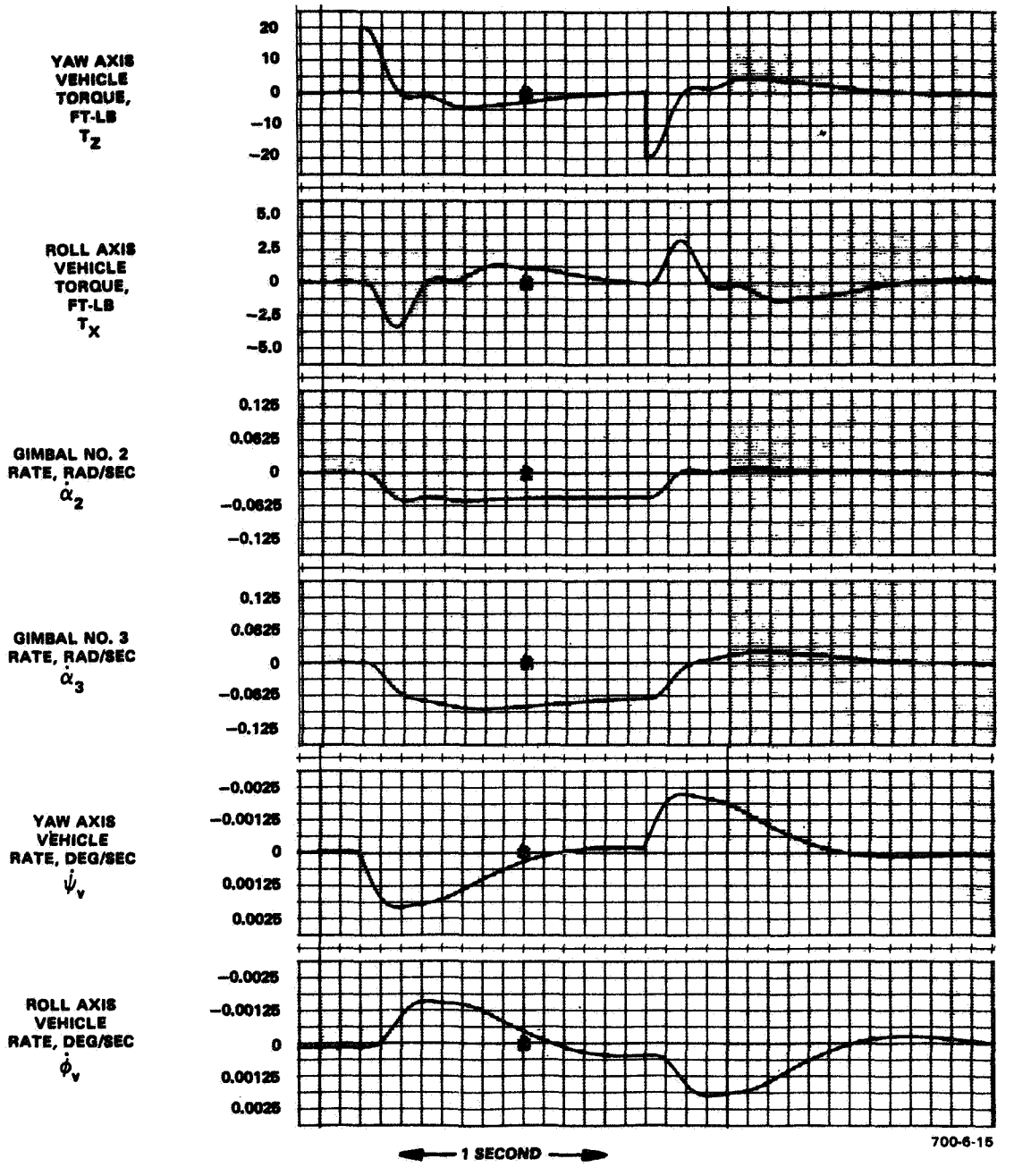

Figure 7-29
Step Torque Disturbance of 20 foot-pounds in Z-Axis, Gyro No. 1 Failed, Constant Gain Steering Law, Stored Momentum: $\left(\frac{H_y}{h}\right) = -0.6$

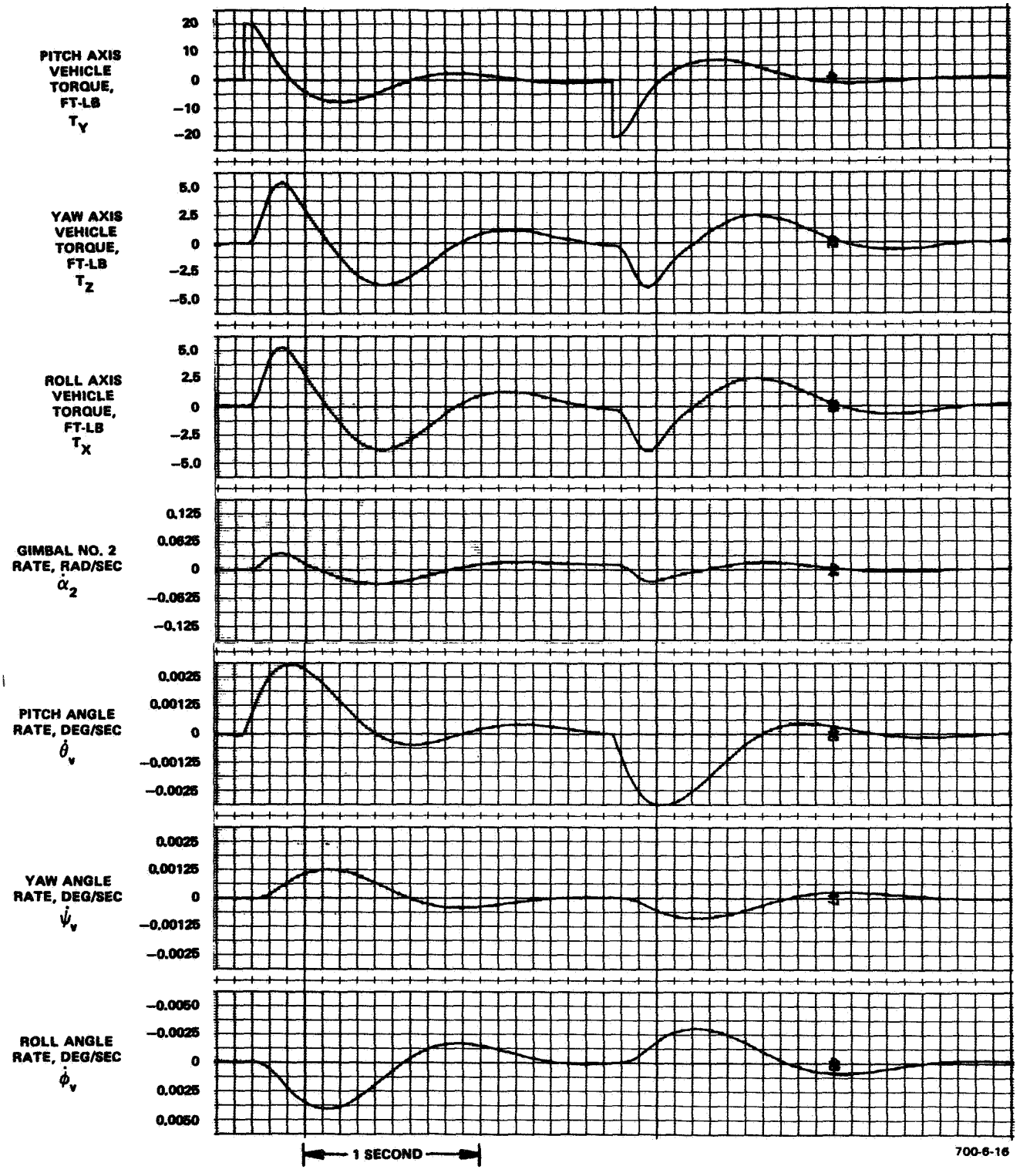

Figure 7-30
Step Torque Disturbance of 20 foot-pounds in Y-Axis, Gyro No. 1 Failed, Constant Gain Steering Law, Stored Momentum: $\left(\frac{H_z}{h}\right) = 0.8$

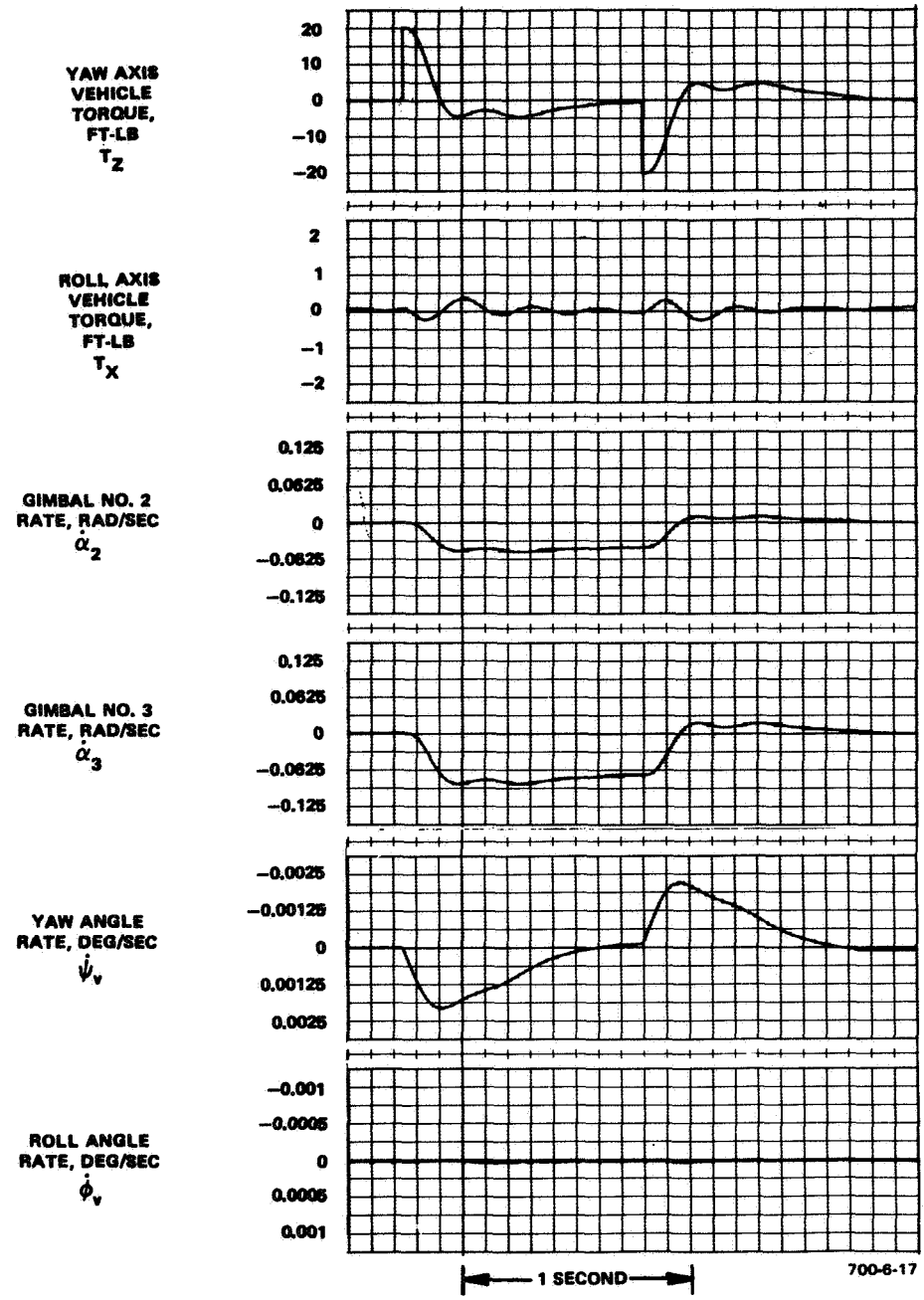

Figure 7-31
Step Torque Disturbance of 20 foot-pounds in
Z-Axis, Gyro No. 1 Failed, Pseudo-Torque
Feedback Steering Law, Stored Momentum: $\left(\frac{H_y}{h}\right) = -0.8$

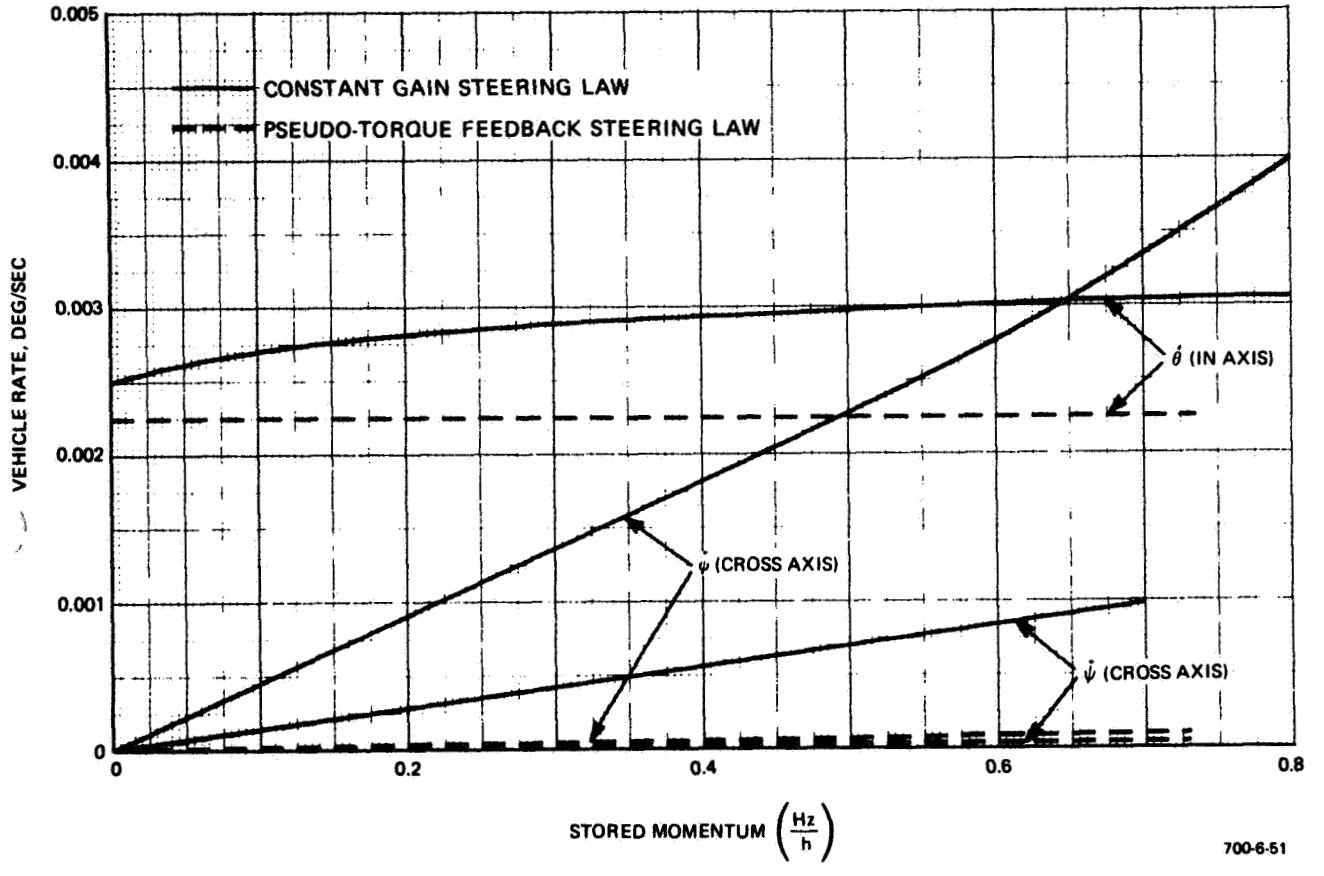

Figure 7-32
Gyro No. 1 Failed, Effect of Stored H_z on Vehicle Rates,
Step Torque Disturbance T_{dz} = 20 foot-pounds

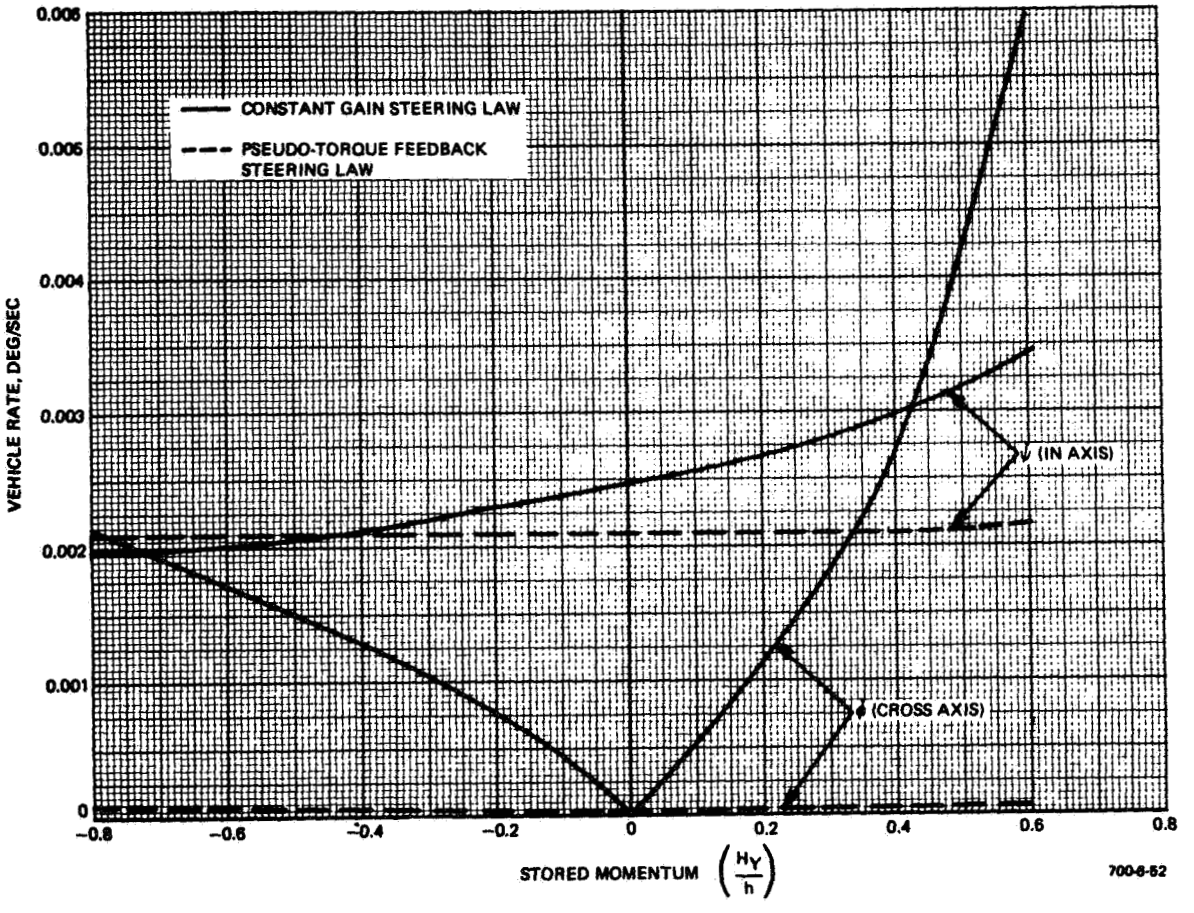

Figure 7-33
Gyro No. 1 Failed, Effect of Stored H_y on Vehicle Rates,
Step Torque Disturbance T_{dy} = 20 foot-pounds

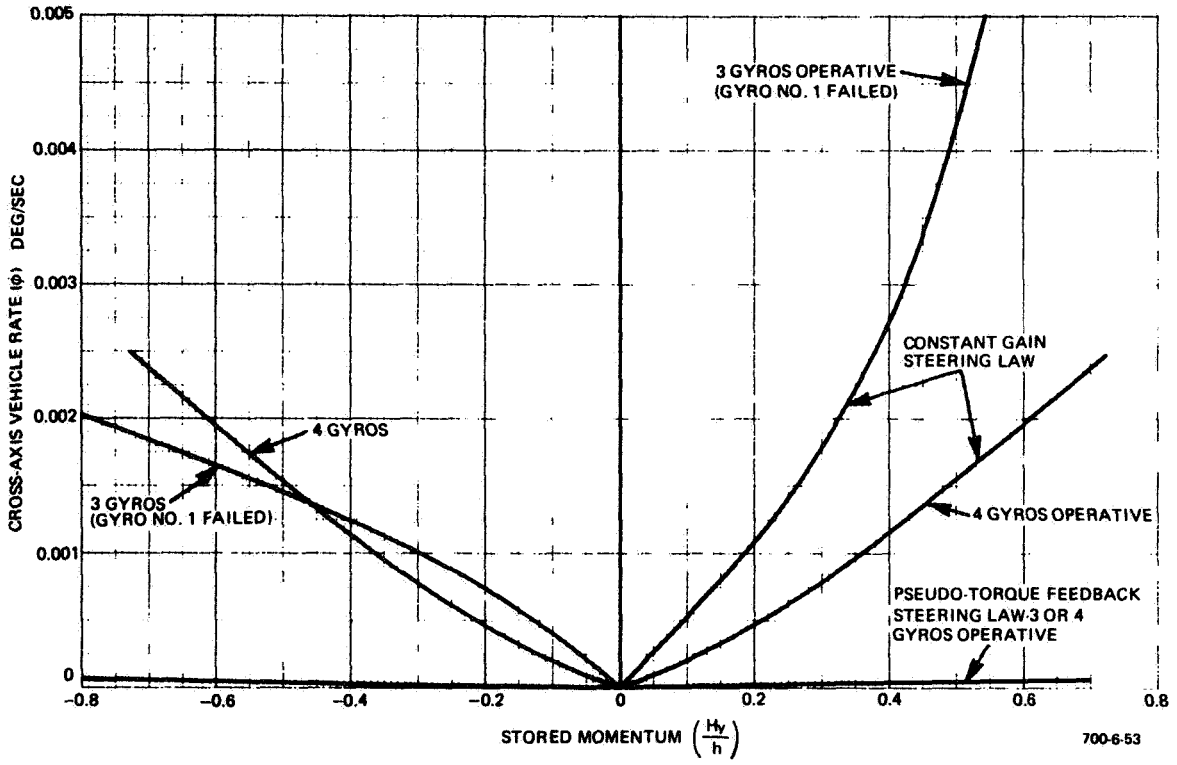

Figure 7-34
Comparison Between Cross-Coupling with Three and with Four Gyros Operative, Momentum Stored in Z-Axis, Step Torque Disturbance T_{dy} = 20 foot-pounds

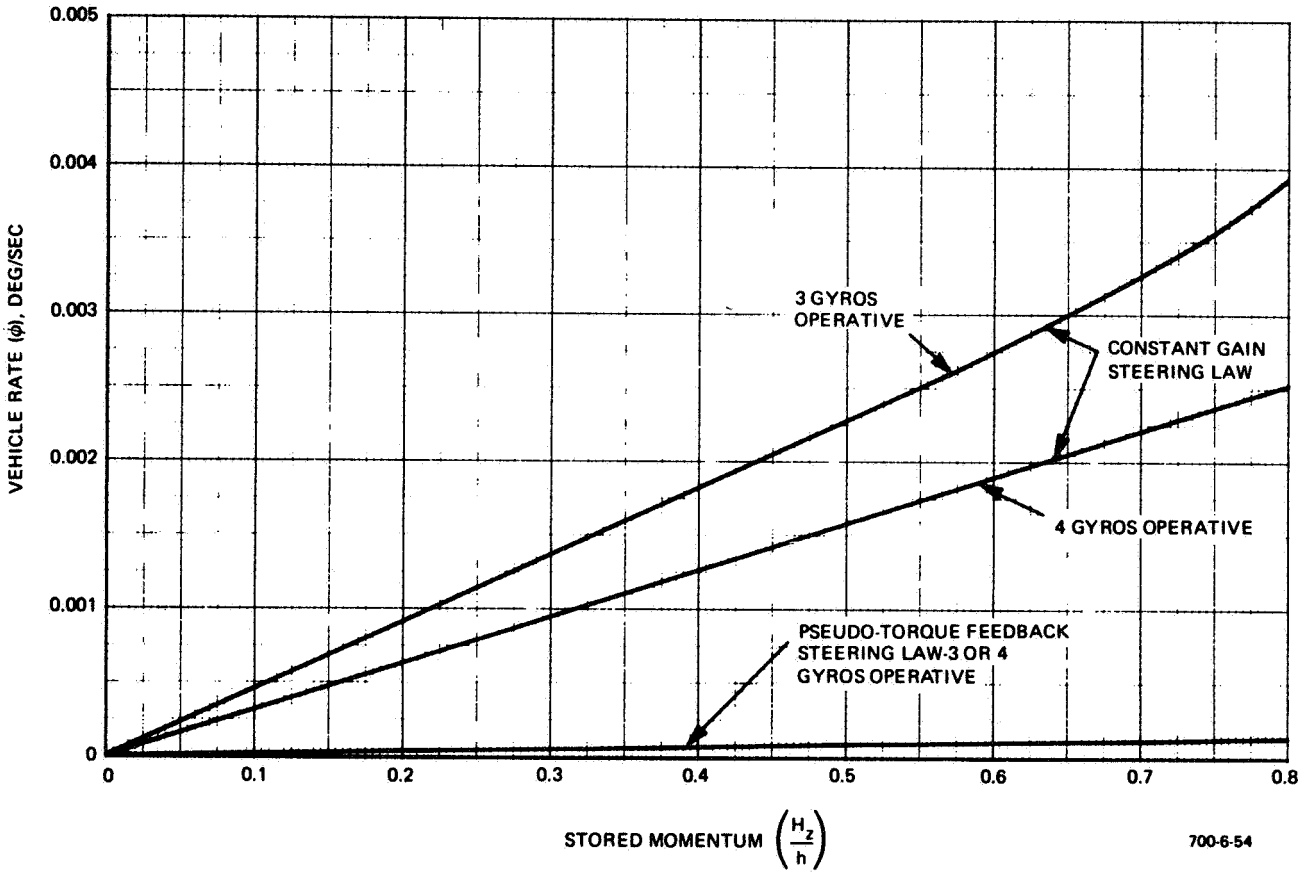

Figure 7-35
Comparison Between Cross-Coupling with Three and with Four Gyros Operative, Momentum Stored in Z-Axis, Step Torque Disturbance T_{dy} = 20 foot-pounds

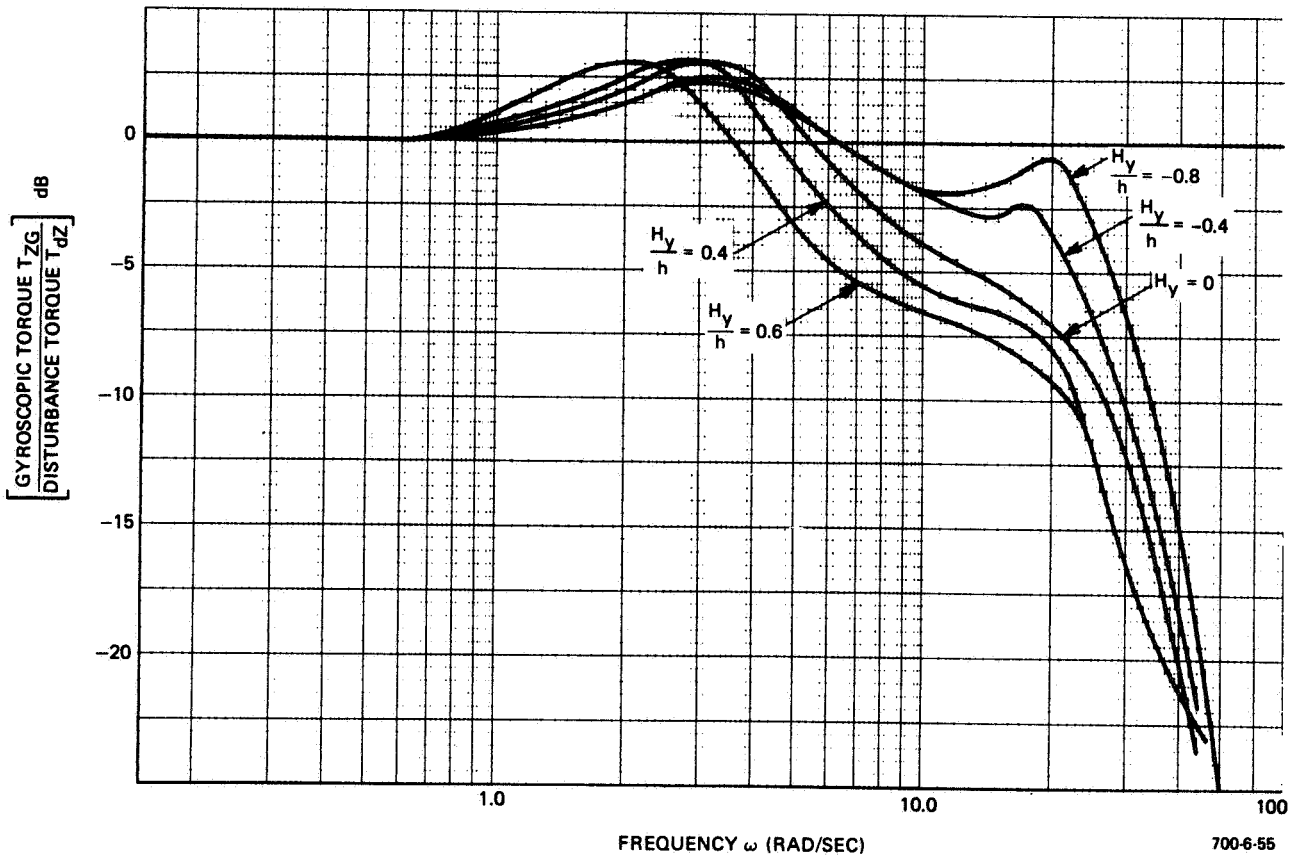

Figure 7-36
4-FACS Frequency Response, Gyro No. 1 Failed, Constant Gain Steering Law, Effect of Stored Momentum in Vehicle Y-Axis, In-Axis Response

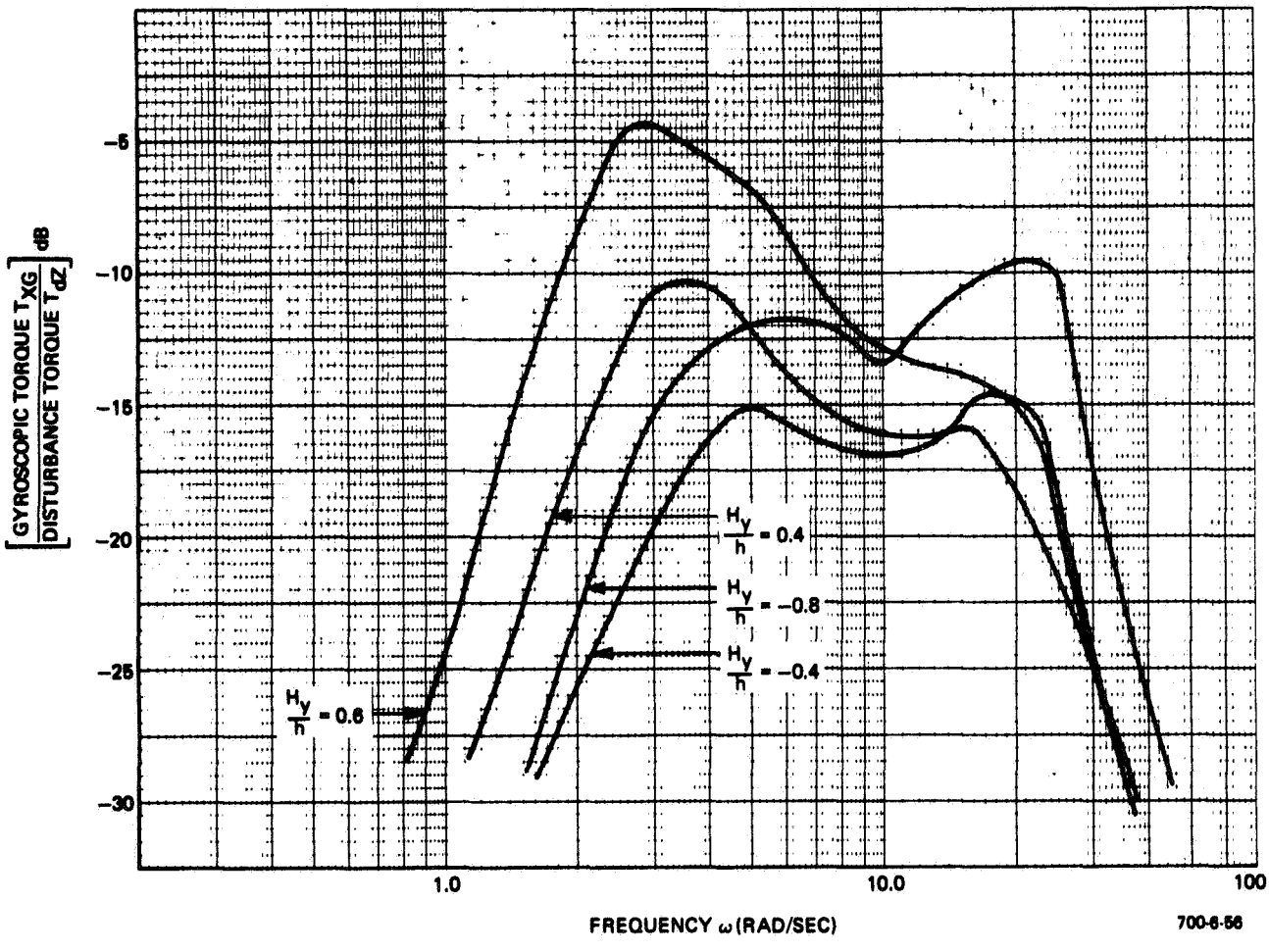

Figure 7-37
4-FACS Frequency Response, Gyro No. 1 Failed,
Constant Gain Steering Law, Effect of Stored
Momentum in Vehicle Y-Axis, Cross-Axis Response

Storing negative momentum in the Y axis causes an X and Z axis drop in gain margin and a rise in the Y axis when the constant gain steering law is employed. An increase occurs with momentum stored along the positive Y axis as shown in Figure 7-38. This asymmetry would be reversed if gyro No. 2 had failed. Nevertheless, the gain margin never drops below the value for four gyros operative. The effect of stored momentum in the Z axis on gain margin is shown in Figure 7-39. The Y axis has a higher gain margin. When one gyro is failed and the constant gain steering law is used, the loop gain in the Y axis is lower than in the other two axes. Adoption of the pseudo-torque feedback steering law gives a constant gain margin of 8 db, independent of stored momentum.

The response to attitude steps with gyro No. 1 failed and the constant gain steering law is shown in Figure 7-40. The amount of cross-coupling is reduced and the response improved when the pseudo-torque feedback steering law is employed (Figure 7-41).

E. MOMENTUM DESATURATION

Two methods of momentum desaturation were investigated: the gimbal position loop method, in which a position loop is closed around each gimbal and the gimbals are driven to their initial positions; and the RJC method, in which momentum is unloaded by commanding torque pulses from the reaction jets. These two methods are described in detail in Subsection VI.D.

When the gimbal position loop method is used, the reaction jets maintain fine attitude and oppose the torque produced by the CMG's. As soon as desaturation is complete, the 4-FACS is reconnected into the attitude loop and the CMG's may be required to reduce a relatively large attitude and rate error, and thus store momentum in the system. The error might be large enough to rate limit the gimbals. As a result, when the 4-FACS is trying to reduce the rate and attitude error to zero, the vehicle rate can increase enough to cause the reaction jets to fire, and thus store momentum and cause incomplete desaturation. In some cases, the vehicle rate at the end of reaction jet firing is large enough to cause the gyro to resaturate in the process of reducing the error. This problem can be eliminated by reducing the switching line and gimbal rate limit during desaturation so that at the end of desaturation the vehicle rates are close to zero. A phase plot for desaturation in the Y axis when the vehicle rate deadband switching line has been lowered by one-half and the gimbal rate limit has been reduced threefold is shown in Figure 7-42. Time histories of gimbal position loop desaturation for various multiple-axis combinations of stored momentum are shown in Figures 7-43 and 7-44; behavior of the gimbal position loop desaturation method is summarized in Table 7-4. The amount of momentum stored at the end of desaturation depends on the vehicle rate at the time the 4-FACS is re-engaged. Hence, the amount of momentum that remains stored in the system when desaturation is completed is difficult to predict a priori.

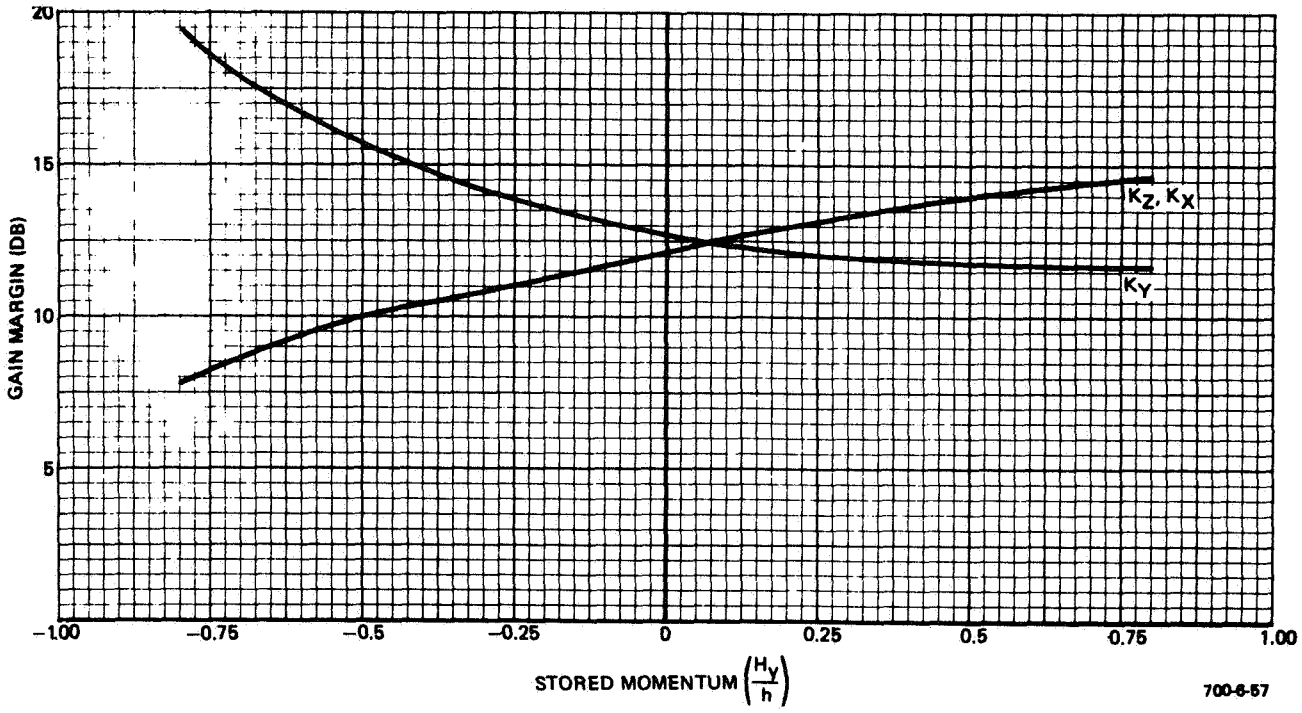

Figure 7-38
Effect of Stored Momentum in Y-Axis Gain Margins with Gyro No. 1 Failed, Constant Gain Steering Law, $H_x = H_y = 0$

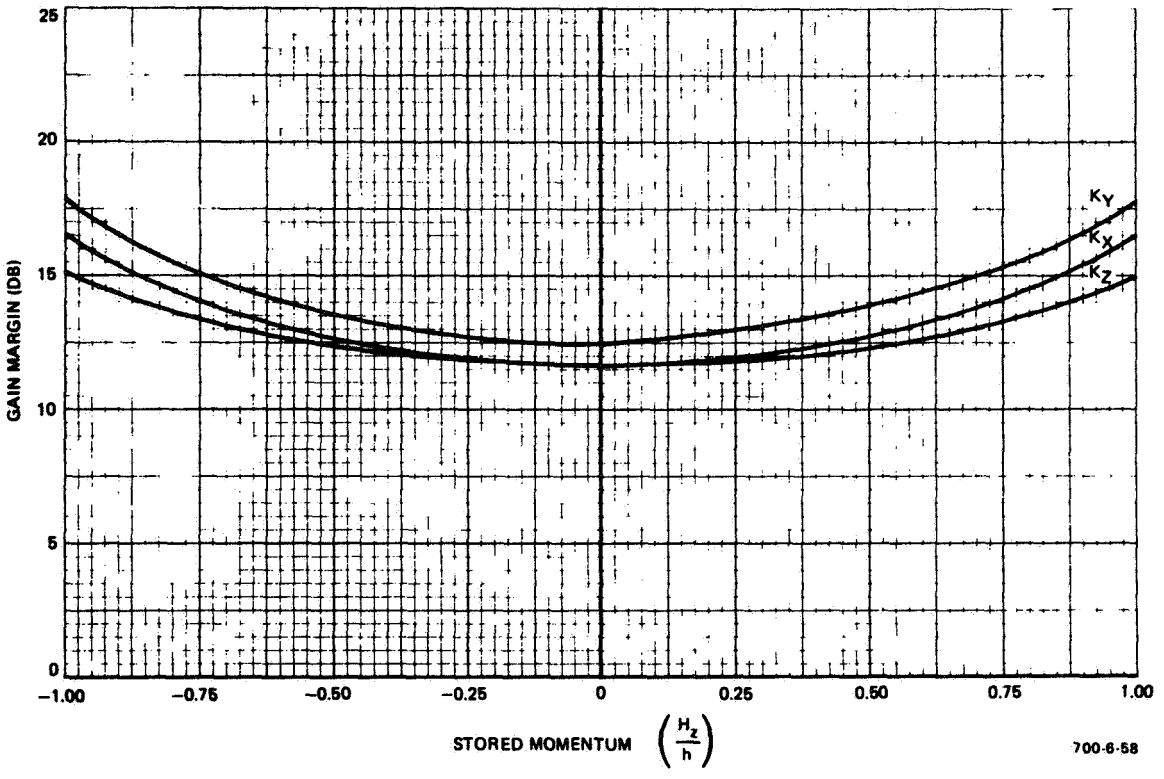

Figure 7-39
Effect of Stored Momentum in Z-Axis on Gain Margins with Gyro No. 1 Failed, Constant Gain Steering Law, $H_x = H_y = 0$

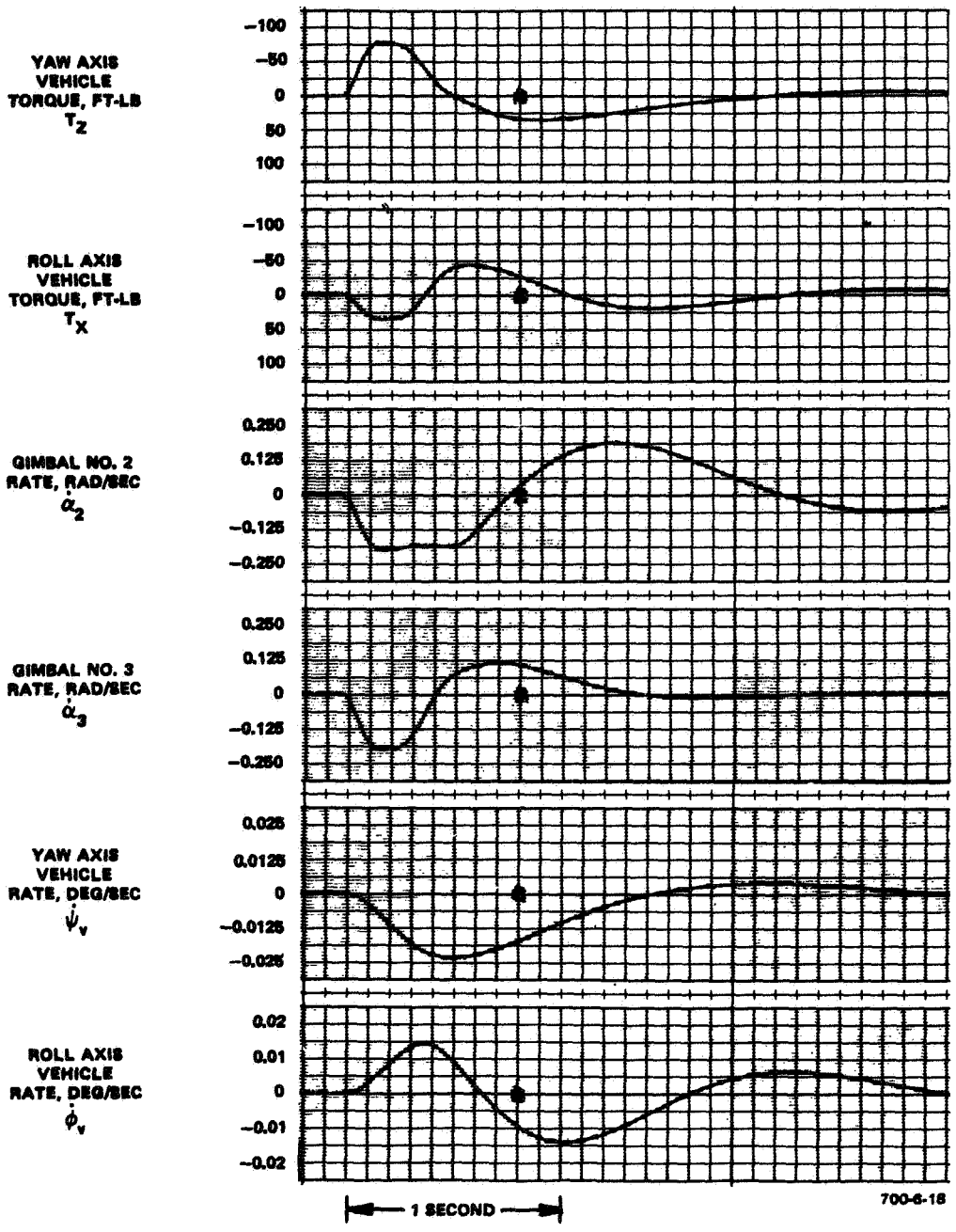

Figure 7-40
Step Response to Attitude Command of 0.015 degree in Yaw Axis, Gyro No. 1 Failed, Constant Gain Steering Law, Stored Momentum: $\left(\frac{H_Y}{h}\right) = 0.6$

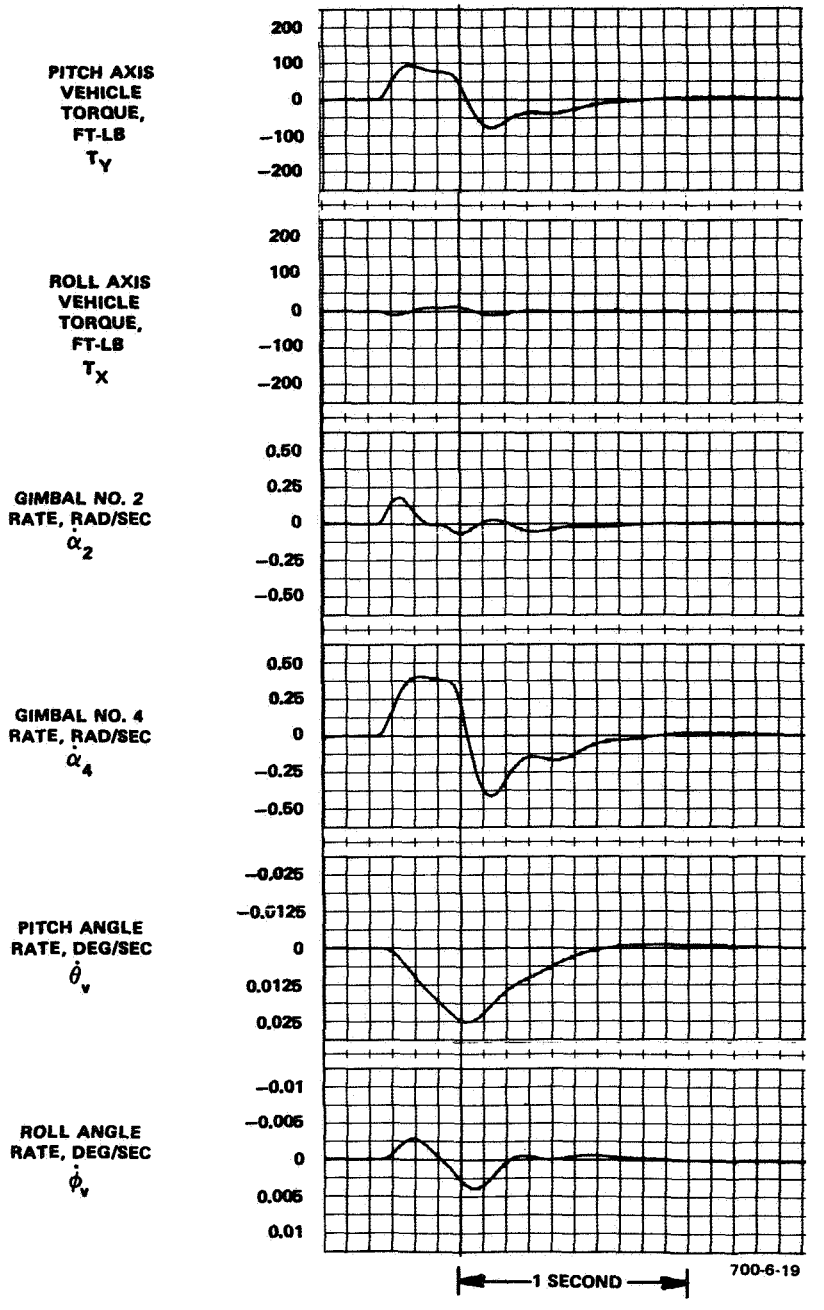

Figure 7-41
Step Response to Attitude Command of 0.015 degree in Pitch Axis, Gyro No. 1 Failed, Pseudo-Torque Feedback Steering Law, Stored Momentum: $\left(\frac{H_z}{h}\right) = 0.4$

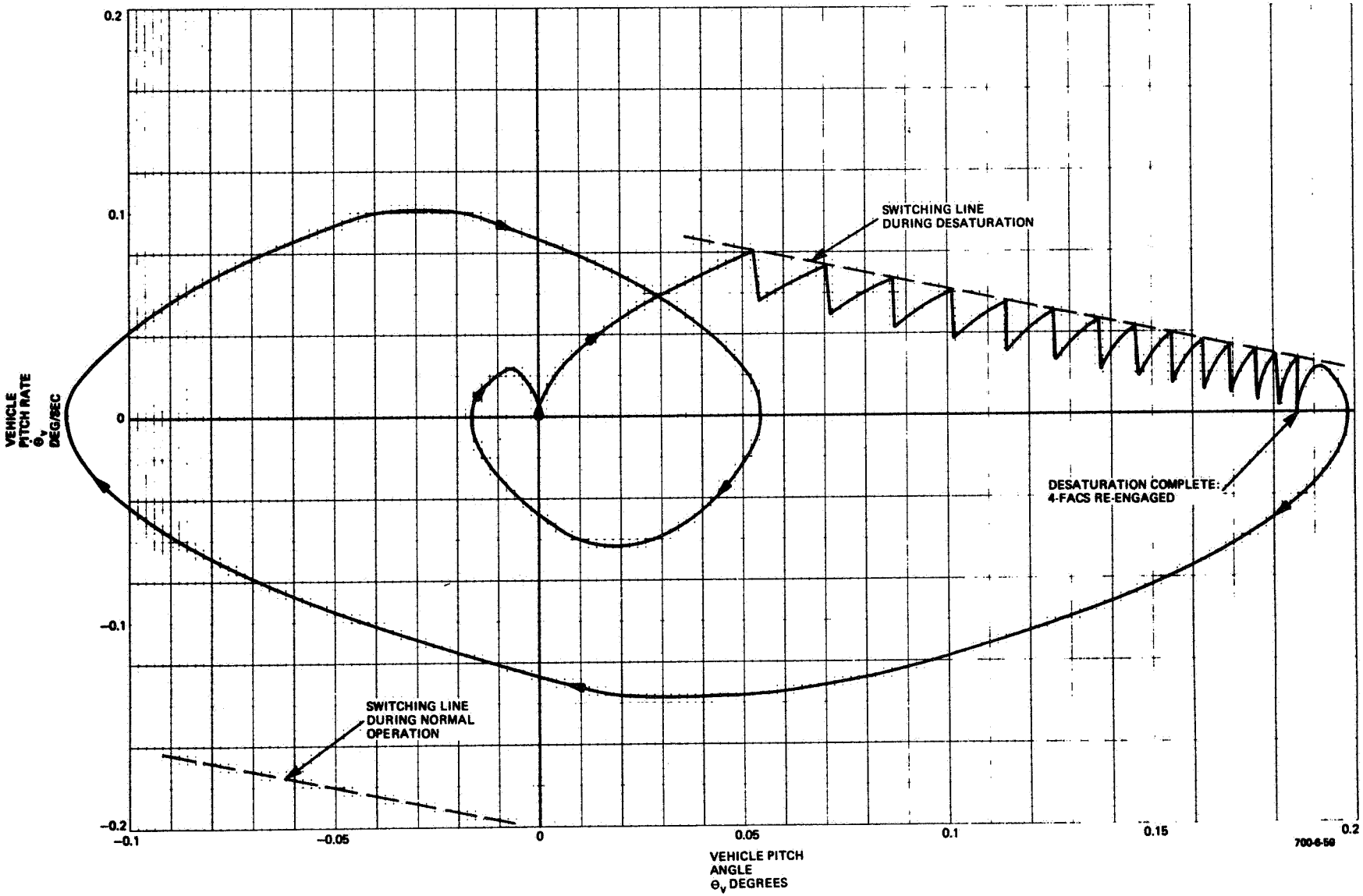

Figure 7-42
Gimbal Position Loop Desaturation, Four Gyros Operative, Phase Plot for Momentum Desaturation in Y-Axis, Gimbal Rate Limit: 0.125 radian per second

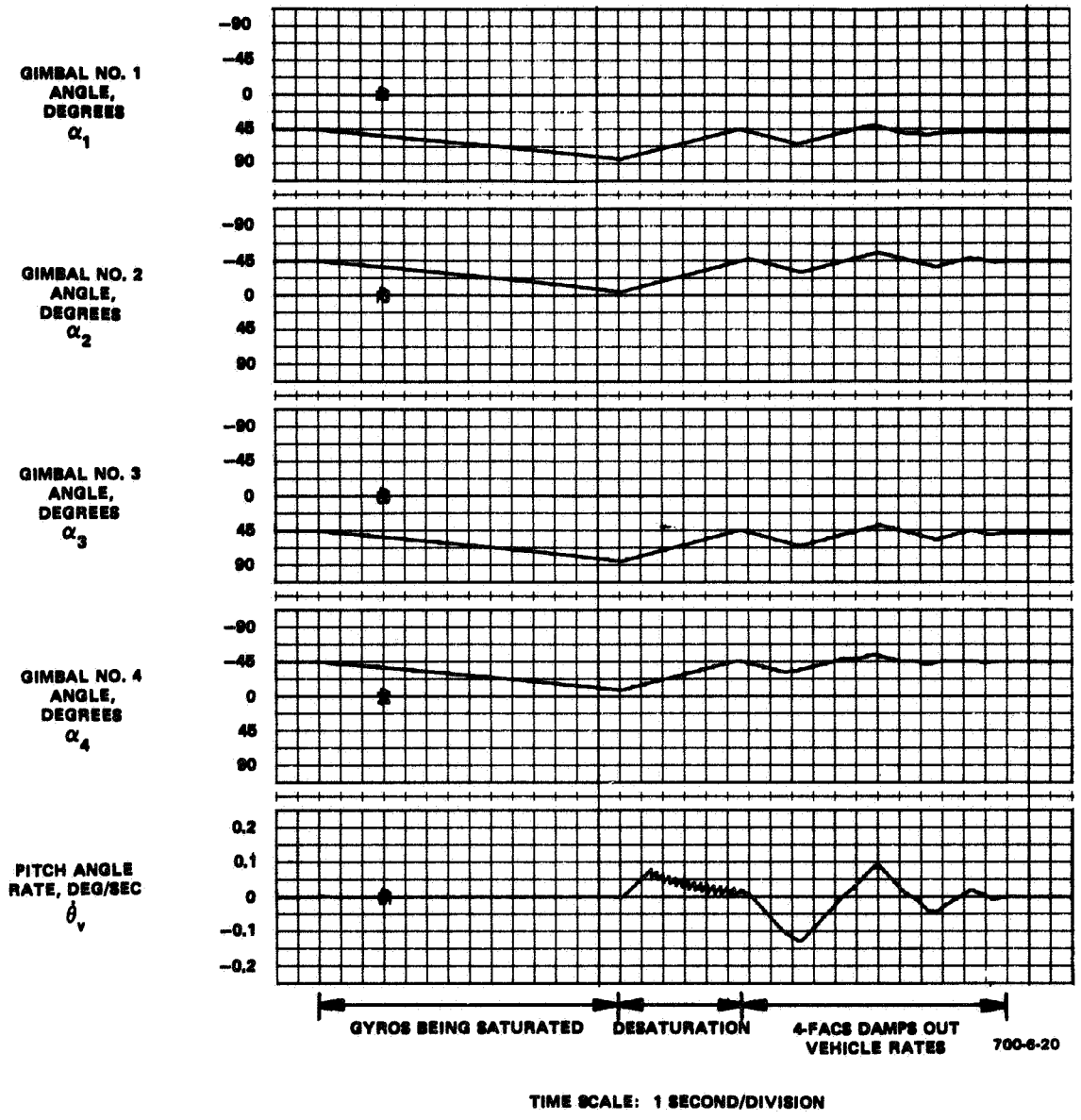

Figure 7-43
Gimbal Position Loop Desaturation,
Momentum Stored in Y-Axis

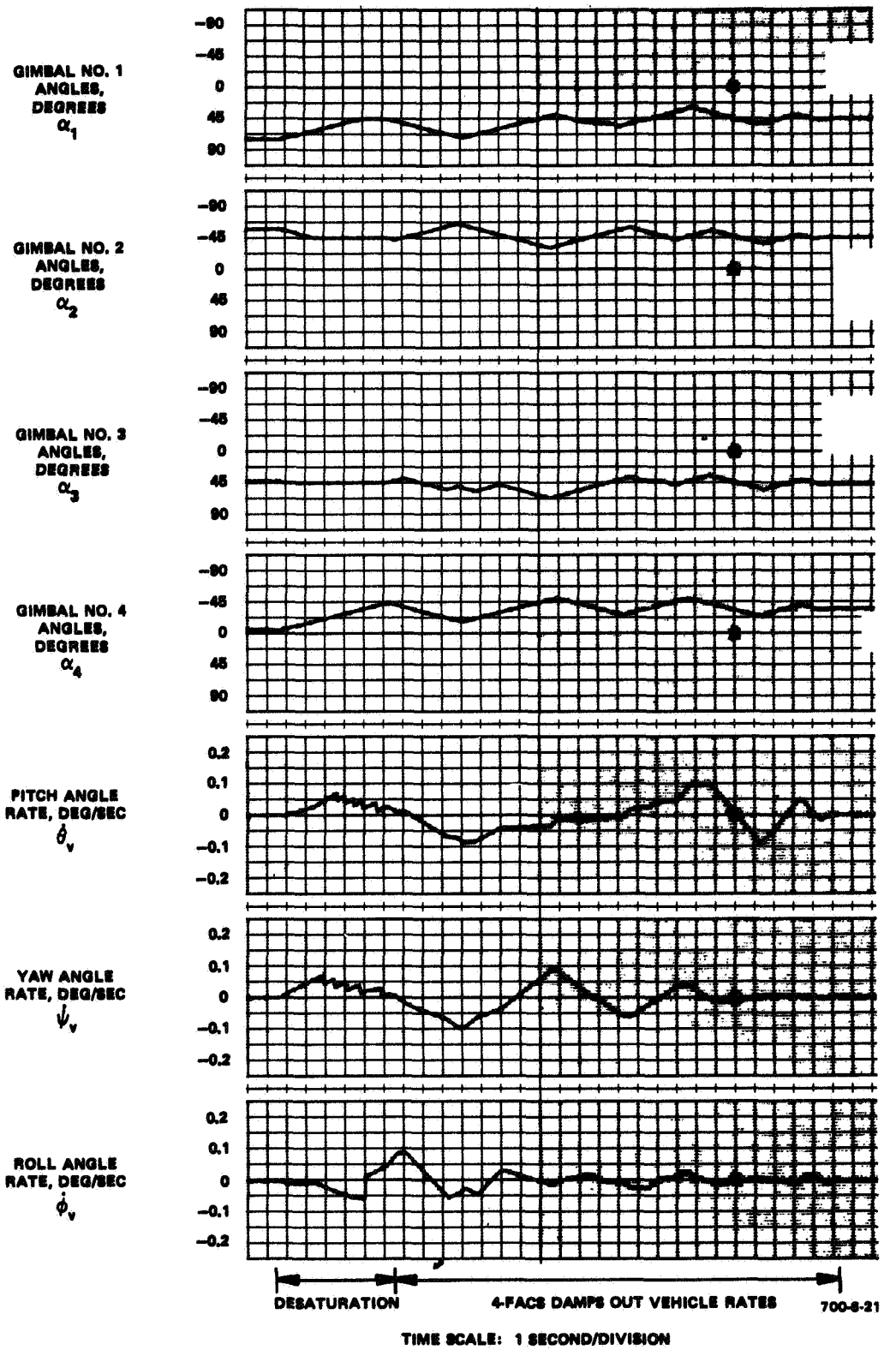

Figure 7-44
Gimbal Position Loop Desaturation,
Momentum Stored in Y- and Z-Axis

TABLE 7-4

MOMENTUM DESATURATION
(GIMBAL POSITION LOOP METHOD)

Momentum Stored			Final Gimbal Angles (degrees)				Momentum Stored at End of Desaturation			
H_x	H_y	H_z	α_1	α_2	α_3	α_4	$\frac{H_x}{h}$	$\frac{H_y}{h}$	$\frac{H_z}{h}$	$\frac{\lvert H \rvert}{h}$
X			44.7	44.4	45.2	45.4	-0.0045	0.002	-0.01	0.0111
	X		48.1	44.2	49.8	44.2	0.0163	0.116	-0.0148	0.118
		X	47.5	47.0	42.6	42.4	-0.0014	0.0108	0.082	0.0825
X	X		44.9	44.2	49.5	40.7	0.0735	0.119	-0.0057	0.140
X		X	54.9	54.0	47.7	47.7	-0.0091	0.008	0.198	0.201
	X	X	44.8	45.2	46.7	34.5	0.0825	0.158	0.1325	0.2225
X	X	X	43.8	40.8	33.6	30.1	0.147	-0.0042	0.049	0.156

When the RJC desaturation method is adopted, the 4-FACS remains in the attitude control loop, so that during desaturation, the attitude error does not exceed the design limit. Examples of RJC desaturation for various combinations of stored momentum are shown in Figure 7-45 and 7-46. The combination of stored momentum in Figure 7-46 is the same as that in Figure 7-44; comparison of the two traces shows how much more predictable the behavior of the RJC system technique is. Behavior of the RJC desaturation method is summarized in Table 7-5. The accuracy of this desaturation method depends primarily on the reaction jet minimum impulse size. For the design mission, the minimum impulse was 1400 ft-lb for 15 milliseconds, or 21 ft-lb-sec; the momentum of each gyro was 200 ft-lb-sec so that in normalized parameters the momentum per RJC firing was 0.105. In all the cases presented in Table 7-5, the momentum left in the system at the end of desaturation was very close to this value.

During the study, asynchronous pulse modulators were used in each axis to avoid having reaction jets in more than one axis firing simultaneously, thus providing a smaller momentum bit during desaturation.

The logic required for the gimbal position loop method is simpler than that needed to implement the RJC method. The RJC desaturation network, however, is in parallel with the fine attitude control system; therefore, no changes are required when desaturation is to take place. The gimbal position loop method, on the other hand, requires disconnecting the fine attitude control system and changing the gimbal loop rate limit and the RJC system deadbands. Moreover, the behavior of the RJC method is more predictable than the behavior of the gimbal position loop method. Notwithstanding its more complex logic, therefore, the RJC momentum desaturation method is preferred.

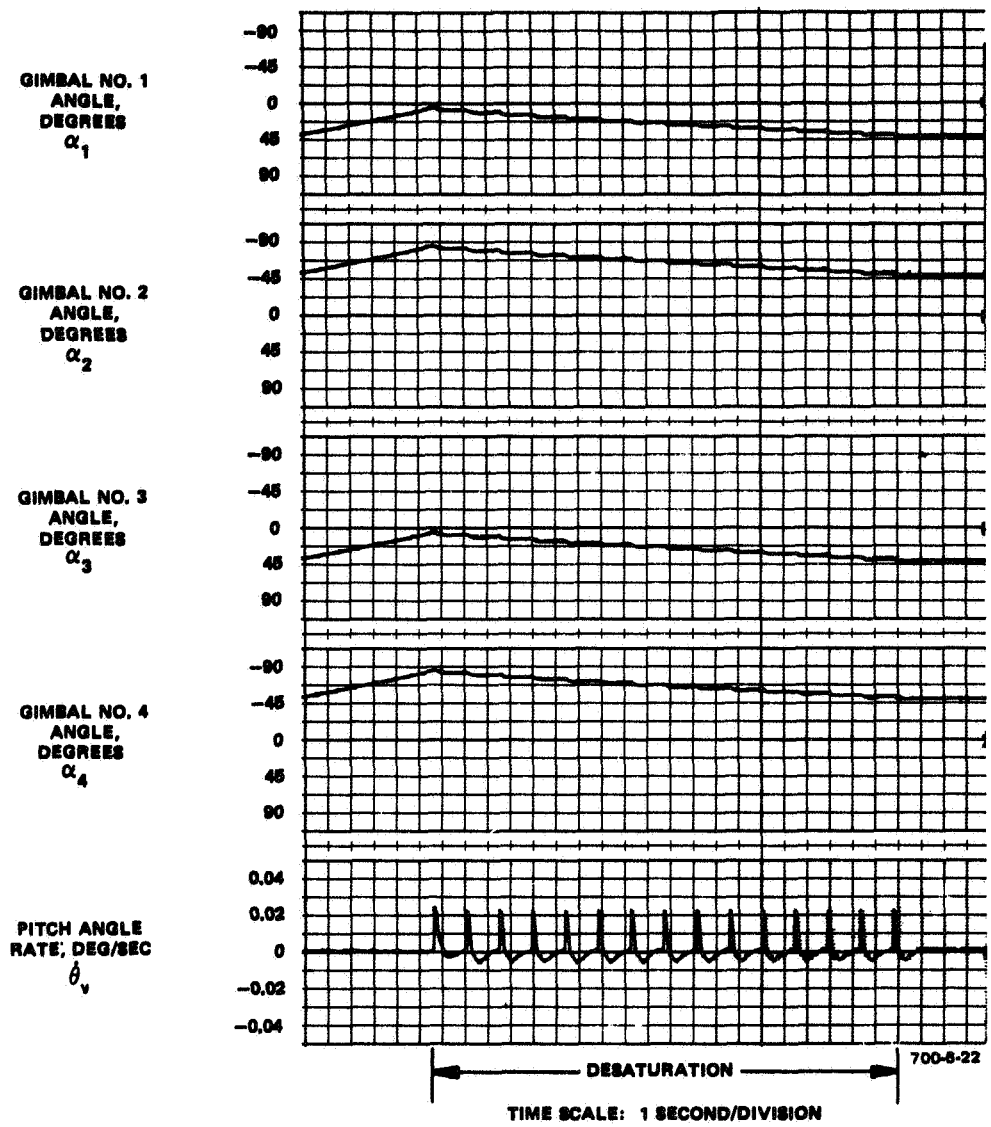

Figure 7-45
RJC Desaturation, Momentum Stored in Y-Axis

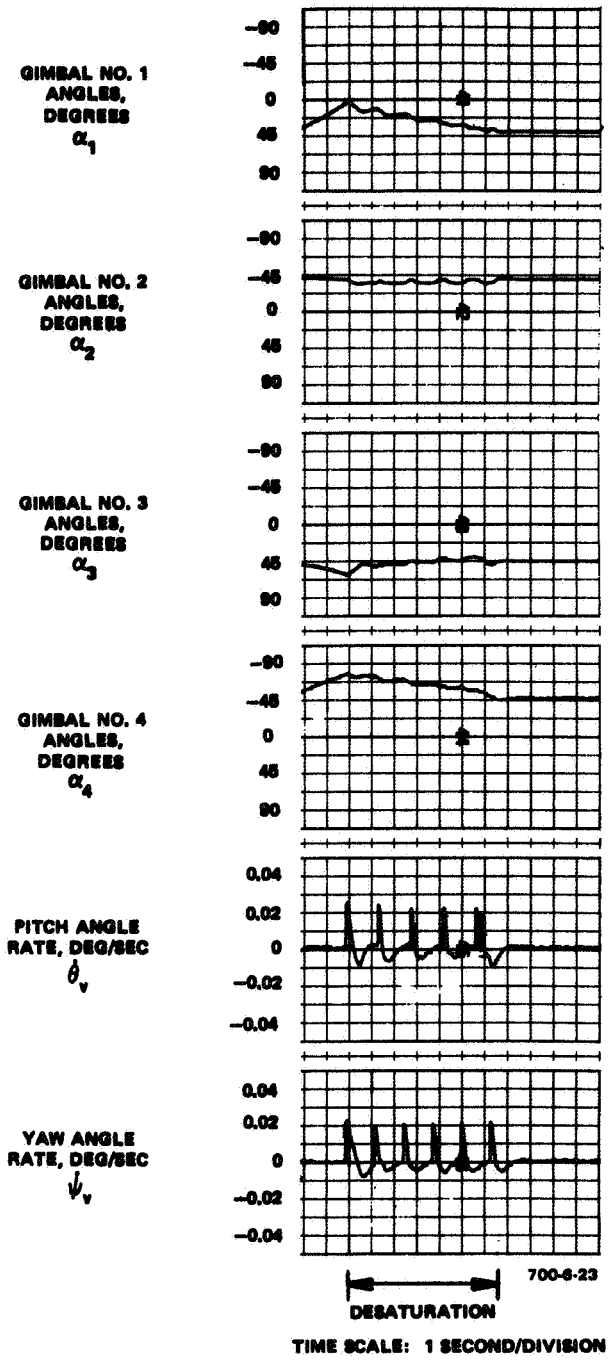

Figure 7-46
RJC Desaturation, Momentum Stored in
Y- and Z-Axis

TABLE 7-5

MOMENTUM DESATURATION
(REACTION JET METHOD)

Momentum Stored			Final Gimbal Angles (degrees)				Momentum Stored at End of Desaturation			
H_x	H_y	H_z	α_1	α_2	α_3	α_4	$\frac{H_x}{h}$	$\frac{H_y}{h}$	$\frac{H_z}{h}$	$\frac{H}{h}$
X			48.1	42.3	46.2	45.2	-0.045	-0.085	-0.005	0.0963
	X		40.6	48.9	41.1	49.5	-0.002	0.1055	-0.010	0.105
		X	41.1	41.1	48.9	48.9	0.0	0.0	-0.135	0.135
X	X		48.9	42.1	44.5	48.4	-0.095	-0.038	-0.015	0.103
X		X	51.4	47.4	51.5	45.9	0.016	-0.110	0.012	0.111
	X	X	39.4	39.4	46.1	45.9	-0.0015	-0.002	-0.111	0.111
X	X	X	49.8	43.6	43.8	51.6	0.127	0.002	-0.002	0.128

F. MISSION PROFILE SIMULATION

The following mission phases were simulated to evaluate the selected manned mission design:

- De-boost and stabilize attitude rates
- Initiate fine attitude hold
- Hold fine attitude
- Re-acquire sun during attitude hold
- Failure of one gyro
- Hold fine attitude with one gyro failed
- Re-acquire sun with one gyro failed

The system used in the mission profile simulation employed a pseudo-torque feedback steering law and RJC momentum desaturation.

During de-boost and stabilization, the sun is acquired and the de-boost rates are damped out by activating the RJC system. The vehicle roll rate being damped out to the RJC limit cycle upon activation of the reaction jet system is shown in Figure 7-47; the other two axes behave similarly.

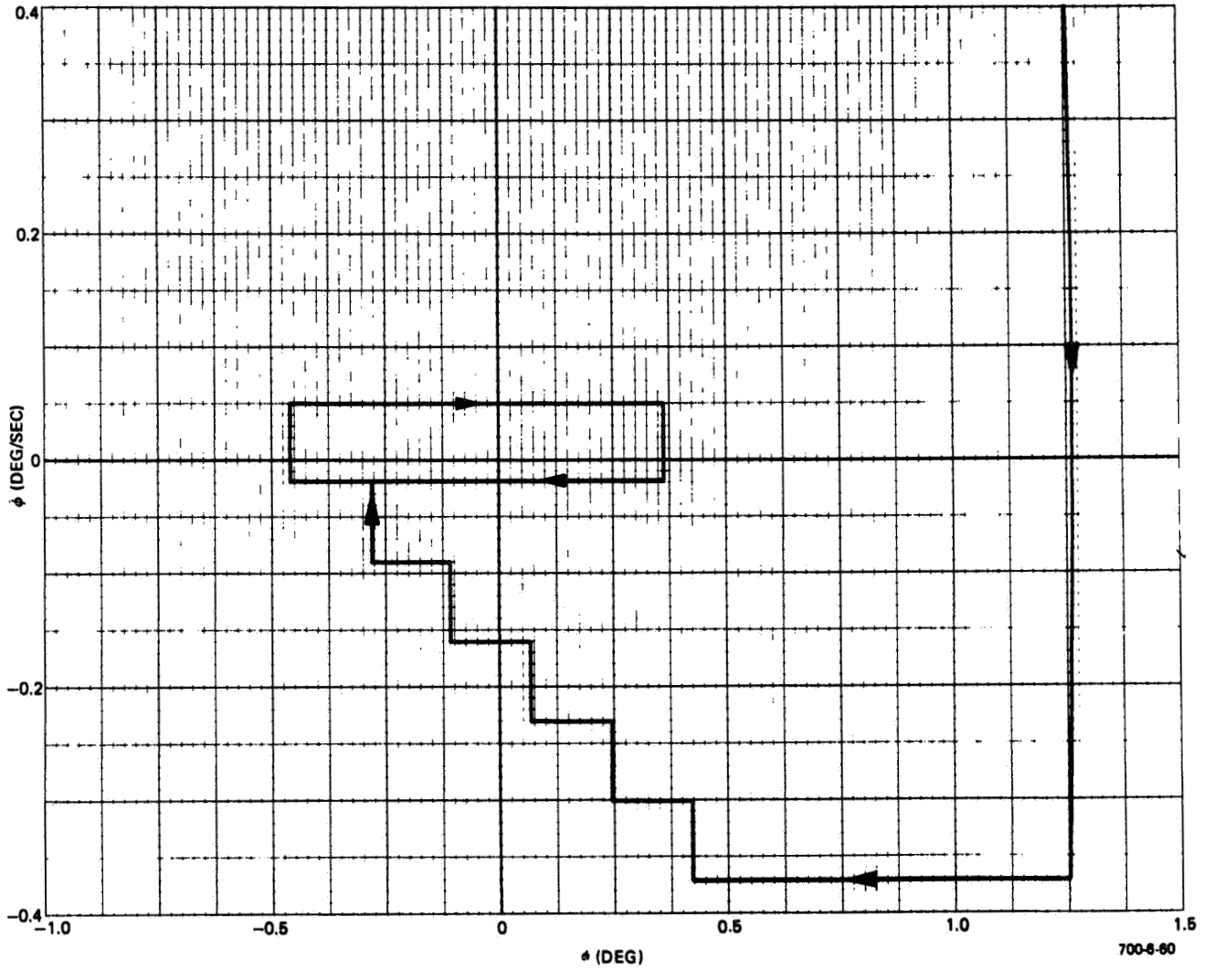

Figure 7-47
RJC Activated, Roll Axis

When the vehicle has established an RJC limit cycle, the 4-FACS is actuated and damps out the rates. If the system is engaged in all three axes at the same time, high gyro torques are commanded and large gimbal angle excursions occur. The best results were obtained by engaging each axis of the 4-FACS individually when the attitude error in that axis is near zero. A phase plot for the Z axis is shown in Figure 7-48; a time history for all three axes is shown in Figure 7-49.

The behavior of the fine attitude control system during fine attitude hold was investigated. Sensor noise was represented in each axis by a sine wave with a peak amplitude of 0.02 degree and frequency of 1 Hz; the X axis sine wave was 180 degrees out of phase with the other two axes. Man-motion torques in the Y axis were reproduced by white noise filtered through a double lag at 1 Hz with an rms amplitude of 10 ft-lb and peaks not exceeding 25 ft-lb. Man-motion torques in the other axes were simulated with manual pots and function switches. The system behavior during fine attitude hold with three and four gyros operative is shown in Figure 7-50. Various combinations of stored momentum were simulated corresponding to different points in the orbit. With both three and four gyros operative, attitude and rate errors were held within the prescribed limits.

Sun reacquisition was simulated by applying simultaneous attitude steps of 0.025 degree in all three axes. An attitude error of 0.025 degree is the maximum to be expected after emerging from the dark side. System behavior with three and four gyros operative is shown in Figure 7-51. As expected, vehicle rates during sun reacquisition exceed the design limit of 0.01 deg/sec. Even with one gyro failed, gimbal angle excursions are not large enough to cause desaturation to occur.

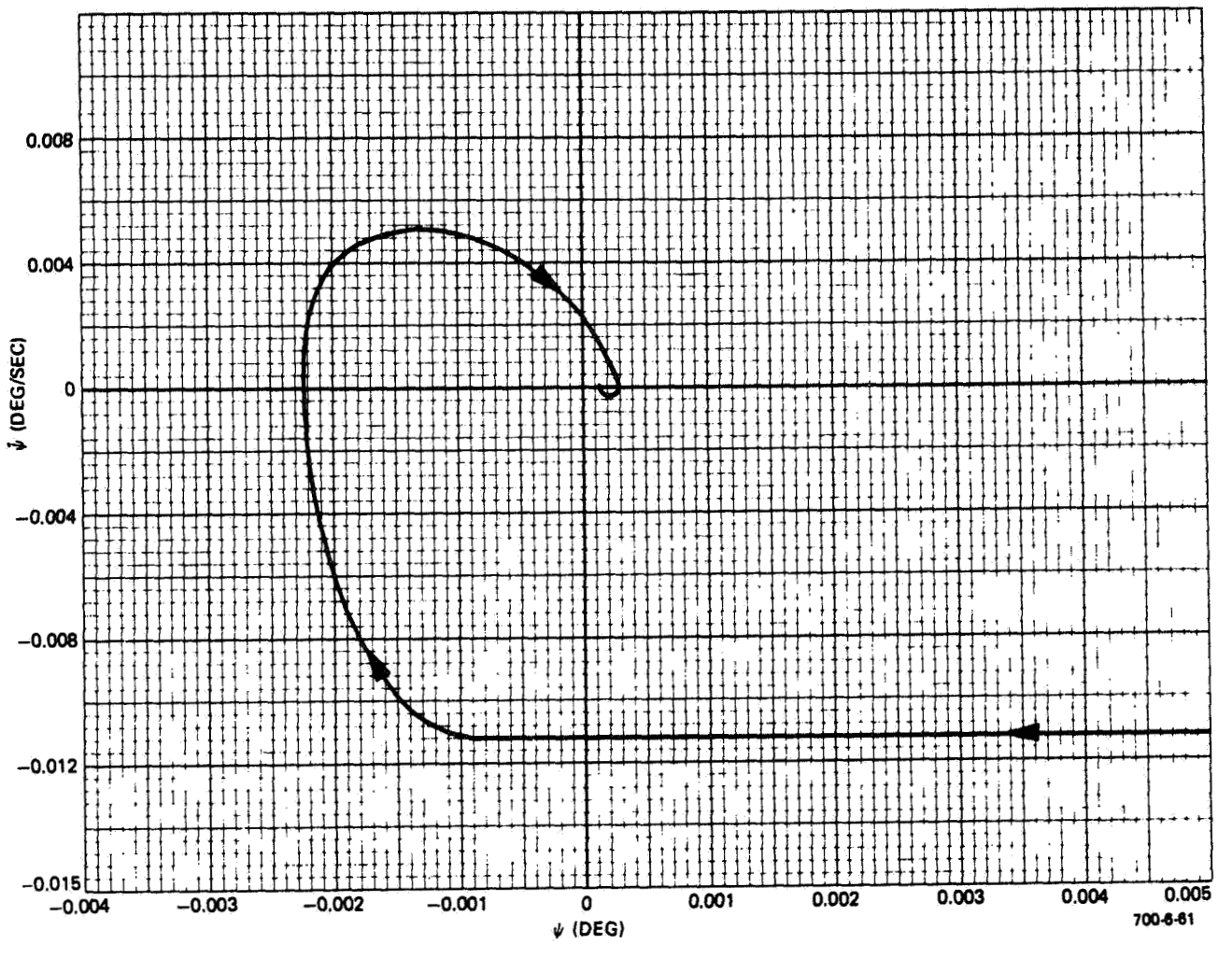

Figure 7-48
Engage Fine Attitude Hold, Yaw Axis

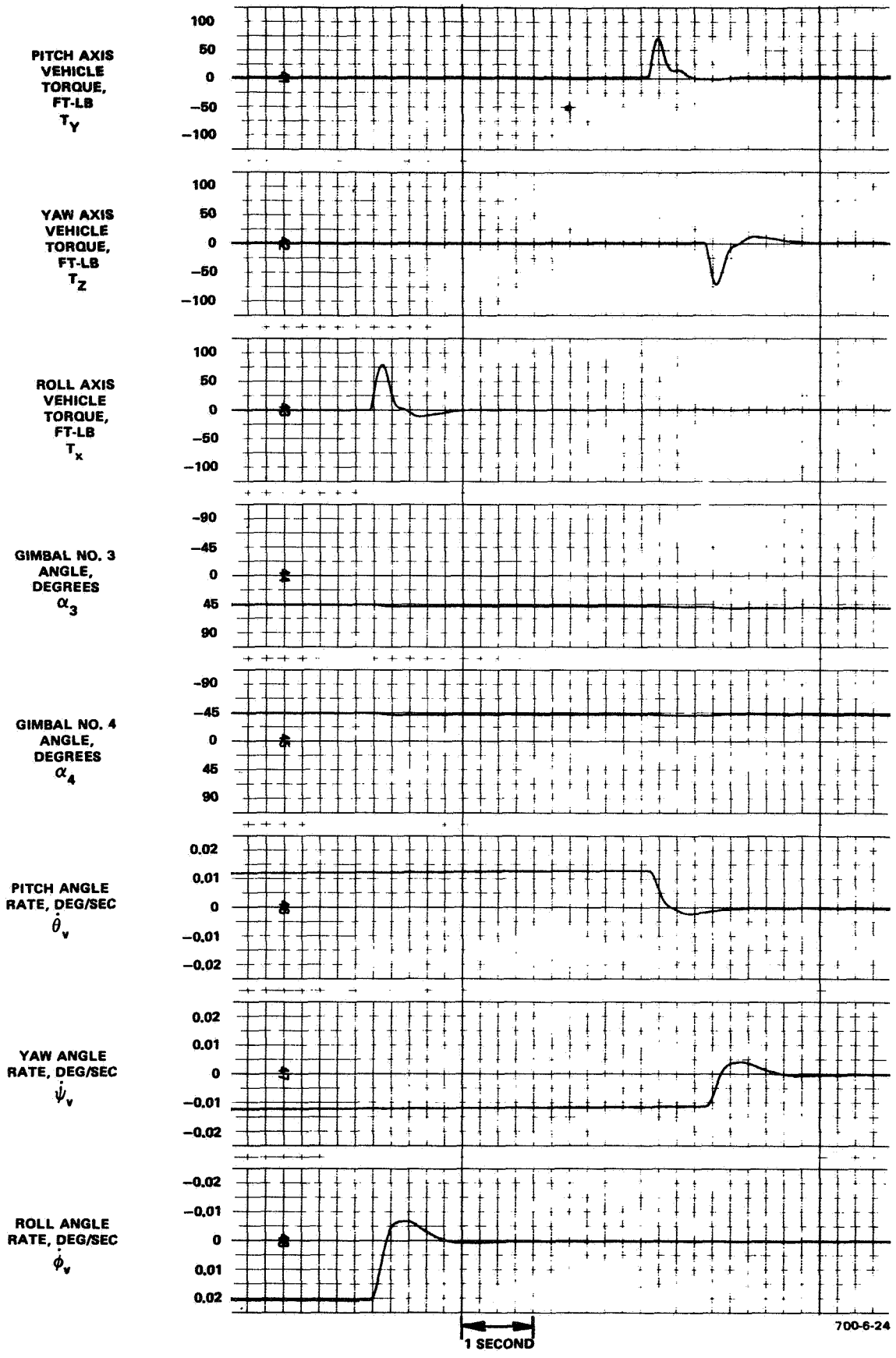

Figure 7-49
Initiate Fine Attitude Hold

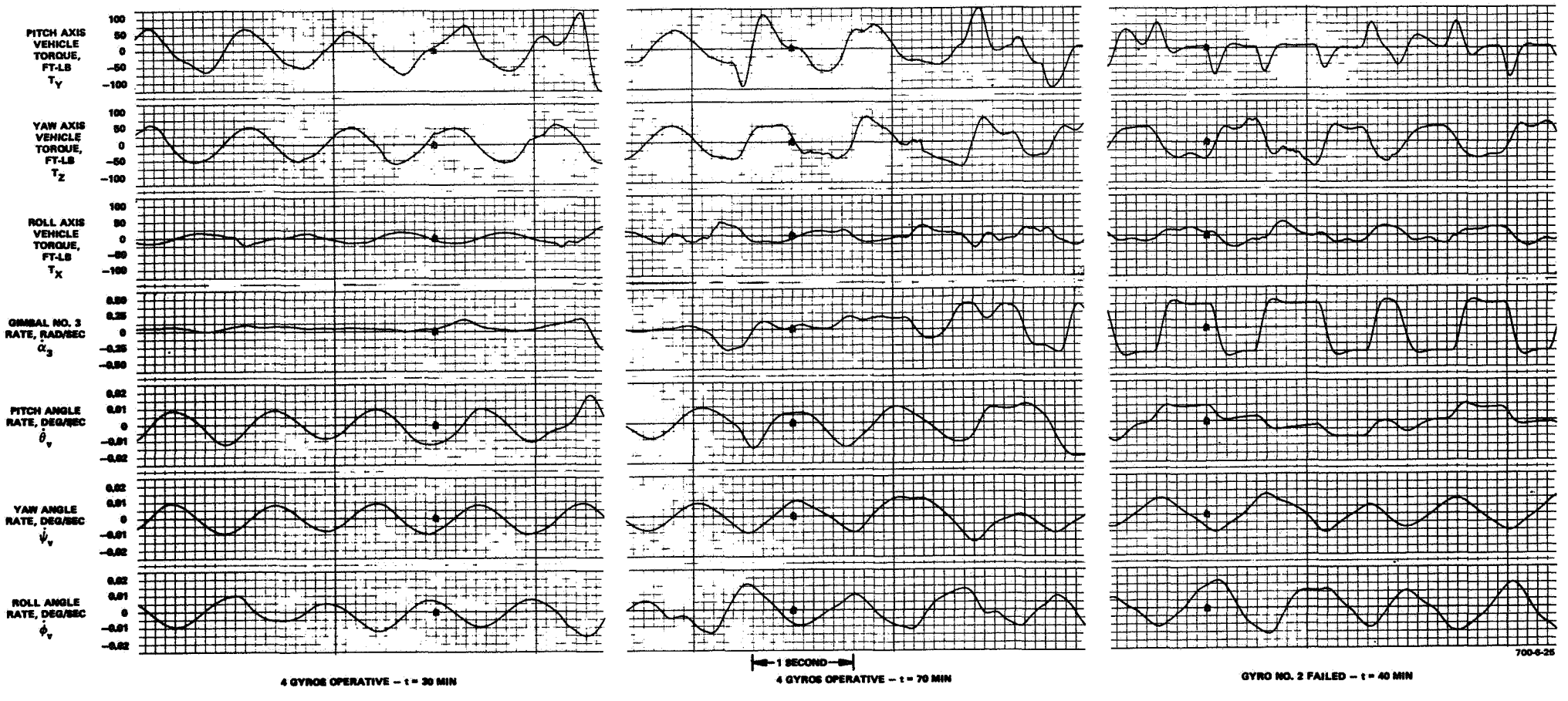

t REFERS TO TIME ELAPSED SINCE BEGINNING OF ORBIT

Figure 7-50
Fine Attitude Hold with 3-Axes
Disturbances, Sensor Noise:
0.02 degree at 1 Hz

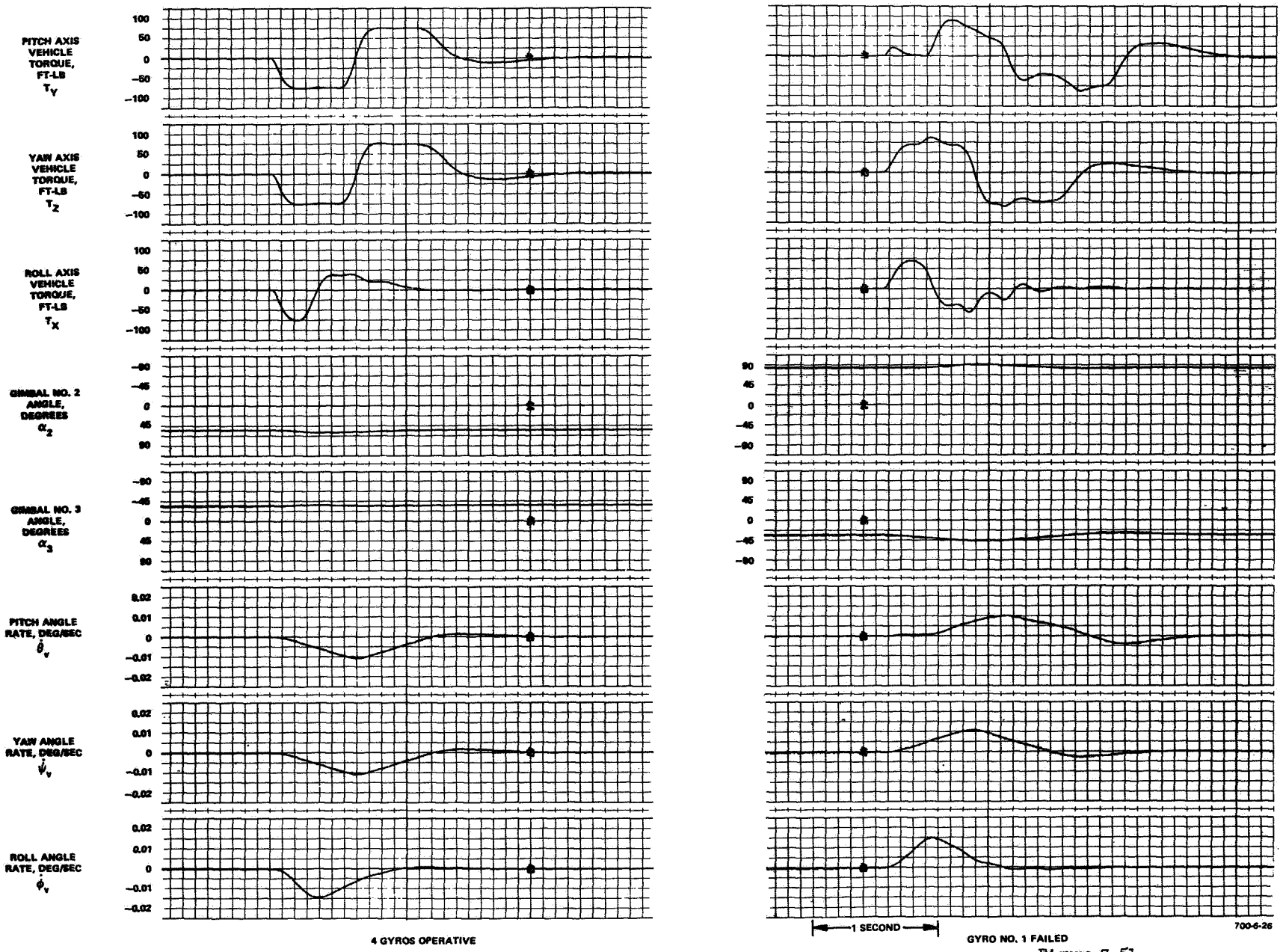

Figure 7-51
Sun Re-Acquisition During Attitude Hold,
Attitude Steps of 0.025 degree,
Momentum Stored in Three Axes

Two different types of gyro failure were investigated. In the first case, a gyro was shut off because an impending failure had been sensed: one example would be a high temperature reading in a bearing, indicating excessive friction. The failed gyro was then disconnected and allowed to spin down, while the steering law and gimbal angle limits were changed to the three-gyro configuration. In the second type of failure investigated, a gimbal angle was driven hardover due to some drastic failure such as loss of gimbal rate feedback. In this case, the discrepancy between commanded and actual gimbal rate was sensed by failure detection circuitry, the gimbal was stopped, and power removed. Then, the CMG system was changed to the three-gyro configuration. The failure was simulated by opening the rate feedback loop. When the discrepancy between commanded and actual gimbal rate was sensed, a first-order lag with a time constant of 0.5 second was closed around the gimbal rate integrator, and thus simulated braking of the gimbal. The system reaction to both types of failure is shown in Figure 7-52. In this case, a desaturation command was given at the time of the failure so that the gimbals were driven to the initial positions for the three-gyro configuration. In practice, this technique may not be necessary and one may wait to desaturate until the system is saturated or until it is desirable to do so. In this case, the first type of failure would have no effect on fine attitude hold; the effect of the second type of failure would be reduced.

The mission profile simulation discussed in this section shows that the 4-FACS does not exceed the "design mission" limits during normal operation and during operation with one gyro failed.

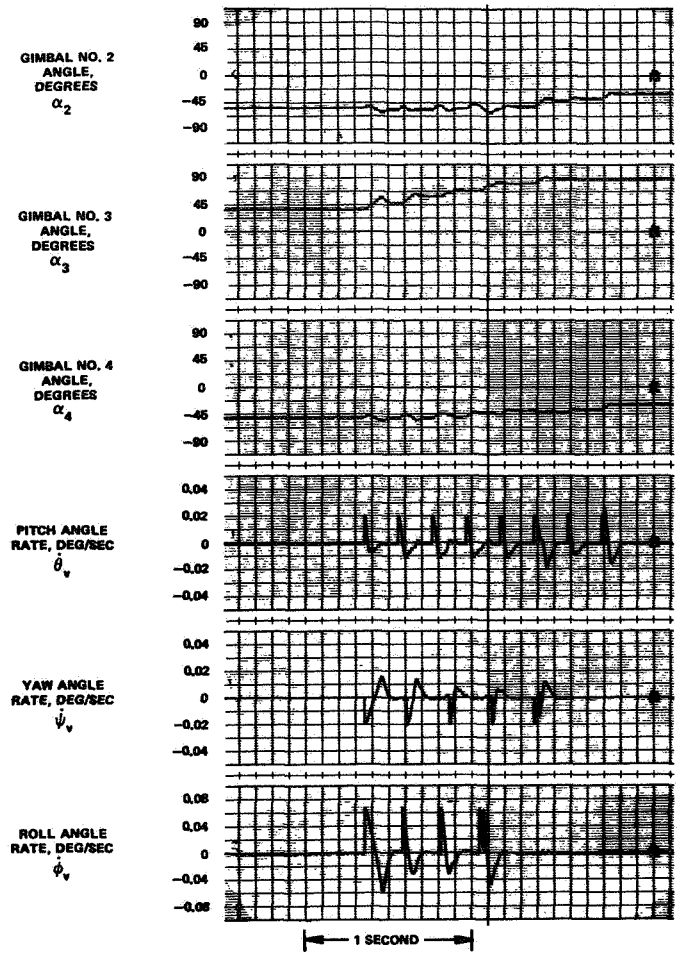

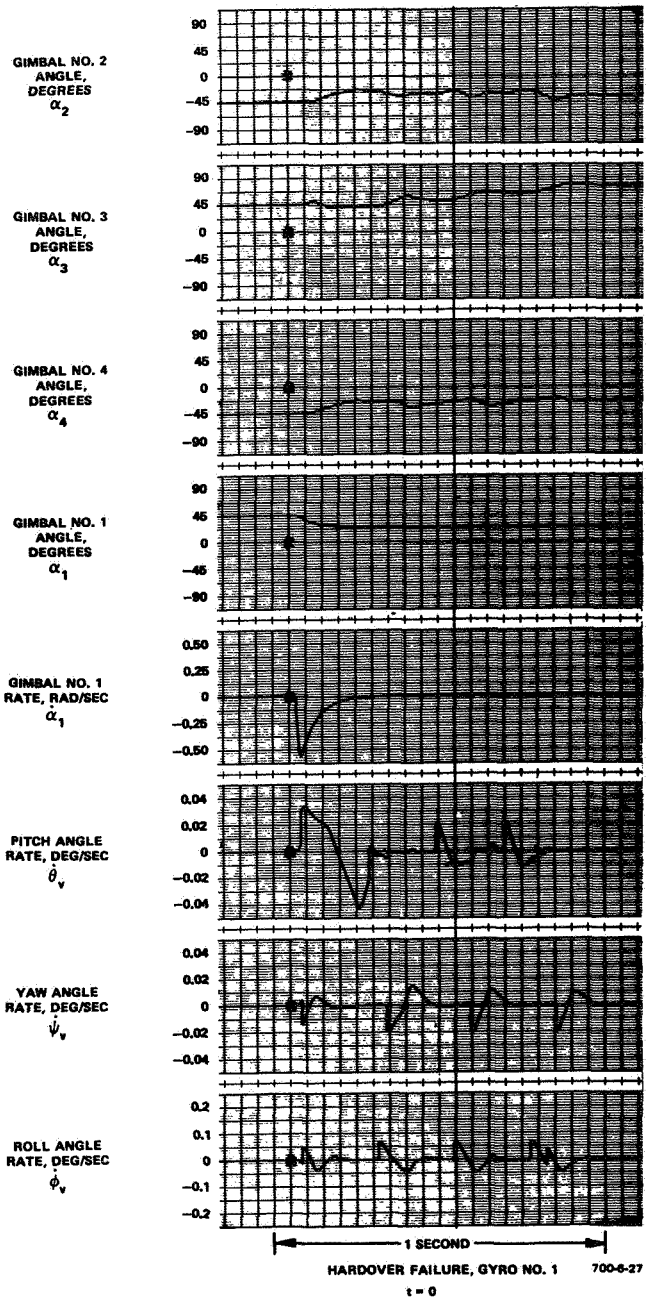

Figure 7-52
Gyro Failure

G. COMPARISON BETWEEN 4-FACS AND SCISSORED PAIR SYSTEM — ONE GYRO FAILED OPERATION

The particular scissored pair configuration used in this comparison is shown in Figure 7-53. Failure of one gyro in the X axis causes coupling in the Y axis but no coupling in the Z axis, so that in this study only the X and Y axes were simulated. The torque produced by this particular configuration with gyro No. 1 failed is

$$\begin{bmatrix} T_y \\ \\ T_x \end{bmatrix} = -h \begin{bmatrix} -\sin\alpha_2 & \cos\alpha_3 & \cos\alpha_4 \\ \\ \cos\alpha_2 & -\sin\alpha_3 & \sin\alpha_4 \end{bmatrix} \begin{bmatrix} \dot{\alpha}_2 \\ \dot{\alpha}_3 \\ \dot{\alpha}_4 \end{bmatrix} \tag{7-1}$$

Two different steering laws were analyzed. In the first one, each pair of gyros were mechanically geared so that two gyros in a pair always had their total momentum vector along one axis. In the second steering law, the gyros were steered electronically so that a pair of gyros did not necessarily have its total momentum vector pointed along one axis. In the event of failure of gyro No. 1, for example, a torque command in the X axis causes gyros No. 3 and 4 to move together with gyro No. 2 so that no coupling occurs in the Y axis.

The steering law for mechanically geared gyros is

$$\begin{bmatrix} \dot{\alpha}_{2c} \\ \dot{\alpha}_{3c} \\ \dot{\alpha}_{4c} \end{bmatrix} = \begin{bmatrix} 0 & 1 \\ \frac{1}{\sqrt{3}} & 0 \\ \frac{1}{\sqrt{3}} & 0 \end{bmatrix} \begin{bmatrix} T_{YC} \\ \\ T_{XC} \end{bmatrix} \tag{7-2}$$

The steering law for electronically steered gyros is

$$\begin{bmatrix} \dot{\alpha}_{2c} \\ \dot{\alpha}_{3c} \\ \dot{\alpha}_{4c} \end{bmatrix} = \begin{bmatrix} 0 & 1/2 \\ \frac{1}{\sqrt{3}} & 1/2 \\ \frac{1}{\sqrt{3}} & -1/2 \end{bmatrix} \begin{bmatrix} T_{YC} \\ \\ T_{XC} \end{bmatrix} \tag{7-3}$$

The pseudo-torque feedback steering law described in Subsection IV.D was also applied to the electronically steered scissored pair configuration and a gain of 200 rad/sec was used as in the 4-FACS simulation.

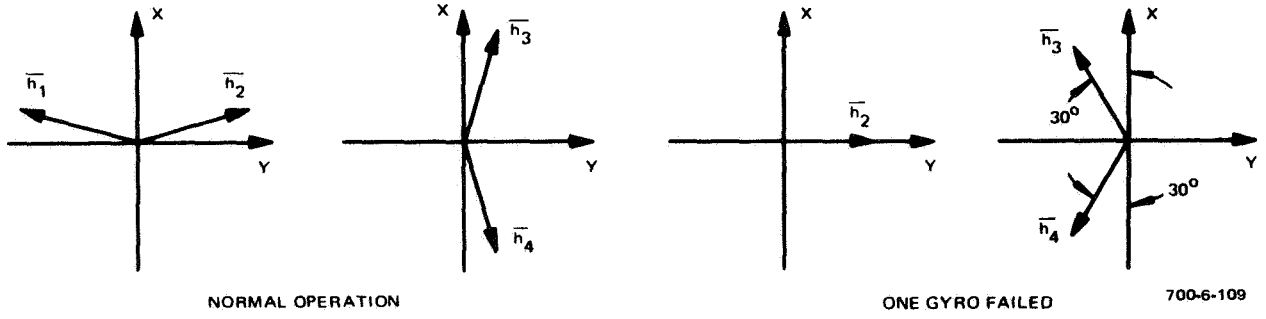

Figure 7-53
Scissored-Pair Operation after One Failure

The momentum limits for the 4-FACS and scissored pair systems are compared in Table 7-6. As shown, the envelope for either scissored pair configuration is considerably larger than the envelope for the 4-FACS configuration. At least one point in the scissored pair envelopes (depending on which gyro has failed), however, is close to a point in the 4-FACS envelope. The limit in the negative Y axis for either scissored pair configuration with a gyro failed in the Y axis is very close to the 4-FACS limit with gyro No. 1 or 3 failed. For this reason, the 4-FACS was compared with scissored pair systems having equal momentum gyros (200 ft-lb-sec). The same gimbal loop and the vehicle characteristics used in the 4-FACS study were adopted.

Step responses of systems with mechanically geared gyros and electronically steered gyros with constant gain steering law and with pseudo-torque feedback steering law are shown in Figure 7-54 through 7-56, respectively. The results are summarized and compared to the behavior of the 4-FACS system in Figures 7-57 and 7-58. When the pseudo-torque feedback steering law is employed, the electronically steered scissored pair and the 4-FACS have equal cross-coupling. When the constant gain steering law is employed, the scissored pair system with electronically steered gyros shows the least cross-coupling but the 4-FACS is still better than the mechanically geared scissored pair.

The 4-FACS with one gyro failed shows the highest steady-state gimbal rates; however, the gimbals are still far from being rate-limited.

The results of the study show that the 4-FACS with one gyro failed is slightly inferior to an electronically steered scissored pair system with one gyro failed. The 4-FACS performance with one gyro failed, however, satisfies the design requirements and is not significantly inferior to the scissored pair performance especially if the pseudo-torque feedback steering law is employed. The added weight and complexity of the two extra scissored pair gyros, therefore, are not justified by the slight improvement in performance.

TABLE 7-6

COMPARISON OF SINGLE AXIS MOMENTUM LIMITS

Configuration		$\frac{H_x \text{ maximum}}{h}$		$\frac{H_y \text{ maximum}}{h}$		$\frac{H_z \text{ maximum}}{h}$	
		+	-	+	-	+	-
4-FACS	Gyro No. 1 or 3 failed	0.598	0.598	0.825	0.992	0.598	0.598
	Gyro No. 2 or 4 failed	0.598	0.598	0.992	0.825	0.598	0.598
Scissored Pair, Gyro Failed in X Axis	Mechanically Geared	2.99	0.99	0.995	0.995	1.99	1.99
	Electrically Steered	2.99	0.99	1.99	1.99	1.99	1.99
Scissored Pair, Gyro Failed in Y Axis	Mechanically Geared	0.995	0.995	2.99	0.99	1.99	1.99
	Electrically Steered	1.99	1.99	2.99	0.99	1.99	1.99
Scissored Pair, Gyro Failed in Z Axis	Mechanically Geared	1.99	1.99	1.99	1.99	0.995	0.995
	Electrically Steered	1.99	1.99	1.99	1.99	0.995	0.995

NOTES: 1. Scissored pair gimbal angle limit: ±85°.

2. Above limits based on stability considerations only.

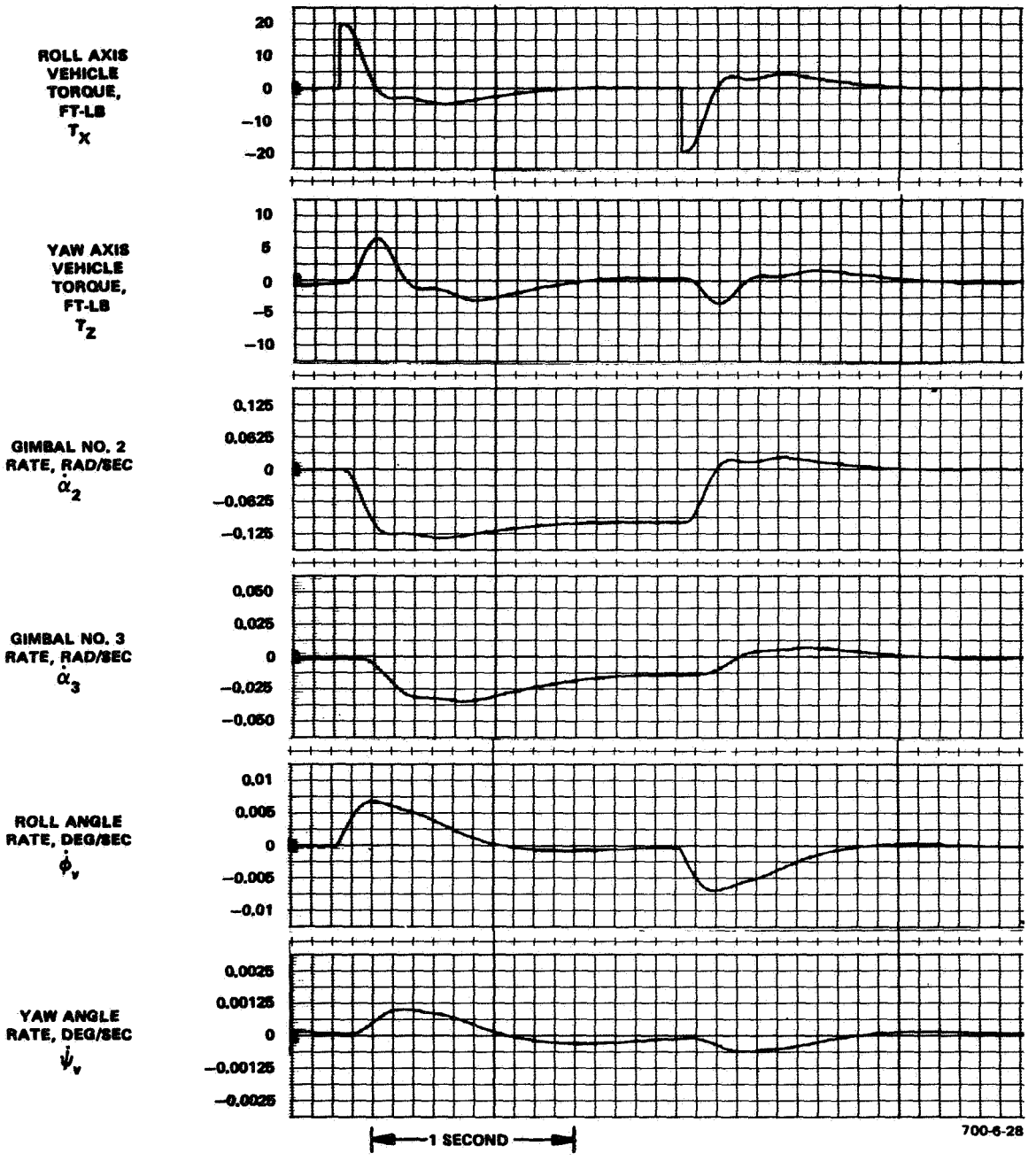

Figure 7-54
Step Torque Disturbance of 20 foot-pounds in Roll Axis, Scissored-Pair Mechanically Geared, Gyro No. 1 Failed, Stored Momentum: $\left(\frac{H_x}{h}\right) = 0.47$

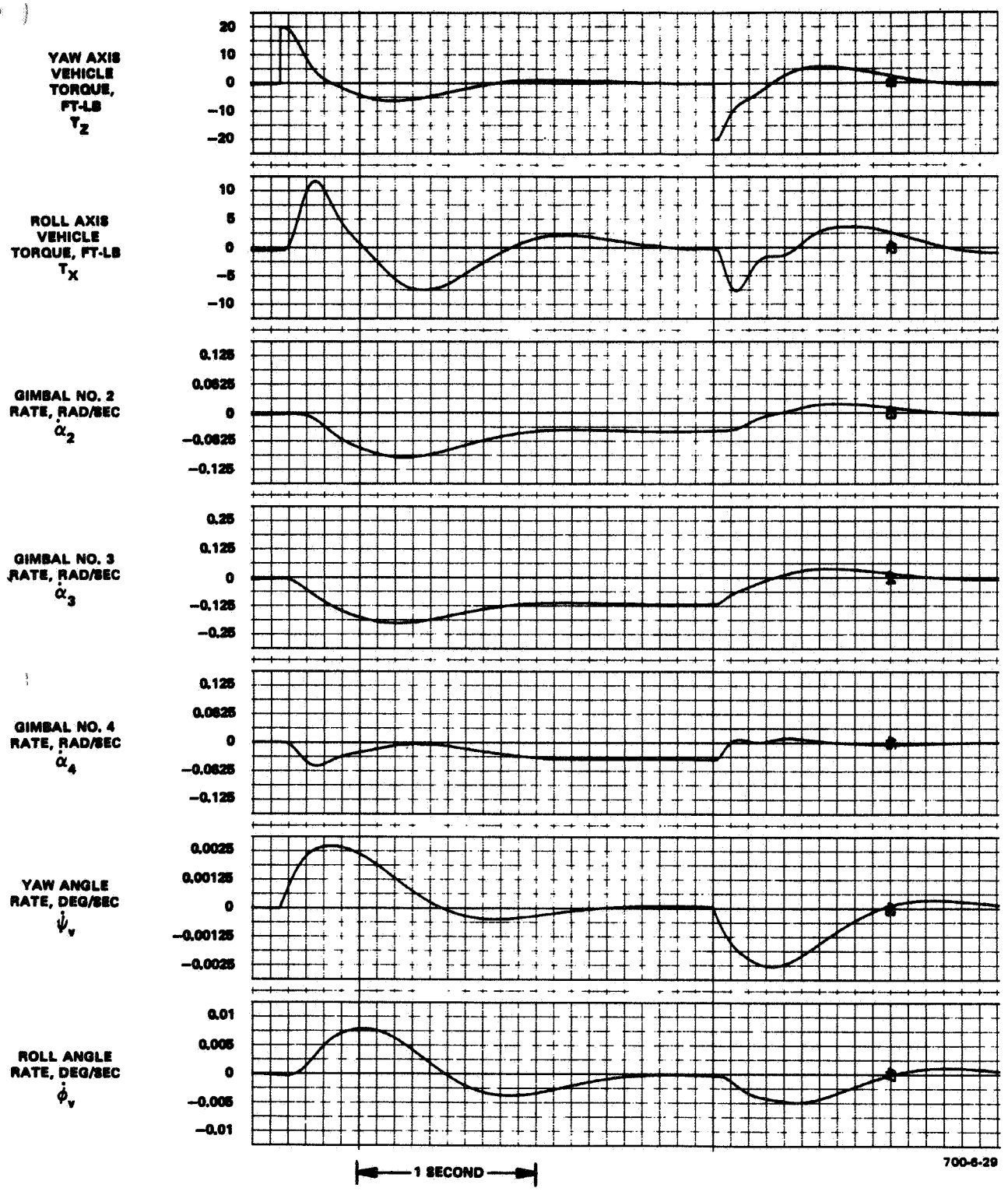

Figure 7-55
Step Torque Disturbance of 20 foot-pounds in Yaw Axis, Scissored Pair Electronically Steered, Constant Gain Steering Law, Gyro No. 1 Failed, Stored Momentum: $\left(\frac{H_x}{h}\right) = 1.4$

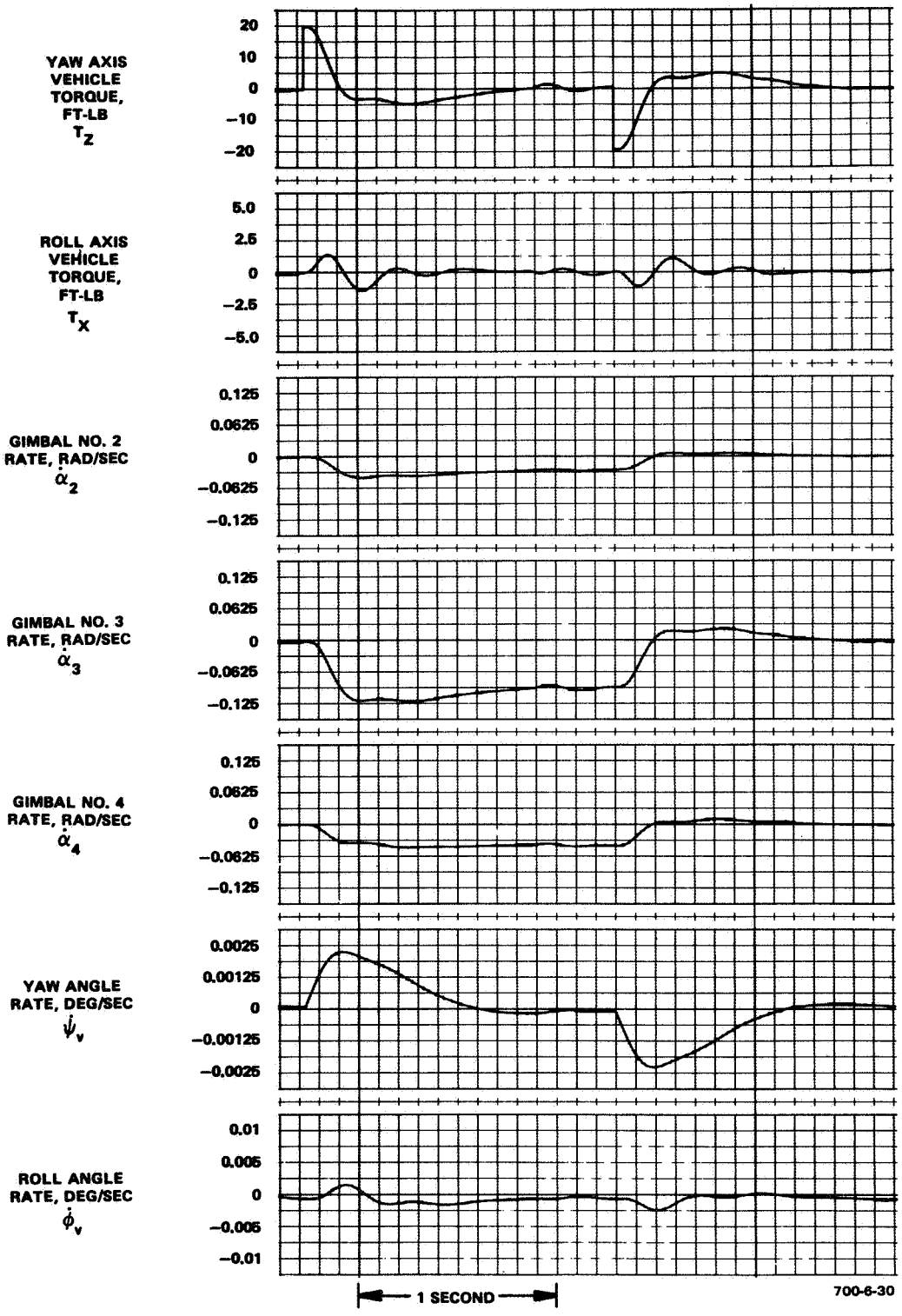

Figure 7-56
Step Torque Disturbance of 20 foot-pounds in Yaw Axis, Scissored-Pair Electronically Steered, Pseudo-Torque Feedback Steering Law, Gyro No. 1 Failed, Stored Momentum: $\left(\frac{H_x}{h}\right) = 1.0$

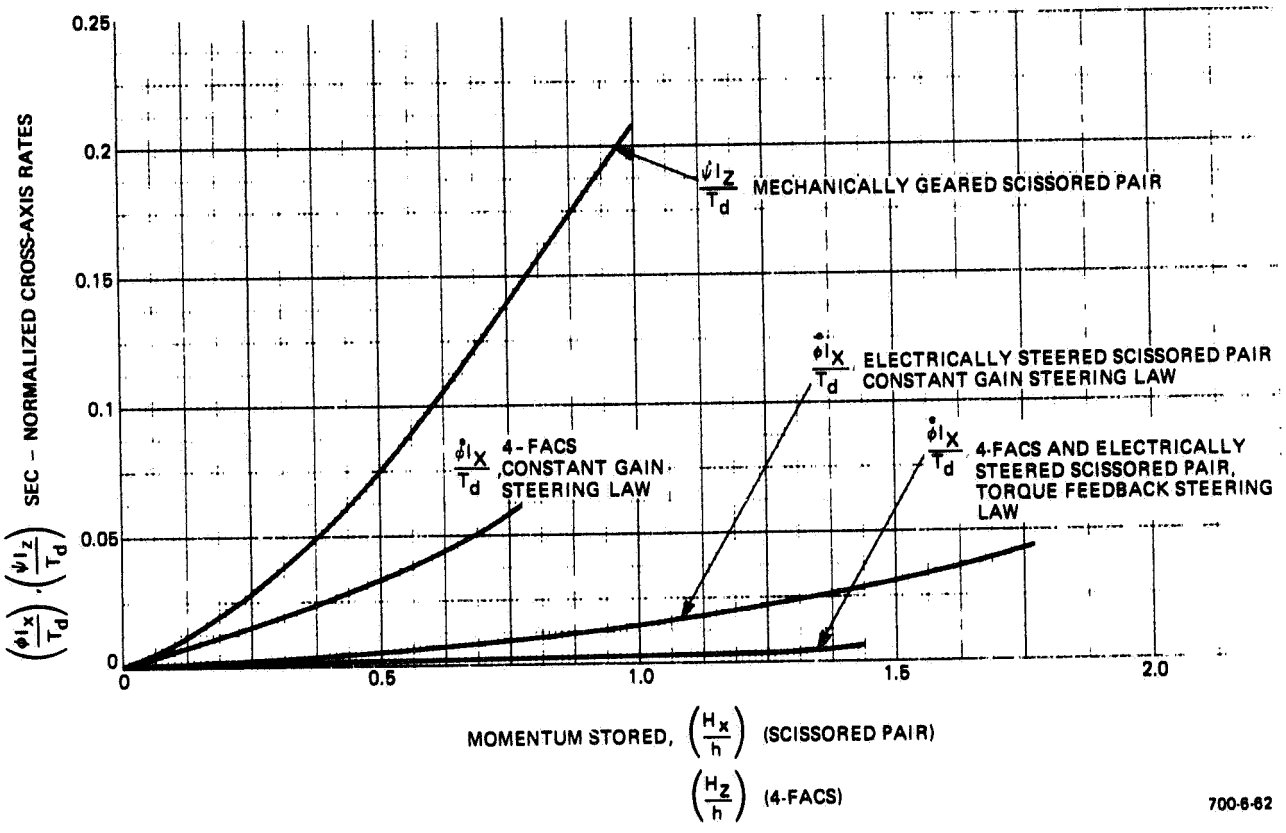

Figure 7-57
Comparison of Cross-Coupling with
One Gyro Failed between 4-FACS
and Scissored-Pair, Step Torque
Disturbance of 20 foot-pounds,
Normalized Variables

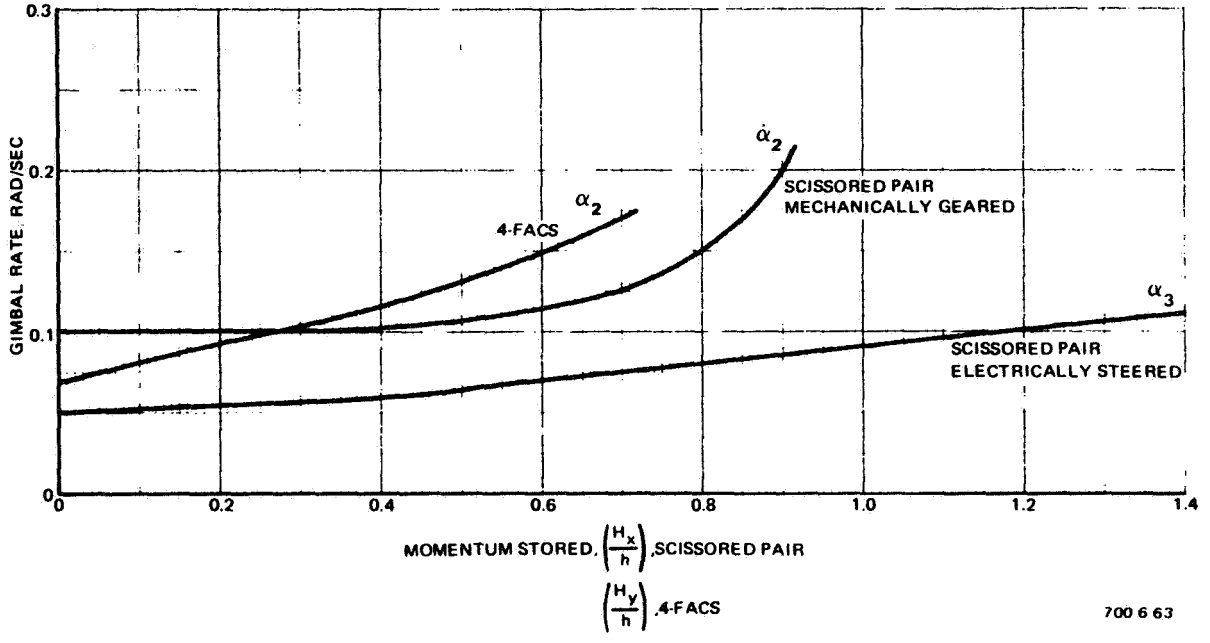

Figure 7-58
Comparison of Steady-State Gimbal Rates between 4-FACS with One Gyro Failed and Scissored-Pair with One Gyro Failed, Step Torque of 20 foot-pounds

H. LOW TORQUE SYSTEM

A preliminary study was conducted to define some characteristics of a low torque, low bandwidth system applicable to unmanned missions. The effect of overall system bandwidth on vehicle rate when subjected to a step torque disturbance was investigated by considering system with various bandwidths. Only one vehicle axis was simulated; the pseudo-torque feedback steering law was used and the 4-FACS gyro and gimbal loop characteristics remained as in the high torque system; the compensation network was altered to give the desired bandwidth. Five basic compensation network configurations were studied as follows:

- Zero at 4 rad/sec, zero at 10 rad/sec, pole at 50 rad/sec
- Zero at 3 rad/sec, pole at 50 rad/sec
- Zero at 2 rad/sec, pole at 50 rad/sec
- Zero at 1.5 rad/sec, pole at 50 rad/sec
- Zero at 1 rad/sec, pole at 50 rad/sec

In each case, a linear digital computer analysis was performed to determine the loop gain which gave a damping ratio of 0.7 and the bandwidth corresponding to that loop gain. The location of the dominant roots for the five cases is shown in Figure 7-59. In each configuration, the bandwidth determined corresponded to loop gains for which the damping ratio was within 15 percent of 0.7; a set of points was thus obtained that spanned a wide range of bandwidths. A step torque disturbance of 1 ft-lb for one second was applied for each point and the response recorded. Examples of step responses are shown in Figure 7-60. The maximum vehicle rate attained in each case was determined and all the points fell within the shaded region in Figure 7-61. The configurations tested did not necessarily have the best compensation for the desired bandwidth. They give, however, a good idea of the behavior of an ideal (linear) 4-FACS at various bandwidths. With the proper compensation, a system can probably be designed, the performance of which will fall at least within the shaded area of Figure 7-61. As shown, when the bandwidth is increased above 10 rad/sec, the low torque system performance is affected very slightly, and therefore no need exists to increase the bandwidth of this system much above 10 rad/sec.

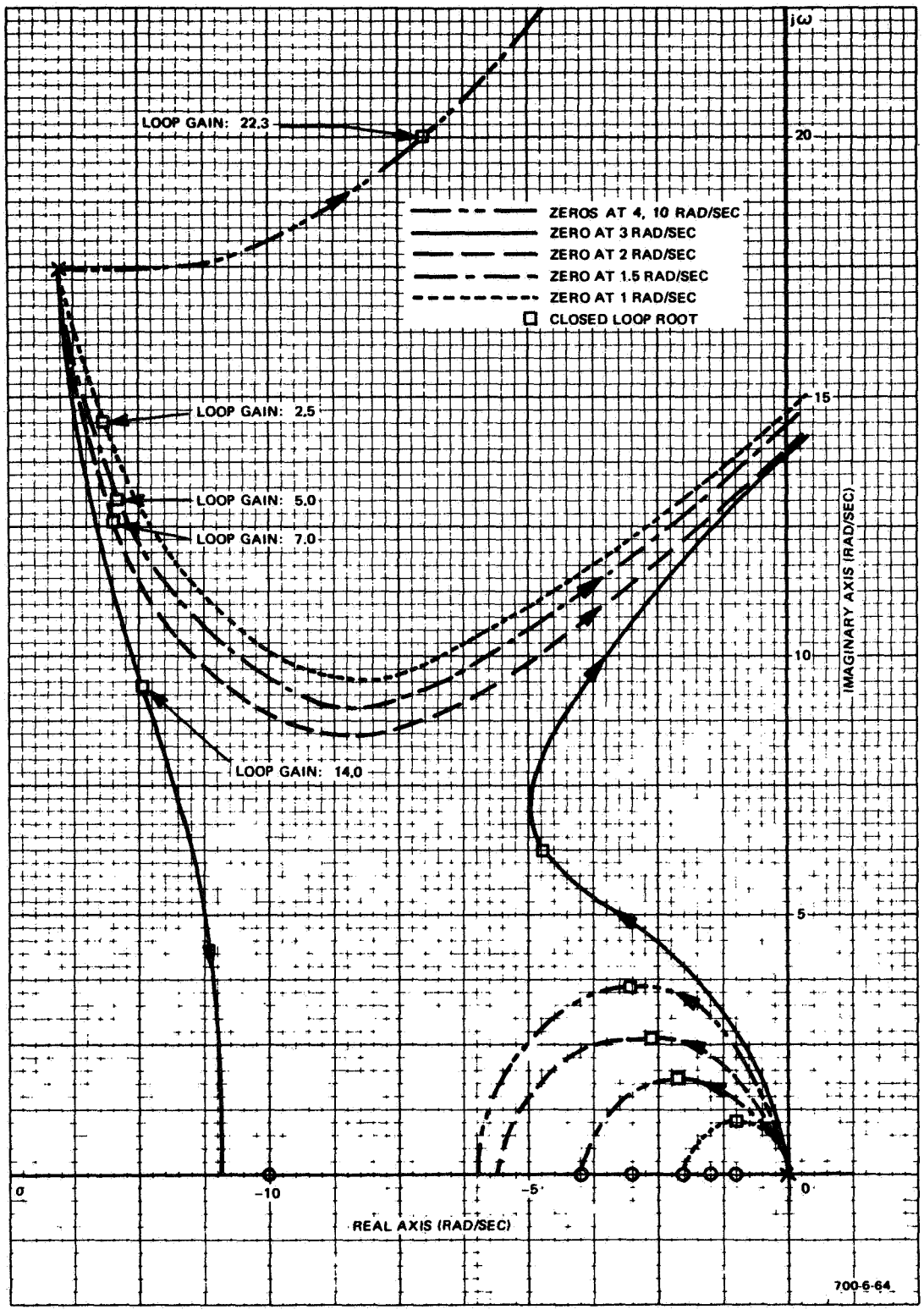

Figure 7-59
Location of Roots for Low-Torque System

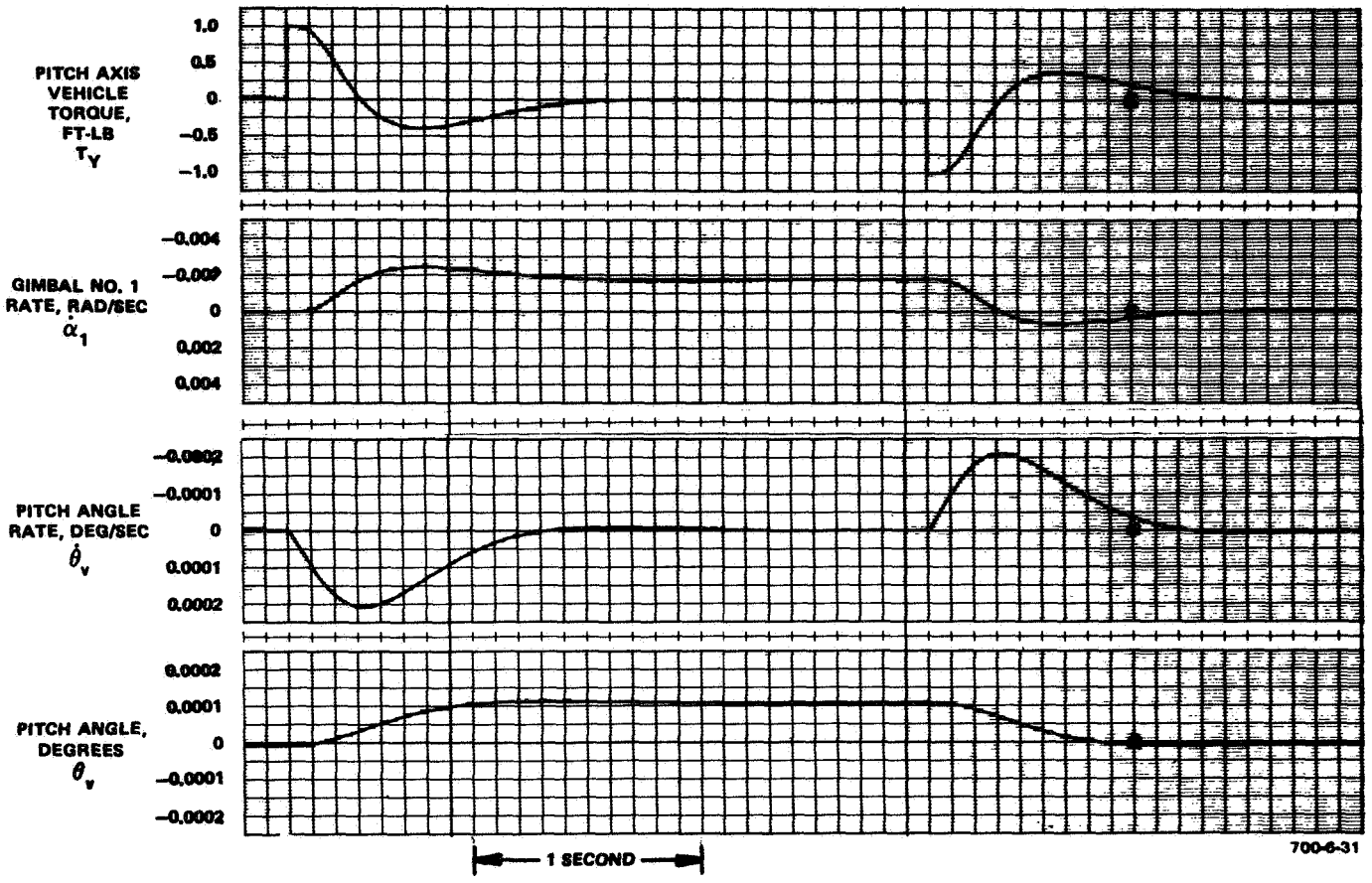

Figure 7-60
Step Torque Disturbance of 1 foot-pound in Pitch Axis, Low-Torque System (Zero at 2 radians per second, 9 radians per second Bandwidth), No Stored Momentum

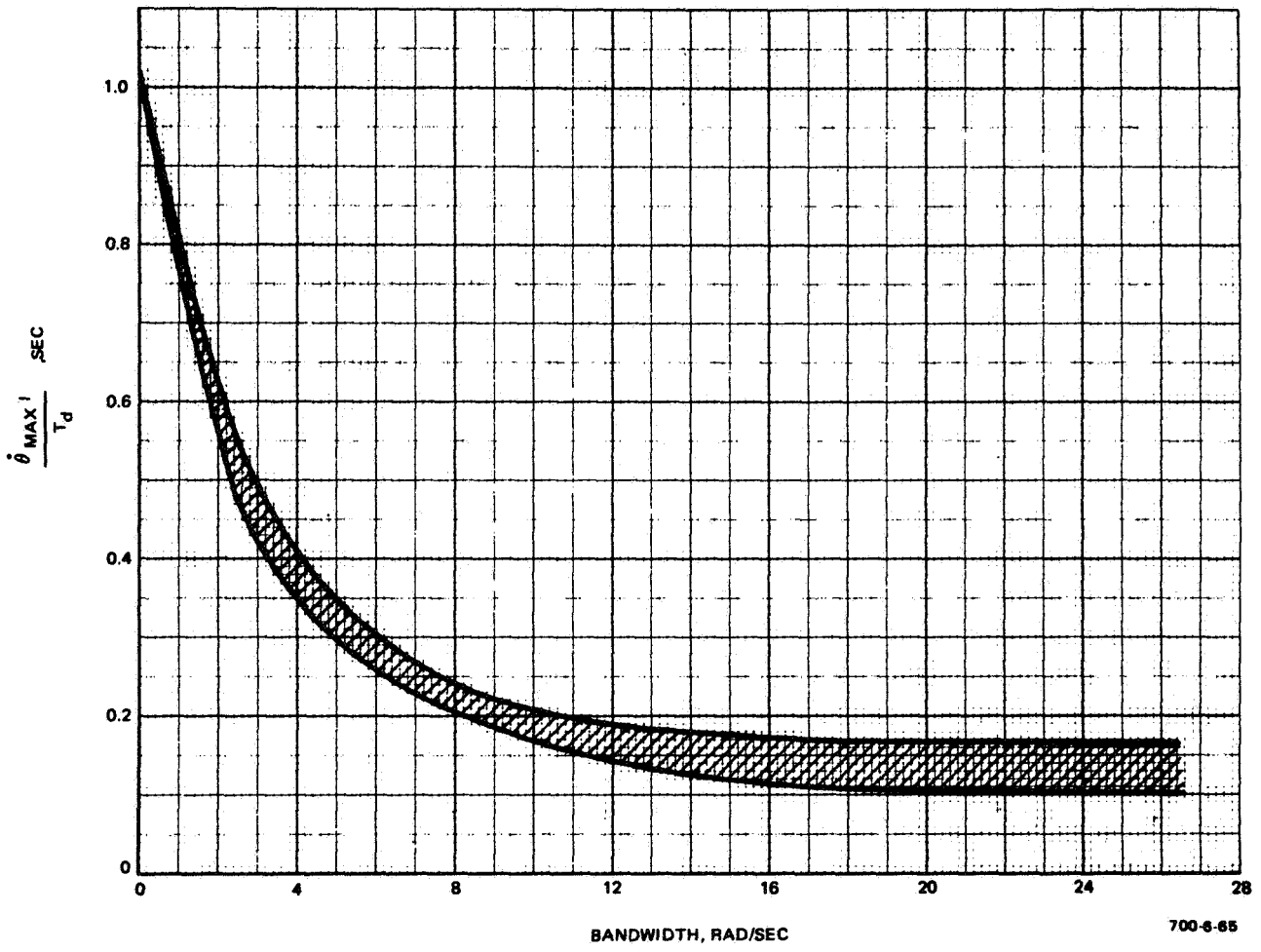

Figure 7-61
Effect of Bandwidth on Vehicle Rate, Step Torque Response, Normalized Curve, Disturbance Torque of 1 foot-pound for 1 second

I. SUMMARY

The analog simulation studies that were conducted show the following characteristics of the 4-FACS CMG configuration when used for fine attitude hold of an Apollo CSM type vehicle:

- Good performance during all mission profile phases
- Attitude error held within 0.1 degree
- Rate held within 0.01 degrees/second for most inputs*
- Ability to maintain a small attitude error while desaturating with RJC method
- Moderate cross coupling with a constant gain steering law**
- Negligible cross coupling with pseudo-torque feedback steering law
- 3.9 Hz bandwidth capability with constant gain steering law and four gyros operative
- 1.35 Hz bandwidth capability with constant gain steering law and three gyros operative
- 3.9 Hz bandwidth capability with pseudo-torque feedback law, constant for 3 or 4 gyro operation
- Adequate gain margin (at least 8 db) for all values of stored momentum
- System performance with one failed gyro competitive with performance of scissored pair system with one failed gyro

The low torque system study showed that the 4-FACS configuration is applicable to such a system. If this study is to be pursued further, a more complete model of the gimbal loop would be needed to investigate the effect on system performance of gimbal loop non-linearities and to establish the ultimate accuracy achievable with the 4-FACS configuration.

---

*One exception is the roll axis rate response to a 25 foot-pound single sinusoidal disturbance torque about the X axis.

**One exception is cross-coupling in the roll axis with input in the Z axis when gyro No. 1 is failed and momentum is stored in the positive Y axis.

SECTION VIII

FAILURE MODES, MONITORING, AND FAILURE DETECTION

SECTION VIII

FAILURE MODES, MONITORING, AND FAILURE DETECTION

This section includes the three related areas of failure modes and effects analysis, parameter monitoring/command, and failure detection. A breakdown of the attitude control system failure modes is presented which tabulates the required corrective action and necessary failure detection networks. A telemetry list is also presented which specifies each parameter to be sent from and received by the vehicle, the bandwidth, and the accuracy requirement. Block diagrams showing the various types of failure detection networks are included.

A. FAILURE MODES AND EFFECTS

The failure modes and effects have been determined for the overall vehicle control system to establish which failures can occur and their effect on system behavior. The results which are listed in this section, include the signals to be monitored to detect a failure, an identification of the detection circuit, the detection method employed, the necessary corrective action and options, and the magnitude of the failure effect. The following ground rules and assumptions were used:

- Only major functional blocks (i.e., attitude reference sensor, rate gyro, etc) are analyzed. A detailed component (resistor, capacitor, relay, etc) level analysis was not attempted within the scope of this task.

- Hardover and open type failures are considered as the only failure modes for each functional block.

- Failure effects are classified as:

  I. Loss of vehicle control
  II. Loss of mission (must repair or replace failed component)
  III. Degraded performance

- When a type II failure occurs, a redundant or backup system is normally put into use; therefore, the fine attitude mission must be terminated and the failed component repaired or replaced. Use of this technique assumes that during a manned mission the crew could make the repair or that during an unmanned mission the vehicle could be returned to a co-orbital repair facility.

- When a type III failure occurs, immediate correction is not always necessary. The influence of the degraded performance on the mission objectives must be evaluated to determine if the mission can still be accomplished successfully.

- The failure mode functional blocks and monitored signals refer to the overall system block diagram shown in Appendix F.

The analysis identifies all CMG failure modes as being of a type II or lesser category. The only possible type I failures exist for RJC failures at particular mission times or in certain rocket combinations. By employing redundancy in the RJC system thrusters and in the electronics all type I failures would be precluded as a result of a failure in the attitude control system.

The failure mode analysis (Table 8-1) only indicates possible failures and their effects, however, and does not indicate at all the probability of a failure occurring. The reliability analysis of Section IX should be used in conjunction with this section to evaluate the acceptability of the overall design.

B. SIGNAL MONITORING AND COMMAND

The attitude control telemetry signals necessary for monitoring the status and activity of the system and the command signals required for system control are listed in Table 8-2. The failure detection networks and control facility are assumed to be either ground based or on board a larger co-orbital vehicle such as a space station or base. As a result, the vehicle can be controlled remotely, continuous verification of failure detection circuitry can be provided, and permanent data storage can be obtained for all system parameters. Each signal tabulated, which is referenced to the overall system block diagram (Appendix F), includes a description of its form, required accuracy, and sampling rate.

TABLE 8-1

FAILURE MODE ANALYSIS

Failure	Signals Monitored	Type Detection Circuit	Detection Method	Corrective Action and Remarks	Failure Effect
Attitude Reference System Sensor	Attitude error A1, A2, A3	A	Monitor for hardover signal.	Switch to alternate reference in failed axis.	
				If alternate reference not available (i.e., sun occluded) switch off failed axis and use rate damping until reference is available.	II
Primary Rate Gyro or Rate Electronics	Primary rate signal B1, B2, B3	A	Monitor for hardover signal.	Switch to backup rate gyro in failed axis.	II
	Primary SMRD M1, M2, M3	F	SMRD signals indicate wheel speed.		
Backup Rate Gyro	Backup rate signal B1', B2', B3'	A	Monitor for hardover signal.	No immediate corrective action.	
	Backup SMRD M1', M2', M3'	F	SMRD signals indicate wheel speed.	Replace backup rate gyro.	II
CMG Vehicle Computer	Output C1, C2, C3	A	Monitor for hardover signal.	Switch to RJC only.	
	Rate and attitude error A1, A2, A3, B1, B2, B3	B	Compute output from A and B signals. Compare to C1, C2, C3.	Turn off CMG.	II

TABLE 8-1 (cont)

FAILURE MODE ANALYSIS

Failure	Signals Monitored	Type Detection Circuit	Detection Method	Corrective Action and Remarks	Failure Effect
RJC Electronics	One shot output N1, N2, N3	C	Monitor one shot signals to detect hardover.	None. Loss of Reaction Jet Control in failed axis.	II possible I
	Output P1, P2, P3 Rate and Attitude Error A1, A2, A3, B1, B2, B3	D	Compute state of output from A and B signals. Compare to P1, P2, P3.	RJC desaturation is still operative and CMG operation can continue. If failure occurs during de-boost, vehicle may be lost.	
CMG Wheel (Spin Motor or Bearings)	Spin motor current, J_1 --- J_4	E	Monitor for excessive spin motor current - indicating bearing friction.	De-spin gyro by dynamic breaking or turning off spin motor power to failed gyro.	III
	Wheel speed I_1 --- I_4	F	Monitor wheel speed.	Switch CMG computer to 3 gyro configuration.	
CMG Spin Motor Electronics	Wheel speed I_1 --- I_4	F	Monitor wheel speed.	Turn off spin motor power to failed gyro. Switch CMG computer to 3 gyro configuration.	III
CMG Gimbal Torque Motor Gimbal Bearings	Gimbal tachometer F1 --- F4 Gimbal rate command D1 --- D4	F	Compare commanded gimbal rate and tachometer signal.	Turn off spin motor power to failed gyro. Turn off power to failed gyro torquer bridge. Switch CMG computer to 3 gyro configuration.	III

TABLE 8-1 (cont)

FAILURE MODE ANALYSIS

Failure	Signals Monitored	Type Detection Circuit	Detection Method	Corrective Action and Remarks	Failure Effect
CMG Gimbal Control Loop Electronics	Gimbal tachometer F1 --- F4 Gimbal rate command D1 --- D4	F	Compare commanded gimbal rate and tachometer signal.	Turn off spin motor power to failed gyro. Turn off power to failed gyro torquer bridge. Switch CMG computer to 3 gyro configuration.	III
CMG Gimbal Angle Synchro	Gimbal angle synchro G1 --- G4	A	Monitor gimbal synchro for hardover signed.	Turn off spin motor power to failed gyro. Turn off power to failed gyro torquer bridge. Switch CMG computer to 3 gyro configuration.	III
CMG Steering Law Computer (Desaturation Section)	Gimbal angle synchro G1 --- G4 Computer RJC outputs H1 --- H3	G H	Monitor output duty cycle for excess authority. Compute correct output signals from gimbal angle signals and compare to computer out outputs.	Turn off CMG system. RJC system maintains control.	II
CMG Steering Law Computer (Gimbal Command Section)	CMG vehicle computer output C1, C2, C3 Steering law torque feedback signals E1, E2, E3	F	Compare command and feedback signals of steering law to verify closed loop.	Turn off CMG system. NOTE: This detection method only senses gross failures. Computational errors are not detected.	II

TABLE 8-1 (cont)

FAILURE MODE ANALYSIS

Failure	Signals Monitored	Type Detection Circuit	Detection Method	Corrective Action and Remarks	Failure Effect
CMG Steering Law Computer (Gimbal Command Section) (cont)	Computer gimbal angle commands D1 --- D4	A	Monitor output for hardover.	RJC system maintains control.	II
CMG Steering Law Computer (Initial Angle and Angle Limit Section)	Gimbal angle synchro G1 --- G4 Desaturation relay R1	This is done manually during data analysis	Monitor gimbal angles at beginning and end of desaturation.	Turn off CMG system.	II
RJC Rocket Logic and Solenoid Driver Electronics	RJC command signals H1, H2, H3 N1, N2, N3 P1, P2, P3 Solenoid current signals K1 --- K16	I	Monitor RJC command signals and compute correct rocket signals; compare to solenoid currents.	If failure is in rocket logic the system may still be operative with degraded performance. If failure occurs in solenoid drive amplifiers, shut off associated rocket fuel. Possible loss of complete RJC system in one axis.	III possible II or I
RJC Rockets	Solenoid currents K1 --- K16 Rocket pressure transducers L1 --- L16	J	Compare rocket commands to pressure transducer traces.	Shut fuel off to failed rocket.	II

TABLE 8-2

FINE ACS TELEMETRY SIGNALS

Symbol	Signal	Signal Form	Sampling Rate (SPS)	Accuracy (percent)	Remarks
A1	Roll Attitude Error	Analog, dc bipolar	50	2	These signals are transmitted from the vehicle.
A2	Pitch Attitude Error		50	2	
A3	Yaw Attitude Error		50	2	
B1	Primary Roll Vehicle Attitude Rate		100	1	
B2	Primary Pitch Vehicle Attitude Rate				
B3	Primary Yaw Vehicle Attitude Rate				
B1'	Backup Roll Vehicle Attitude Rate				
B2'	Backup Pitch Vehicle Attitude Rate				
B3'	Backup Yaw Vehicle Attitude Rate				
C1	Steering Law Torque Command, Roll				
C2	Steering Law Torque Command, Pitch				
C3	Steering Law Torque Command, Yaw				
D1	CMG Gimbal Rate Command, CMG 1				
D2	CMG Gimbal Rate Command, CMG 2				
D3	CMG Gimbal Rate Command, CMG 3				
D4	CMG Gimbal Rate Command, CMG 4				
E1	Steering Law Torque Feedback, Roll				
E2	Steering Law Torque Feedback, Pitch				
E3	Steering Law Torque Feedback, Yaw	Analog, dc bipolar	100	1	

TABLE 8-2 (cont)
FINE ACS TELEMETRY SIGNALS

Symbol	Signal	Signal Form	Sampling Rate (SPS)	Accuracy (percent)	Remarks
F1	CMG Gimbal Rate, CMG 1	Analog, dc bipolar	100	1	
F2	CMG Gimbal Rate, CMG 2				
F3	CMG Gimbal Rate, CMG 3				
F4	CMG Gimbal Rate, CMG 4				
G1	CMG Gimbal Angle Synchro, CMG 1				
G2	CMG Gimbal Angle Synchro, CMG 2				
G3	CMG Gimbal Angle Synchro, CMG 3				
G4	CMG Gimbal Angle Synchro, CMG 4	Analog, dc bipolar	100	1	
H1	Steering Law RJC Command, + Roll	Discrete positive pulse	200	-	ON-OFF signal
H2	Steering Law RJC Command, - Roll			-	
H3	Steering Law RJC Command, + Pitch			-	
H4	Steering Law RJC Command, - Pitch			-	
H5	Steering Law RJC Command, + Yaw			-	
H6	Steering Law RJC Command, - Yaw	Discrete positive pulse	200	-	CMG Rotor Tachometer pulses are preconditioned in gyro electronics.
I1	CMG Rotor Speed, CMG 1	Analog, dc positive	10	1.0	
I2	CMG Rotor Speed, CMG 2				
I3	CMG Rotor Speed, CMG 3				
I4	CMG Rotor Speed, CMG 4	Analog, dc positive	10	1.0	

TABLE 8-2 (cont)

FINE ACS TELEMETRY SIGNALS

Symbol	Signal	Signal Form	Sampling Rate (SPS)	Accuracy (percent)	Remarks
J1	CMG Spin Motor Current, CMG 1	Analog, dc positive	10	1.0	
J2	CMG Spin Motor Current, CMG 2	↓	↓	↓	
J3	CMG Spin Motor Current, CMG 3	↓	↓	↓	
J4	CMG Spin Motor Current, CMG 4	Analog, dc positive	10	1.0	
K1-K16	Reaction Jet Commands	Discrete positive pulse	200	-	
L1-L16	Reaction Jet Pressure Transducers	Analog, dc positive	↓	5	
N1	Reaction Jet Electronic One Shot Output, Roll	Discrete positive pulse	↓	-	
N2	Reaction Jet Electronic One Shot Output, Pitch	↓	↓	-	
N3	Reaction Jet Electronic One Shot Output, Yaw	↓	200	-	
P1	Reaction Jet Electronic Output, Roll	↓	100	-	
P2	Reaction Jet Electronic Output, Pitch	↓	100	-	
P3	Reaction Jet Electronic Output, Yaw	↓	100	-	
R1	Desaturation Signal	↓	10	-	
S1	Sun Sensor Acquisition Signal	↓	10	-	
T1	Steering Law Gyro Failure Signal	Discrete positive pulse	10	0	

TABLE 8-2 (cont)
FINE ACS TELEMETRY SIGNALS

Symbol	Signal	Signal Form	Sampling Rate (SPS)	Accuracy (percent)	Remarks
X1	CMG Spin Motor Power Command, CMG 1	Discrete (on-off)	10	-	These signals are commands sent to the vehicle.
X2	CMG Spin Motor Power Command, CMG 2			-	
X3	CMG Spin Motor Power Command, CMG 3			-	
X4	CMG Spin Motor Power Command, CMG 4			-	
X5	CMG System Engage Command			-	
X6	CMG System Disengage Command			-	
X7	CMG System Desaturate Command			-	
X8	CMG Failure, CMG 1			-	
X9	CMG Failure, CMG 2			-	
X10	CMG Failure, CMG 3			-	
X11	CMG Failure, CMG 4			-	
X12	Rate Gyro Failure, Pitch			-	
X13	Rate Gyro Failure, Roll			-	
X14	Rate Gyro Failure, Yaw			-	
X15-31	Reaction Jet Fuel Control Commands			-	
X32	Star Tracker Failure			-	
X33	Yaw Attitude Reference Failure			-	
X34	Pitch Attitude Reference Failure	Discrete (on-off)	10	-	

C. FAILURE DETECTION NETWORKS

This subsection describes the failure detection networks needed to detect the failures described in the FMEA Subsection VIII-A. These networks receive the processed telemetry signal (dc or discrete form) and provide a logical output signal indicating a functional failure. These outputs can be combined into a failure priority and logic network which issues automatic commands to the vehicle via the telemetry link when a failure occurs. Most networks contain comparison or level detection circuitry combined with a first order filter which, in turn, provides signal smoothing and prevents false triggering by large transient spikes. This filter, however, creates a time delay in the failure detection path and would be not only designed to minimize the delay and provide quick correction but also to smooth the signal sufficiently. The circled letters in the figures (i.e., A1) refer to the overall block diagram in Appendix F. The ten types of failure networks considered are described in the paragraphs that follow and shown in Figure 8-1.

(A) Hardover Detector

The hardover detector provides a failure indication whenever the monitored signal exceeds a preset magnitude. An attitude error signal is shown as a typical signal in Figure 8-1.

(B) Compute and Compare Detector

The compute and compare detector computes a signal, C_1, from a combination of monitored signals and compares it with another monitored signal. If the required signals do not track within a predetermined amount a failure is indicated. A first order filter precludes false triggering caused by transient mistracking. This type detector is used to monitor the output of a multiple input network.

(C) Hardover One Shot Detector

The hardover one shot detector determines if a one shot circuit output exceeds a specified pulse duration. A quickly resettable integrator and a latching level detector are employed.

(D) Compute and Compare Detector

The compute and compare detector is similar to the previously described compute and compare detector, except that a threshold and hysteresis network is necessary to obtain a comparison signal, P_1. This network is used to monitor the RJC electronic output commands.

(E) Gyro Spin Motor Current Detector

The gyro spin motor detector verifies that the spin motor current is maintained within a predetermined percentage of a nominal current, I_0. During runup or for dual speed operation the nominal current and limits may be changed.

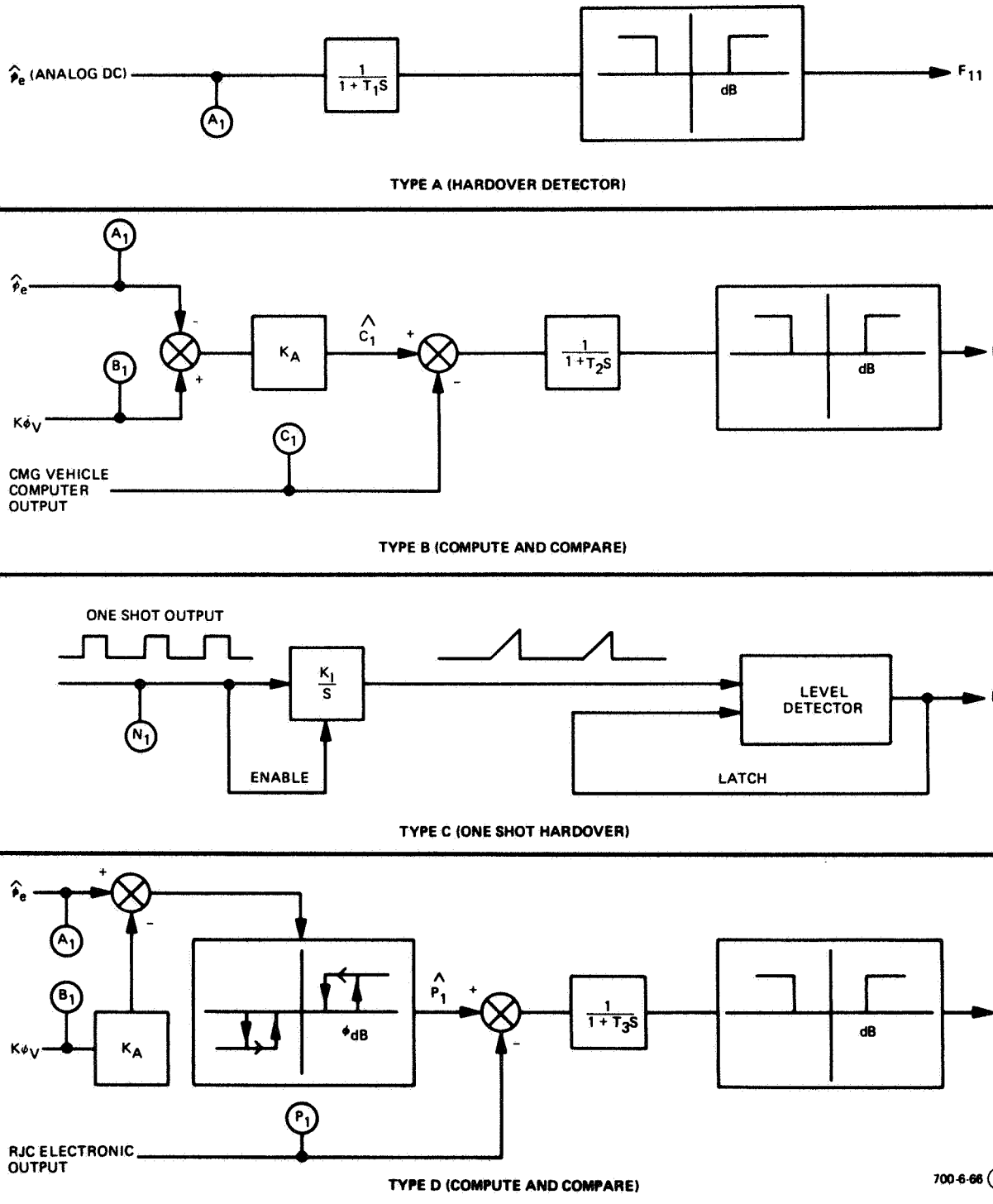

Figure 8-1
Failure Detection Networks
(Sheet 1 of 3)

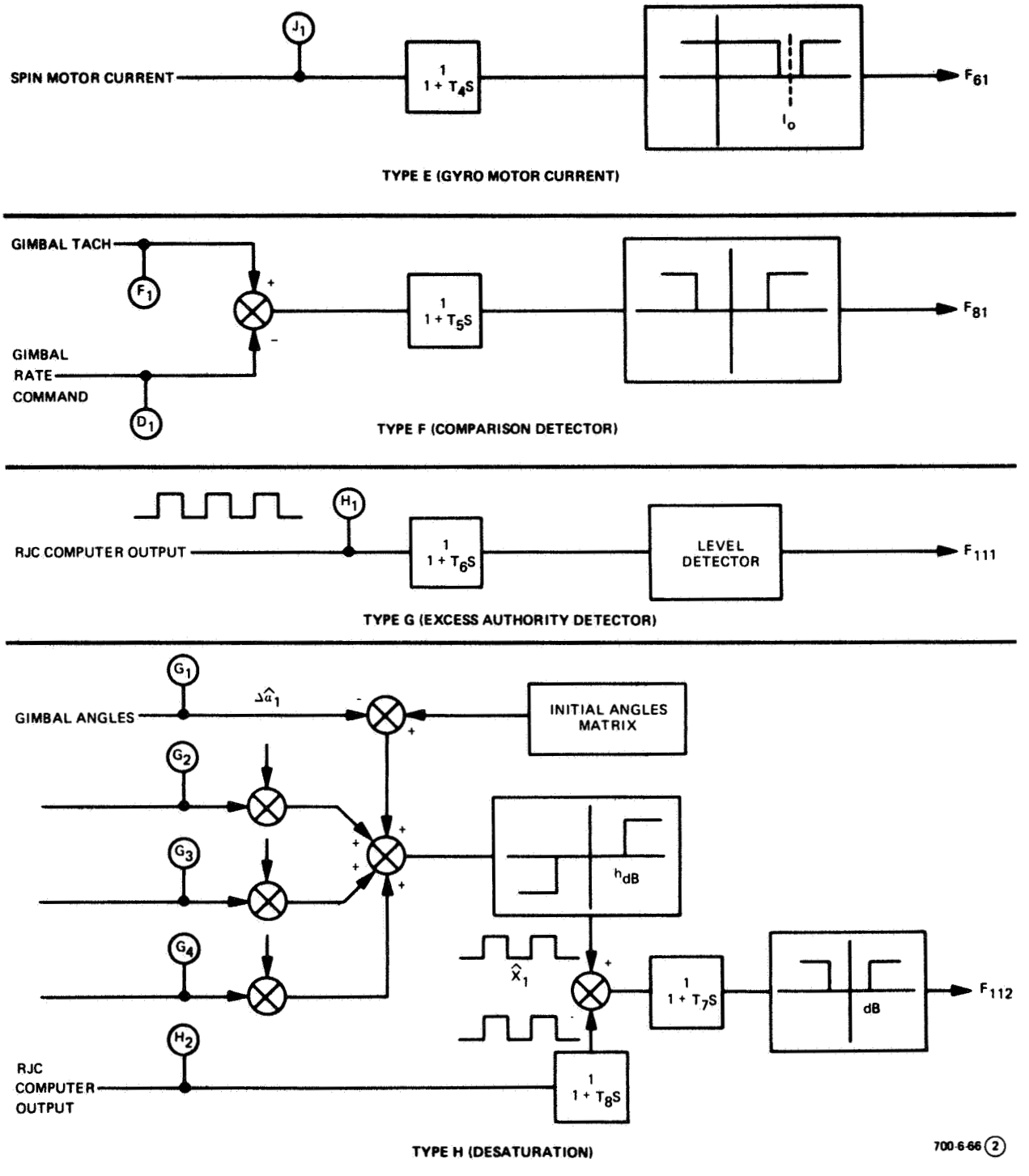

Figure 8-1
Failure Detection Networks
(Sheet 2 of 3)

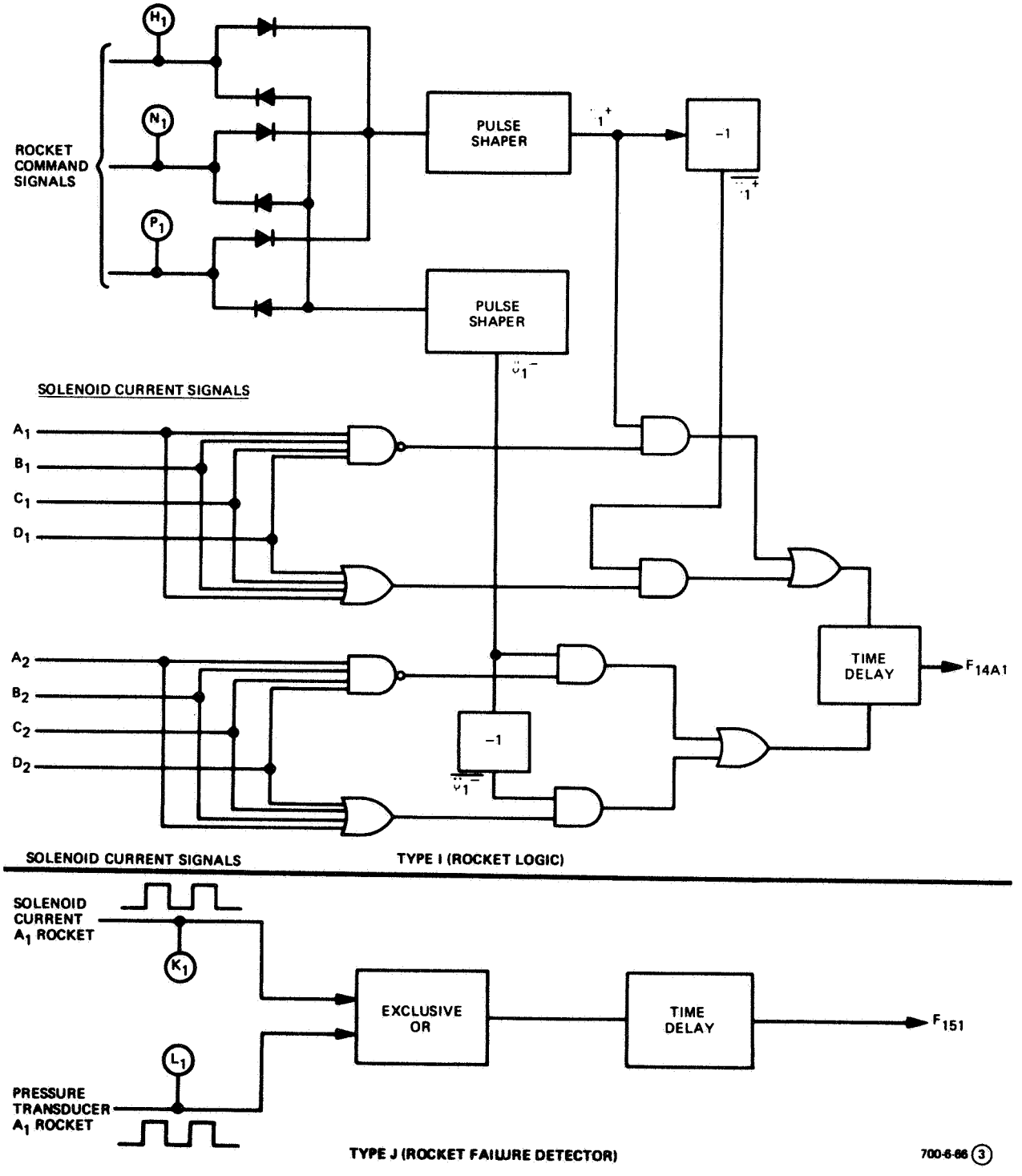

Figure 8-1
Failure Detection Networks
(Sheet 3 of 3)

(F) Comparison Detector

The comparison detector simply compares two signals (input/output or input/feedback) and issues a failure indication if they do not track.

(G) Excess Authority Circuit Detector

This excess authority circuit detector computes the average value or duty cycle of the input pulse train and indicates a failure when it exceeds a predetermined level. This circuit is used during desaturation to ensure that the RJC system torque authority does not exceed that of the CMG system.

(H) Desaturation Detector

The desaturation detector performs computations on the gimbal angle signals similar to those in the CMG steering law computer to provide a signal X_1 which can be compared to the steering law RJC commands during desaturation. If the compared signals do not track sufficiently, a failure is indicated.

(I) Rocket Logic Network Detector

The rocket logic network detector determines if the correct rocket commands are given for a particular channel command. Thus, the rocket logic which determines the rocket conbination that should be fired is verified. The logic is given by the following equation:

$$\text{Fail} = \left[\ddot{\phi}_1^{+} \cdot (\overline{A_1 \cdot B_1 \cdot C_1 \cdot D_1})\right] + \left[\bar{\ddot{\phi}}_1^{+} \cdot (A_1 + B_1 + C_1 + D_1)\right] + \left[\ddot{\phi}_1^{-} \cdot (\overline{A_2 \cdot B_2 \cdot C_2 \cdot D_2})\right] + \left[\bar{\ddot{\phi}}_1^{-} \cdot (A_2 + B_2 + C_2 + D_2)\right] \quad (8\text{-}1)$$

where

$\dddot{\phi}_1^{+}$ = Positive, roll axis, acceleration command

$\ddot{\phi}_1^{-}$ = Negative, roll axis, acceleration command

A_1 = Rocket A_1 command signal

A_2 = Rocket A_2 command signal

10. Rocket Failure Detector

The rocket failure detector compares the rocket solenoid currents and the pressure transducer signals for each rocket in an "exclusive or" type circuit. Rocket stuck open and stuck shut failures can thus be determined. A time delay network allows for rocket buildup and decay times during pulse operation.

SECTION IX

RELIABILITY ANALYSIS

SECTION IX

RELIABILITY ANALYSIS

A reliability analysis of the 4-FACS was conducted to determine the following: the interdependency of the various system components, the areas which required redundancy, and the overall probability of success for 1000 hours. The system was divided into major subsystem blocks, and the reliability diagram shown in Figure 9-1 was derived. The diagram was constructed from the major component failure rates listed in Table 9-1 and derived in Appendix E, in conjunction with the overall system block diagram of Appendix F. Although derived from standard sources, the reliability failure rates used in this study are not to be construed as absolute predictions. Instead, they are used to establish a relative comparison of different subsystems. The value of the analysis is predicated on having a consistent set of data.

Various techniques with different levels of complexity can be used to establish the overall system reliability. For instance, each mission phase can be considered separately, the duration and environment of each considered, and the probability of success data generated. This data can then be combined along with contingency modes of operation to establish an overall reliability estimate. Another technique would be to consider the separate RJC and CMG subsystems and each individual axis channel separately, and derive individual probability of success data. Then, this data would be combined to obtain an overall estimate. In this study, a simplified alternate approach has been used which treats all mission phases and axes, simultaneously. The series flow of subsystems that must operate to make a successful mission is shown in Figure 9-1; the frequency of use or "duty cycle" over the 1000-hour mission is taken into account when computing the failure rate data for each component. A mission failure is defined as follows: the occurrence of a component failure such that fine attitude hold cannot be maintained and the performance specifications are not achieved. A short discussion of each system block follows.

The telemetry system is considered in computing the overall reliability since orbital ephemeris data is necessary to establish a roll attitude reference and failure detection, monitoring, and command signals require an operational telemetry system. Only that portion of the telemetry system on-board the vehicle is considered in the reliability calculations.

The attitude reference system considered is the fine pointing section only, consisting of the sun sensor and two-gimbal star trackers. A loss of the single-degree-of-freedom rate integrating gyros is allowed and therefore not included since the system could be permitted to drift during the orbital dark period and re-acquire the sun with the RJC system. Although this technique would require more attitude rocket fuel the mission could be continued.

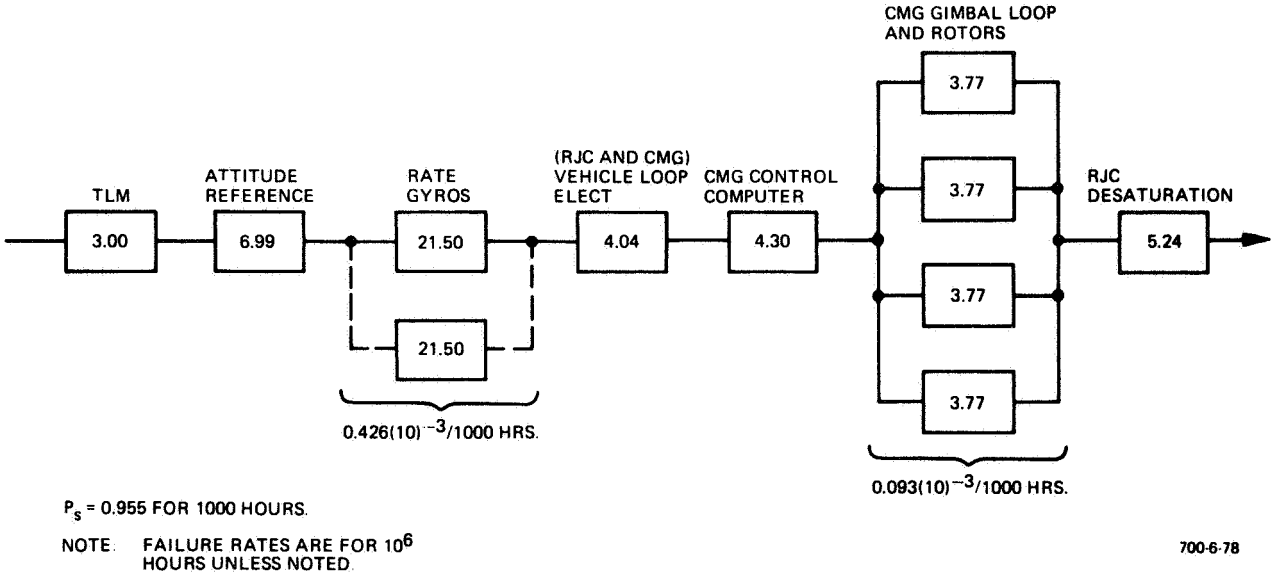

Figure 9-1
Overall CMG FACS Reliability Block Diagram

The rate gyros and processing electronics are necessary to provide vehicle rate damping during all operational modes. Loss of a rate gyro results in an unstable vehicle. A redundant rate gyro triad used for standby, backup operation is, therefore, necessary to ensure a safe vehicle; this backup gyro however does not improve the probability of success for maintaining fine attitude hold since a ground rule is imposed which requires termination of the fine attitude hold mission whenever a backup mode is employed, which, if subsequently failed, could cause vehicle loss. After the backup rate gyro is used, the vehicle must be serviced by either an on-board crew or a co-orbital vehicle; therefore, fine attitude hold mode must be discontinued after a primary rate gyro failure. The rate gyro is the most probable component to fail during a 1000-hour mission; however, component improvement may decrease this failure rate by an order of magnitude during the 1975-1980 time period. Alternate techniques such as derived rate from the attitude signals may also be successfully employed, and, thereby, lower the failure rate. Further investigation, however, must be conducted to ensure that sensor noise is sufficiently small to make this technique feasible. When computing the probability of success with a failure defined as loss of vehicle (rather than loss of mission), the parallel reliability of the rate gyros as shown in Figure 9-1 can be considered.

The RJC and CMG vehicle loop electronics are considered together as one block since both are necessary for a fine pointing mission success.

The CMG control computer includes the steering law, desaturation, and initial angle circuitry. Redundancy is not considered necessary for the control computer during this mission because its failure rate is of the same order of magnitude as all other components. The overall reliability, therefore, would not be significantly enhanced by computer redundancy unless all major blocks employed backup systems also.

The CMG gimbal loop and rotor are considered as four parallel units, any three of which operating provide fine attitude hold. The overall configuration probability of success, $P_{s(\tau)}$ is then

$$P_{s(\tau)} = P_s^4 + 4 P_s^3 \lambda_s \qquad (9\text{-}1)$$

where

P_s = probability of success of a single CMG

$\lambda_s = (1 - P_s)$; probability of failure of a single CMG

factoring equation (9-1) gives

$$P_{s(\tau)} = P_s^3 [1 + 3\lambda_s] \qquad (9\text{-}2)$$

Expanding equation 9-2 in terms of gyro failure rate, λ_s, the overall 4-FACS failure rate is:

$$\lambda_{s(\tau)} = 1 - P_{s(\tau)} \simeq 6\,\lambda_s^2 \qquad (9\text{-}3)$$

where

$\lambda_{s(\tau)}$ = Overall configuration failure rate

Note that the individual gyro failure rate, λ_s, is effectively squared when the redundant 4-FACS configuration is used. Since λ_s is a very small fraction, squaring lowers the failure rate many orders of magnitude. The probability of attaining fine attitude hold with the 4-FACS CMG configuration, therefore, is 0.99991 for 1000 hours, a marked improvement over the individual gyro probability of success (0.9962 for 1000 hours).

The RJC desaturation block consists of the attitude rockets, jet logic, and rocket driver electronics. These components are necessary to desaturate the CMG configuration and allow it to return to a zero momentum state. If an alternate desaturation technique is used which does not use reaction jets, the overall reliability may be improved.

Combining all the failure rates listed in Figure 9-1 provides an overall fine attitude control mission probability of success of 0.955 for 1000 hours. The probability that the vehicle is not lost due to failures is 0.975 for 1000 hours.

TABLE 9-1

MAJOR COMPONENT RELIABILITY SUMMARY

Major Component	Failures/10^6 Hr
Gyro Rotor and Case	0.787
Gyro Rotor Electronics	0.767
Gimbal Torquer and Angle Control	0.123
Gimbal Control Electronics	2.094
Gimbal Angle Synchro	0.038
CMG Control Computer	4.298
Vehicle Loop Electronics (CMG)	2.082
Vehicle Loop Electronics (RJC)	1.956
Rate Gyro and Electronics	21.500
Two Axis Sun Sensor and Electronics	0.758
Two Gimbal Star Tracker and Electronics	5.934
RJC Drive Electronics	2.644
RJC Attitude Rockets: X-Axis	0.220
Y-Axis	2.220
Z-Axis	0.440
Failure Detection and Switching Network	0.788
Telemetry	3.000

SECTION X

SELECTED SYSTEM DEFINITION

SECTION X

SELECTED SYSTEM DEFINITION

The selected fine attitude control system for both the manned and unmanned missions considered is a 4-FACS CMG configuration using a pseudo-torque feedback control law, reaction jet desaturation technique, redundant rate gyros, and a two-axis sun sensor and a two-gimbal star tracker attitude reference system.

The 4-FACS CMG configuration provides the required attitude hold with four 200 ft-lb-sec single-gimbal CMG's weighing less than 65 pounds each. Operation after a single-gyro failure is made possible by re-orienting the gyros about their gimbal axis and slightly modifying the steering law. A pseudo-torque feedback steering law provides essentially uncoupled torque actuation form the CMG configuration, thereby, simplifying the control task and minimizing gyro torquer power. By employing a reaction jet desaturation technique, repeatable and efficient gimbal angle convergence is accomplished during momentum unloading. Body-mounted rate gyros give vehicle damping and are used in a redundant configuration to give sufficient system reliability.

The attitude reference system employs a two-axis sun sensor and a two-gimbal star tracker in the primary attitude hold mode. This maintains the X-vehicle axis pointed at the sun and the Y-axis in the orbital plane. During the dark part of the orbit, three Single-Degree-Of-Freedom (SDOF) rate integrating gyros establish the attitude reference.

The principal system characteristics are summarized in Table 10-1. Other sections of this report contain detailed information about the different subsystems. Two performance specifications released separately: "A 200 ft-lb-sec Single-Gimbal CMG Performance Specification " and "A 4-FACS Steering Law Computer Performance Specification " supply detailed design specifications for the principal CMG components.

TABLE 10-1

4-FACS SYSTEM CHARACTERISTICS

Characteristics	Value		Unit
	Manned	Unmanned	
Attitude Hold Accuracy	<0.1	<0.001	deg
Attitude Hold Rate Error	<0.01	<0.0001	deg/sec
Control Torque	25	2	ft-lb
Bandwidth	3.5	1.5	Hz
Reliability (1000 Hr), P_s =	0.955	0.955	-
Number of CMG's	4	4	Single Gimbal
CMG Momentum	200	200	ft-lb-sec
CMG Unit Weight	61	48	lb
Overall System Weight	305	252	lb
Overall System Average Power	92	117	W

SECTION XI

CONCLUSIONS AND RECOMMENDATIONS

SECTION XI

CONCLUSIONS AND RECOMMENDATIONS

A. SUMMARY

After considering the design mission requirements, deriving the vehicle disturbance torques, and performing a system comparison study, the 4-FACS CMG configuration was chosen as the preferred fine attitude control system. The 4-FACS configuration was selected since it has the best combination of low system weight and power, good accuracy capability and high reliability. The other systems considered were a reaction wheel system, scissored-pair CMG system, and a reaction control jet system. The 4-FACS was synthesized, CMG's sized to meet the performance requirements and an analog computer simulation was conducted to evaluate system performance. Three-axis simulations were run to investigate the following:

- 4-FACS Constant Gain Steering Law
- 4-FACS Pseudo-Torque Feedback Steering Law
- 4-FACS One-Gyro Failed Operation
- Momentum Desaturation Techniques
- Scissored Pair CMG Configuration with One Gyro Failed
- Low Torque System (Unmanned)

The simulation results indicate that the 4-FACS CMG configuration will give acceptable performance with some cross-coupling when operating with a simplified constant gain steering law; however, a pseudo-torque feedback steering law provides much better performance and was chosen as the preferred law. The pseudo-torque law essentially eliminates gyro cross-coupling and enables the CMG performance to remain unchanged during momentum storage and even after a single gyro failure. The selected desaturation technique computes the stored momentum about each vehicle axis and pulse-modulates the reaction jets to unload the CMG system. This method provides stable and repeatable convergence for all three-axis-momentum combinations within the CMG envelope. A scissored-pair CMG configuration with one failed gyro was also simulated and compared to the failed 4-FACS configuration; no particular advantage was found when the scissored-pair gyros were used. A brief, low-torque, 4-FACS CMG simulation was also run to identify accuracy and bandwidth relationships for an ideal linear CMG control system.

Other related accomplishments during the study were:

- Development of 4-FACS momentum envelope models
- Derivation of 4-FACS stability envelopes
- System reliability analysis
- FMEA and failure detection analysis

- Definition of Operational Procedures
- Generation of 200 ft-lb-sec CMG Performance Specification
- Generation of 4-FACS CMG Steering Law Computer Performance Specification

B. CONCLUSIONS

The following principal conclusions can be drawn from this study:

- A 4-FACS CMG system can precisely hold spacecraft attitude for both manned and unmanned missions
- A 4-FACS CMG configuration is preferred over reaction wheel, CMG scissored pair, and reaction jet attitude control systems for the chosen missions
- A 4-FACS CMG configuration performs acceptably even after one gyro failure
- The 4-FACS CMG system is lightweight, consumes a moderate amount of electrical power, and has high reliability

C. RECOMMENDATIONS

This study has proven the feasibility of using the 4-FACS CMG configuration for fine attitude hold and has established its merits relative to other control techniques. Now it is necessary to apply the configuration to a particular vehicle design and investigate in detail the system performance when detailed CMG models are employed. In addition, during this study other interesting concepts for using CMG's and momentum exchange devices were discovered; however, these concepts were not investigated because of the limited scope of the study. As a result, recommendations for further study are:

- Conduct a system design study which will establish the ultimate accuracy which the 4-FACS configuration can provide. A particular mission and vehicle should be selected for this design task.
- Consider the influence of CMG non-linearities, by using detailed math models, on the 4-FACS CMG system performance.
- Compare the 4-FACS configuration to other 4-CMG configurations capable of operation when one gyro has failed.
- Determine the effectiveness of the 4-FACS CMG configuration to provide slew and track capability as well as fine attitude hold.
- Consider dual rotor speed CMG operation. This could provide maneuvering capability at high speeds and precision control at low speeds.
- Consider the use of variable rotor speed CMG's in a 4-FACS configuration.
- Consider hybrid momentum exchange configurations using reaction wheels and CMG's to provide maneuvering and precision control capability for space vehicles.

SECTION XII

REFERENCES

SECTION XII

REFERENCES

1. Sabroff, A.E. - "Advanced Spacecraft Stabilization and Control Techniques" AIAA Journal of Spacecraft and Rockets, Vol 5, No. 12, December 1968, pp 1377-1393.

2. Greensite, A.L. - "Analysis and Design of Space Vehicle Flight Control Systems", Vol XII "Attitude Control In Space", NASA CR-831, August 1967.

3. Jenson, J., et. al. - "Design Guide to Orbital Flight", McGraw-Hill Book Co, New York, 1962, pg 752-753.

4. Tewell, J.R. and C.H. Murrish - "Engineering Study and Experiment Definition for an Apollo Applications Program Experiment on Vehicle Disturbances Due to Crew Activity", NASA CR-66277, March 1967.

5. Murrish, C.H. and G. Smith - "The Effects of Crew Motion on the Attitude of a Manned Orbiting Spacecraft", AIAA Guidance, Control, and Flight Dynamics Conference, August 12-14, 1968, Paper No. 68-867.

6. Davis, L.P. - "Optimization of Control Moment Gyroscope Design" - Sperry Flight System TM-LJ-1252-0765, May 1967.

7. "Reliability Stress and Failure Rate Data for Electronic Equipment" MIL-HDBK-217A; December 1965.

8. Earles, D.R. - "Reliability Engineering Data Series, Failure Rates" - AVCO Corp, April 1962.

9. Ergin, E.I., et. al. - "Techniques for Analysis of Nonlinear Attitude Control Systems for Space Vehicles" - ASD-TDR-62-208, Vol. I, p 77, Wright Patterson Air Force Base, June 1962.

10. Davison, P.H. - "Passive Aerodynamic Stabilization of a Near Earth Satellite" - WDD-TR61-133, Vol. II - Aerodynamic Analysis, Wright Patterson Air Force Base, March 1964.

APPENDIX A

DISTURBANCE TORQUE DERIVATION

APPENDIX A

DISTURBANCE TORQUE DERIVATION

This appendix derives the gravity gradient and aerodynamic disturbance torque equations used in the study.

A. GRAVITY GRADIENT TORQUE

To derive the gravity gradient torque acting on a rigid body satellite in a cicular orbit a useful set of equations (ref 9) is:

$$L_{xg} = \frac{3\, G_e\, R_e^2}{R_o^3} (\vec{\mu}_r \cdot \vec{Y}_v) (\vec{\mu}_r \cdot \vec{Z}_v) (I_{zz} - I_{yy})$$

$$L_{yg} = \frac{3\, G_e\, R_e^2}{R_o^3} (\vec{\mu}_r \cdot \vec{Z}_v) (\vec{\mu}_r \cdot \vec{X}_v) (I_{xx} - I_{zz}) \qquad \text{A-1}$$

$$L_{zg} = \frac{3\, G_e\, R_e^2}{R_o^3} (\vec{\mu}_r \cdot \vec{X}_v) (\vec{\mu}_r \cdot \vec{Y}_v) (I_{yy} - I_{xx})$$

where:

L_{xg}, L_{yg}, L_{zg} = Gravity gradient torque magnitudes

G_e = Gravitational acceleration at earth's surface

R_e = Mean radius of earth

R_o = Distance from earth's center to spacecraft

$\vec{X}_v$, $\vec{Y}_v$, $\vec{Z}_v$ = Body oriented spacecraft vectors

I_{xx}, I_{yy}, I_{zz} = Spacecraft moment of inertia

$\vec{\mu}_r$ = Gravity vector

The vector dot products can be evaluated for the design mission by referring to the coordinate geometry, Figure A-1. The vehicle is always oriented such that the X_v axis is maintained parallel to the Y_s axis (sun line) and the Y_v axis is held in the orbital plane X_o - Y_o. The vehicle's position in the orbital plane with respect to the Y_o axis is given by the angle, η, and the vector from the center of the earth to the vehicle's center of mass is given by $R_o \bar{\mu}_r$. The dot products are derived by obtaining the projection of the gravity vector, $\vec{\mu}_r$ into the vehicle coordinate system with the X_v and Y_v axis in the orbital plane

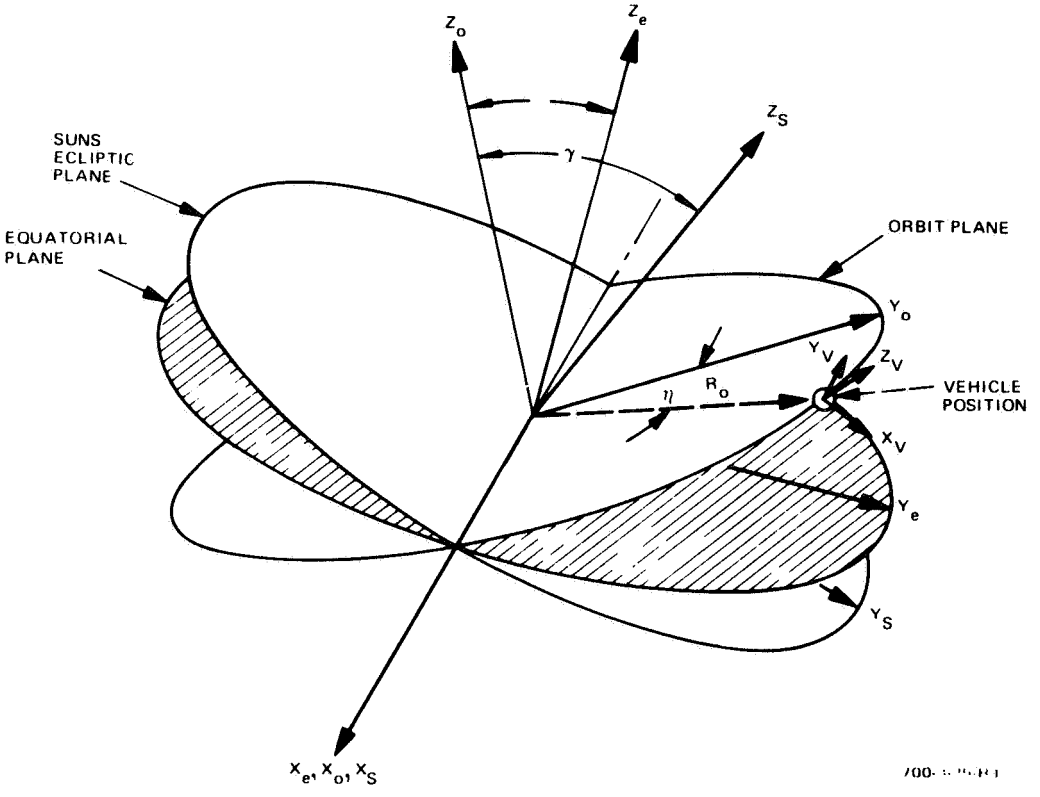

Figure A-1
Coordinate Geometry

$X_o - Y_o$, and then rotating the vehicle about the Y_v axis by an amount γ; the angle between the orbital and ecliptic plane.

$$\begin{bmatrix} \vec{\mu}_r \cdot \vec{X}_v \\ \vec{\mu}_r \cdot \vec{Y}_v \\ \vec{\mu}_r \cdot \vec{Z}_v \end{bmatrix} = \begin{bmatrix} \cos\gamma & o & -\sin\gamma \\ o & 1 & o \\ \sin\gamma & o & \cos\gamma \end{bmatrix} \begin{bmatrix} \cos\eta \\ \sin\eta \\ o \end{bmatrix} \tag{A-2}$$

$$\begin{bmatrix} \vec{\mu}_r \cdot \vec{X}_v \\ \mu_r \cdot \vec{Y}_v \\ \vec{\mu}_r \cdot \vec{Z}_v \end{bmatrix} = \begin{bmatrix} \cos\gamma\cos\eta \\ \sin\eta \\ \sin\gamma\cos\eta \end{bmatrix} \tag{A-3}$$

Substituting equation (A-3) into equation (A-1) and letting $\eta = \omega_o T$, where ω_o = orbital rate, gives:

$$\begin{bmatrix} L_x \\ L_y \\ L_z \end{bmatrix}_{gr} = \frac{3\,G_e\,R_e^2}{2R_o^3} \begin{bmatrix} (I_{zz} - I_{yy}) & (\sin\gamma)\sin 2\,\omega_o T \\ (I_{xx} - I_{zz}) & \frac{1}{2}(\sin 2\gamma)(1 + \cos 2\,\omega_o T) \\ (I_{yy} - I_{xx}) & (\cos\gamma)\,\sin 2\,\omega_o T \end{bmatrix} \tag{A-4}$$

For the design mission under consideration at a 250 N.M. circular orbit:

$$R_e = 2{,}093(10)^7 \text{ ft}$$

$$G_e = 32.2 \text{ ft/sec}^2$$

$$I_{xx} = 18{,}200 \text{ slug-ft}^2$$

$$I_{yy} = 56{,}100 \text{ slug-ft}^2$$

$$I_{zz} = 60{,}000 \text{ slug-ft}^2$$

$$\gamma = 56.45 \text{ degrees}$$

Substituting these values into equation (A-4) gives:

$$\begin{bmatrix} L_x \\ L_y \\ L_z \end{bmatrix}_{gr} = \begin{bmatrix} 0.613 & \sin 2\,\omega_o T \\ -3.63 & (1 + \cos 2\,\omega_o T) \\ 3.96 & \sin 2\,\omega_o T \end{bmatrix} (10)^{-2} \text{ ft-lb} \tag{A-5}$$

B. AERODYNAMIC TORQUE

The approximate aerodynamic torques acting on a rigid body vehicle in a circular orbit are derived using the following simplifications:

- A constant atmospheric density which is the average of "day" and "night" atmospheric densities
- A constant vehicle drag coefficient

The vehicle in Figure A-2 is the simplified CSM model used in deriving the aerodynamic torques. The center of pressure (CP) is located in the Y_v - Z_v plane at station 982.5". The center of gravity is offset from the CP such that

$$l_x = 32 \text{ inches}$$

$$l_y = 1.3 \text{ inches}$$

$$l_z = -6.1 \text{ inches}$$

The total normal surface area, A_n, is 254 square feet. The drag coefficient for a 90-degree angle-of-attack (perpendicular to the longitudinal axis) can be calculated using equations developed by Davison (ref 10), employing free molecular aerodynamic theory.

$$C_D \Big|_{\gamma = \frac{\pi}{2}} = \frac{3\pi}{8S_\infty} \frac{T_\omega}{T_\infty} + \frac{\pi D}{2 L S_\infty} + 2 \qquad \text{(A-6)}$$

which for this mission gives $C_D = 2.15$. The average dynamic pressure, q, at a 250-N.M. orbit using the ARDC 1959 atmospheric model density $\rho = 7 \times 10^{-15}$ sl/ft^3 is:

$$q = \frac{1}{2} \rho V^2 = 2.21(10)^{-6} \text{ lb/ft}^2$$

and the maximum normal drag force, D_M becomes

$$D_M = q C_D A = 1.2(10)^{-3} \text{ pounds} \qquad \text{(A-7)}$$

With the vehicle orientation and orbit of Figure A-1, the normal drag force acting on the CP will be:

$$D_N(t) = \left[D_y^2(t) + D_z^2(t) \right]^{\frac{1}{2}} \qquad \text{(A-8)}$$

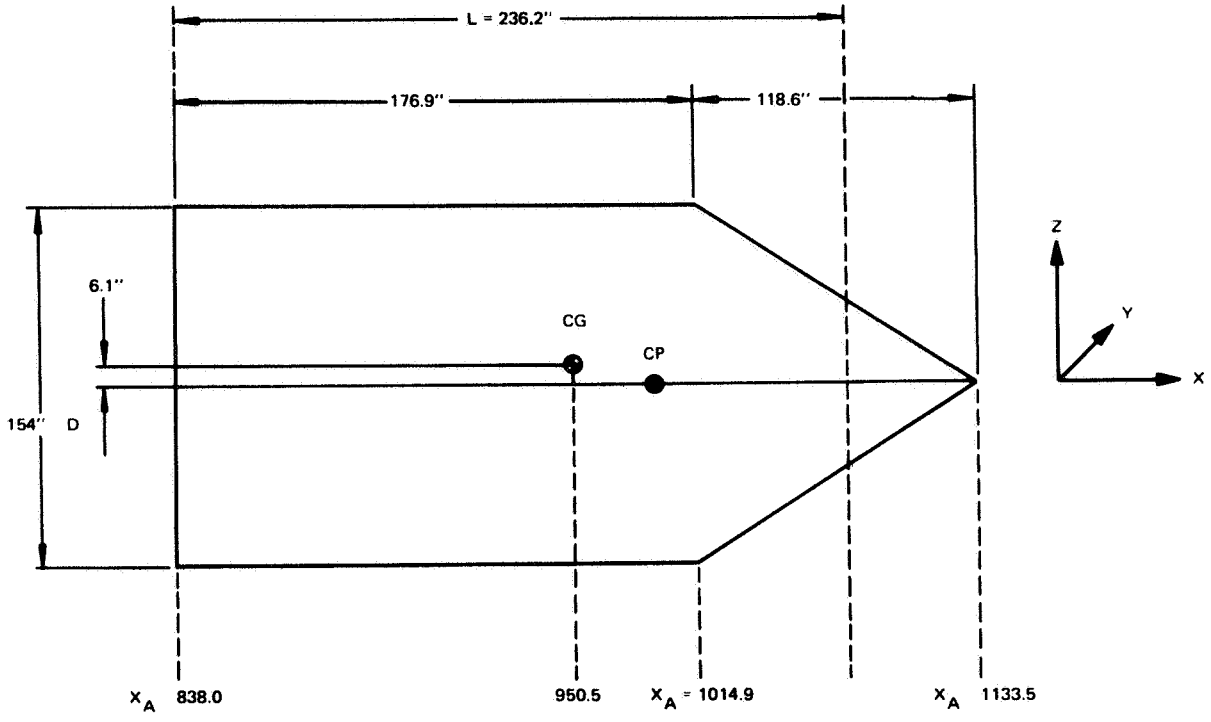

CG	CP	INERTIAS
X_A = 950.5 IN	X_A = 982.5	I_{XX} = 18,000 SL-FT^2
Y_A = 1.3 IN.	Y_A = 0	I_{YY} = 56,000
Z_A = 6.1 IN.	Z_A = 0	I_{ZZ} = 60,000

700 3 26

Figure A-2
Command and Service Module Configuration

$D_y(t)$ and $D_z(t)$ can be obtained by deriving the drag on the vehicle when X_v and Y_v are in the orbital plane, and then pitching the vehicle by the angle between the orbital and ecliptic plane.

$$\begin{bmatrix} D_x(t) \\ D_y(t) \\ D_z(t) \end{bmatrix} = \begin{bmatrix} \cos\gamma & o & -\sin\gamma \\ o & 1 & o \\ \sin\gamma & o & \cos\gamma \end{bmatrix} \begin{bmatrix} \cos\omega_o t & \sin\omega_o t & o \\ -\sin\omega_o t & \cos\omega_o t & o \\ o & o & 1 \end{bmatrix} \begin{bmatrix} o \\ D_M \\ o \end{bmatrix} \quad \text{(A-9)}$$

or:

$$\begin{bmatrix} D_x(t) \\ D_y(t) \\ D_z(t) \end{bmatrix} = \begin{bmatrix} \cos\gamma \sin\omega_o t \\ \cos\omega_o t \\ \sin\gamma \sin\omega_o t \end{bmatrix} \quad \text{(A-10)}$$

Substituting the results of equation (A-10) into equation (A-8) gives:

$$D_N(t) = D_M (1 - \cos^2\gamma \sin^2 \omega_o t)^{1/2} \quad \text{(A-11)}$$

Finally, the aerodynamic torque will be the cross product of the vehicle drag forces and moment arms between the CP and CG: $[T]=[l] \times [F]$. Therefore, the aerodynamic torque is:

$$\begin{bmatrix} T_x \\ T_y \\ T_z \end{bmatrix}_{Aero} = \begin{bmatrix} o & -l_z & l_y \\ l_z & o & -l_x \\ -l_y & l_x & o \end{bmatrix} \begin{bmatrix} \cos\gamma & o & -\sin\gamma \\ o & 1 & o \\ \sin\gamma & o & \cos\gamma \end{bmatrix} \begin{bmatrix} \cos\omega_o t & \sin\omega_o t & o \\ -\sin\omega_o t & \cos\omega_o t & o \\ o & o & 1 \end{bmatrix} \begin{bmatrix} o \\ D_N(t) \\ o \end{bmatrix} \quad \text{(A-12)}$$

For the design mission under consideration with $\gamma = 56.45$ degrees and the moment arms previously listed equation (A-12) reduces to:

$$\begin{bmatrix} T_x \\ T_y \\ T_z \end{bmatrix}_{Aero} = D_N(t) \begin{bmatrix} -0.5 \cos\omega_o t \\ -1.95 \sin\omega_o t \\ 2.67 \cos\omega_o t \end{bmatrix} \quad \text{(A-13)}$$

where:

$$D_N(t) = D_M (1 - 0.3 \sin^2\omega_o t)^{1/2}$$

C. AN ALTERNATE ORIENTATION (XOP)

As discussed in this report, the size of the momentum exchange system is largely determined by the magnitude of the secular gravity gradient torque; therefore, an alternate orientation which places the X-axis in the orbital plane (XOP) and reduces the secular torque should be considered if other mission constraints allow it.

The X-axis can be placed in the orbital plane by simply rotating -90 degrees about the Z-axis. Then, the Y- xis points at the sun and the X-axis is in 180-degree opposition to the vehicle velocity vector. For this orientation the gravity gradient torques acting on the vehicle axes are

$$\begin{bmatrix} L_x \\ L_y \\ L_z \end{bmatrix} = \begin{bmatrix} 0.613\ (1 + \cos 2\ \omega_o T) \\ 3.63 \sin 2\ \omega_o T \\ -3.96 \sin 2\ \omega_o T \end{bmatrix} (10)^{-2} \text{ ft-lb} \qquad \text{(A-14)}$$

As demonstrated by comparing equation (A-14) with equation (A-5), the secular torque has been reduced by approximately six times. Consequently the total momentum caused by the secular torque per orbit is only about 40 instead of 200 ft-lb-sec. The Y- and Z-axis have approximately equal cyclic requirements which call for equal momentum capability about those two axes. Of course, the aerodynamic and solar torque must also be considered for this new orientation. Assuming their contribution to the momentum requirements remain small at this altitude, the momentum envelope is approximately a 40 ft-lb-sec cube.

APPENDIX B

ATTITUDE REFERENCE SYSTEM

APPENDIX B

ATTITUDE REFERENCE SYSTEM

An attitude reference system capable of meeting the mission requirements and consisting of a two-axis, sun sensor assembly; two-gimbal star tracker; and three strapdown, single-degree-of-freedom rate integrating gyros is described in this section. This system is meant to be representative of a fine attitude reference capable of satisfying the manned mission requirements and is not intended to be the optimum choice. To choose the "best" attitude reference, a more detailed comparison, which considers power, weight, reliability, non-linearities, alignment errors, etc, would be necessary and is beyond the scope of this study.

The X_v-axis of the vehicle is pointed at the sun by using a two-axis sun sensor to provide pitch and yaw axis control as shown in Figure B-1. During the sunlight part of the orbit, an electronic switch, shown schematically as a relay, is in the position shown. The attitude error signal from the sun-sensor is used for vehicle control. Two single-degree-of-freedom rate integrating gyros aligned to the pitch and yaw axis are placed in a follow or caged mode during the sun sensor control period. This technique keeps the gyro pickoff signal at zero by torquing the gyro gimbal axis to follow the strapdown case motion and prohibits gyro drift from causing loss of reference. When the vehicle enters the twilight or dark portion of the orbit, the sun sensor output is disconnected from the channel input and the rate integrating gyros are uncaged to provide an attitude reference signal.

When the vehicle loses sun acquisition for 15 minutes during the orbit, the gyros, which possess random drift, cause attitude errors to exist at time of re-acquistion. To avoid large attitude error inputs and excessive maneuvering when the sun sensor hold mode is resumed, the rate integrating gyros must not let the reference drift more than 0.025 degree; therefore the gyro random drift rate must be less than 0.1 degree per hour.

The roll axis attitude reference system aligns the Y_v-axis into the orbital plane by employing a two-gimbal star tracker as shown in Figure B-2. The star tracker is mounted to a base within the inner gimbal of a two gimbal platform arrangement. The outer gimbal axis is colinear with the vehicle Y_v-axis and the inner gimbal axis is colinear with the X_v-axis. When the gimbal axis $\delta_1 = \delta_2 = 0$, the tracker and vehicle axis are coincident. An attitude reference computer operates with the star tracker platform to provide search and track operational modes as well as to compute the roll attitude error from platform angle and orbital ephemeris information.

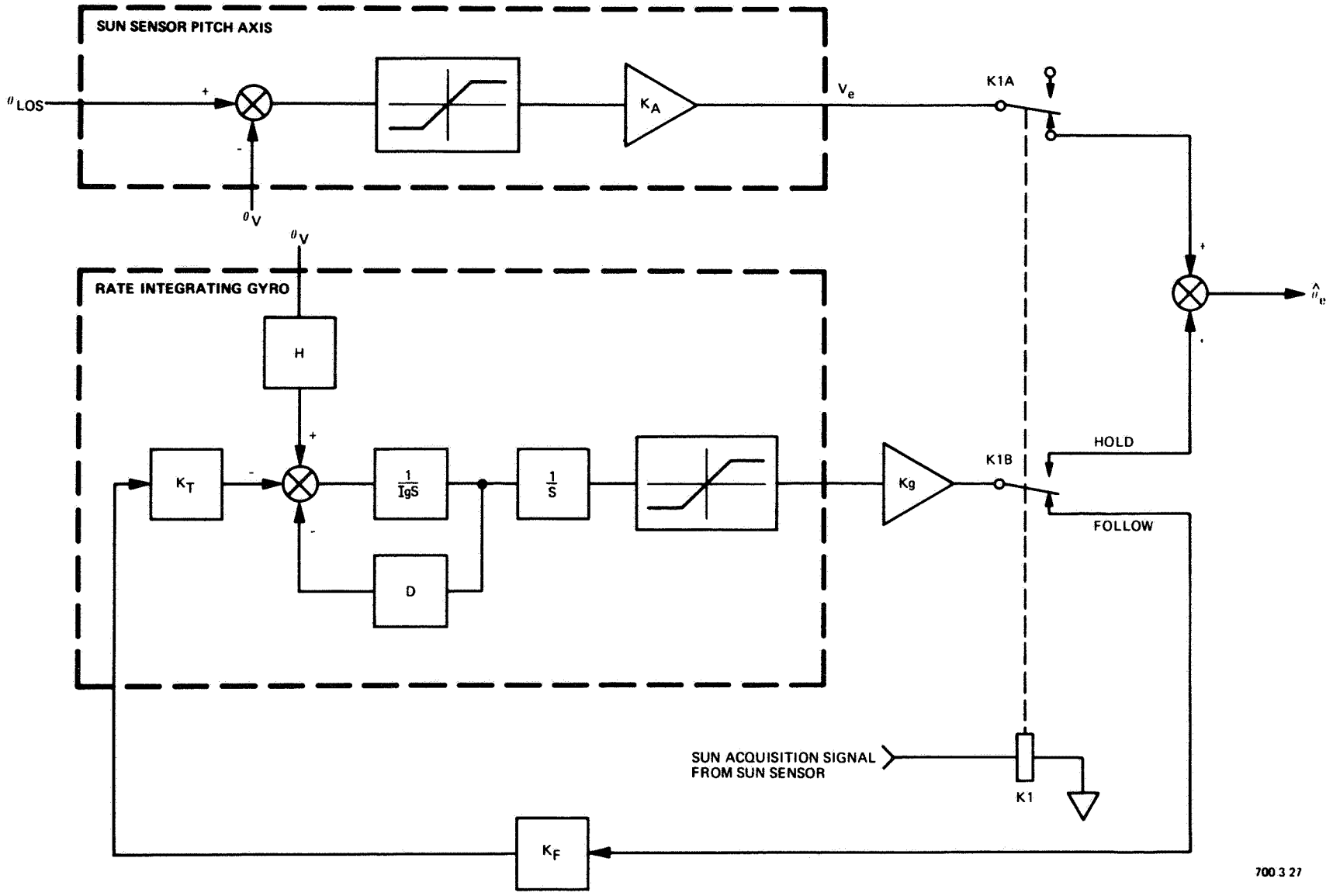

Figure B-1
Pitch Axis Attitude Reference
(Yaw Axis Similar)

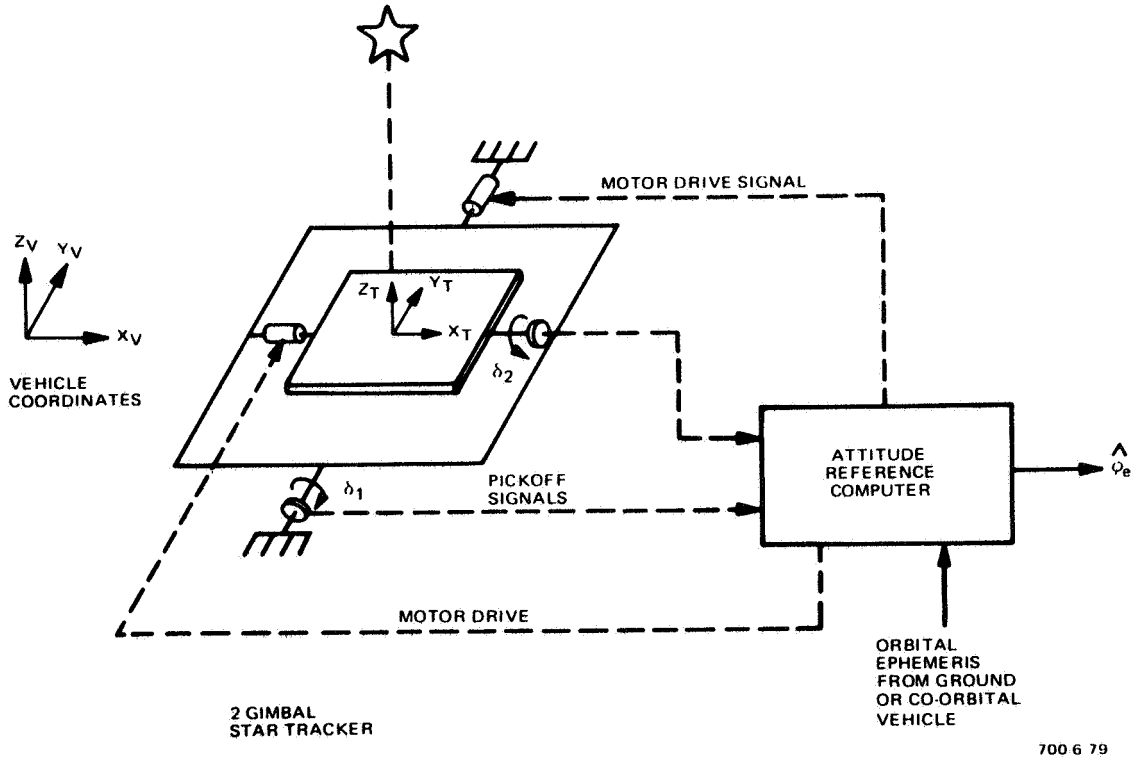

Figure B-2
Roll Axis Attitude Reference System

When the attitude reference system is in operation and after sun acquisition is achieved, the star tracking system is motor-driven in the search mode until a known star is acquired. The gimbal angles, δ_1 and δ_2, are compared in the computer with the gimbal angles that would exist if the Y-axis were aligned in the orbital plane. Of course, orbital ephemeris information from ground track or a co-orbital vehicle is necessary to establish the desired angles δ_{1D} δ_{2D}. With the star tracker in a track mode, the platform angle errors are:

$$\begin{bmatrix} \delta_{1E} \\ \delta_{2E} \end{bmatrix} = \begin{bmatrix} \delta_{1D} - \delta_1 \\ \delta_{2D} - \delta_2 \end{bmatrix}$$

This error is used to create a roll attitude error, $\hat{\phi}_e$ and maneuver the vehicle so that δ_{1E} and δ_{2E} are driven to zero. Subsequently, the attitude reference system continues to track and produce an attitude error signal. An accuracy capability of 0.05 degree is expected with this technique if sufficient accuracy is contained in the orbital ephemeris data and the required resolution is available in the platform angular pickoffs.

During the dark time of the orbit, a Single-Degree-Of-Freedom (SDOF) rate integrating gyro is used to generate the roll attitude error signal in a similar manner to that employed in the other two axes.

Some component specifications of available type sun sensor, rate integrating gyro, and gimballed star tracker which would satisfy the requirements are presented in Table B-1.

TABLE B-1

ATTITUDE REFERENCE SYSTEM

- Two-Axis Sun Sensor Assembly

  Angular Range = ±5 degrees
  Angular Accuracy = ±2 arc minutes
  Power = 1.2 watts at 28 vdc
  Weight = 2 pounds
  Output = 2 vdc/deg

- Three Single-Degree-of-Freedom Rate Integrating Gyros

  Angular Momentum = $5\ (10)^5$ dyne-cm-sec
  Output Axis Freedom = ±1 deg
  Random Drift = 0.01 deg/hr
  Power = 25 watts
  Weight = 3 pounds

- Two Gimbal Star Tracker Assembly

  Angular Range = ±85 degrees
  Angular Accuracy = ±3 arc minutes
  Slew Rate = ±5 deg/min
  Power = 10 watts
  Weight = 10 pounds

APPENDIX C

CONTROL MOMENT GYRO DESCRIPTION

APPENDIX C

CONTROL MOMENT GYRO DESCRIPTION

This section briefly describes the mechanical design, a typical installation, and the vehicle interface of the 4-FACS gyro specified in Section V.C. The 4-FACS gyro requiring 200 ft-lb-sec momentum capability uses a design similar to the 100 and 500 ft-lb-sec gyros already successfully built and tested at Sperry. The twin gyro assembly and vehicle installation is a suggested design for implementing the 4-FACS CMG configuration into the Apollo Service Module. Many other techniques can also be used to implement the 4-FACS configuration and the final scheme selected would depend on a detailed configuration study of the combined gyro and vehicle systems.

A. MECHANICAL DESIGN

The basic design features of the single gimbal CMG proposed for the 4-FACS installation are the following:

- Bimetal shell type rotor
  - Large inertia to weight ratio
  - High strength
  - Good balance stability
  - High stiffness
- Direct Drive Torquer Module
  - Simplified Design
  - High reliability
  - No gear backlash
  - Extremely good angular resolution
- Long Life Spin Bearing and Lubrication Scheme
  - Bearings preloaded in duplex pairs
  - High reliability self-contained lubrication system
- Inner Gimbal Position Sensed by Resolver and Synchro
- Speed Pickoff
- Brushless DC Spin Motor

Design studies have shown that these features satisfy the requirements for a fine attitude hold CMG. The Sperry high torque single gimbal CMG is shown as an example of a typical minimum equivalent weight design. A cutaway drawing of this gyro is shown in Figure C-1 and the 4-FACS CMG would be very similar in its basic design. The primary difference being that the 4-FACS CMG will employ a direct-drive rather than a dual torquer. Outline dimensions for the proposed 4-FACS CMG are given in Figure C-2.

B. GYRO INSTALLATION

The 4-FACS CMG installation will consist of two twin gyro assembly units mounted on beam supported shelves. Schematic drawings of the twin gyro assembly and the mounting structure are shown in Figure C-3. The truss type support of the CMG's consist of 0.50 O.D. tubular aluminum members, which will provide a high stiffness to weight ratio. The twin gyro assembly design allows installation of the system with a minimum volume penalty.

Mounting within the Apollo service module would be on a shelf that consists of a ring which is tied to the module wall structure by support beams. The center ring of the twin gyro assembly mounts directly to the shelf ring. This installation provides adequate stiffness to ensure that axis alignment is maintained within required limits. Overall dimensions of the twin gyro assembly are given in Figure C-4.

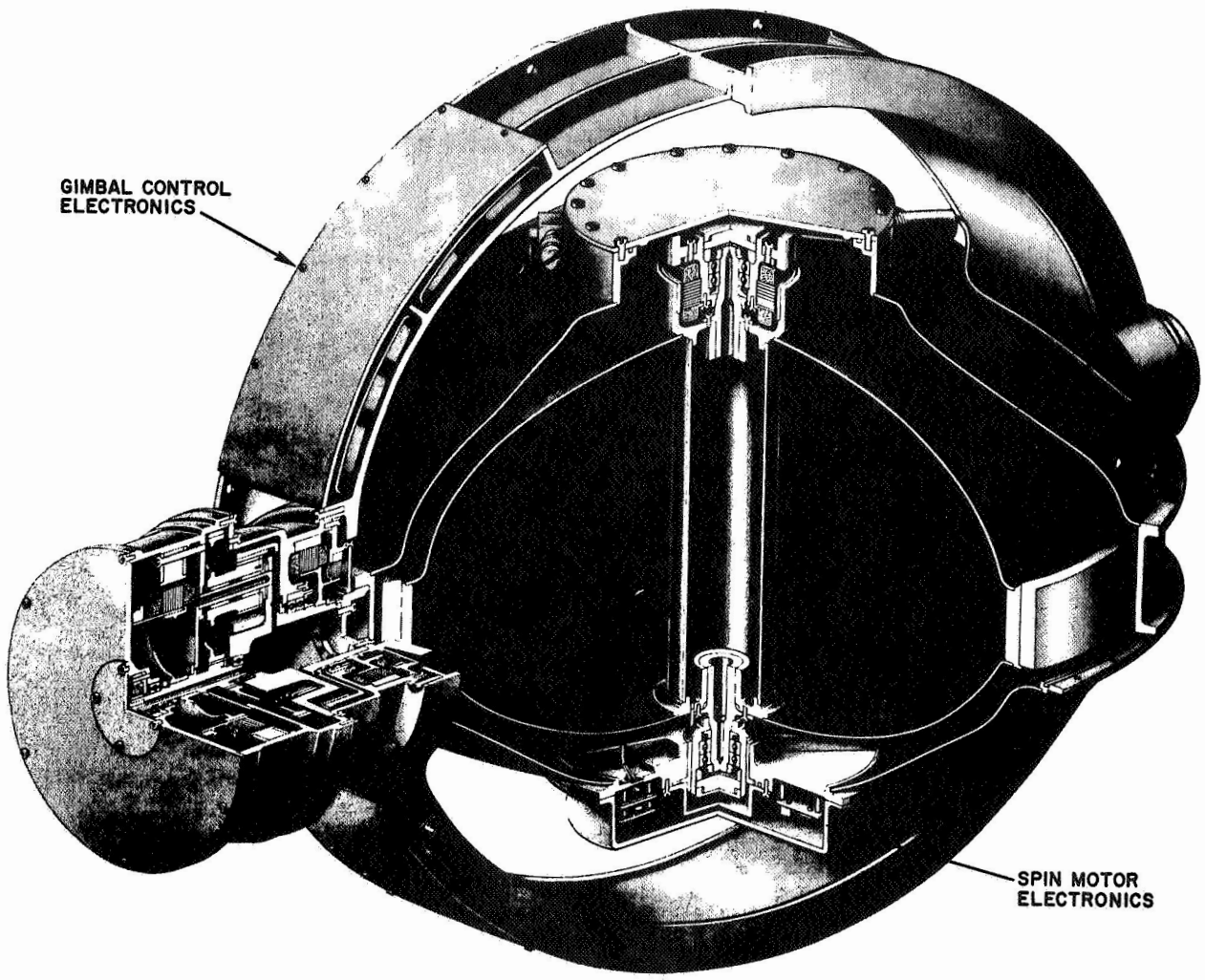

Figure C-1
Sperry High Torque Single-Gimbal CMG

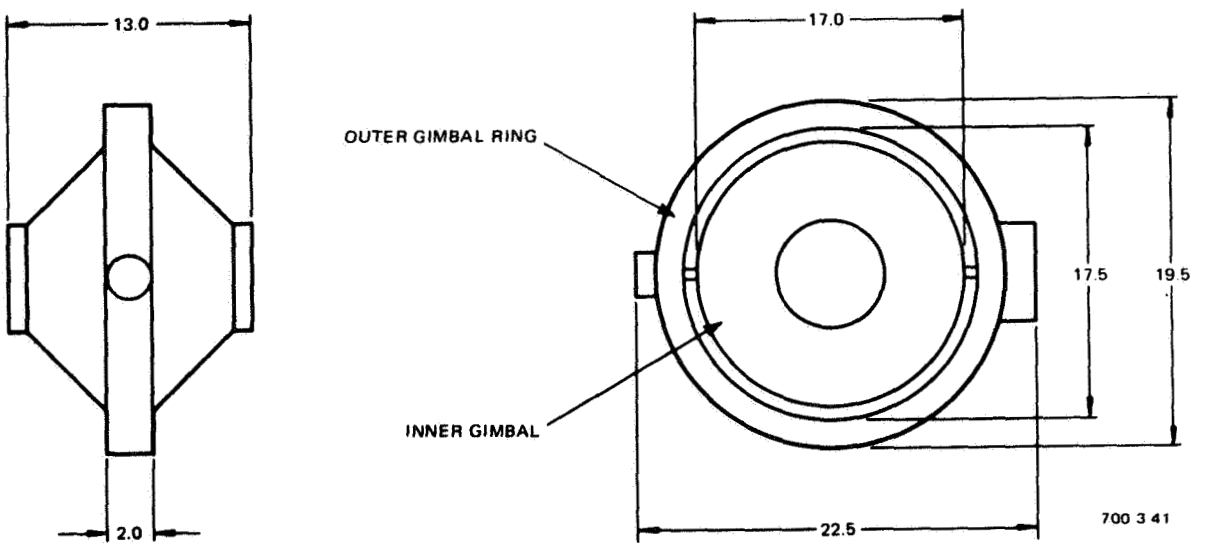

Figure C-2
Outline Dimensions Proposed, 4-FACS CMG

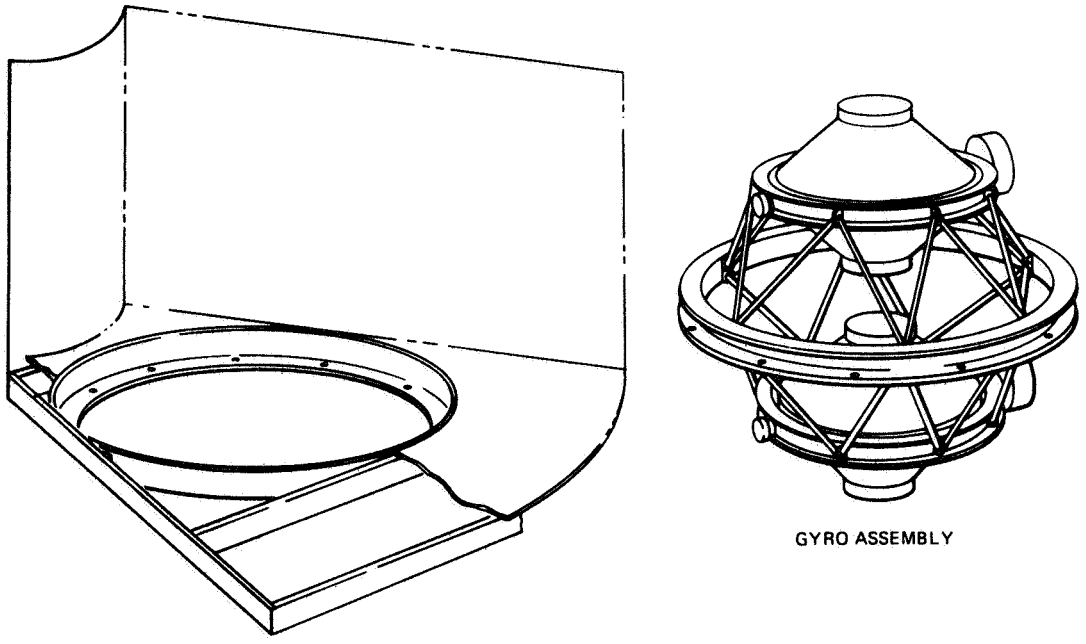

Figure C-3
4-FACS CMG Installation

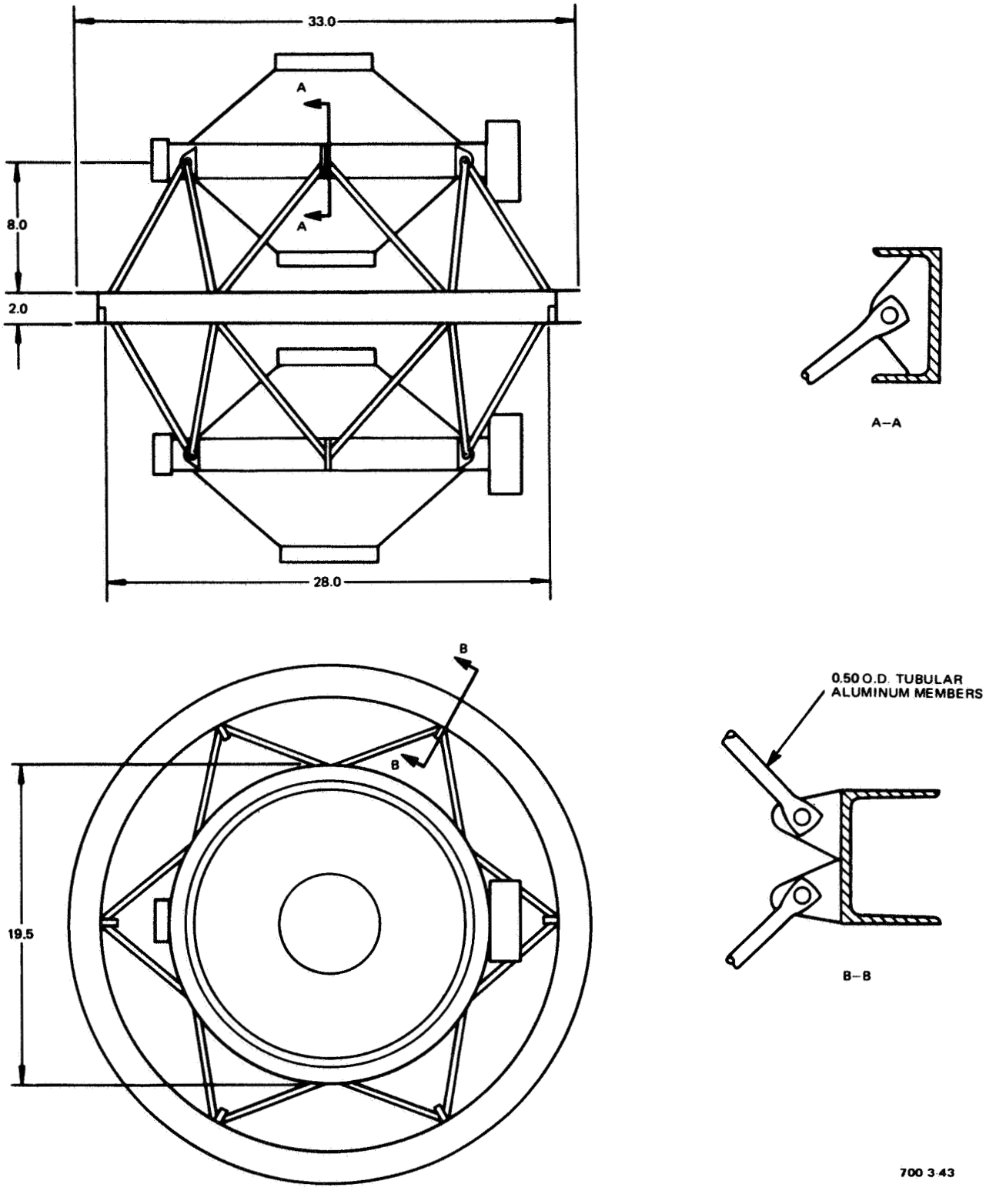

Figure C-4
Dual CMG Assembly

APPENDIX D

ANALOG COMPUTER DIAGRAMS

APPENDIX D

ANALOG COMPUTER DIAGRAMS

Diagrams of the AD-4 analog computer networks used in the simulation discussed in Section VII are included in this section.

Symbols used in the diagrams are shown in Figure D-1; a complete diagram of the 4-FACS simulation is shown in Figures D-2 through D-5. The basic model (vehicle, constant gain steering law, gimbal dynamics, momentum transfer) is shown in Figure D-2; diagrams for the RJC system, in Figure D-3. Pseudo-torque feedback steering law is shown in Figure D-4; desaturation and gyro failure schemes as well as the network for engaging the 4-FACS, in Figure D-5. A diagram for the low-torque 4-FACS simulation is shown in Figure D-6; the scissored pair system diagram, in Figure D-7.

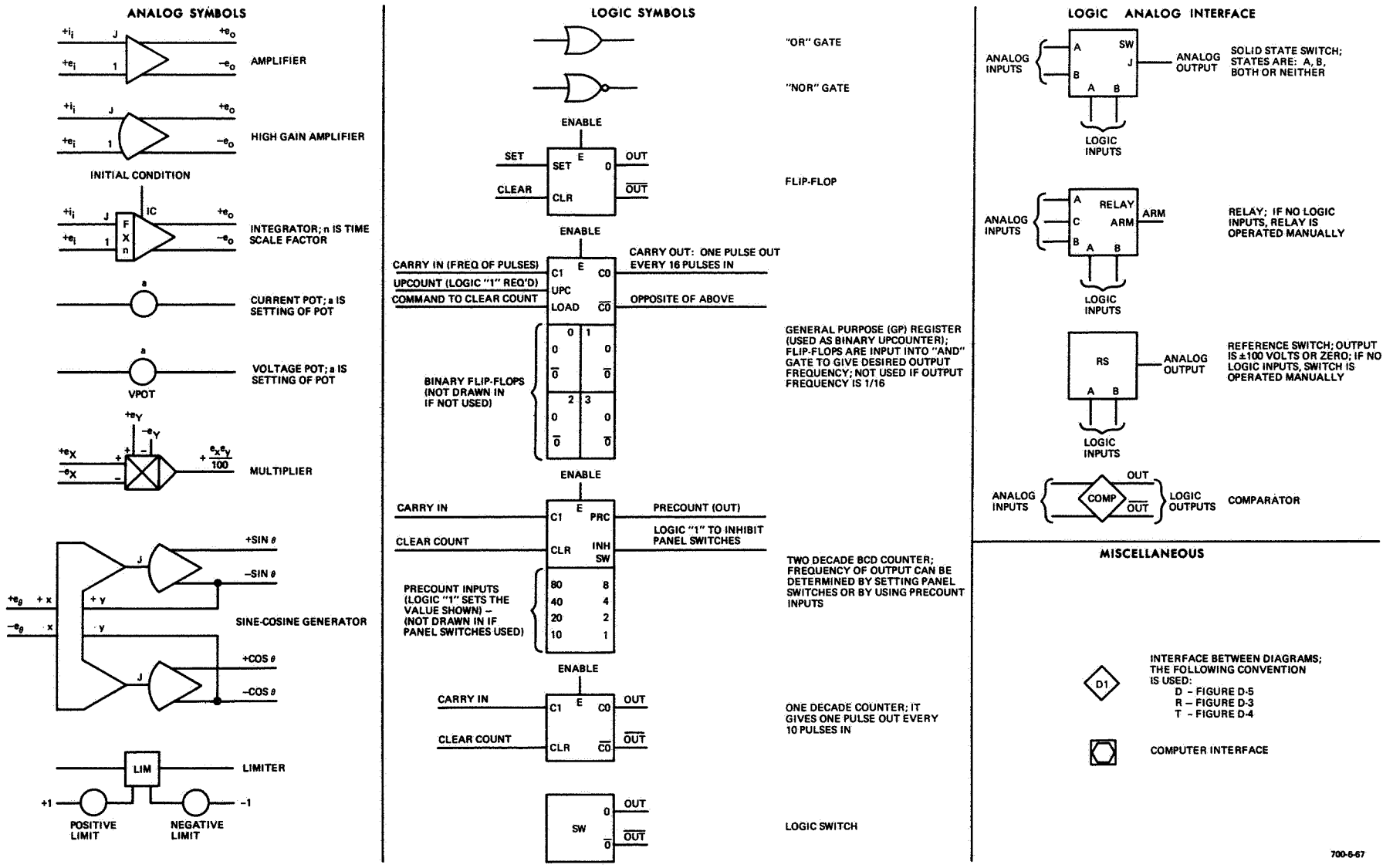

Figure D-1
List of Symbols used in Analog Computer Diagrams

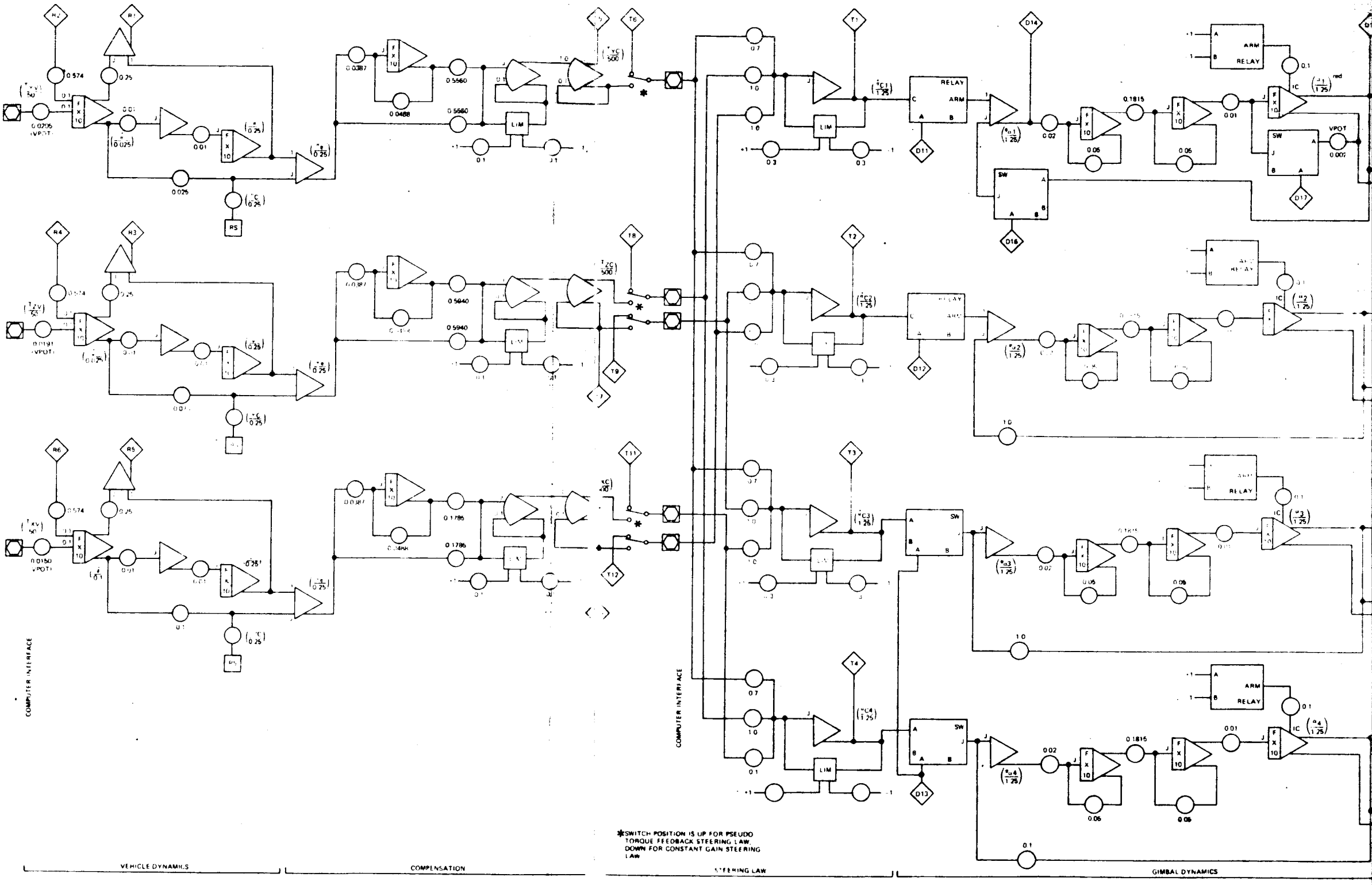
COMPUTER INTERFACE
COMPUTER INTERFACE
VEHICLE DYNAMICS
COMPENSATION
STEERING LAW
GIMBAL DYNAMICS
*SWITCH POSITION IS UP FOR PSEUDO TORQUE FEEDBACK STEERING LAW, DOWN FOR CONSTANT GAIN STEERING LAW
RELAY
ARM
SW
LIM
VPOT

FOLD-OUT #1

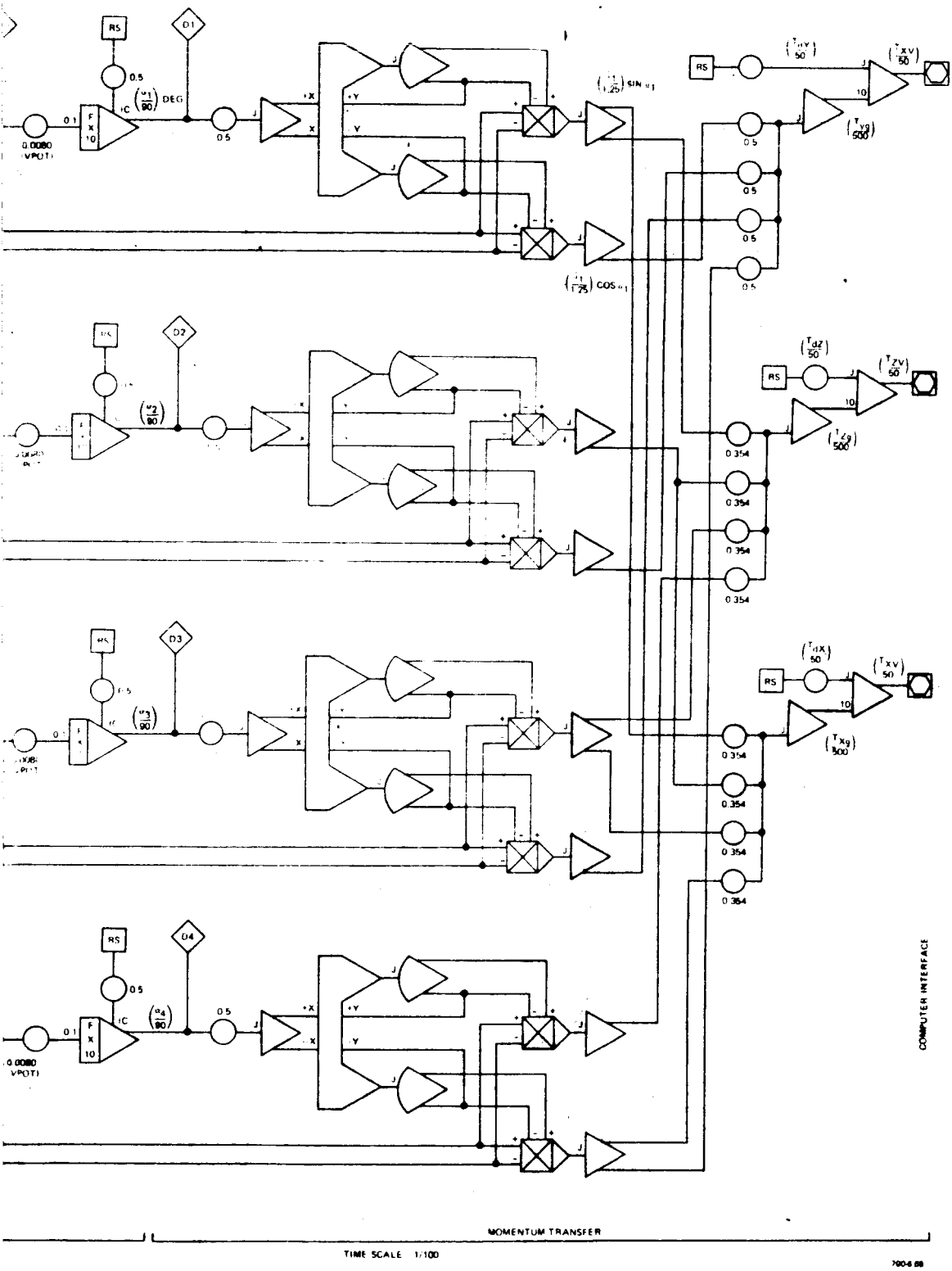

FOLD-OUT #2

Figure D-2
Vehicle Dynamics, Compensation, Constant Gain Steering Law, Gimbal Dynamics, Momentum Transfer Analog Computer Diagram

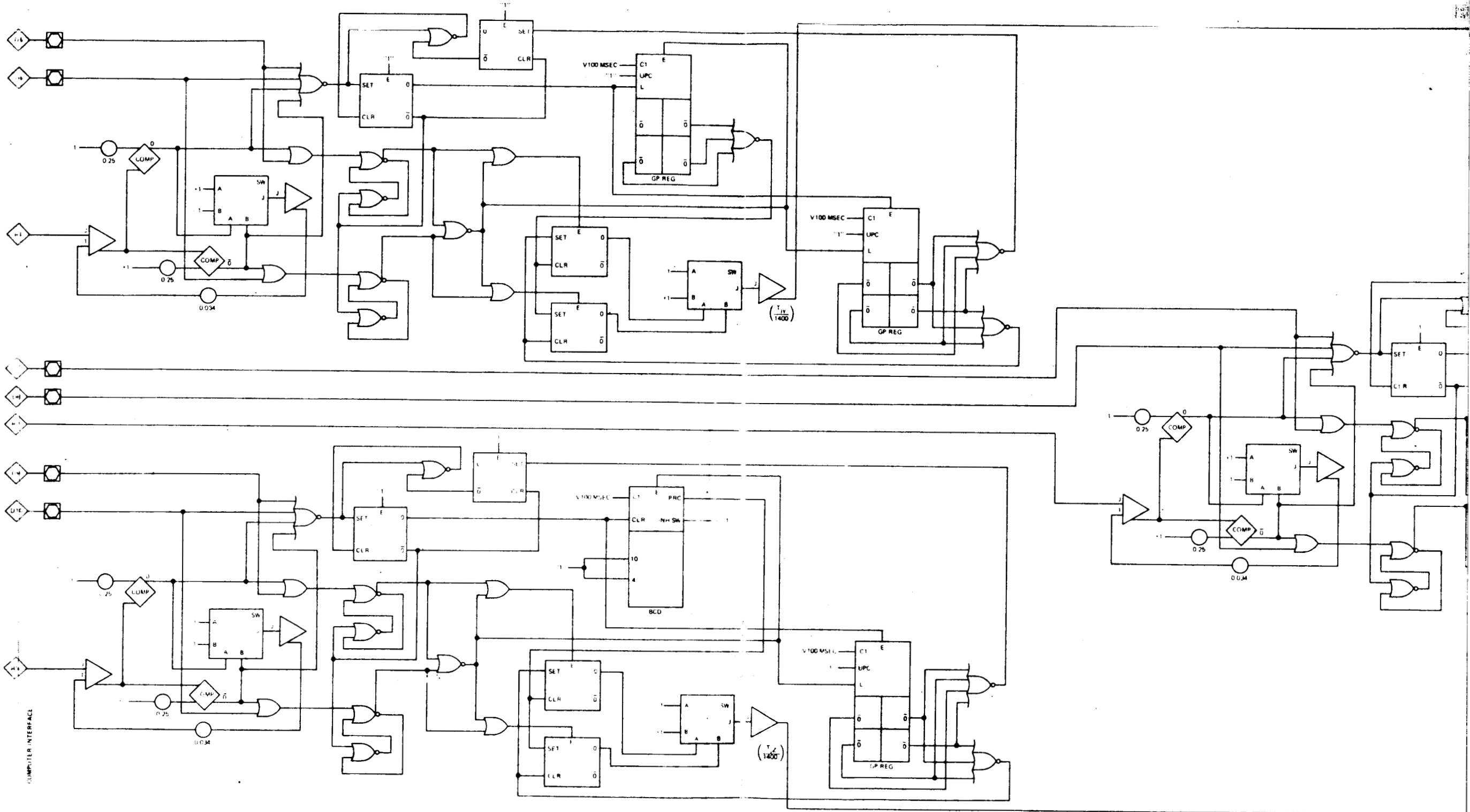

FOLD-OUT #1

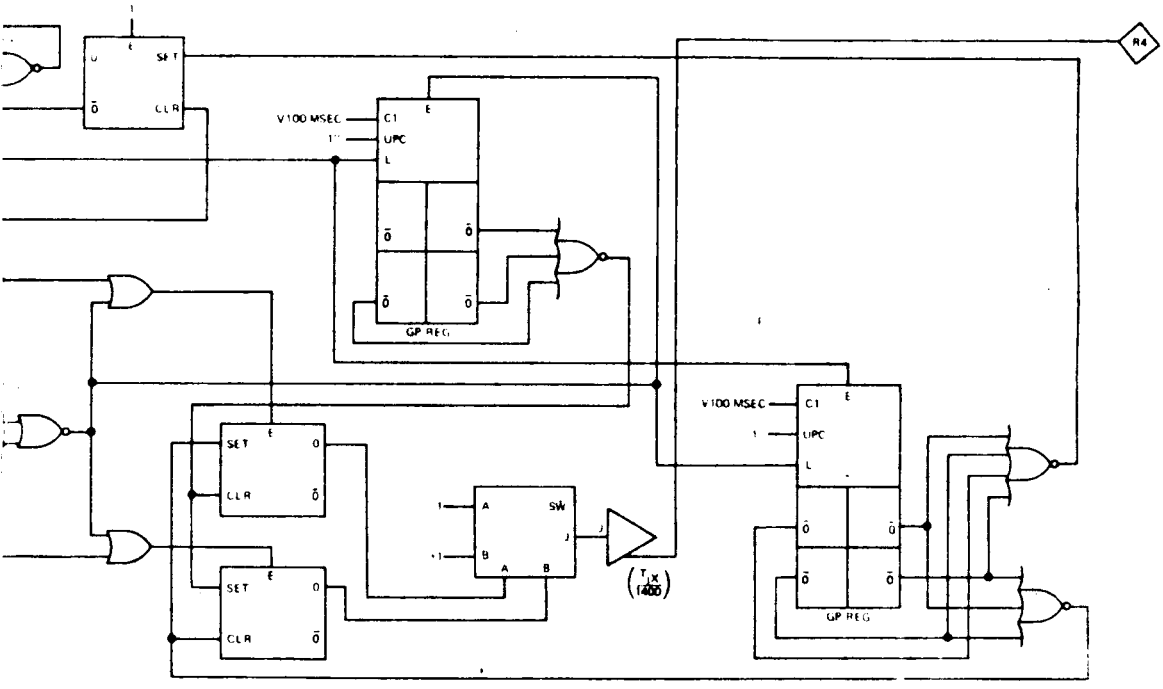

FOLD-OUT #2

Figure D-3
Reaction Jet System Analog
Computer Diagram

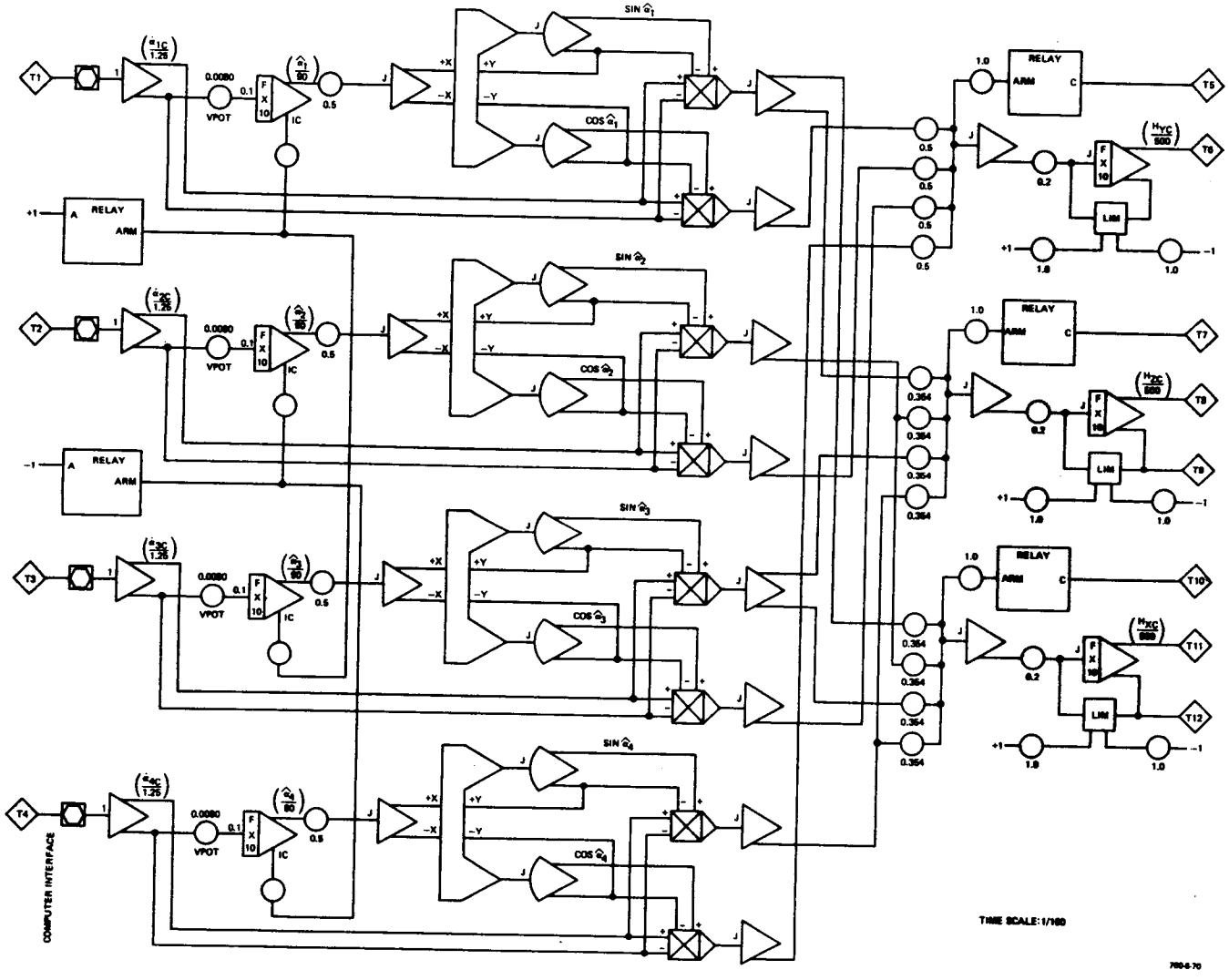

Figure D-4
Pseudo-Torque Feedback Steering Law
Analog Computer Diagram

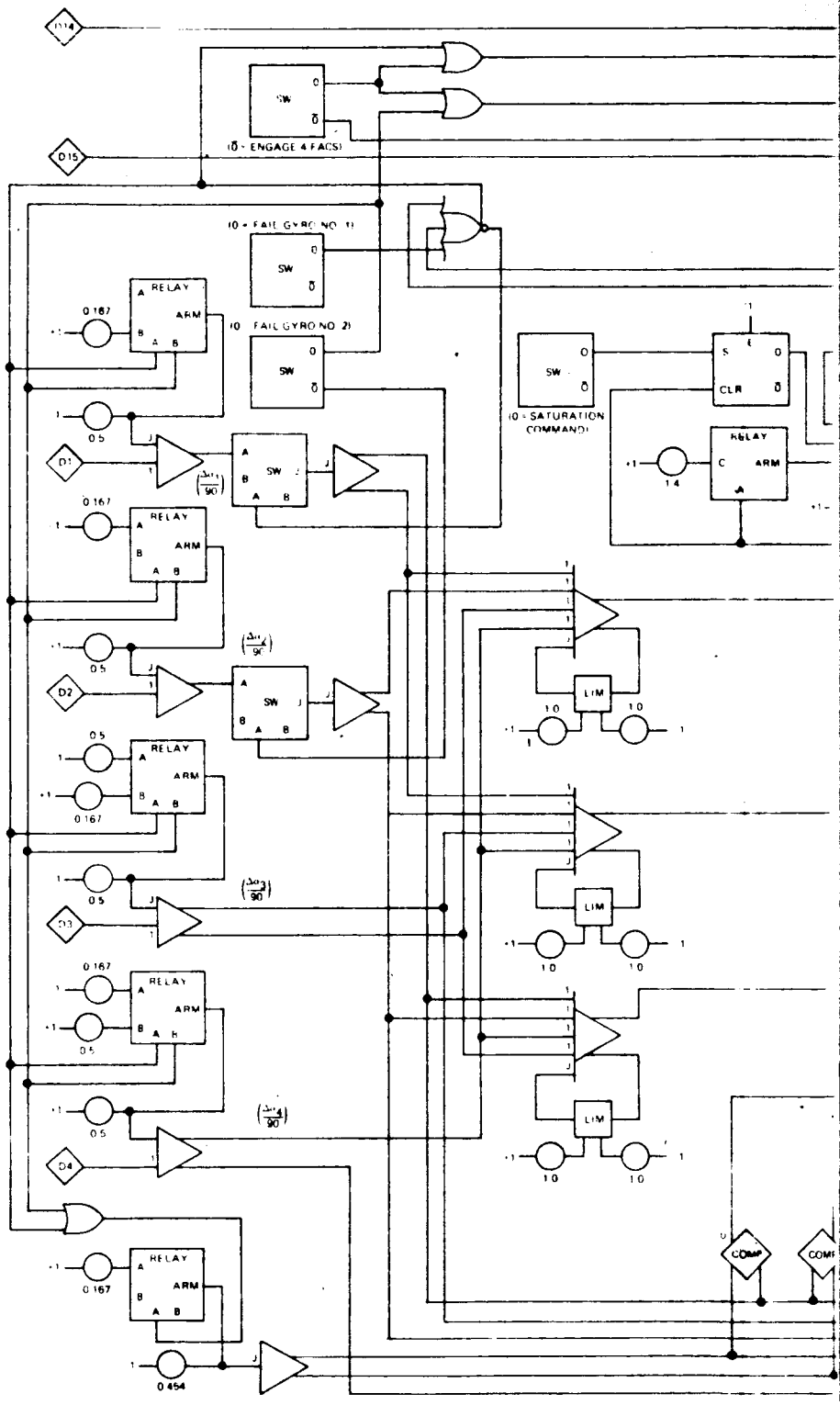
SW
(0 - ENGAGE 4 FACS)
(0 - FAIL GYRO NO 1)
(0 - FAIL GYRO NO 2)
(0 - SATURATION COMMAND)
RELAY
ARM
LIM
CLR
COMP
D1
D2
D3
D4
D15
0.167
0.5
0.454

FOLD OUT #1

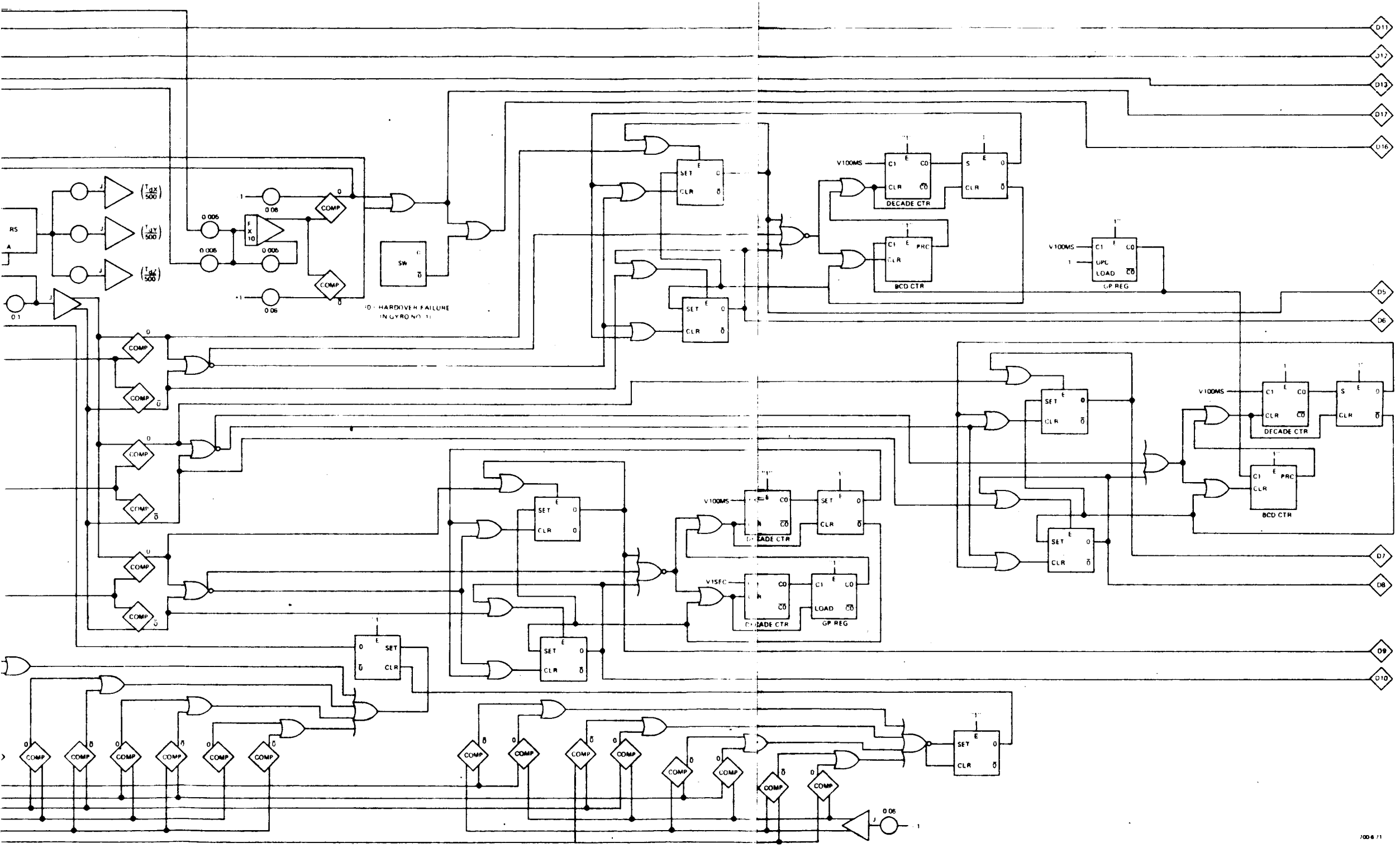

FOLD OUT #2

Figure D-5
RJC Desaturation, Gyro Failures
Engage 4-FACS
Analog Computer Diagram

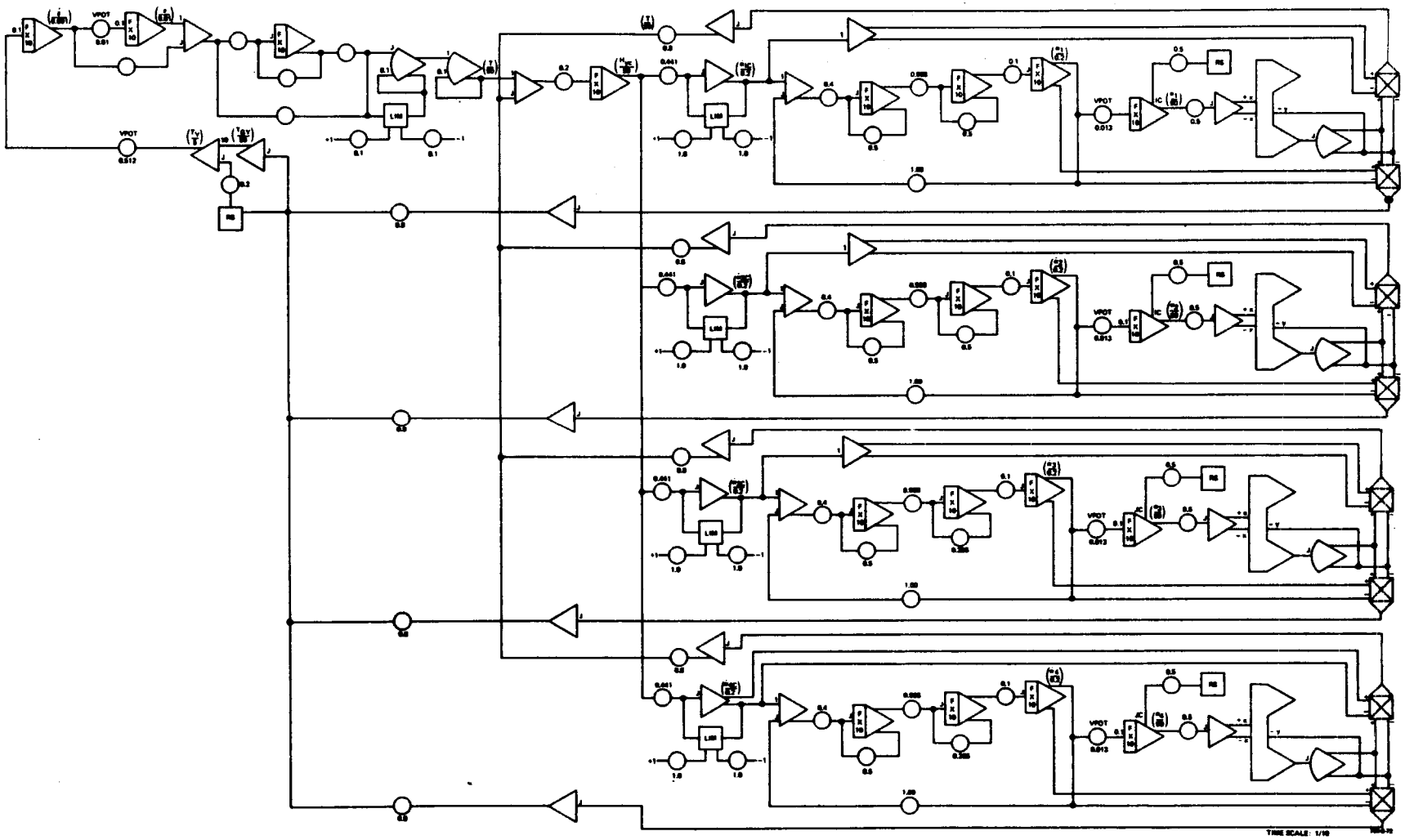

Figure D-6
Low Torque 4-FACS

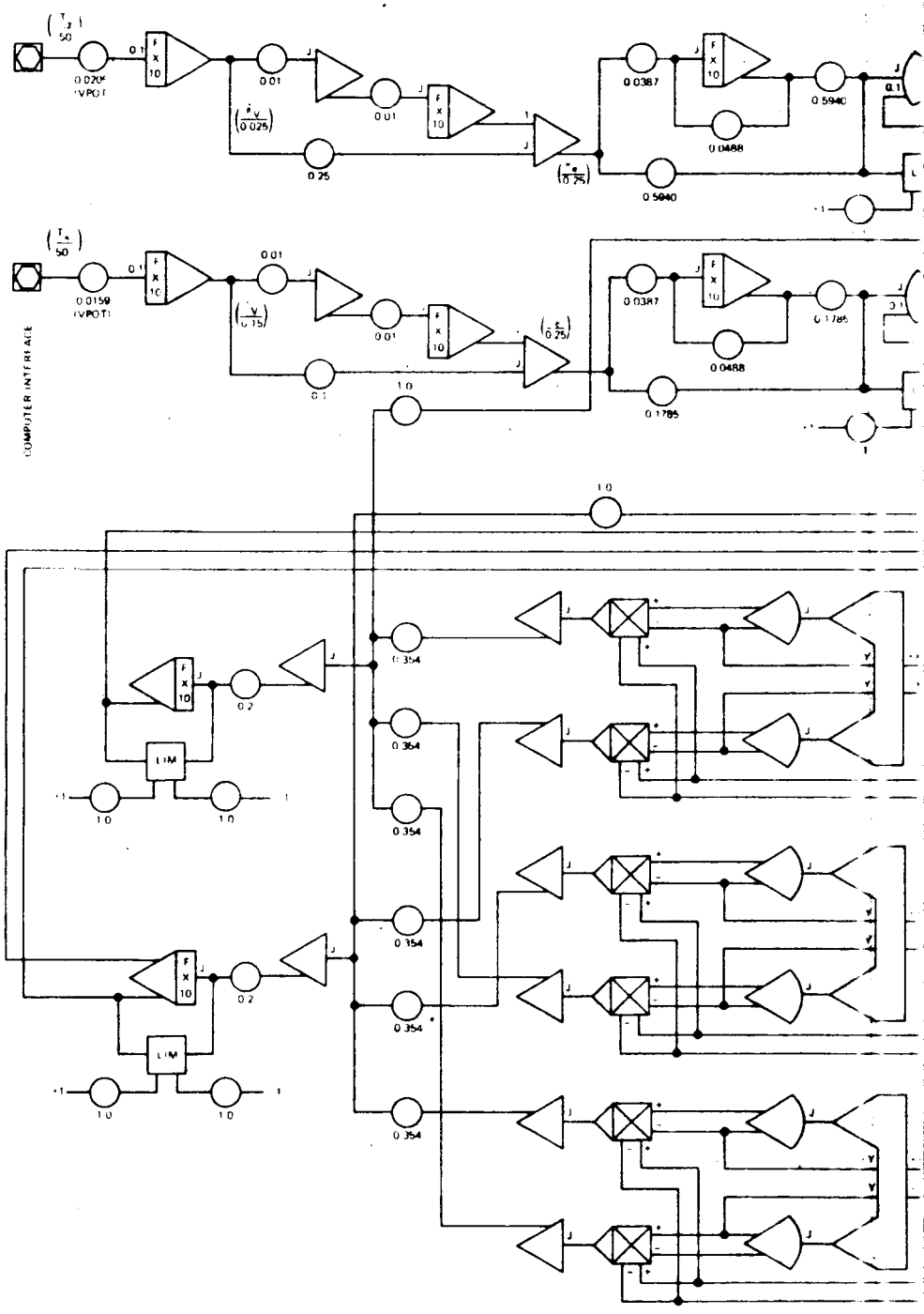

FOLD OUT #1

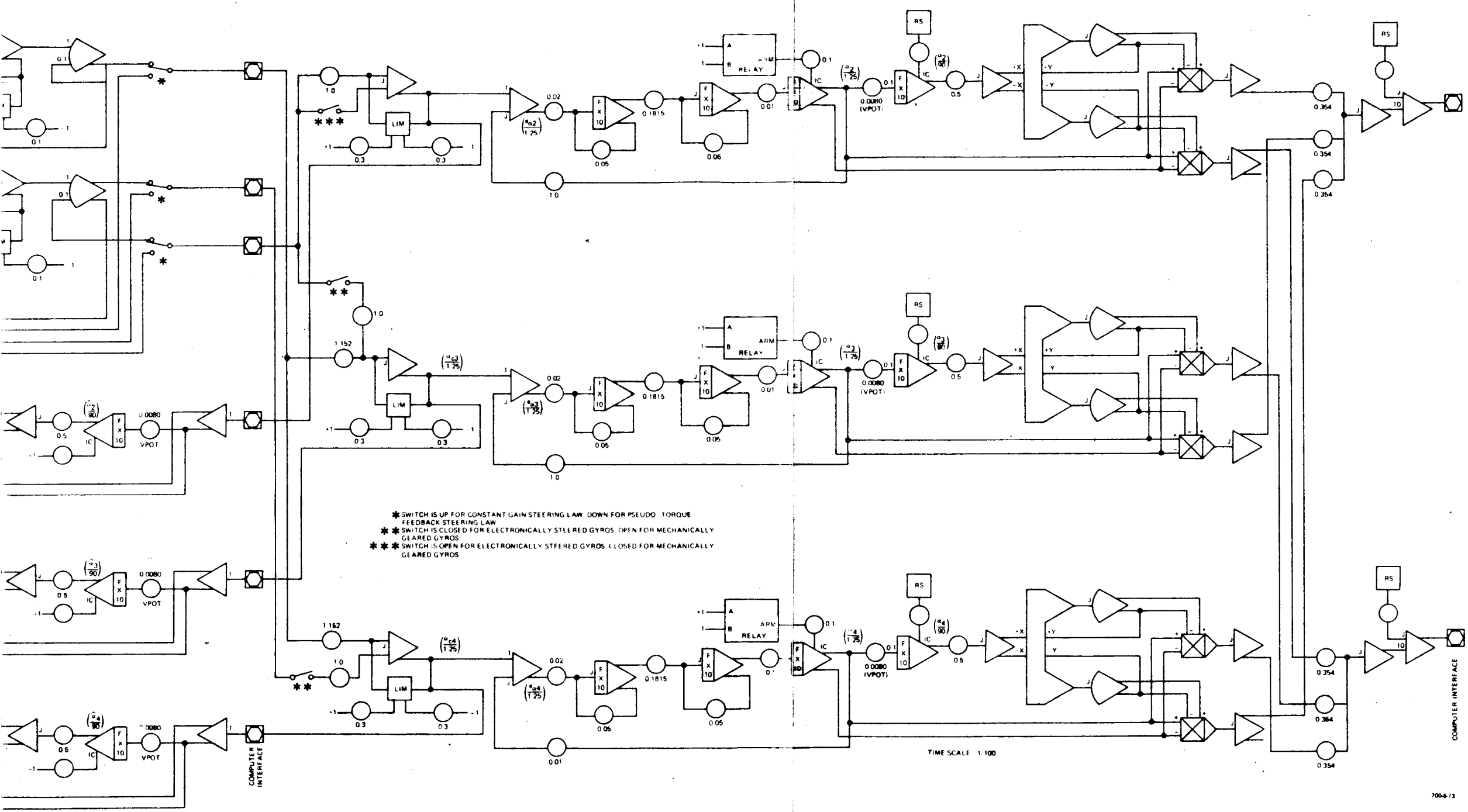

FOLD-OUT #2

Figure D-7
Scissored-Pair System Analog
Computer Diagram

APPENDIX E

COMPONENT FAILURE ANALYSIS

This appendix presents the piece part failure rates of each system component listed in Table 9-1. The failure rate information is from many standard sources including Sperry in-house gyro life test and field data as well as standard sources such as references 7 and 8. Mission related stress factors have been applied to the basic failure rates to derive the part failures per million hours. Each major electronic component includes a regulated dc power supply, and thus maintains isolation between unit failures. The rate gyro has the largest failure rate which is predicated on standard inertial grade rate gyro field data such as the Sperry RG1000 field data. It is anticipated that a high reliability unit with component improvements can be produced in the 1975 - 1980 period that will lower this failure rate by an order of magnitude.

Quantity	Component	Part Failure 10^6 hr	Total Failure 10^6 hr
	CMG GYRO ROTOR AND CASE		
1	Spin Motor	0.089	0.089
4	Spin Bearings (Duplex Pairs)	0.146	0.580
3	Slip Rings	0.020	0.060
1	Hermetic Seal	0.058	0.058
	OVERALL		0.787
	CMG GYRO ROTOR ELECTRONICS		
1	Rotor Tachometer	0.013	0.013
1	Inverter - (20% Duty Cycle)	0.754	0.754
	OVERALL		0.767
	CMG GIMBAL TORQUER AND ANGLE CONTROL		
1	Torquer Motor	0.085	0.085
4	Gimbal Bearings	0.002	0.008
1	Tachometer	0.030	0.030
	OVERALL		0.123

Quantity	Component	Part Failure 10^6 hr	Total Failure 10^6 hr
	CMG GIMBAL CONTROL ELECTRONICS		
8	Operational Amplifiers (IC)	0.05	0.400
60	Resistors	0.005	0.300
12	Transistor (Low Level)	0.02	0.240
12	Capacitors	0.003	0.036
6	Transistors (High Level)	0.05	0.300
12	Diodes (Switching)	0.01	0.120
2	Transformers	0.1	0.200
400	Solder Joints	0.0001	0.040
1	DC Regulated Supply	0.458	0.458
	OVERALL		2.094
	GIMBAL ANGLE SYNCHRO		
1	5 Wire Synchro	0.038	0.038
	OVERALL		0.038
	CMG VEHICLE LOOP ELECTRONICS		
12	Operational Amplifiers (IC)	0.05	0.600
6	Transistors (Low Level)	0.02	0.120
3	Flip-Flops	0.035	0.105
6	Logic Gates	0.03	0.180
80	Resistors	0.005	0.400
18	Capacitors	0.003	0.054
12	Diodes	0.01	0.120
450	Solder Joints	0.0001	0.045
1	DC Regulated Power Supply	0.458	0.458
	OVERALL		2.082

Quantity	Component	Part Failure 10^6 hr	Total Failure 10^6 hr
	CMG CONTROL (STEERING LAW) COMPUTER		
20	Operational Amplifiers (IC)	0.05	1.000
100	Resistors	0.005	0.500
30	Transistor (Low Level)	0.02	0.600
30	Logic Gates	0.03	0.900
30	Diodes	0.01	0.300
50	Capacitors	0.003	0.150
2	Transformers	0.100	0.200
1	Connector (20 pin)	0.100	0.100
900	Solder Joints	0.0001	0.090
1	DC Regulated Power Supply	0.458	0.458
	OVERALL		4.298
	RJC VEHICLE LOOP ELECTRONICS		
9	Operational Amplifiers (IC)	0.05	0.450
3	Transistors (Low Level)	0.02	0.060
12	Logic Gates	0.03	0.360
90	Resistors	0.005	0.450
6	Capacitors	0.003	0.018
12	Diodes	0.01	0.120
400	Solder Joints	0.0001	0.040
1	DC Regulated Power Supply	0.458	0.458
	OVERALL		1.956
	RATE GYRO AND ELECTRONICS		
1	Miniature Inertial Rate Gyro	20.0	20.0
1	Demodulator Electronics	0.50	0.50
1	Pickoff Excitation Electronics	0.50	0.50
1	Spin Motor Electronics	0.50	0.50
	OVERALL		21.5

Quantity	Component	Part Failure 10^6 hr	Total Failure 10^6 hr
	DUAL DC REGULATED POWER SUPPLY		
8	Diodes (Switching)	0.010	0.080
2	Diodes (Zener)	0.015	0.030
4	Transistors (Switching)	0.020	0.080
2	Transistors (Power)	0.050	0.100
6	Capacitors	0.003	0.018
10	Resistors	0.005	0.050
1	Transformer	0.100	0.100
	OVERALL		0.458
	RJC DRIVE ELECTRONICS (JET LOGIC AND SOLENOID DRIVERS)		
39	Transistors (Low Level)	0.020	0.780
12	Transistors (Power)	0.050	0.600
90	Resistors	0.005	0.450
27	Diodes	0.010	0.270
12	Capacitors	0.003	0.036
500	Solder Joints	0.0001	0.050
1	DC Regulated Power Supply	0.458	0.458
	OVERALL		2.644
	RJC ATTITUDE ROCKETS		
4	Y-Axis Rockets [6.4 $(10)^6$ cycles] (213 ft-lb-sec/orbit)	$0.347/10^6$ cycles	2.22
4	Z-Axis Rockets [1.28 $(10)^6$ cycles] (48 ft-lb-sec/orbit)	$0.347/10^6$ cycles	0.44
4	X-Axis Rockets [5.6 $(10)^5$ cycles] (8 ft-lb-sec/orbit)	$0.347/10^6$ cycles	0.22
	OVERALL		2.88

Quantity	Component	Part Failure 10^6 hr	Total Failure 10^6 hr
	TWO-AXIS SUN SENSOR AND ELECTRONICS		
4	Solar Cells	0.01	0.040
2	Operational Amplifiers (IC)	0.05	0.100
15	Resistors	0.005	0.075
50	Solder Joints	0.0001	0.005
1	Connector	0.08	0.080
1	DC Regulated Power Supply	0.458	0.458
	OVERALL		0.758
	TWO-GIMBAL STAR TRACKER AND ELECTRONICS		
2	Gimbal Torquer and Angle Control	0.123*	0.246
2	Gimbal Control Electronics	2.094*	4.188
1	Star Tracker Sensor and Electronics	0.50	0.500
1	Roll Reference and Update Computer	1.0	1.000
	OVERALL		5.934
	VEHICLE ON-BOARD TELEMETRY SYSTEM		
1	On-board Receiver Decoder/ Transmitter	3.0	3.0
	OVERALL		3.0
	FAILURE DETECTION AND SWITCHING NETWORK		
2	Operational Amplifiers (IC)	0.05	0.100
1	Logic Gate	0.03	0.030
4	Transistors (Switching)	0.020	0.080
16	Resistors	0.005	0.080
2	Diodes (Zener)	0.015	0.030
100	Solder Joints	0.0001	0.010
1	DC Regulated Power Supply	0.458	0.458
	OVERALL		0.788

*Gimbal control complexity assumed equal to gyro gimbal loop complexity.

APPENDIX F

OVERALL SYSTEM BLOCK DIAGRAM

APPENDIX F

OVERALL SYSTEM BLOCK DIAGRAM

The overall 4-FACS CMG Fine Attitude Control System is shown in the block diagram following this page. The complete three-axis system is shown in this block diagram which depicts the interconnections between main functional areas. Telemetry monitoring points are indicated by encircled letters (i.e., (A1)) and refer to the signals listed in Subsection VIII.B.

The primary functional blocks shown are the following:

- Attitude Reference System
- Rate Gyro System
- RJC Vehicle Electronics
- CMG Vehicle Electronics Computer
- CMG Control (Steering Law) Computer
- CMG Gimbal Rate Loop
- Vehicle Model

NASA — MSC — Coml., Houston, Texas

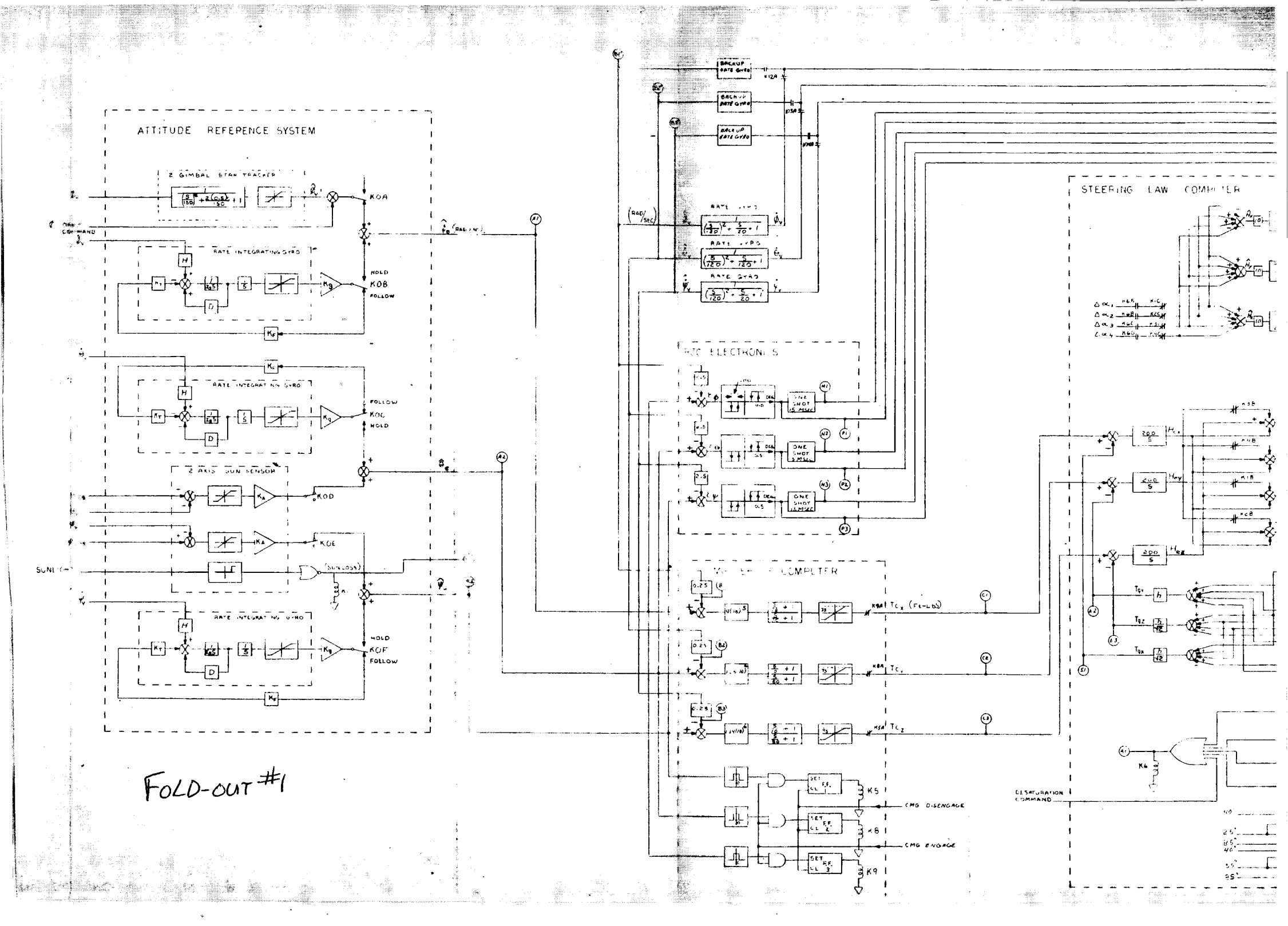
ATTITUDE REFERENCE SYSTEM
2 GIMBAL STAR TRACKER
RATE INTEGRATING GYRO
HOLD
FOLLOW
2 AXIS SUN SENSOR
SUNLOSS
BACKUP RATE GYRO
RATE GYRO
RCS ELECTRONICS
ONE SHOT 15 MSEC
ONE SHOT 3 MSEC
ONE SHOT 15 MSEC
STEERING LAW COMPUTER
SET FF
CMG DISENGAGE
CMG ENGAGE
DESATURATION COMMAND

FOLD-OUT #1

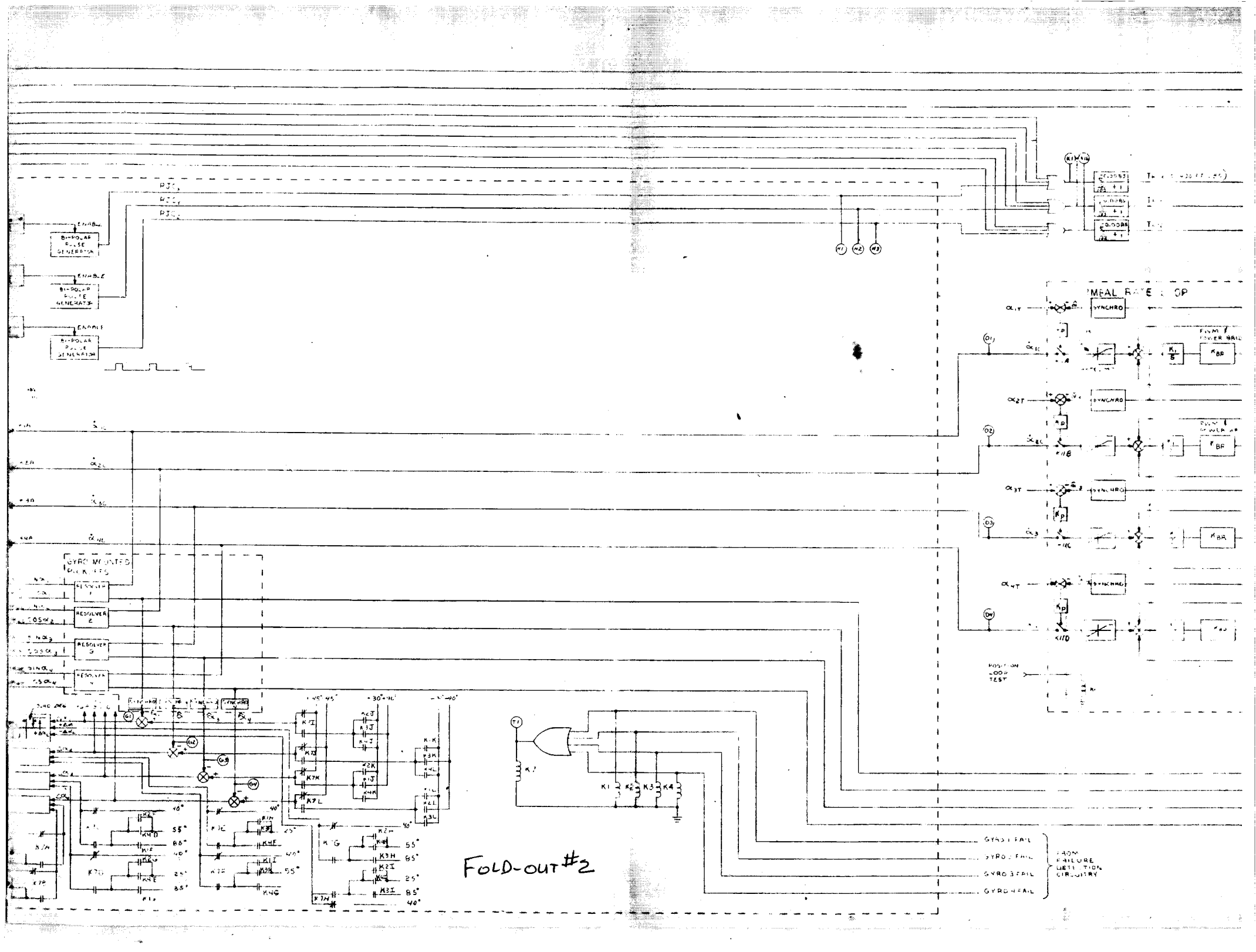
BI-POLAR PULSE GENERATOR
ENABLE
GYRO MOUNTED ELECTRONICS
RESOLVER 1
RESOLVER 2
RESOLVER 3
RESOLVER 4
SYNCHRO
K1
K2
K3
K4
K7
GYRO 1 FAIL
GYRO 2 FAIL
GYRO 3 FAIL
GYRO 4 FAIL
FROM FAILURE DETECTION CIRCUITRY
POSITION LOOP TEST
FOLD-OUT #2

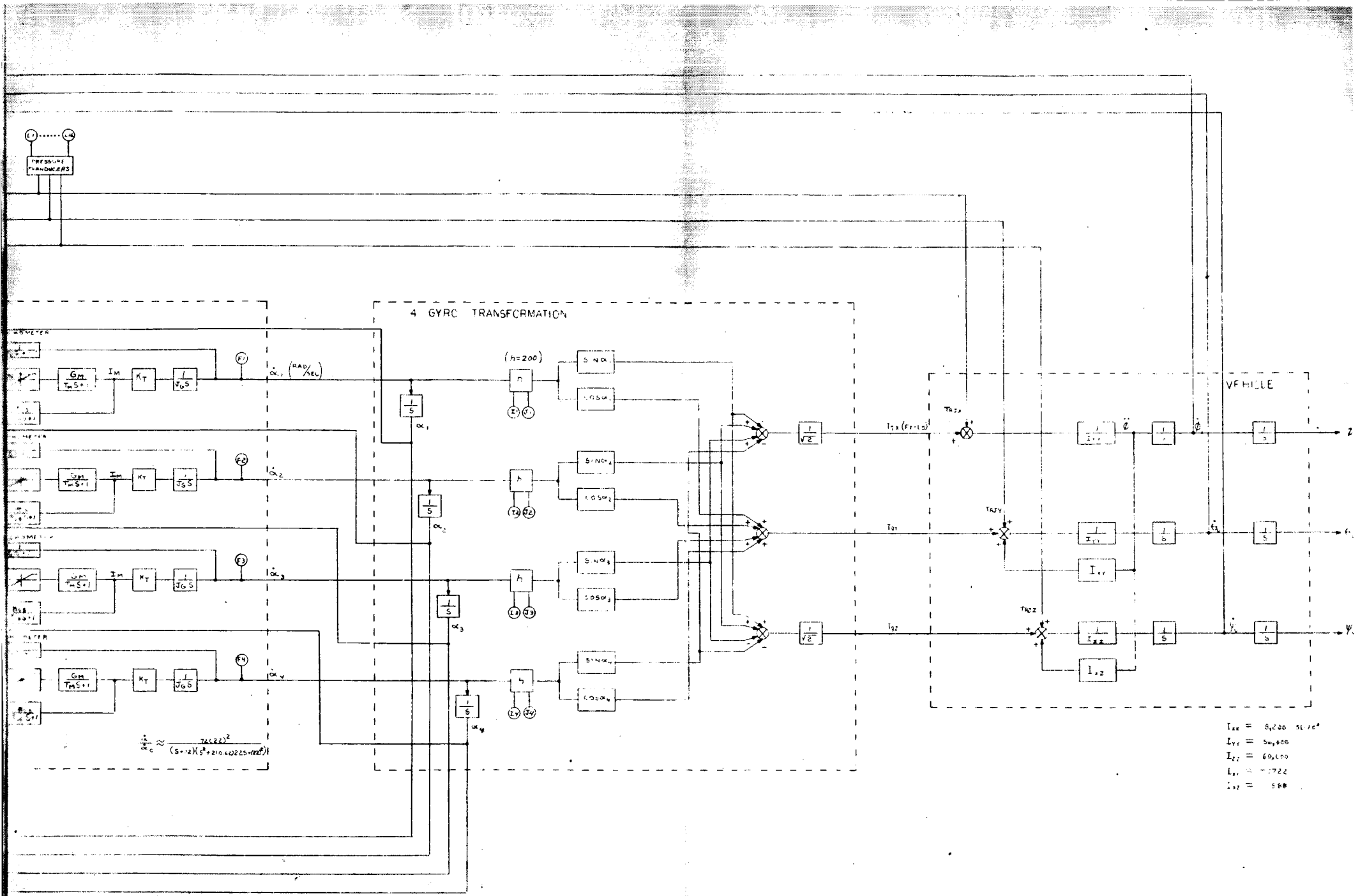
TREASURE HANDLERS
4 GYRO TRANSFORMATION
(h=200)
VEHICLE
I_{xx} = 5,200 SLUG-FT²
I_{yy} = 54,000
I_{zz} = 60,000
I_{xy} = -1722
I_{xz} = 588

FOLD-OUT #3

...ANS)

4-FACE CMG FINE ATTITUDE CONTROL SYSTEM

DRAWN BY M. KELLY DATE 6-12-70

APPROVED BY [signature] DATE 6/12/70

FOLD-OUT #4